SINGLE MOLECULE CONDUCTANCE OF DITHIAHEXYL-ARYL COMPOUNDS

Thesis submitted in accordance with the requirements of the University of Liverpool for the degree of Doctor in Philosophy

by

Edmund Leary

September 2008

ABSTRACT

This thesis describes an investigation into electron transfer across redox active and redox inactive molecular wires. The molecules we studied consisted of three parts; a saturated alkyl 'tunnelling barrier' connected to a central conjugated group (lower in energy than the alkyl groups) which was also connected to another alkyl group, all in a linear fashion. Thiols were mainly employed as the terminal binding groups to the gold contacts. A primary aim was to explore detailed mechanisms of current flow across a single molecule bridge between two metallic contacts by altering the electrochemical gating potential. *N,N'*-(bis(thiahexyl))pyrollotetrathiafulvalene was chosen for this as it has easily accessible redox states and has a symmetric structure which is similar to a previously studied viologen compound. Further investigations were targeted at studying the nature of the bridge molecule and how its structure could determine electron transport mechanisms. Concepts such as the size of the 'barrier indentation' provided by the conjugated group were tested. In particular, simple aromatic systems were explored in the form of substituted or unsubstituted benzene rings. Investigations were also carried out into the conjugation extent and metallic character of the centre group. The current-distance (I(s)) and current-time (I(t)) techniques employing an STM were used to study the electron transfer. Characterisation of monolayers and sub-monolayers of the thiol compounds on gold were carried out by XPS, PMIRRAS, cyclic voltammetry and *in situ* STM imaging.

PREFACE

The understanding of the underlying mechanisms at work in electron transfer on the nano-scale (1 – 100 nm), in particular across single molecules, is still very much in its infancy. Several novel techniques have been developed over the last ten years to study the phenomenon which involve the use of the STM, the scanning tunnelling microscope. We have used two such techniques, namely the I(s) and the I(t) methods, extensively in this thesis to explore the conductance properties of many organic and metal-organic molecules, in particular paying close attention to the relation between chemical structure and conductivity.

- Chapter three begins by addressing the potential to 'switch' a molecule's conductance between a high and a low state. This behaviour would be paramount amongst molecular components as switches are a basic constituent of an electronic circuit. Pyrrolotetrathiafulvalene and viologen based systems were investigated and differences in structural changes upon electrochemical transitions resulted in the two groups displaying quite different switching behaviour.

- Chapter four investigates whether non-redox active aromatic groups can behave in a similar manner to the redox active groups discussed in the previous chapter in that they serve as an effective indentation in the tunnelling barrier of the alkane chains. This effect was verified and, by modifying the chemical substituents on the central benzene ring, it was found that that more electron-rich benzene rings give higher conductances, consistent with hole conduction via the benzene HOMO.

- Chapter five examines the effect of varying the length (and hence degree of conjugation) of the π-conjugated unit. For this oligothiophenes were selected as oligothiophenes, polythiophenes and their derivatives have been extensively investigated as semiconductors in organic thin film transistors and photovoltaic devices. We found that across a series of four oligomers the conductance remained practically constant, a trend which could not be rationalised in the context of advanced DFT calculations (which predicted that the conductance should drop by orders of magnitude). To explain this we investigated, both experimentally and theoretically, the effect of a water environment around the molecules and found that water cause the anomalous length independency. By removing the water from the system we showed that the length dependence followed the predicted decrease with length.

- Chapter six investigates a particular compound which contains a small platinum metal cluster. Similar in structure to the molecules discussed thus far, it consists of two alkyl chains on opposing sides of the cluster fragment forming another 'double tunnel barrier' arrangement. The I\V behaviour was studied and found not to fit a modified Simmons model well, which is possibly a reflection of the double-barrier characteristics of the junction. The high conductance of the molecule (up to 8 nS) for its length (2.4 nm) marks the start of using stable metal containing molecules in molecular electronics.

- Chapter seven looks at a much simpler molecule than those discussed in the majority of this thesis in considerable detail. The molecule discussed is octanedithiol, a simple fully saturated alkane compound. The effect of different experimental conditions was monitored in terms of the histogram profile. Under an argon

atmosphere one conductance group was present in the histogram analysis which agrees with the low value reported using the break-junction technique. However, in the presence of ethanol on the surface, this conductance group practically disappeared in favour of an even lower group a factor 6 lower. This result is in contrast to the effect water had upon the oligothiophenes, however, it can be explained in terms of a gold-thiol contact change in the presence of ethanol, which may restrict the mobility of thiols into their optimal co-ordination sites on the gold surface.

- Chapter nine presents the overall conclusion to this work.

CONTENTS

LIST OF FIGURES

Number *Page*

ACKNOWLEDGMENTS

I would like to express sincere appreciation to Dr Simon Higgins and Professor Richard Nichols for their assistance during my PhD and in the preparation of this manuscript. Particular thanks go to Dr Harm van Zalinge for help and constant discussion. I would also like to thank the people with whom I have collaborated over the past four years – Professor Colin Lambert and the theory group based in Lancaster University and Professor Jens Ultsrup from the Technical University of Denmark for their very good discussions. Finally I would like to thank the past members of the Higgins' group, Sam Badria and Ian Liverseige, who helped me with chemical synthesis at the beginning of my PhD.

Chapter 1

Introduction

Chapter 1. Introduction

1.1 The concepts of Molecular Electronics

As the miniaturisation of electronic components reaches the nanometre scale new principles of how to tailor structure-property relationships at the molecular level are vital in order to overcome the physical and economic limitations of conventional silicon electronics. Silicon technology is based on the 'top down' approach, which progressively removes material by lithography [1] and etching[2] to make a device. So called 'bottom up' self assembly of well defined nanoscale structures are composed of molecules,[3] quantum dots,[4] and nanowires [5] and display properties which can be manipulated by controlling size, morphology and chemical composition. This form of technology presents an enticing alternative to current electronic manufacturing. Building electronic devices is one of the goals of Molecular Electronics (ME), and indeed nanotechnology as a whole. ME represents a breakthrough in conceptualising new ways of designing electronic components and should allow us to continue to fulfil the prophecy of Henry Moore,[6] for the time being. In order to achieve this it will be necessary to measure, control and understand electron transport through these nano-scale building blocks.

ME is a topic of great interest in basic physics and chemistry. On the one hand, a molecule is governed by the laws of quantum mechanics, so

studying individual molecules gives insight into mesoscopic electron transfer processes, similar to research into inorganic-semiconductor quantum dots.[7] On the other hand, the study of molecular electronics can be seen as essentially a continuation of several decades of electron transfer research on donor-molecule-acceptor type systems.[8, 9] Richard Feynman gave the conceptual origin of nanotechnology and molecular electronics in 1959 in a lecture entitled 'Plenty of Room at the Bottom'. It considered the possibility of direct manipulation of individual atoms as a more powerful form of synthetic chemistry than those used at the time. [10] At the time it was impossible to manipulate matter at the individual molecule / atom level. The advent of the scanning tunnelling microscope (STM) [11] in the early 1980s changed this by making it possible to control the position of matter at the sub-molecular level to a degree unprecedented even to this day. Since then the STM has been applied in many disciplines, such as the imaging of biological compounds (DNA for instance) [12] or elucidating the adsorption geometries of many organic compounds on different surfaces.[13] In particular its application concerning the formation an electrical circuit with a single molecule[14] has generated huge scientific interest, allowing an almost limitless design of molecules to study in this way. It is this function of STM which we are concerned with in this thesis. We study STM in different environments with molecules of differing chemical structure to probe the relationships between molecular structure and electrical properties.

The question "What is the conductance of a single molecule?" has proved a difficult one to answer.

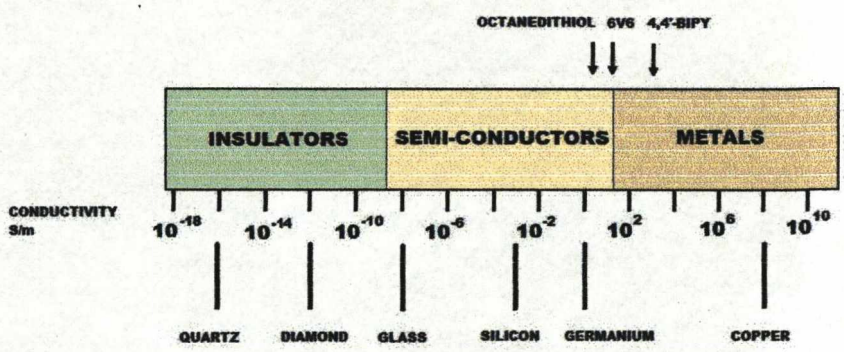

Figure 1.1. Conductivity of various bulk materials compared to some single organic molecules. [14, 15]

To determine the conductance of a single molecular wire one must tether the molecule reliably to (at least) two electrodes. Herein lies the main problem we are faced with, that as the current passed across a molecule between two metal electrodes depends on several factors. Firstly it depends on the intrinsic properties of the molecule, but also the electrode material [16] and how the molecule is attached to the electrodes.[17, 18] Creating identical contact geometries is an experimental hurdle for each experimental procedure lacks atomic level structural information, and hence control, during a conductance measurement. Significant progress has been made, however, both experimentally and theoretically, since the subject's inception more than a decade ago. These advances include: (1) the demonstration of simple molecular device functions and (2) the

development of many different experimental ways to measure electron transfer through single (or a few) molecules. As can be seen in figure 1.1, the conductivities that have been measured for single organic molecules places them within the region of good semi-conductors/poor metals. The conductivity (Sm^{-1}) of octanedithiol (a hydrocarbon compound with eight saturated carbon atoms and two terminal thiol groups) is similar to bulk germanium, a group 4 semi-conductor. Thus the conductivities of single molecules measured so far relate well with the established properties of classic electronic materials.

We shall continue this chapter with an overview of the experimental techniques, discussing their advantages and disadvantages, and investigate whether we can make comparisons between the various procedures for measuring molecular conductance. Subsequently we will address some of the more fundamental concepts of the subject of *single* molecule conductance, providing a detailed description of electron transport across many types of molecular junction.

1.2 The measurement of molecular junctions

Many experimental techniques have been devised and refined to measure and control current through molecules. They can be categorized under two main headings: (1) molecular films and (2) single molecule measurements. Further sub divisions of each category are (a) two terminal (electrode)

devices and (b) three terminal devices. We shall look first at molecular films between bulk electrodes.

1.2.1 Bulk electrodes

The concept of the bulk electrode approach is to trap a molecular film of monolayer, or multilayer, dimensions between two electrodes. The approach was applied initially to the study of thin films formed via Langmuir-Blodgett (L-B) or molecular self assembly methods, where molecules are initially immobilised on a surface and form a thin film. This was first demonstrated by Ratner and Aviram in the early 1970s when they prepared and characterised various donor-acceptor species. Such a compound is divided into three main parts, the donor, which is an electron rich species; an acceptor, which is an electron deficient species; a bridge, which connects, whilst keeping separate, the donor and the acceptor. The theory stated that they would behave in an analogous fashion to a silicon *p-n* junction and show molecular rectification.[19] There results suggested superexchange as the transport mechanism, some were also retracted, yet they represent historically the first attempts to predict and characterise a molecular scale electronic phenomenon.

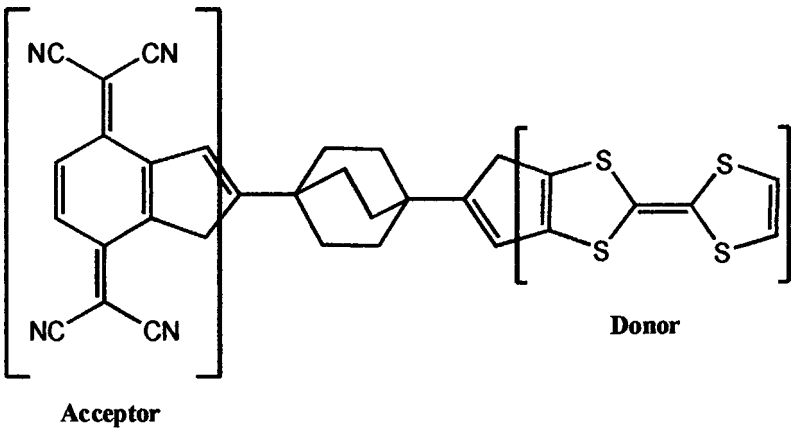

Figure 1.2. An example of a D-A compound with a tetrathiafulvalene donor moiety and a tetracyanoquinodimethane acceptor moiety connected by a methylene bridge. Calculations performed on this compound showed rectification to be possible. [19]

Rectification occurs when electron transfer across the molecular backbone is more facile at one bias than the opposite sign and occurs because of the different relative alignments of donor and accepter HOMO/LUMO with the metal electrode Fermi level. Recent progress in this area has come from the work of Metzger and co-workers [20] who have studied L-B films of γ-(*n*-hexadecyl)quinolinium tricyanoquinodimethanide between metal electrodes observing strong rectification (figure 1.3).

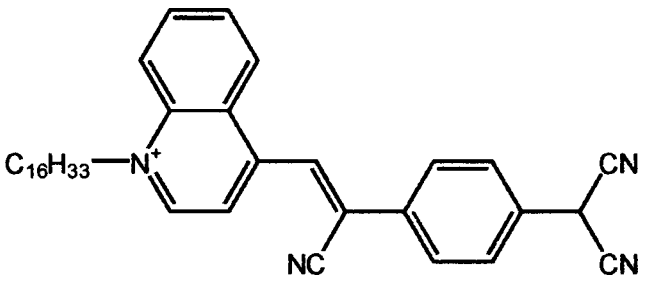

Figure 1.3. D-A compound from reference 20.

This compound is good at forming L-B films thanks to its long polymethylene chain, however determining the mechanism of rectification has been problematic. For Aviram and Ratner's compound (figure 1.2) the transport mechanism proposed involved electron transfer to/from metal electrodes to a neutral ground state molecule, creating a zwitterionic form that, by intervalence transfer (IVT), is able to return to the neutral form. The overall electron transfer is actually from acceptor to donor. Metzger's compound (fig. 1.3) is already charged so the first step is IVT to form a neutral species followed by electron transfer to and from the metal electrodes to recover the charged form. Metzger's compound, however, showed a larger rectification when four L-B layers where created between the electrodes compared to just one. It has been suggested that this difference occurs due to conduction through defects in the thicker layers.[20] This highlights the need to control precisely the number of layers and amount of defects in order to obtain reliable rectification behavior.

The placement of an electrode on top of the film is often the most difficult part of the experiment, and many methods have been developed, which include vapour deposition,[21, 22] electro-deposition[23-25] and mercury drop methods.[26-28] Problems with these procedures can include short circuiting between the top and bottom electrodes via penetration of metal atoms into the film through defect sites. The electrochemical approach of adsorbing metal ions on top of the film followed by reduction to the metal has proven quite successful.[29] Angle-resolved x-ray photoelectron spectroscopy showing that the top contact indeed sits on the film with no penetration. The mercury drop approach is also relatively straight forward and has shown some high yield devices.

Perhaps, though, the problem most difficult to overcome is that of finding the number of molecules contained between the two electrodes. To make a direct comparison between different molecular films one should know, ideally, the exact number of molecules passing current. At best the number can only be estimated from the area of the contacts and the volume occupied by a molecule on the surface. Thus it is not possible to say, with any great deal of certainty, whether one type of film is a better conductor than another because of the lack of knowledge of the number of molecules and defects/grain boundaries between the electrodes. It is, therefore, desirable to measure only *one* molecule in an experiment and make comparisons based on the fundamental properties of the individual

molecule in question. To carry this out the electrodes have to be made much smaller than the bulk electrodes discussed up until now.

1.2.2 Nanoelectrodes

The number of measured molecules can be reduced by using nano-scale electrodes. This has several important advantages over large films of molecules. In addition to those mentioned above, nano-gaps allow greater exposure of molecules to the environment which opens facilitates the study of environmental effects upon molecular electronic properties.[30] Most of the molecules studied as films can be studied using nano-electrodes, but also molecules which don't form ordered films well can be studied.

Nanoelectrodes can be generated using atomic force microscopes (AFM), STMs and cross-wire junctions[31]. AFM is a scanning probe technique where surface structure can be obtained along with controlled force applied to the molecular film. The cross-wire junction sandwiches a molecular layer between two perpendicular metal wires. At the point where the two wires cross the contact area is small, and hence a relatively small number of molecules bridge the gap.

Nanopores, fabricated in a thin solid membrane, have been used to reduce the number of molecules spanning the junction.[32] Using this method large negative differential resistance (NDR) of molecules as a function of the

sample bias has been observed. In this technique one side of the membrane is first covered with a thin metal layer followed by molecular monolayer formation on the metal inside the pore. Then a second metal layer is deposited on the molecular film in the nanopore. It is important that defects and electromigration induced effects are not allowed to dominate electron transfer. A further issue is how a molecule interacts with their nearest neighbour(s) as such an interaction can suppress conformational fluctuations making it difficult to make any direct comparison between the average conductance per molecule in a junction and a single molecule in a junction. Hence, it is critical that we aim to measure single molecular junctions.

1.3 Measuring the conductance of a single molecule

The measurement of the conductance of a single molecule requires certain guidelines and provisions in order that we can be certain about the observations we make. The following list deals with these issues in no particular order. To begin with, we need a recognisable signature to pick out the conductance of an individual molecule from an ensemble of molecules. We must ensure that we can establish proper contact between both ends of the molecule with the electrodes (in a two terminal device). We must make each measurement of a single molecule as similar to any

other single molecule measurement to give reproducibility between experiments, hence making for reliable comparisons. Currently there are only a couple of techniques which can fulfill all these criteria. They are the scanning probe techniques of STM, AFM, along with mechanically controlled breakjunctions[33] of the cantilever type.

STM- Scanning tunnelling microscopy is a unique tool for single molecule studies. It allows the direct visualisation of molecules before and after a conductance measurement, and also to image the electrode surface on which the molecules are attached. CAFM, conducting atomic force microscopy, is related to STM but provides information about the mechanical forces involved at the same time as measuring the molecular conductance. CAFM generally has a lower image resolution than STM, however, STM tips that are used for single molecule measurements can become quite poor due to etching by the thiol groups of the molecule.

In an STM or AFM experiment the molecules of interest are firstly adsorbed onto the substrate. This is normally gold, due to its high affinity towards the thiol group, but could, theoretically, be any other conductive material. The molecular adlayer can be relatively well defined, however, the tip-molecule-substrate arrangement is generally less well defined during an actual measurement, due to the variability in adsorption geometries on the tip (which generally has a non-crystalline structure). Essentially three STM based approaches have been developed.

1.3.1 STM-Breakjunction technique

The STM breakjunction method was introduced by NJ Tao[14] in 2003 and it involves the repeated mechanical contact between an STM tip and a metal substrate. The tip is first moved into mechanical contact with a dithiol covered surface (experiments are generally performed in a solution of the compound). Once contact has been established the tip is withdrawn, ultimately forming an atomic chain of metal atoms. When this chain cleaves a gap is left into which a dithiol molecule can bind, creating a metal-molecule-metal junction. During the initial stages of breaking tip contact with the substrate, the measured conductance decreases in a stepwise fashion, each step corresponding to an integer number of the conductance quantum $G_0 = 2e^2/h$. After the atomic chain has broken, by pulling further on the tip an extra sequence of steps at a lower conductance is apparent in the presence of molecules (figure 1.4). The conductance steps are due to the formation of stable molecular junctions, and a histogram analysis reveals the value of the lowest, single molecule junction.

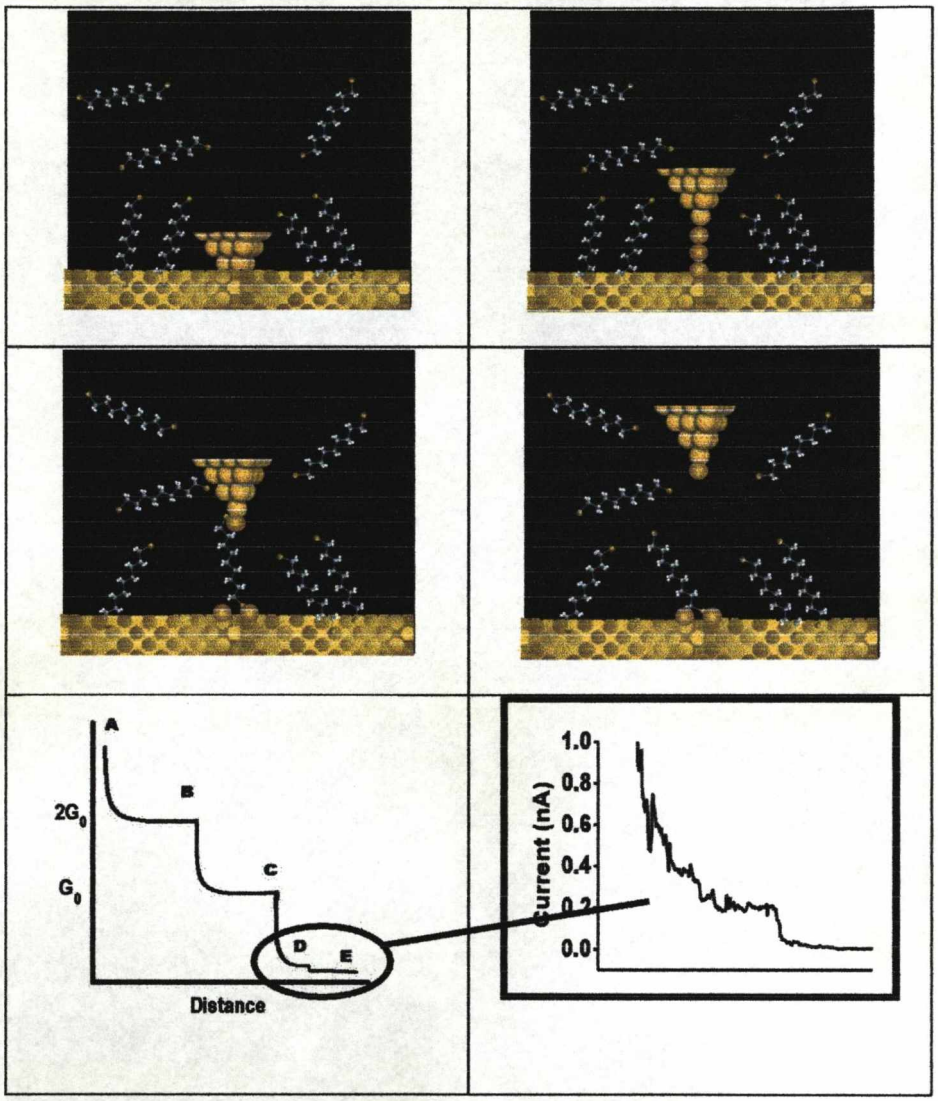

Figure 1.4. An illustration of the steps in the breakjunction technique and the corresponding features in the current-distance traces.

1.3.2 I(s) technique[15]

The approach developed in Liverpool, and mainly adopted in this thesis. It employs a similar experimental set-up as the breakjunction method, however, rather than making mechanical contact between the gold tip and the gold atoms in the surface, the tip is positioned at a defined distance from the surface whilst maintaining a constant *x-y* position. From this initial position, which is close enough for molecules to bridge the gap spontaneously, the tip is withdrawn until such a distance that cleavage of the metal-molecule-metal bridge is complete.

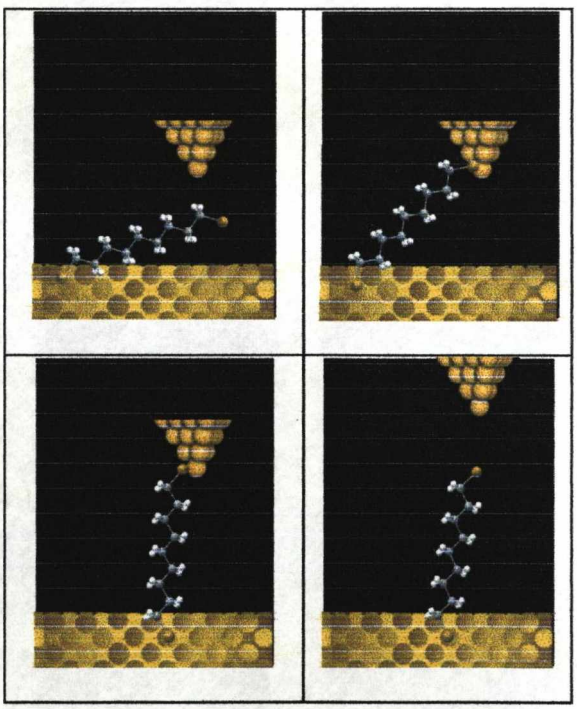

Figure 1.5. An illustration of the different steps in an I(s) measurement.

Two distinctive classes of $I(s)$ scans are observed when performing the experiment. One is a fast exponential decay which is typical of tunnelling between a tip and a bare metal (curve 1 in Figure 1.6). The other is a less abrupt decay followed by a characteristic current plateau (I_W) (curve 2 in Figure 1.6).

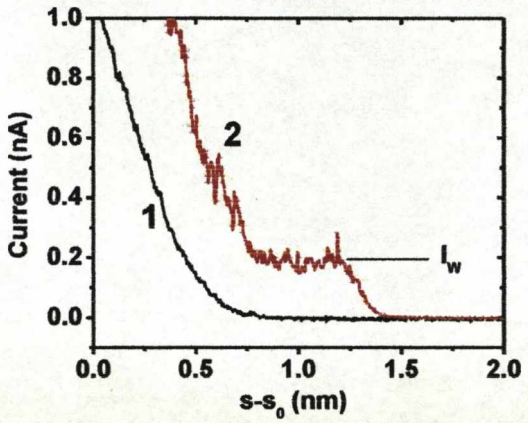

Figure 1.6. Current decay curves ($I(s)$ scans). (1) Baseline for a clean Au surface. (2) for the dithiol compound $6Th_56$ on Au(111).

The experiment is repeated many times, and the results are analysed statistically. The data points in I(s) scans containing molecular plateaus are finally added together into one histogram, which gives peaks at the values characteristic of the average plateau positions in the measurements.

1.3.3 I(t) technique

The I(t) techniques is another way to measure the electrical conductivity of single molecules and is also based on trapping molecules between an STM tip and a substrate. The spontaneous attachment and detachment molecular wires in the time domain are measured in this way. The measurements are performed by placing the tip at different locations on the substrate surface at a distance determined by the tunnelling parameters. After positioning the tip, the feedback loop is disabled and the current is monitored over a fixed period of time. When molecules in a low coverage monolayer spontaneously attach and detach between the tip and the surface a sudden and abrupt change in the tunnelling current is observed. The low coverage conditions are necessary to obtain single molecule events. The difference between the current before the jump and after the jump is attributed to the current which passes through a single molecule (when a statistical analysis is performed).

1.3.4 Matrix Isolation technique[34]

Another scanning probe approach to forming single molecule junctions involves the use of a self assembled monolayer (SAM) of an insulating matrix, usually alkanethiols, into which a relatively small number of dithiol

molecules are inserted (generally 1:1000). This is achieved by having a dilute solution of the dithiol compound in the presence of a more concentrated amount of monothiol. In this way when the SAM is formed, by immersing the gold substrate in the thiol containing solution, the concentration of dithiols is low enough to have isolated dithiol molecules embedded in the insulating matrix of monothiols. Once the surface has been passivated by the SAM the surface is exposed to another solution containing gold nanoparticles. The nanoparticles can then adsorb to the vacant thiol groups of the dithiol molecules which lie at the top of the SAM (which is upright standing). The nanoparticles can be imaged using STM or AFM. This subsequently allows the positioning of the tip directly above a given particle. Once situated above the nanoparticle (and molecule) the tip is pressed onto the particle (or moved into close proximity) completing the circuit and allowing a current to be measured. The current depends, therefore, on the molecule connecting the nanoparticle to the surface as it generally has significantly the largest resistance.

All three techniques have, until recently, yielded differing values of conductance for identical molecules. Indeed, the breakjunction technique has shown multiple sets of conductance values within a single set of data. This technique often gives higher values of conductance than the I(s) approach, which may reflect a difference in the way the molecules are

connected to the electrodes in the different techniques. However, it does appear that the longer the molecule is the better the two techniques agree. Interestingly, the matrix isolation method has also shown different conductance values, agreeing both with the breakjunction and the I(s) values. The nature of thiol bonding to a nanoparticle was little understood until recent x-ray crystallographic structures were obtained[35] which shed light on the true nature of the interaction. More recently, it has been shown that the two STM based techniques, breakjunction and I(s), can yield similar results but these depend strongly on the chosen experimental parameters.[36]

1.4 An introduction to STM

Scanning tunnelling microscopy is one of the most powerful tools for the examination of surfaces, and the research and development of its many applications is still making rapid progress. The physical concepts used in the instrumentation of STM are simple. Indeed, the quantum mechanical principles have been known for a long time. Yet the interpretation of the STM results can be very complicated, due to the convolution of several interactions that take place during the measurement process. This is true not only for STM imaging, but also for STM spectroscopy. As the STM has only been used for a very short time to measure single molecule

conductance (since 2003) the issues surrounding these complications are not yet fully understood. However, if we look at the problems encountered in STM imaging then we may be able to draw some parallels. One cause of artefact or error during surface imaging could also cause unexpected results during single molecule spectroscopy.

1.4.1 The main principles of STM

During the real-space visualisation of an atomic scale surface it is either the spatial variation of the tunnelling current which is converted into an image, or the spatial variation of the tip height. The tunnelling current decreases exponentially with the increasing tip-sample distance and at any given location of the tip over the sample, the electron transfer involves only one or a few atoms at the tip apex, and at the closest point on the surface. This makes the tip-sample separation one of the most important factors controlling electron transfer between the two electrodes. There can be different processes of electron transfer occuring depending on the distance between tip and surface or the energetic barrier of the intervening medium. The theoretical studies of Ciraci[37] show that as the tip-sample separation decreases, the electron transfer changes from the conventional tunnelling regime to the electronic contact regime and then to the mechanical contact regime where the metallic wavefunctions of atoms in the surface and on

the tip apex begin to interact strongly. This may have implications when considering the conduction behaviour of short molecules (<1nm) or long molecules (>3nm).

1.4.2 The conventional electron tunnelling regime

The electron transfer process in metallic tip – insulator – metal systems is classified into three mechanisms on the basis of the current vs voltage (I\V) relationship. In tunnel emission, when the applied voltage (V) is much less than the effective barrier height (Φ) of the insulator ($V << \Phi/e$), the current is proportional to the applied voltage ($I \propto V$). In field emission, with $V >> \Phi/e$, the I\V dependence is given by the equation

$$I \propto V^2 \exp(-\text{const}/V).$$[38]

In Schottky emission, where the potential barrier is low and $V >> k_BT/e$), the current is proportional to $\exp(\text{const}/V^{1/2})$. In the topographiner (the predecessor of the STM), which employs the field emission phenomenon, the tip-sample separation is around 100 nm. In the electron tunnel regime, the tip-sample separation is much less, generally 0.5 – 1 nm and the I\V dependence is linear.[39]

In the tunnel regime the tip and the sample can be regarded as separate and independent entities and the electron transfer between them can be described by the perturbation approach, using the wavefunctions of the free electrons. Representing the tip by an atom with a single s-orbital and assuming a small bias voltage between tip and sample, Tersoff and Hamman showed that on the basis of the perturbation approach the spatial variation in the tunnelling current can be described by the partial electron density distribution $\rho(r, E_F)$ of the sample as $I_{tun} \propto \rho(r, E_F)$. The partial electron density is associated with the energy levels lying in the vicinity of the Fermi level E_F. The evaluation of this density distribution at the tip-sample distance of r_0 (from the sample surface) gives rise to the partial density plot $\rho(r, E_F)$, which simulates the observed STM image.

1.4.3 Electronic and Mechanical Contact Regimes

When the tip-sample separation is lowered below a certain distance, the overlap of the tip and the sample's wavefunctions increases such that the potential barrier between the electrodes is gradually lowered. This causes rearrangement of both their electron density distributions and introduces short range attractive forces (adhesion) and displacement of atoms in the tip and in the sample. The local electronic and structural modifications are significant but they are reversible. Furthermore, the transport of the current

takes place via a tunnelling mechanism that is substantially modified compared to larger separations.

As the tip-sample distance decreases, direct contact begins with a quantum dot contact, for which the diameter of the contact area is smaller than the mean free path of an electron. In this regime electron transport occurs in the absence of any barrier (i.e. ballistic transport with phase coherence). On further shortening the gap resistance R_{gap} reaches the limiting value of the quantum (or Sharvin) resistance (i.e. $4\pi^2e/h^2 = 13\ k\Omega$). Below this value of R_{gap} ohmic conductance is observed (and the I\V dependence is linear).

1.4.4 STM in different environments

The considerations above apply to the situation of ultrahigh vacuum (UHV) STM, for which it was originally designed. However, it became clear that the equipment for STM could also be used in ambient conditions, under liquid for example, in an electrochemical environment or simply in air. The main difference between UHV-STM and ambient STM is the barrier height for electron tunnelling. The I\V dependence found for ambient condition STM is consistent with Schottky emission,[40] which suggests that the electron transfer is facilitated by much lower barrier pathways. This is believed to result from the contamination layer present between the tip and the surface which includes water, plus oxides or other compounds present in the atmosphere (for oxidisible surfaces). The low

barrier heights may originate for localised intermediate states present in the tip-sample gap.

1.4.5 The operating principles and main components of an STM

Common parts of a scanning tunnelling microscope include the piezoceramic scanner, on which the moving element is mounted, and the coarse mechanism by which the tip and the sample are brought close together so that the probing interaction can be measured using a detector. The detector signal is used for feedback control to adjust the tip-sample distance during the scanning.

1.4.5.1 Scanner

In the STM the movement of the tip is performed by a piezoceramic actuator, which can change its dimensions under an applied voltage. In a hollow tube scanner the tip can move in all three mutually perpendicular directions. The outside surface of the tube is separated into four longitudinal segments, on which four electrodes are attached. An additional electrode is placed on the inside of the tube. The application of different voltages to each pair of oppositely located outer electrodes induces a tube

bending, which provides the lateral movement for the tip attached to the tube. Application of voltages to the inner and outer electrodes shrinks or extends the tube, which causes the tip to move in the vertical direction. In some STM setups the piezo operates the sample, and the tip's position is fixed. Our apparatus operates with (calibrated) piezomechanical co-efficients in the 10-20 Å/V range, which allows the movement of the tip with sub-angstrom precision.

1.4.5.2 The electronic feedback

The strength of the local probing interaction (i.e. tunnelling current) between the tip and the sample is only measurable when the tip is positioned close enough to the sample surface. This distance, which is in the range 0.5 – 2 nm, is controlled by an electronic feedback loop. Initially the tip and sample are brought close to one another using high-precision screws incorporated in the microscope stage. Using optical procedures it is possible to bring the tip to within a few micrometers of the sample surface. After this, closer approach is performed with a stepper motor, which closes the gap until control can be taken over by the scanner (i.e. to the tunnelling distance).

If the outgoing signal of a system is inserted back into the system this is called feedback. If this reinserted signal has a different sign compared to the original input signal this is called negative feedback. Two circuits are

used in our system, and most others, which are a proportional circuit and an integral circuit. A P-controller is a (non-inverting) amplifier inserted in a negative feedback loop. In a STM feedback loop the following will happen. Whenever the tip is within tunnelling range of the surface a tunnel current will flow. This tunnel current is amplified and converted into a voltage, V to be compared to a reference voltage, Vr. If the tip is not at the right height, or the right current is not flowing, there will be a non-zero error-signal:

$$e(t) = Vr - V(t) \neq 0$$

This error signal is used to generate the new position of the tip above the sample. Due to the inertia of the piezo electric crystal, there is some time delay in the feedback loop, which means that a high proportional gain would give a relatively fast approach of the reference position, while a low gain would give a relatively slow approach. However, if the proportional gain is set too high, the system will be corrected too quickly and by too much. This will cause the system to oscillate around the reference position, which means also that the tip height will oscillate and potentially it can crash into the sample surface.

The integrator circuit makes a sum of all error signals from the moment the feedback loop is switched on. The integrator acts as a "memory" of what

has happened to the system at earlier times. This memory helps to eliminate the steady state error.

The feedback mechanism can be operated in one of two ways. In one method the tip maintains a constant height above the surface, and thus the tunnelling current is modified so as to account for regions of higher or lower transmission (protusions, adatoms, surface vacancies or surface adsorbates). This method is perhaps only suitable for very smooth samples where the risk of crashing the tip is minimal. The other method of operation is to keep the tunnelling current (I_{set}, setpoint current) constant and to vary the tip-sample distance. Because the risk of a tip crash is eminent especially when the surface is very rough and / or covered with a layer of organic material, the "constant current mode" is generally used for, or in between, most STM single molecule measurements. For constant current mode a voltage is applied to the piezo electric crystal such that the distance between the tip and the sample is modulated. The speed of the response of the feedback loop is varied by changing the integral and the proportional gain settings.

1.4.5.3 STM tips and Current Detection

In STM, the ideal tip should have a monoatomically sharp apex and be symmetric. This applies not just to STM in general, but to single molecule studies too. If the tip geometry was always defined in this manner, then the

number of binding geometries of a molecule to the tip and the surface could be quite few. This would, in theory, make single molecule experiments highly reproducible as molecules would be limited to the number of ways of bridging the tip-substrate gap. Tips of high quality can be prepared and characterised by means of field-ion microscopy.[41] However, most laboratories do not have access to such facilities and it is more practical to use tips prepared from a metallic wire (gold, tungsten, Pt/Ir, Rh/Ir) by mechanically cutting or by electrochemical etching.[42] In this way, though, the tip apex is poorly defined and can change during scanning. In fact, during single molecule conductance measurements, where molecular bridges are made and broken repeatedly, there is little reason to beginning with ideal tip geometry as the tip is likely to become non-ideal during the course of the measurements. Although the outermost atom, or few atoms, of the tip are expected to participate in electron tunnelling, experimental images and single molecule conductance measurements can exhibit variations and artefacts caused by the non-ideal tip geometry.

For ambient-condition STM, gold and Pt/Ir tips are used in preference to tungsten as tungsten tips oxidise easily in air.[43] Tungsten tips are most commonly used in UHV STM, where oxidation is much less likely to take place. Gold tips are, however, favourable to the study of single molecules due to the strong affinity of sulphur to gold. For these reasons Pt/Ir, Ni and

Ag tips are less common. Silver in particular has little affinity towards thiols. Nickel has a strong affinity for thiols, but oxides easily in air.

For studies on atomically flat samples the results are only slightly improved when using an electrochemically etched tip over a mechanically cut tip, as on the sub-micron scales both types of tip have poorly defined and complex apex profiles.[44]

1.4.5.4 Bias voltage

The bias voltage V_{bias} determines which levels of the sample electronic states will participate during the tip-sample electron transfer interaction. Values of V_{bias} are generally in the range 0.001 to 5 V, whilst bias voltages are kept below about 1V for single molecule studies due to the instability of metal-molecule bond above this voltage. In most STMs electrons flow from the tip to the sample when the bias voltage is positive, but, from the sample to the tip when the bias voltage is negative. Thus, at positive voltages the tip-sample electron transfer process involves the lowest unoccupied levels of the sample and the highest occupied levels of the tip. At negative voltages it is the reverse situation and electron transfer involves the lowest unoccupied levels of the tip and the highest occupied levels of the sample (with the tip grounded).

1.4.5.5 Scanning Tunnelling Spectroscopy

Scanning Tunnelling Spectroscopy (STS) is the study of the tunnelling current as a function of the tip-sample bias at a constant tip-sample separation. During some types of STS the feedback loop is switch off, and in general this analysis requires very stable conditions (low drift, low noise etc). The purpose of STS is to examine the bias dependence of the tunnelling current, which can lead to information about the electronic structure of the material between the tip and the substrate. STS of a surface can be conducted in several different ways, one of which is to take repeated images (one after the other) at different bias voltages and to examine the changes in the topography of the images. The tip-sample bias can also be changed on a line-by-line basis during a single scan. This method creates two interleaved images at different biases. Another way of performing spectroscopy is to do single point spectroscopy. In this method the 'sample-and-hold' circuit freezes the voltage applied to the z piezo, which freezes the tip-sample distance, at the desired location allowing I-V measurements without the feedback system responding.[45] The tip-sample bias is swept between the specified values, and the tunneling current is recorded. After the spectra acquisition, the tip-sample bias is returned to the scanning value, and the scan resumes. This method can be performed on single molecules by imaging the surface first and then placing the tip over an individual, generally isolated, molecule. In this method, however,

there is always an asymmetry in the junction as the molecule is adsorbed to the surface, but not to the tip, thus keeping a tunnelling barrier in the junction. This is less of a problem under UHV conditions, where contaminant compounds are less likely, than under ambient conditions where contaminant, or solvent, molecules could interfere with the spectroscopy.

In terms of scanning tunnelling spectroscopy on single molecules studied under non-UHV conditions it is preferable to have the molecule adsorbed to both electrodes, so that the tunnelling pathway is only through the molecule, reducing, but not ruling out, effects of contaminant molecules. STS performed on molecules using the I(s) methods is therefore the optimal way to measure the I\V behavior of single molecules.

The shape of the tip is of critical importance for the reliability of STS information. The tip density of states always affects information obtained by STS since the spectra are a convolution of the electronic structure of the tip and the sample. In order to obtain an atomic-resolution topographic image, the tip needs to be very sharp. Unfortunately, atomically sharp tips can have prominent, non-uniform electronic structure and produce very unreliable spectroscopy. Very blunt tips with poor spatial resolution are, however, more likely to produce reliable spectroscopy.

It is well known that the shape of the probe-tip apex can dramatically influence the appearance of STM images; on the atomic scale, individual corrugation maxima may be elongated in a particular direction by an

asymmetric tip, or effects of multiple tips can distort and complicate the images. Similarly, the electronic properties of a probe-tip can influence spectroscopic measurements, leading to apparent band gaps or voltage offsets around zero volts, or in worse cases to distinct features in the spectrum. Such effects were fully appreciated in early examples of STS measurements and efforts were made to clean the tips to ensure good metallic character. Enough spectroscopy data were collected using different tips and samples so that individual spurious results could be discarded. It is for this reason that it is necessary to record many single molecule conductance events, and to produce a histogram of such events, in order to lessen the impact of unwanted, spurious, data. Also, however, it is important to take the average of many single events precisely because two events are rarely identical.

Usually I/V curves of samples measured in ambient conditions have limited use because of the poorly defined experimental conditions. Nevertheless, it is important to study the behaviour of samples under different experimental conditions as the information gathered could highlight important differences in the response of a sample to its environment – an important issue especially for molecular electronics. That said, in single molecule studies where the molecules form chemical bonds between the tip and the surface tunnelling is presumed to carry out only through the bonds of the intervening molecule. This could prove to the

advantage of molecular electronics as environmental contaminants could play less of a role than when the molecule is only adsorbed on the surface. The different types of I/V curve that are generally obtained using STS are shown in figure 1.7. Metals show linear I/V spectra, defect free semi-conductors show, generally, a linear regime at low bias, followed by a change in the slope at larger biases. P-type semi-conductors will show rectification, with a larger current flowing at positive bias. N-type semiconductors also show rectification, but with a larger current flowing at negative biases.

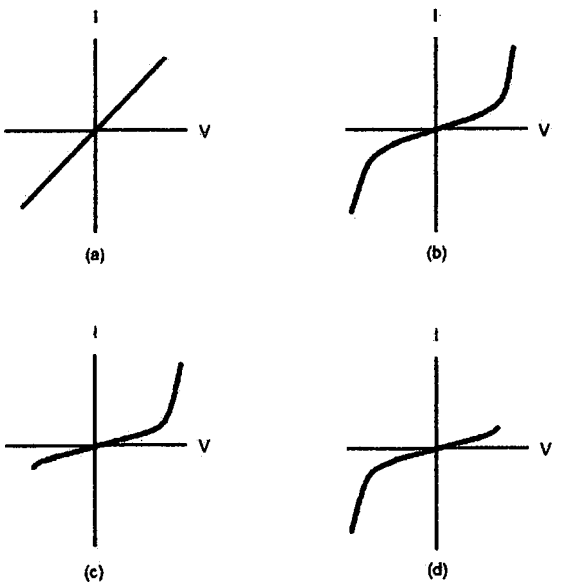

Figure 1.7. Schematic representation of the I/V curves expected for (a) metals; (b) defect free semi-conductors; (c) p-type semi-conductors; (d) n-type semiconductors.

These can be referred to when performing spectroscopy on single molecules to see if the molecules can fit into one of these categories, or perhaps a different category. Another type of I/V behaviour seen for certain semi-conductor heterojunctions, and for some molecules, is known as negative differential resistance (NDR) where at some particular bias the slope of the curve becomes negative (fig. 1.8). This translates to a fall in the current as the bias is increased, corresponding to the process whereby an energy level in the junction is moved out of alignment with the metal Fermi levels, generating a lower transmission probability.

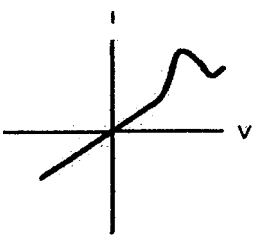

Figure 1.8. Schematic representation of an NDR effect in an I/V curve.

1.4.6 Forces in STM

An understanding of tip-sample interactions is essential in STM because the tip is placed very close to the sample surface. When two surfaces are brought into close proximity, forces of various origins appear as a result of

physical and chemical interactions. At subnanometer separation, forces of chemical origin can result in the formation and rupture of chemical bonds. These strong forces decay exponentially so that above one nanometer (in UHV) only electrostatic forces due to contact potential differences, or induced by charges and electrical dipoles from adsorbates, step edges, etc., and the weaker van der Waals forces remain.[46]

A calculation for the interaction force between two atoms using the Lennard-Jones potential (which describes the attractive, dispersive, force at large distances, and the short range repulsive electrostatic forces) shows that around a separation distance of 0.4 nm between the two atoms, a small attractive force is seen. When the separation distance becomes even smaller the repulsive force increases steeply. The Lennard-Jones potential is an approximation, however, its physical origin is related to the Pauli principle: when the electronic clouds surrounding the atoms start to overlap, the energy of the system increases abruptly.

According to Lifshitz theory,[47] the van der Waals forces are considered as dispersion forces associated with the electromagnetic fluctuations. The magnitude of the van der Waals (VDW) forces for the model metal/metal tip-sample systems relevant to STM (and AFM) are estimated to be in the 1 – 20 nN range (for a distance of 1 nm and tip curvature radius of 100 nm).[46] If the tip is brought much closer then the forces can increase significantly by orders of magnitude. The relevance of this for single molecule studies using STM is that these forces can cause deformation to

the sample surface atoms and also to the molecule being studied. Any type of sample deformation will modify the density of states in the locality of the force interactions. This may make comparison between long and short molecules complicated by the different forces experienced at different tip-sample separations. Indeed, the presence of a molecule in the tip-sample gap will likely induce different local forces, not apparent in the absence of a molecule. These forces would act to modify somewhat the atomic positions in the tip apex and on the surface. This has implications also for theoretical modeling and understanding of these systems, where, as of yet, dispersion or van der Waals forces are neglected and only well defined surfaces are considered.

When the STM tip and sample are immersed in an electrolyte solution, they are subject to a force not predicted by Lifshitz theory. This is due to ions of opposite charge which assemble near the tip and the sample to form double layers.[48] Both repulsive and attractive forces can develop when the two double layers begin to overlap. For two planar surfaces immersed in an electrolyte and separated by a distance D larger than the Debye length (the characteristic length of repulsion associated with the medium), the electrostatic repulsive forces between the double layers varies exponentially as exp(-D/L). This leads to overall attractive forces at distance lower than about 3 nm.[49] Immersion of the tip in a highly polar solvent, like water or ethanol, is found to reduce the VDW forces, at small tip-sample distances, by up to two orders of magnitude with respect to the

vacuum.[50] It is important to realise that in water (and therefore in air) many surfaces are charged. This surface charging comes about from the dissociation of surface groups (e.g. thiols and carboxylic acids dissociating into thiolates, carboxylates and protons) increasing the ion concentration in the vicinity of the sample. The theoretical analysis by Butt[51] shows that the electrostatic force between the tip and the sample is repulsive, increases with surface charge density, and decreases roughly exponentially with distance. To bring the tip into close contact with the surface, the external applied force should exceed this electrostatic repulsion. In terms of imaging this means that if the forces are not overcome, then what is actually imaged is the surface charge distribution rather that the surface topography.

In terms of single molecule conductance, these considerations raise important issues about the necessary precautions to make reliable and comparable measurements. Care should be taken in making assumptions about the absolute distance between the tip and sample, especially at short tip-sample distances, when calibrating the absolute set point distance. If short molecules are measured (i.e. < 1nm), the forces acting on the tip and the sample may be different than when measuring longer molecules in the 2 – 3 nm range.

1.4.7 Optimising the conditions of STM experiments

Careful consideration is needed over the experiment conditions involved in STM single molecule measurements in order to understand properly the reasons for the behaviour seen. For example, the choice of tip-sample bias is not crucial for metallic samples, but is crucial when investigating semi-conducting samples. Metals should have the same conductance regardless of the sample bias, as the electron transport is always between the occupied states and the unoccupied states across a single barrier (under UHV conditions). Semi-conductors, on the other hand, have a band-gap, which means that a certain bias threshold must be reached before significant overlap of occupied states and unoccupied states allows any significant current to flow. A similar situation exists in molecules due to the gap between their highest occupied molecular orbital (HOMO) and lowest unoccupied molecular orbital (LUMO) – H/L gap. Thus, depending on the magnitude of the bias used to probe a single molecule, the alignment between metal Fermi levels and molecule levels can be different, which can lead to a different conductance at different biases.

To minimise the tip-sample force interaction in the imaging of metallic samples, a scan is normally carried out with a high gap resistance, R_{gap} (by using a low set-point current below about 1 nA, and a high bias voltage roughly around 0.6 to 1.0 V). Scanning under these conditions is likely to produce an image with relatively low signal to noise ratio at the expense,

perhaps, of some resolution. Decreasing the gap resistance, which effectively reduces the tip-sample distance, can then lead to better resolved images, but may also lead to image distortion as the tip-sample force increases, and may even lead to surface etching due to larger electric fields. In terms of single molecule conductance measurements the size of the molecule determines the initial tip-sample separation, and hence gap resistance. Thus, for quite long molecules a high gap resistance can be used causing minimal tip-sample forces. On the contrary, short molecules (those less than 1 nm in length) require lower gap resistances in order for them to bridge the tip-sample gap. It is therefore possible that the local environment about a shorter molecule is different than for a longer molecule during an actual conductance measurement. A change in the local environment of atoms in the tip and surface could strongly affect, amongst other parameters, the local density of states which, in turn affect the transport properties of the junction.

1.5 Eletronic measurements on single molecules with metal electrodes

1.5.1 The quantum point contact

Compared to electrochemical and optically induced electron transfer, the proecess of transferring an electron, or passing a current of electrons, from one metal electrode to another via a single molecule coupled to both, differs in some important ways. The behaviour of electron transfer through a molecule is determined purely be quantum mechanical phenomena. Below length scales of roughly 40 nm, the typical mean free path of an electron in copper at room temperature, the concept of resistivity no longer applies. It is understood that the resistance of a single quantum channel is given by the Landauer-Büttiker, equation 1[52];

$$R = 2e^2/h \,.\, (1\text{-}T)/T \quad (1)$$

Here, the first term is the quantum resistance (13 kΩ = 77.4 μS) and T is the transmission coefficient through the gap. For single chains of metallic atoms with one conductance channel, the resistance is found to be quantized in units of $2e^2/h$.[53] Indeed, it has been demonstrated

theoretically that the quantum resistance is also related to the valency of the atoms involved,[54] implying that if the channel consists of multiple bonds from one end to the other, then the I\V behaviour in the single atom contact regime cannot be described by a single channel theory.

1.5.2 Tunnelling between two metals in a vacuum – the coherent transport regime

In the typical case of a metal tip brought close to a metal surface in a vacuum, as in UHV STM, the gap between the tip and the surface provides an insulating barrier. When the bias voltage is zero, their Fermi levels are equal (providing the metals are identical) and there is no tunnelling current between them. If, now, a positive potential is applied (with say the sample grounded) then the energy levels of the tip are lowered by eV_{Bias} so that the electrons in the occupied levels of the sample (between e_f and e_f - eV_{Bias}) tunnel into the unoccupied levels of the tip.

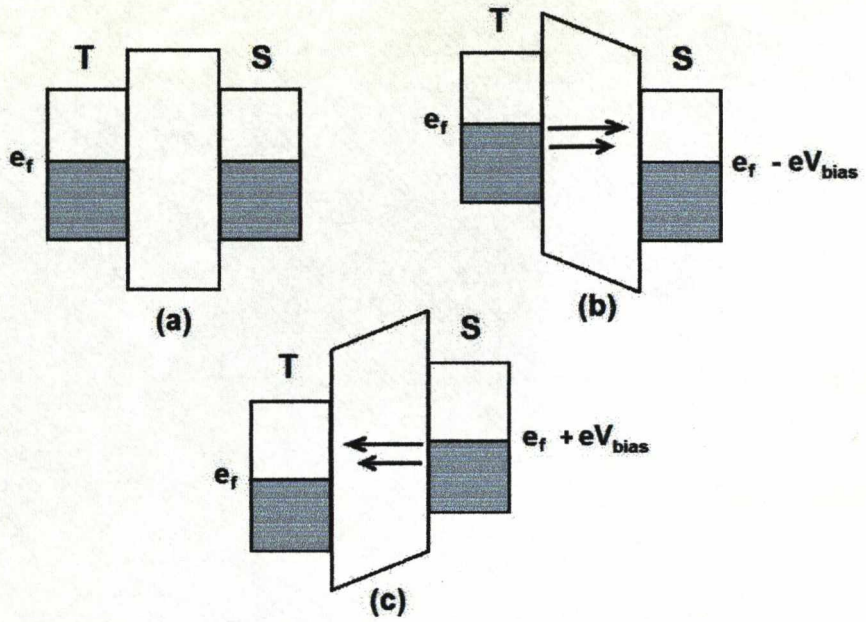

Figure 1.9. Energy bands associated with the metal – insulator – metal junction between a metallic tip and a metallic sample: (a) $V_{Bias} = 0$; (b) $V_{Bias} < 0$; (c) $V_{Bias} > 0$.

When V_{Bias} is negative (with the substrate grounded) the energy levels of the tip are raised by eV_{Bias} so that the electrons in the occupied levels of the tip (between e_f and $e_f + eV_{Bias}$) tunnel into the unoccupied levels of the sample. The transmission probability of tunnelling is largest for the electrons at the Fermi level of the negatively biased electrode and steadily decreases as the energy is lowered from that level (shown by the shorter arrow is figure 1.9). In general, most of the tunnelling electrons come from within 0.3 eV of the Fermi level of the negatively biased electrode.

1.5.3 The strong coupling regime

An essential point to consider when dealing with molecules connected to metals is the degree of mixing that occurs between metal states and molecular states. This hybridisation that occurs strongly alters the characteristics of a molecule as measured in a vacuum environment as charge can be transferred to or from the molecule. The energetics of molecule-metal interfaces are often quite complicated, however the charge transfer can be understood in simple terms of electron affinity differences between the molecule and the metal, and the desire of the system to obtain a lower overall energy. Surface spectroscopy techniques, such as ultraviolet photoelectron spectroscopy (UPS) and x-ray photoelectron spectroscopy, can provide useful information about the energy level alignments at molecule-surface interfaces.[55] STM tunnelling spectroscopy has also been employed to study the electronic states of molecules adsorbed on surfaces. However, the rather unique, and specific, arrangement of a single molecule in a metal junction is very difficult to characterise ex situ, and one cannot easily reproduce the same conditions used to measure the conductance of a molecule whilst performing external spectroscopy.

Thus, the behaviour of molecular junctions in the strong coupling limit is unlikely to be as simple as in the weak coupling regime, and any

theoretical efforts should consider the whole system as one, rather than as isolated components.

1.5.4 Metal-molecule-metal junctions

Consider a molecule weakly coupled to two electrodes. Weak, in this situation, implies that the resistance due to the molecule is large compared with the Landauer resistance (G_0) and thus T<< 1. the simplest picture of electron transfer is that of a one dimensional tunnelling barrier with a potential barrier height V_0 and a width L. The energy of the incident electron is given by equation 2,

$$E = \hbar^2 k^2 / 2m \quad (2)$$

with the wavefunction inside the barrier region changing to $e^{-\kappa x}$, with $\hbar^2 k^2 / 2m = V_0 - E$. The transmission probability through the barrier is approximately proportional to $e^{-\beta L}$, with the decay function β being 2κ. This means that for monoenergetic electrons, the current which passes through the barrier decreases as the barrier thickness increases or the barrier height becomes greater. The rate of decrease β depends on the electron energy as $\beta = 2\sqrt{(2m\varphi/\hbar^2)}$, where φ is the barrier height $V_0 - E$.
In terms of a molecule we consider the barrier to be represented by a single, or set of, molecular orbitals, making φ equal to the difference in

energy between the molecular orbital and the Fermi level of the metal electrodes.

$\varphi = (E_{LUMO} - E)$, for tunnelling through the LUMO.

$\varphi = (E_{HOMO} - E)$, for tunnelling through the HOMO.

The barrier height is affected by changing the bias voltage, which alters the energy of the electrons in the metal contacts.

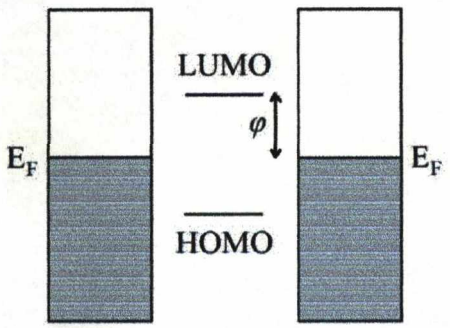

Figure 1.10. Schematic plot of the energy versus distance in a metal-molecule-metal junction.

Changing the bias voltage can give an indication of how close a molecule is to resonance (i.e when $E = E_{LUMO/HOMO}$). In a simple theory certain assumptions can be made about the effect of applying a bias across the molecule junction. If a voltage is applied to the right contact, it changes the electron energy of that contact by V relative to the left contact. We assume

that the molecular charge density is spread uniformly over the molecule, which results in the energy of the LUMO to be V/2 with respect to the contacts. When the molecular orbitals 'line up' with the metal Fermi level, $\varphi = V/2$, and resonant tunnelling occurs. In this model, β goes to zero, and T, the transmission probability can be unity, making the molecular resistance equal to the Landauer resistance. In conditions other that under a strict vacuum and helium temperatures, it is unlikely to achieve these low resistances due to effects such as electron coupling to molecular vibrational modes or environmental broadening of the levels.

In this simple view of the system we neglect the manner in which the molecule is coupled to the electrodes. Two issues arise, however, when making this consideration. First is the type of physical, chemical, contact between molecule and electrode. There is usually a resistance associated with this contact, which is assumed to be a constant. The term describing the contact resistance is the pre-exponential factor A in the equation $T_{mol} = \underline{A}e^{-\beta L}$. It may be related to the strength of chemical bond between binding group and metal electrode, so a strong chemical bond, like the Au-S bond, would imply a low contact resistance. If the molecule contains groups which strongly decouple the frontier orbitals from the electrodes, the tunnelling may or may not actually involve these levels.[56] It remains to be seen whether the electron transfer tunnelling process always involves the lowest energy orbitals, or whether it involves only those orbitals which have density spread across the entire molecule.

1.5.5 Tunnelling through single and double barrier systems

A lot of attention has been focussed, both theoretically and experimentally, on the study of alkanedithiols in single molecule conductance studies. Alkanedithiols, which possess two thiol groups in the α-ω positions of a polymethylene $(CH_2)_n$ chain, are regarded as archetypal single tunnel barrier resistors. They are very useful to study as they are among some of the simplest molecules to model theoretically using the latest computational methods. They are used as test beds to acquire knowledge concerning the fundamental aspects of charge transport in molecular wires, and to allow the comparison of different techniques of measuring single molecules. However, alkanedithiols are not ideal molecular wires due to their relatively low conductivity and lack of functionality. In terms of molecular electronics it is useful to search for molecular devices capable of performing basic electronic functions. Molecules designed to act as molecular wires,[57] switches[15, 58, 59] and diodes[60] have recently been examined theoretically and/or experimentally,[61] and devices have been produced which show rectification[20] and negative differential resistance (NDR)[62] behaviour at the single molecule level. One important type of device architecture in the semi-conductor field is the double tunnel barrier (DTB) junction,[63] shown in figure 1.11. If two single tunnelling barriers are placed a reasonably small distance apart (in the same structure, less

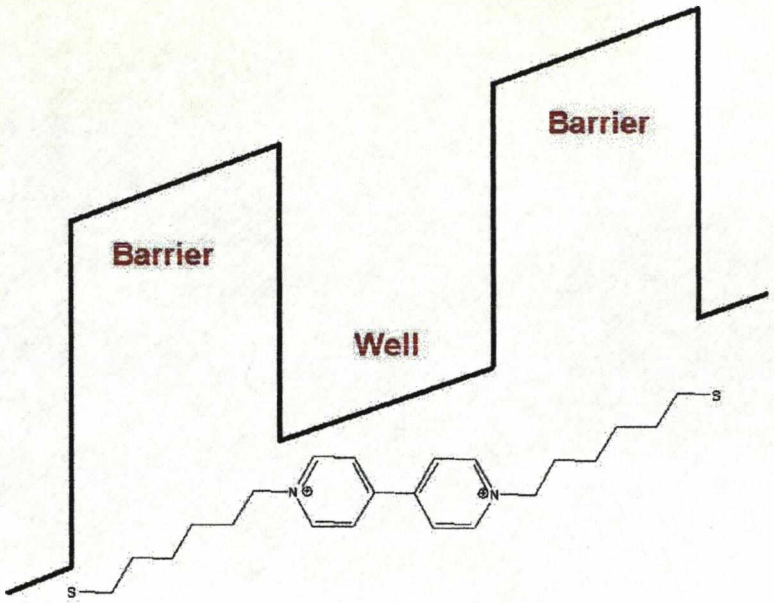

Figure 1.12. A schematic representation of a double barrier with the 6V6 molecule shown below.

Simple tunnelling theories suggest that when the bias applied to a junction aligns the Fermi level of the metal with a molecular orbital of the molecule, resonant tunnelling should be observable in the current–voltage relationship. It remains to be seen, however, if resonant tunnelling is a viable mechanism for electron transfer across single molecules, or whether a 'hopping' mechanism, with level relaxation, (vide infra) is a better description. Resonant tunnelling has not been observed for molecular systems studied so far, most conductivities fall well below G_0. For molecules in an aqueous environment environmental electronic level broadened and relaxation may wash out resonant processes. Molecules may have to be studied in ultra high vacuum conditions for resonant

particle be localised inside the two barriers. This means that the energy of the level between the two barriers must equal that of the energy level from which the particles are injected, the so called resonance energy. In other words, the particle tunnels through the first barrier, appears inside the well and resides there for some period, and finally tunnels out of the well. This is considered a quasi-two step process. At energies away from this value, the tunnelling particle cannot be localised between the barriers, and no resonance occurs. The total transmission becomes proportional to the product of the transmission coefficients through the different regions of the system, and decays exponentially with distance and barrier height.

If a molecule is synthesised which contains a group with an extended pi-system, such as an aromatic ring, chemically placed between two alkanethiol groups, and subsequently contacted to metal electrodes via the thiol groups, then it can be regarded as the single molecule equivalent of DTB junction. The justification is that the frontier orbital energies for the alkyl barriers lie far from the gold Fermi energy (E_F), while the frontier orbitals of the π-system (barrier indentation) are much closer in energy. This is represented in figure 1.12.

Resonant tunnelling involves the transmission of a particle through the two barriers with (notionally) zero resistance, i.e. 100 % transmittance. Resonant tunnelling may be understood, conceptually, by the destructive interference which occurs between the electron waves reflected by the first barrier and, critically, the second barrier. In particle tunnelling there are always two components to a wave; the transmitted part (which passes through the barrier by tunnelling, moving from left to right in the conventional picture), and the reflected part (moving from right to left and not penetrating the barrier). If the dimensions are such in a double tunnel barrier device that the reflected wave from the second barrier, propagating to the left in figure 1.11, can destructively interfere with the reflected wave from the first barrier, also propagating to the left, then the two can cancel each other by destructive interference, specifically a wave phenomenon, making the only wave component seen that of the transmitted wave passing through both barriers. As, in reality, the incident electron comes from only one side of the barrier (due to the bias potential applied across the barriers) the situation is asymmetric, so the transmitted wave is not cancelled by an incident beam from the left of the two barriers. Another process that can happen is constructive interference inside the two barriers as, once inside, the particle can reflect off both the first and the second barrier, interfering constructively with itself and increasing its amplitude inside the well. Both these processes contribute to the increased transmission probability through the two barriers, but they require that the

assumption of a rectangular barrier. In the case of UHV STM, with no matter between the tip and the surface, V_B is simply the vacuum barrier; so for states at the Fermi level, $V_B - E$ is just the workfunction of the metal. The transmission probability, or tunnelling current, decays exponentially with barrier width d as shown in equation 5,

$$I \propto e^{-2\kappa d} \quad (5)$$

1.5.5.2 The double barrier case

The double tunnel barrier is an interesting structure in quantum physics. Intuitively, if two barriers are placed in sequence then one would expect the transmission across both barriers to be less than across just one of the barriers. Classical resistors lined up in series give a total resistance proportional to the sum of the individual resistors (i.e. 1 Ω + 1 Ω = 2 Ω). If two tunnel resistors are 'lined up' in series, one would expect the total transmission to be the product of the two resistors (i.e. $T_1 . T_2 = T^2$, if $T_1 = T_2$). However, the physical size of such double tunnel devices can be close to that of the de Broglie wavelength for the tunnelling electron (approx 0.5 nm), making their electron transport properties subject to the laws of quantum wave mechanics where the phenomenon of resonant tunnelling becomes important in such nanoscale structures.

when approaching a barrier, the wavefunction actually exists on the other side of the barrier – as opposed to simply reflecting off it. If the function, therefore, describes the particle as being on the other side of the barrier, the particle has "tunnelled".

One way of quantifying the proportion of particles that tunnel through the barrier is in terms of the *transmission coefficient*. This is defined as the probability that any single electron incident to a barrier structure will tunnel and contribute to the current flow through the barrier. The transmission coefficient of a wave incident on a simple single barrier can be easily calculated. If we consider weak transmission, common in STM, then the solutions of the Schroedinger equation inside a simple rectangular barrier in one dimension (denoted z) have the form

$$\Psi = e^{-\kappa z} \quad (3)$$

The parameter κ (also β later on) is the electron attenuation factor, where

$$\kappa^2 = 2m(V_B - E)/\hbar^2 \quad (4) \text{ (see Gamow)}$$

Here, m is the electron mass (for electron tunnelling), $\hbar$ is Planck's constant divided by 2π, E is the energy of the state, and V_B is the potential in the barrier. In general, V_B may not be constant across the gap, but it usually adequate to assume the average barrier height so as to maintain the

Quantum well heterojunctions based on doped inorganic semiconductors can now be made on the nanometer scale[65], however, they must be grown layer by layer in ultra pure conditions to avoid contamination which may hinder the devices' performance. We have synthesised and studied organic molecular analogues of these semiconductor devices in the hope of exploring the scope of such materials in semiconductor applications.

1.5.5.1 The single barrier case

In quantum mechanics, quantum tunnelling (or simply tunnelling) is a phenomenon where a particle (for example electrons or hydrogen) violates the principles of classical mechanics by penetrating a potential barrier with higher energy than the kinetic energy of the particle. A barrier, in terms of quantum tunnelling, may be a form of energy state analogous to a "hill" or incline in classical mechanics, which classically suggests that passage through or over such a barrier would be impossible without sufficient kinetic energy. On the quantum scale, objects exhibit wave-like behaviour; in quantum theory, quanta moving against a potential energy "hill" can be described by their wave-function, or, more specifically by a probability amplitude ($\Psi^*\Psi$) which represents the chance of finding a particle in a certain location on either side of the barrier. The wavefunction (vide infra) of a particle decays exponentially through space from its point of origin, so there is a certain probability that

than a few nm) then the system is known as a *double tunnel barrier, DTB,* (or in some cases a quantum well) structure.

Since their invention by Esaki and Tsu in the 1970s, semiconductor quantum wells have evolved from scientific curiosities to a means of probing the fundamentals of quantum mechanics, and more recently into creating many working semiconductor devices, a practical example of which is in a CD player. The laser that reads information of the discs is a quantum well laser which confines electrons by sandwiching materials together. A double tunnel device consists of a semi-conductor, e.g. GaAs, which is confined between two other semi-conductors with a larger band gap, e.g. GaAlAs. The source and drain are connected to opposite barriers.

DTBs have quite different transmission properties to single barriers of equivalent dimensions. DTB junctions can exhibit negative differential resistance (NDR) and resonant tunneling. The two barriers can be either symmetric or asymmetric in terms of both their height and their width. Asymmetric barriers may also behave as diodes and rectifiers[64].

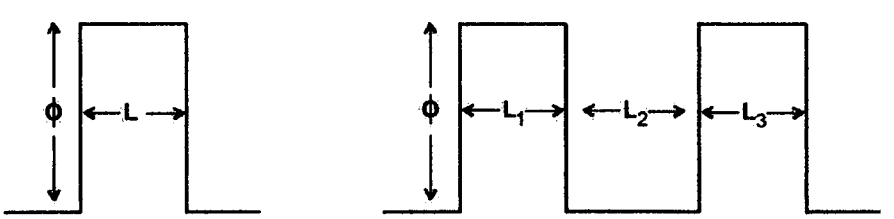

Figure 1.11. Single and double tunnel barrier structures. Φ represents the height of the barrier, whilst L_n are the lengths of the respective barriers.

tunnelling effects to become manifest. For molecules with intermediate levels, an intermediate mechanism such as superexchange, may operate under the Breit-Wigner formalism.

1.5.6 Transport calculations on single molecules

Most transport calculations are based on the Landauer-Büttiker equation (1), with the transmission coefficient, T, calculated from quantum mechanical scattering theory.[66-68] The current at zero bias is generally given by equation 4,

$$I(V) = 2e^2/h \int T(E, V)\left[f(E - eV/2) - f(E + eV/2)\right] \quad (4)$$

where $T(E,V)$ is the transmission function, f is the Fermi function, and V is the voltage. The transmission function is calculated using a Green's function matrix of the coupled system. For small systems, although non-trivial, these elements can be worked out using standard quantum chemical methods. For larger systems, which require a great deal of computational time, the density functional (DFT) methods based on the local density approximation (LDA) and the generalised gradient approximation (GGA) can be employed to approximate core orbitals.[69]

1.5.7 A review of molecules for electronic studies

One of the great aspects of molecular electronics is the almost limitless design of molecules which have been used to try to understand the nature of electron transport in organic systems. Many compounds can be purchased directly for use from suppliers, whilst established organic synthetic procedures allow us to design and build a very large number of molecules with which to test our theories. The next pages will present an overview of some of the main types of molecule that have been studied in the area of single molecule conductance.

1.5.7.1 The test bed – alkanedithiols[14, 34, 36, 70]

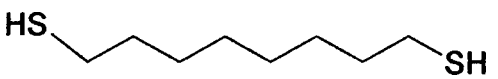

Figure 1.13. Example of an alkanedithiol (octanedithiol – HS-$(CH_2)_8$SH).

Alkanedithiols represent a simple class of compounds with the formula HS-$(CH_2)_n$-SH. These molecules have large gaps between their highest occupied molecular orbitals (HOMO) and their lowest unoccupied molecular orbitals (LUMO). They are considered as poorly conducting wires, and as such are not studied for any potential application, rather as test beds of the experimental techniques and theoretical calculations of

single molecule conductance. Experiment and theory have both determined that the conductance of alkanedithiols decrease exponentially with the number of methylene (CH_2) units and can be described by the formula $G = A\exp(-\beta L)$,[71] where A is a constant (normally assumed to represent the contact resistance between metal and molecule) and β is a decay constant of approximately 1 $Å^{-1}$. The conductance features of exponential length dependence, temperature independence and I/V behaviour suggest that electron transport in these molecules is via non-resonant tunnelling. However, the comparison between absolute conductance values is not particularly straight forward, particularly as some experiments measure an unknown number of molecules. It has now been discovered, also, that even in the same experiment the histogram analysis can reveal two (or more) conductance values of the same compound. The reasons for this are as yet rather unclear, however, the atomistic nature of the contact is considered significant.

The type of contact the molecule makes to the metal can be systematically varied by changing the head groups. Thiols, chosen for their affinity to gold, are often used, however, other groups will bind to gold as well. These include carboxylate ($-COO^-$),[72, 73] amine ($-NH_2$)[72, 74] and isothiocyanate (-NCS).[75]

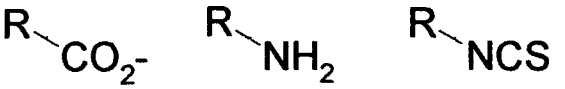

Figure 1.14. Various head groups studied for alkane wires.

Multiple sets of conductance have been seen for each group studied, and this makes it difficult to compare the absolute effect of each group on the conductivity of the wire. For example, the high conductance series reported for alkanediamines is virtually identical to the low conductance series for alkanedithiols.[72] As breakjunction measurements do not allow for atomistic control of the contacts there is no way of finding out whether these series correspond to the same adsorption geometry, or are fortuitous (or unfortunate) coincidences. The ratios observed, however, between the different conductance regimes do differ from group to group. Thiols, which are now known to exhibit at least three different conductance values,[36] have a factor of approximately four between the series. Amines and carboxylates display a factor of ten between series,[72] whilst isothiocyanates show a factor 12.5 between series.[75] The probability of finding high conductance events and low conductance events of alkanedithiols and alkanedisothiocyanate was studied. It was found that the ratio of high to low was 63:37 for the thiols, whilst it was only 34:58 for the isothiocyanates (the remaining 8 % contained both high and low events). The low conductance was therefore ascribed to adsorption on a top site because the low events always follow the high events in the 'pulling' type experiments. The high conductances are thus ascribed to adsorption in a hollow site of gold(111). They found this statistical ratio to be in agreement with theoretical calculations which suggested that for isothiocyanates, adsorption on the top site of a gold(111) is more stable

than in the hollow sites, and hence a larger number of junctions occur with the group in the top site.[76]

Regardless of the type of contact though, all alkane bridges show a lack of temperature dependence of their conductivity when measured using the breakjunction technique.[18] This indicates that charge transfer involves coherent tunnelling rather than sequential hopping. This is, however, in contrast to a temperature effect which has been observed for alkanedithiols using the I(t) technique.[77, 78] Using this technique, molecules form spontaneous bridges with a large degree of conformational freedom. Hence, this effect was interpreted by a change in the population of shorter conformers at elevated temperatures. It is expected that in the breakjunction technique the all-trans conformation dominates due to the stretching of the molecule in the junction, and such an effect would not be expected.

1.5.7.2 Conjugated molecules

As previously stated, saturated alkane chains, although robust compounds, are poor conductors and measuring the conductance over distances greater than 2 nm is practically impossible. For long distance charge transport, molecules with a higher degree of electronic connection between one end and the other are required and conjugated molecules with alternating double and single, or triple and single, bonds are the best candidates.

Conjugation is based on the idea of delocalised bonding across a number of chemical bonds – the simplest conjugated molecule being buta-1,3-diene (H_2C=CH-CH=CH_2). Conjugation usually involves pi-orbitals, but can include d-orbitals and lone pairs of electrons also. These molecules have lower HOMO-LUMO gaps than saturated compounds, and generally levels which are quite close to the gold Fermi level (-5.2 eV relative to the vacuum), which makes them more efficient charge transporters. However, for most short conjugated molecules, electron tunnelling is still the likely conduction mechanism as an offset between energy levels in the molecule and on the metal contacts remains. Also, it is believed that energetic level alignment takes place at the metal-molecule interface in which charge transfer takes place in order to create an energetically more stable system. This modifies the levels of molecules compared to the gaseous state and leads to different HOMO-LUMO gaps and energies.

1.5.7.2.1 Carotinoid polyenes[79]

Systematic studies of the length dependence of the conductance of single conjugated molecules are quite rare. One such example was with carotinoid polyenes with different lengths. The measured β was (0.22 ± 0.04) $Å^{-1}$, which demonstrates that the conductance is less sensitive to length than it is for saturated alkanes.

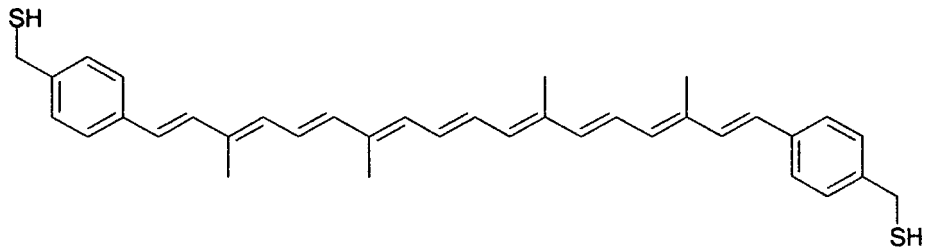

Figure 1.15. 7,7'-Bis(4-thiomethyphenyl)-7,7'-diapocarotene conjugated molecular wire.

The carotinoid compound in figure 1.15, with nine double bonds terminated by benzylthiol groups, contains a total of 28 carbons in its backbone, yet has a resistance comparable to decanedithol, where N = 10 carbons. This demonstrates the long range electron transfer abilities of conjugated molecules.

1.5.7.2.2 Benzenedithiol[80, 81]

One of the simplest conjugated molecules to be studied thus far, however, is benzenedithiol (BDT). This molecule is a benzene ring with thiol groups in the 1,4 (*para*) positions. It has a reported upper, high, conductance of 0.011 G_0 (852 nS) using the STM breakjunction method, which means that only one percent of the potential current can flow through the wire under these conditions. BDT has been studied extensively by several groups, both experimentally and theoretically, in an effort to investigate the conductance of these 'building block' compounds. Depending on the models and approximations used by the different groups, the theoretical values of the

conductance often vary from the experimental values by (at worst) several orders of magnitude. Again, contact geometries, and the strength of the molecule-electrode coupling, have been pointed out as crucial factors to consider when comparing theory with experiment in the case of a short, conjugated molecule. However, the theories are at best only approximations, with limitations due the use of various assumptions of binding site and computational details like the exchange correlation function (the description of the core orbitals).

Also studied has been benzenedimethanethiol (BDMT)[81] shown in figure 1.16.

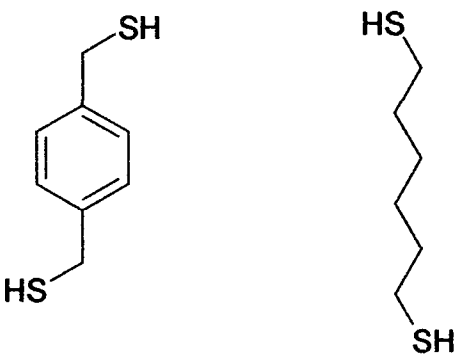

Figure 1.16. Benzenedimethanethiol (left) and hexanedithiol (right).

Both compounds have approximately the same S-S distance (~1 nm) and contain six carbons between the terminal thiol groups, considering only one half of the benzene ring in BDT. Thus their measured conductivities should highlight the differences between conjugated and saturated bonds. Larger conductivities are expected for the conjugated systems due to

electron delocalisation and the low lying pi-system. The largest conductance reported for BDMT is 6 x 10^{-4} G_0 (46.5 nS), whereas HDT has reported conductances of 1 x 10^{-3} G_0 (108 nS) and 2.6 x 10^{-4} G_0 (20 nS), (ref Tao and Wand) high and low values respectively. Intuitively BDMT should be significantly more conductive than HDT if one assumes the rule of thumb about conjugated and saturated bonds, however, this is practically not the case. The β decay factor between BDT and BDMT from the experiment is 1.4 CH_2^{-1}, or 0.82 $Å^{-1}$ (based on the through bond distance). These values are the same as those found in alkanedithiols, so the effective barrier height in these small aromatic compounds must be higher than expected when compared to alkanes of the same length. The barrier heights often measured for alkane monolayers are in the region 1 – 1.5 eV, whereas thermoelectric measurements on single BDT molecules adsorbed between electrodes gives also an effective barrier height of 1.2 eV.[82] These values are much smaller than half the HOMO-LUMO gap (approximately 4 eV) Although the only data on alkane compounds is based on full monolayers, whilst the Seebeck measurements were performed with single molecules, the similar measured effective barrier heights do explain the similar conductance for BDMT and HDT in the single molecule studies (single molecule studies are, however, invariably performed with monolayer coverage of the surface electrode and so may be comparable). This does leave the question of why do alkanedithiols present such low *effective* barriers? The value of 1-1.5 eV seems too low in light of

ultraviolet photoelectron spectroscopy (UPS) experiments that show the HOMO* on the chain atoms to be about 5 eV away from the Fermi level for an octadecanethiol monolayer on Au.[83, 84] It seems not to make sense to view the ET mechanism as pure tunnelling through a single, as the Simmons model describes. Such a barrier does not adequately describe the situation for an organic molecule chemically bound between two electrodes. Instead of a single energy level, a density of states arises in the molecular junction as a result of the mixing of molecular orbitals and metal electrodes.[85, 86] Therefore, the interpretation of the equations describing a square barrier[87] cannot be implemented, and rather the measured barrier height should be thought of only as the overall *effective* barrier to transport. The effective barrier is smaller than would be predicted due to the in-gap DOS that results from coupling of the molecule to the electrodes.

Still, however, one would expect that for conjugated molecules, the electronic coupling, and by extension the effective barrier height, should be such that, length for length, the conjugated system is more conductive than the non-conjugated system. The measured similarity remains a mystery.

1.5.7.2.3 Effect of conjugation extent in diaminoarenes[88]

For aromatic containing compounds it has been shown that the conductance correlates well with the molecular redox potentials.[89] In the series of diamine compounds 1,4-diaminobenzene, 1,4-diaminonapthalene

and 9,10-diaminoanthracene, the conductance increases with the number of benzene rings.

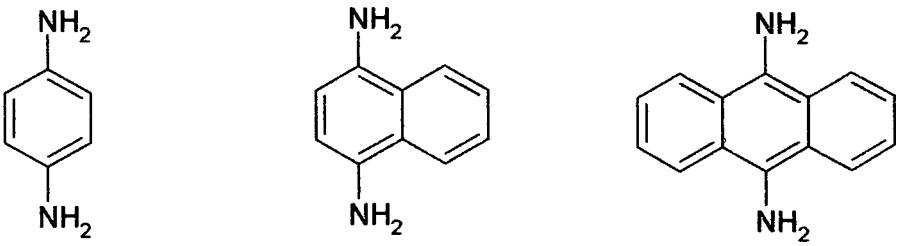

Figure 1.17. Aminobenzene derivatives with different degrees of conjugation.

In this case the distance between the two amino groups remains constant, however, the conductance decreases with the number of rings if the benzene rings are coupled by single bonds, as in the series 1,4-diaminobenzene, 1,8-diaminobiphenyl, and 1,12-diaminoterphenyl. This can be explained by the less significant increase in conjugation in this series which is primarily caused by the existence of a twist between the rings lessening the overlap of the pi-orbitals. The conductance also decreases with the number of carbons for the series 1,4-diaminobenzene, 2,6-diaminonaphthalene and 2,7-diaminoanthracene. This shows that tunnelling, or superexchange, are the likely conductance mechanisms and highlights the interplay between the barrier height (determined usually by the HOMO or the LUMO energy) and the distance over which tunnelling takes place.

1.5.7.2.4 Bis-9,10-phenyl-ethynylanthracene derivatives[90]

A way of decoupling a conjugated aromatic molecule from the electrodes was demonstrated by varying the position of the thiol anchor groups on a molecular rod. The two rods studied consisted of a bis-9,10-phenyl-ethynylanthracene core and acetyl protected thiol anchor groups in the *meta* and *para* positions respectively.

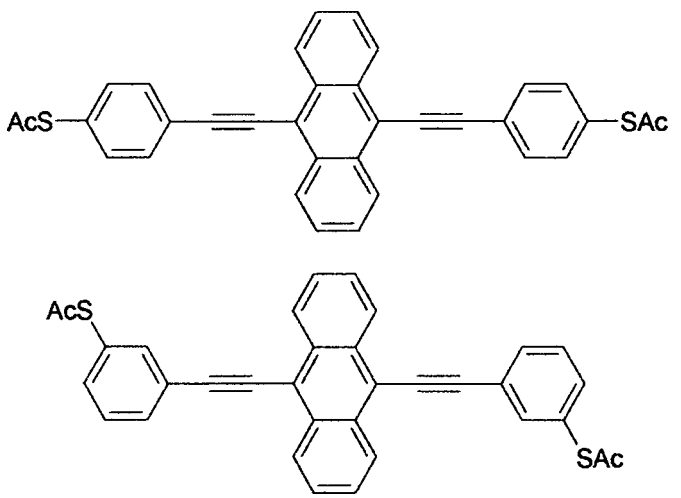

Figure 1.18. *Para* (top) and *meta* (bottom) derivatives of a bis-9,10-phenyl-ethynylanthracene core molecular wire.

The reduced conjugation extent when the thiol groups are in the *meta* position reduced the electronic coupling to the electrodes (double bonds can be moved across the whole of the *para* compound which is not the case for the *meta*). This results in a one order of magnitude lower conductance for the *meta* compound compared to the *para*. The poorer conducting *meta*

compound did, however, form more stable junctions under higher bias potentials compared to the *para* compound. This could be an indication that the flow of a current across the junction can interfere with the metal-molecule bond. This may become an important issue for molecular electronics in terms of long term device stability .

1.5.7.2.5 A molecular rectifier based on a 1,8-(bisphenylethenyl)biphenyl

A molecular rectifier was demonstrated using an asymmetric molecular wire containing two separated conjugated pi-systems. This was achieved by incorporating a biphenyl unit with two methyl groups in the *ortho* position to the biphenylinic C-C bond, which causes the two rings to twist out of conjugation with each other. Two thioacetyl substituted phenylethenyl groups were joined to the biphenyl unit to complete the symmetric wire, whilst the asymmetric wire contained one phenylethenyl and one tetrafluoro-phenylethenyl unit.

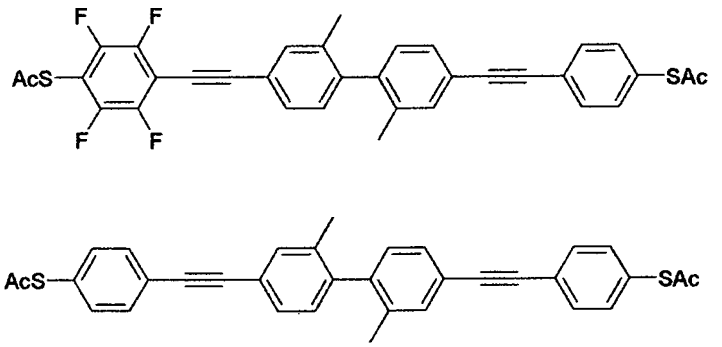

Figure 1.19. Single molecule rectifier (top). Non-rectifying molecule (bottom)

In the original work by Aviram and Ratner[19] the rectification behaviour resulted from different thresholds for electron injection at positive and negative bias. In the single molecule case, however, the diode-like shape of the I/V is connected to the different step heights of the current in positive and negative bias directions. The steps in the I/V are believed to result from molecular energy levels crossing the Fermi level, which are not equidistant from E_F at zero bias. One difference between these molecular diodes and the Aviram-Ratner diodes is that these may not involve molecular donor-accepter charge transfer, but rather that transport becomes more facile in one direction due to, perhaps, different molecule-electrode coupling strengths.

1.5.7.2.6 Oligothiophenes

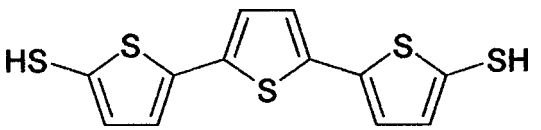

Figure 1.20. Structure of α,ω-bis thiol terthiophene.

Charge transport across oligothiophene molecular wires has been reported by several groups primarily because of the use of polythiophene compounds in semi-conductor transistor devices.[91] Polymers are too large to study using conventional single molecule techniques, so it is necessary to study shorter oligomers, capped generally with thiol groups for linkage to gold. An example is the compound α,ω-bis thiol terthiophene (figure 1.20), which has been studied using several techniques, including one in which the compound is adsorbed on two facing gold electrodes of a mechanically controllable break junction.[92] Current-voltage (*I-V*) characteristics were recorded at room temperature giving zero bias conductances in the 10–100 nS range. These values tend to agree with other literature accounts of the same molecule measured by various techniques.[93] An increase in the conductance of thiophene oligomers with length was reported by Tao et. al.[94] The quater-thiophene, although longer, was more than twice as conductive as the ter-thiophene, and the behaviour was attributed to the decrease in the HOMO – LUMO

separation. Interestingly, though, a set of conducting–atomic force microscopy (cAFM) measurements gave the opposite trend, and showed the conductance to decrease exponentially with length, starting from thiomethyl thiophene up to thiomethyl quater-thiophene. The β decay constant found was 0.41 $Å^{-1}$, which agreed well with quantum chemical calculations.[95] The experiments were carried out on full monolayers, under an atmosphere of nitrogen, which, compared to Tao's measurements, are substantially different conditions to the breakjunction measurements, which are performed on single molecules in toluene solvent.

1.6 Electrochemistry in Molecular and Organic Electronics.

Electrochemistry is becoming increasingly important in molecular and organic electronics studied on surfaces, and shows great potential for creating new electronic devices which use electrochemistry to control an electrical response. Electrochemical processes have been implicated in controlling the electrical behavior of a number of molecular devices such as rotaxane based switches and negative differential resistance (NDR)[62] devices, although it has not been straightforward to ascertain the mechanism. As a basic task in molecular electronics, understanding transport mechanisms through single molecules is increasingly being

investigated through solution-electrochemistry studies. The type of experimental setup is based on established techniques of measuring single molecule conductivities and involves using the STM in an aqueous environment. This allows us to probe the electronic levels of molecules in a controlled manner. However, this method of performing STM is in complete contrast to the ultra high vacuum and cryogenic environments where surface structure can be well understood. Since the advent of single-crystal, atomically planar electrode surfaces[96] combined with in-situ electrochemical STM, monolayer and sub-monolayer studies of well defined systems have been achieved.

Organic molecules containing redox centres are chemical species whose oxidation state, and thus electronic structure, can be changed, usually in a reversible way, relative to a reference electrode inserted in the same solution. One way to shift and align the molecular energy levels relative to the Fermi level(s) of the enclosing metal electrodes by adjusting the electrochemical (over)potential of the working electrodes with respect to the reference electrode. When sandwiched as molecular layers between the two working electrodes in an electrochemical STM arrangement (the tip and the surface), redox molecules display highly promising functional behaviour such as electrical switching between conductive 'on' states and insulating 'off' states. It has recently been demonstrated that the electrical properties of single molecules incorporating redox groups (e.g. viologens[97, 98] oligophenyleneethynylenes,[99] perylene tetracarboxylic

diimides (PTCDI)[100], oligo-anilines[101] and transition metal complexes) can be characterized as they are electrochemically switched between redox states. This opens the possibility to examine directly the link between redox state and conductance of individual molcules. Questions are raised such as can we link an increase or a decrease in conductance with certain redox states of a molecule? If so, then by how much does the conductance change around a redox transition, if it does so at all?

Such experiments typically are based on a scanning tunnelling microscope (STM) apparatus, with individual redox active molecules, held under potential control, tethered via Au–S bonds between the (generally) gold substrate and gold tip (figure 1.21). Mechanically controlled break junctions (MCBJs)[102] can also been used instead on an STM to create metal|molecule|metal junctions in this manner, but the principle, however, remains the same.

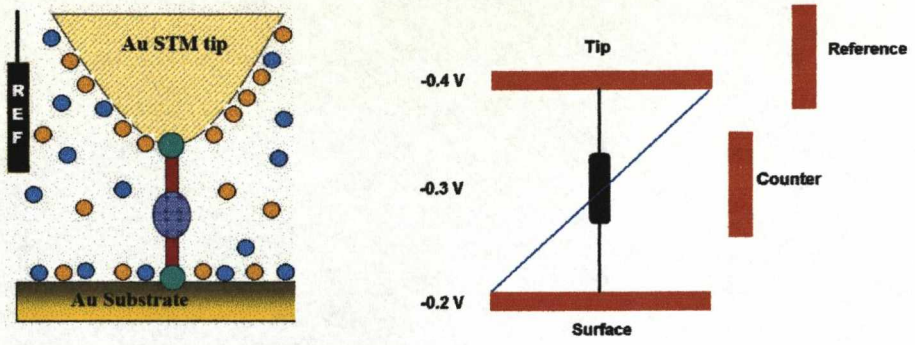

Figure 1.21. Schematic illustration of our approach for electrochemical measurement of single molecule charge transfer of redox molecules. The molecule is trapped between an STM tip and the surface in the presence of an aqueous electrolyte (ions represented by the coloured circles), counter and reference electrodes. The blue line represents the approximate bias drop across the molecule.

Redox molecules are attractive for molecular electronics applications because they can be reversibly oxidized and reduced by controlling the electrochemical gate voltage, leading to field effect switching behaviour. In this experimental setup there is an analogy to silicon based transistors,[103] with the tip and surface act as source and drain, I_{SD} being the current flow between these two electrodes, while the reference electrode acts as a "gate" controlled *via* a reference electrode (figure 1.21). The system is controlled through a bipotentiostat, which allows the independent control of tip and surface potentials. To avoid unwanted current between the tip and the counter electrode, the tip is coated with an insulating wax leaving only its apex exposed to interact with the surface.

1.6.1 Gating the molecular conductance

Ideally, the source and the drain electrodes should exchange electrons (or holes) through the molecular levels, whilst the third, gate, electrode should tune the energy of the molecular level. In order for the molecular redox levels to be tuned in this manner, the gating field must act within a few angstroms of the molecule.[104] This is difficult to achieve using solid state device configurations (i.e. using back gates). However, by placing the STM in an electrochemical cell, where the molecular junction is immersed in an electrolyte solution, the reference electrode behaves as a gate electrode. In an electrochemical STM experiment the tip and the substrate are the 'source' and 'drain' electrodes, and are biased with respect to the reference electrode, which is also inserted into the electrolyte. It is this reference electrode which controls the gating field across the molecule. An applied gating field falls across the double layer at the reference electrode/electrolyte interface, the electrolyte between the gate electrode and the source/drain electrodes, and the interface between the electrolyte-source/drain electrodes. Since there is practically no current between the source/drain electrodes and the reference electrode, the potential drop in the electrolyte is considered to be zero. Thus, the thickness of the double layer at the source/drain electrode-electrolyte interface determines the effective gating distance.

The overall effect of controlling the voltage between working and reference electrodes is to shift up or down the Fermi level of the metal electrodes with respect to the molecular levels. The concentration of ions in the double layer controls the chemical potential at the metal surface, which is defined as the amount by which the energy of the system would change if an additional particle (electron) were introduced (entropy and volume fixed). This, therefore, controls the energy of the electrons at the surface and is the principle behind the gating effect. In order to maximise the effect of the gate field, the redox molecule, or redox unit of the molecule, should be outside of the electrochemical double layer during a measurement. The thickness of the double layer is quoted in terms of an inverse screening length (k^{-1}, see equation x). This factor must be significantly smaller than the junction size for the electrostatic field to be effective. If it is not, then the ionic field may only partially screen the molecule, and the relations between the potentials of the electrodes and the effective energy of the molecular electronic levels would become similar to those in gas-phase (non-ionic) STM.[105] This would make the levels of both the molecule and metal move rather less independently. As the source-drain distance in a molecular FET is determined by the length of the molecule, it is necessary to choose molecules with length greater than the size of the double layer (or layers depending on how one views the situation at the tip). The longer the molecule becomes, the less conductive it becomes, normally, so there is a paradigm in designing compounds of

suitable length, but also of reasonable conductance for such studies. Obvious candidates are conjugated molecules, which tend to be the most conductive types of molecules. Other candidates are those based on semiconductor double barrier junctions, such as the viologen compound, 6V6, already mentioned. Double barrier compounds have the unique potential to be very insulating when the redox level is off-resonant, whilst becoming very conductive when on-resonant. This is the type of switching behaviour required if single molecules are to be used in integrated circuits, where the difference between 'on' and 'off' conductivities determines the effectiveness of the switch.

1.6.2 The structure of the electrochemical double layer

When an electrode surface is in contact with a surrounding electrolyte ion accumulation will occur at the interface between the electrode and the solution. The metal may become negatively charged by gaining electrons from the aqueous electrolyte, which attracts positive ions from the solution. This positive layer will then attract negative ions which form into a second layer. Several theories of the way in which charge is arranged at the interface have been proposed. In the Helmholtz model of the double layer the solvated ions arrange themselves along the surface of the electrode but are held away from it by their solvation spheres. This layer of charge, which exists as a plane of charge running along the solvated ions, is known

as the Outer Helmholtz Plane (OHP) and consists of ions also opposite in charge to the surface. Ions can also exist closer to the surface, but these are considered chemically bound and form the inner Helmholtz plane (IHP). This model considers the ionic structure at the surface as being rigid and thermal motions, which tend to break up the structure, are ignored. The potential drop across the interface

occurs completely in the region between the electrode surface and the Outer Helmholtz Plane (OHP), which is the radius of the counterions.

In the Gouy-Chapman model the disordering effect of thermal motion is taking into account resulting in the picture of a diffuse double layer. Ions of opposite charge congregate close to the electrode whilst ions of the same charge are repelled from it. In this case the potential drop is mainly in the region closest to the electrode surface but some charge is now further away from the electrode than the OHP.

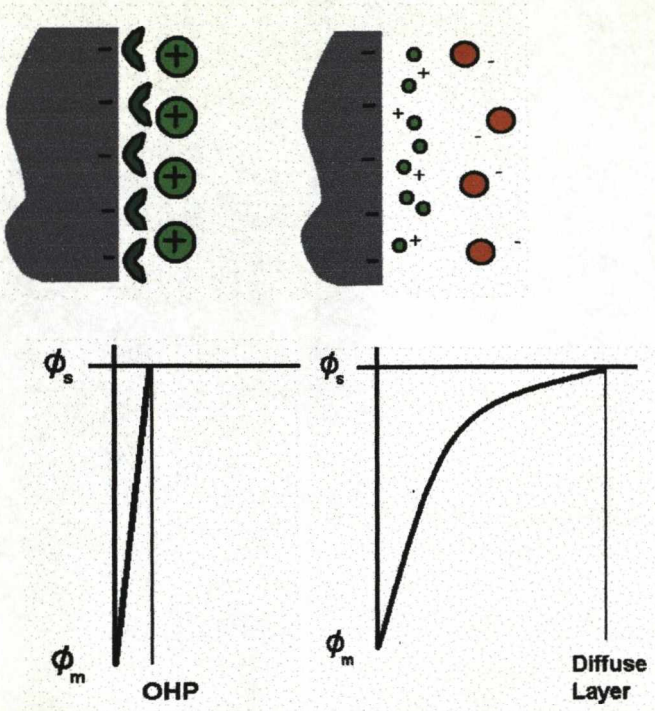

Figure 1.22. Helmholz model (left). Gouy Chapman model (right).

Neither model is a perfect representation of the double layer interface. The former overemphasizes the rigidity of the system, whilst the latter underestimates its structure. The Stern model develops both models into a more complete theory by combining aspects of the two together. In the Stern model the ions closest to the electrode are constrained into a rigid Helmholtz plane while outside this plane the ions are dispersed as in the Gouy-Chapman model, having a minimum distance of approach (OHP). This results in a sharp potential drop between the electrode and the OHP and then a gradual potential drop across the diffuse layer to the bulk solution. The adsorbed fixed layer and the diffuse mobile layer together are

the Electrical Double Layer. The double layer acts as a capacitor, with a 'fixed plate' (the fixed layer) and a 'moveable plate' (the mobile layer, and is a kind of electrolytic capacitor).

1.6.3 Thickness of electrical double layer

The electric field distribution is a crucial factor for considering the current-voltage characteristics of a molecular junction. For low currents and when there is no charging of the molecule the distribution of the potential is controlled only by the distribution of ions in the electrolyte. The length characterizing the decrease with distance of the potential in the double layer is called the Debye length, k^{-1}, and given by equation 5[106]

$$1/k = \left[\varepsilon_r \varepsilon_0 RT / \left(F^2 \sum_i c_i z_i^2\right)\right]^{1/2} \quad (5)$$

(rationalized four-quantity system) where ε = static permittivity = $\varepsilon_r\varepsilon_0$, ε_r = relative static permittivity of solution; ε_0 = permittivity of vacuum, R = gas constant, T = thermodynamic temperature, F = Faraday constant , c_i = concentration of species i, z_i = ionic charge on species i.

For common inorganic electrolytes, containing phosphates or sulphates, the Debye length is on the order of a few nanometers, depending on the concentration. At high concentrations of electrolyte the Debye length

decreases and ion paring may become an issue for redox molecules. Ion pairing has been shown to have a strong influence on the kinetics and mechanisms of electrochemical reactions as reflected by the location of the corresponding half-wave (or peak) potential.[107] At low electrolyte concentrations (milli-molar say) the Debye length is quite large compared to the tunnel gap and the potential distribution in the gap is nearly linear.[108] An analysis of the bias-voltage dependence of the position in the maximum tunnelling current versus overpotential relation was performed by Kuznetsov. [108] This analysis showed that generally the Debye potential screening in the tunnel gap by the supporting electrolyte affects the maximum position and width of the peak.

Another aspect of the Debye length compared to the bridge molecule is that when the Debye screening length becomes less than the length of the molecular bridge, the molecular energy levels, as a consequence of being influenced by the potential distribution in the gap, can be significantly altered close to the electrodes compared to the centre of the bridge. Even for symmetric, homogeneous, junctions like Au|alkanedithiols|Au the centre would, theoretically at least, feel a different enough potential to cause a rectifying effect in the current\bias-voltage relation.[109]

1.6.4 Electrostatic potential distribution in single molecule electrochemical STM measurements

A description of the potential drop occurring in solution was given recently by Corni.[110]

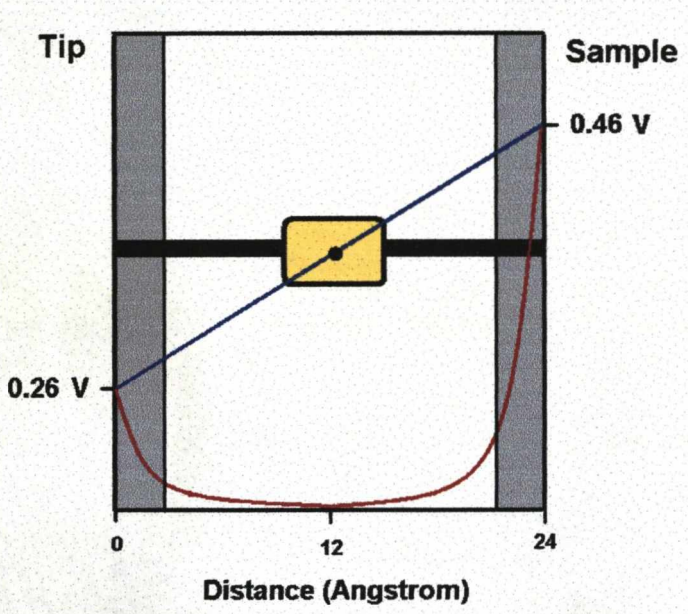

Figure 1.23. Modelling the bias potential drop across a single molecule in a metal junction. The yellow square represents the redox centre. The red line is the Gouy-Chapman potential drop between tip and sample.

When the solute is relatively large, like a protein,[111] the electrostatic potential distribution in the tip-substrate gap is complex. The space occupied by the solute is not accessible to the ions, which cannot screen the surface charge potentials of the tip and the surface. Hence, for small

molecules, like 6V6,[15] the redox site can be fully screened from the surface, whilst for large, bulky, molecules, like proteins, the potential drop could be intermediate between the two limiting cases (full screening / gas-phase - non ionic). In this model most of the potential drops inside the double layer region (represented approximately by the grey shaded area). This diagram is schematic as the surface potential is, of course, determined relative to the reference electrode which is at microscopic distances, not nanoscopic. Also the Debye length depends on electrolyte concentration. The GC analysis neglects ion sizes and non-linear screening effects, which could be an issue for tunnel junctions. A rigorous theory may also consider strongly and weakly coupled molecules as the number of electrons flowing through the junction could significantly affect the potential distribution too.

1.6.5 Electron transfer across redox-inactive molecules

The way in which molecules are considered redox active or redox inactive depends on the accessibility of the energy levels, under the experimental conditions, relative to the electrodes. The size of the potential 'window', where background electrochemical processes are minimal, is of the order of 1 eV in aqueous solution. Thus molecules whose levels lie within a fraction of an eV from the gold Fermi level can only be considered redox active for our measurements.

In terms of in situ-electrochemical STM studies of single molecules the classic series of redox inactive molecules are the alkanedithiols. These compounds have large HOMO-LUMO separations in the order of 8 eV,[112] with the levels far removed from, especially, the gold Fermi level of -5.2 eV relative to vacuum. The prevailing transport mechanism depends on the electronic structure of the molecule and electrodes and on the environment. It is not always straightforward to assert which mechanism dominates in a given junction. When the contribution of the intermediate states is negligible, one may speak about direct tunneling. The bridge molecule in direct tunneling simply represents a barrier for electron, which is, however, lower than that in the absence of the bridge[77] because of long-range electrostatic or short-range interactions of the tunneling electron with the bridge molecule, e.g., the interactions with the polarization of the molecule.

The energy levels of the intermediate states in superexchange are strongly off-resonance of the energy of the tunneling electron, and the interaction with the environment is weaker. These levels enhance electron tunneling compared with direct donor–acceptor ET by favorable nearest-neighbor electronic overlap. The superexchange mechanism has been considered for alkanedithiols.[113] Current\bias-voltage and current\overpotential relations largely reflect the wide molecular HOMO and LUMO spacing, i.e. single barrier behaviour with linear I\V and no NDR.[114, 115] Attempts have been made to fit the data to the Simmons model of tunnelling, which

is a pure tunnelling model.[116] A value of the apparent barrier height, Φ_B, in alkanedithiols SAMs was found to be circa 1.3-1.5 eV by Reed *et.al* [116] where several thousand molecules are sandwiched between two metallic contacts. The HOMO-LUMO gap in Au|Alkanedithiol|Au junctions has not been reported, however, a value of 8 eV is commonly assumed. As the Fermi level of the (gold) electrodes is normally found between the H-L gap, the value of Φ_B reported (essentially E_F-$E_{H/L}$) is rather low and suggests Fermi level alignment – probably as a result of neglecting the favourable nearest neighbour overlap.

Redox inactive compounds such as the alkanedithiols are not ideal molecular conductors, presenting a relatively large barrier to electron transfer. However, they permit the testing of ideas about electron transfer, and through the understanding of their behaviour, will allow for the evolution of the more advanced concepts necessary in complex systems such as those which involve redox states. The areas most important to interfacial electron transfer for which these test-bed compounds give insight are the molecule-electrode contacts, dynamics of the molecule/electrode binding, and dynamics of the molecular structure itself reflected in temperature dependent "gating" of the molecular conductivity.[77] Until recently there have been large discrepancies over several orders of magnitude between not only theory and experiment, but also between various experimental methods. In particular the results of break-junction experiments have largely disagreed with those from the

softer I(s) technique of Haiss et. al. These discrepancies are now largely being interpreted in terms of the molecule – electrode contact configuration,[18] and further investigation has revealed significant overlap of results between the techniques.[117] Both techniques, however, agree that no conductivity switching can be attained with redox inactive alkane molecules, which fits in with the notion of off-resonant transport in these molecules.

1.6.6 Electron transfer across redox active molecules

If the molecule in the metal junction possesses a low lying, redox active, energy level, then this level may participate in the tunnelling process.[78] It can be either oxidised or reduced, depending on the occupancy of the level, during electron transfer across the molecule. If the level can be brought into alignment with one of the electrodes connecting the molecule, an increase in the current can be expected. This can either be observed, as in the study of inorganic heterojunctions, by measuring the current as a function of the bias voltage V between the working electrode and the STM probe. However, if the measurements are performed in an electrochemical environment, one may tune the alignment of the molecular level(s) by adjusting the potentials of the working electrodes (at a constant bias voltage) relative to a reference electrode also in the electrolyte. This form of control is analogous to that in field effect transistors.

The ability to control electron transport in an analogous manner to a field effect transistor is an important task to achieve in the development of the field of single molecule electronics. Not only will it lead to the development of single molecule switches capable of being integrated in functional electronic circuitry, these studies also provide a unique opportunity to study charge transport at a fundamental level.

Usually the process is thought of in terms of a two step mechanism of electron transfer. One can think of the process involved in terms of the parabolas which describe the isosurface potential of the reaction coordinate[118] (this was shown to be an effective method by Marcus[119]). Figure 1.24 shows a schematic representation of a two step process in electron transfer involving a localized stated.

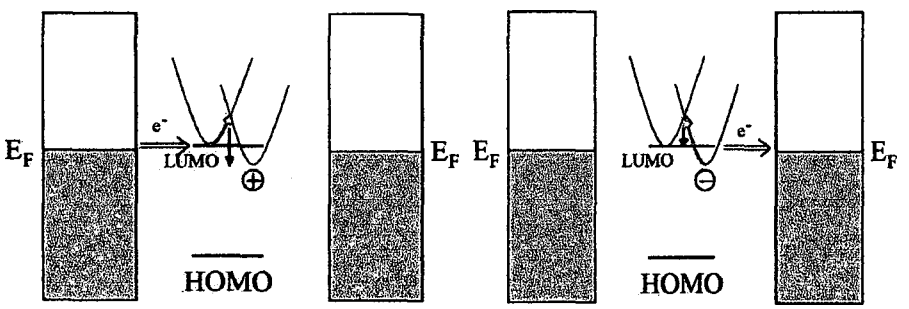

Figure 1.24. Representation of electron transfer involving redox states as a function of the ET reaction coordinate. The positive and negative signs describe the occupation state of the redox level. The lower parabola is the reduced state whilst the higher (energetically) parabola represents the oxidised state of the redox level.

The parabola that sits on top of the LUMO state represents fluctuations away from the local minimum caused by the coupling of the electronic level to environmental fluctuations. The second parabola represents the reduced state of the redox level. In the first step of the charge transfer process, fluctuations eventually take the LUMO parabola up to an energy where it intersects the REDOX parabola (light arrow). At that point, total electronic energy is lowered by occupation of the REDOX level and the electron relaxes down to this level, now trapped on the molecule. In the second phase of the charge transfer (second step in Figure 1.24), the trapped electron is released as a fluctuation takes the energy of the occupied REDOX state back into degeneracy with the energy of the unoccupied LUMO state. Now the electron can lower its energy still further by passing on to the Fermi level in the right electrode (which is lowered through the application of a bias voltage across the electrodes). In this picture, the redox state can be formally occupied even if the level is not formally in perfect energetic alignment with the gate electrode.

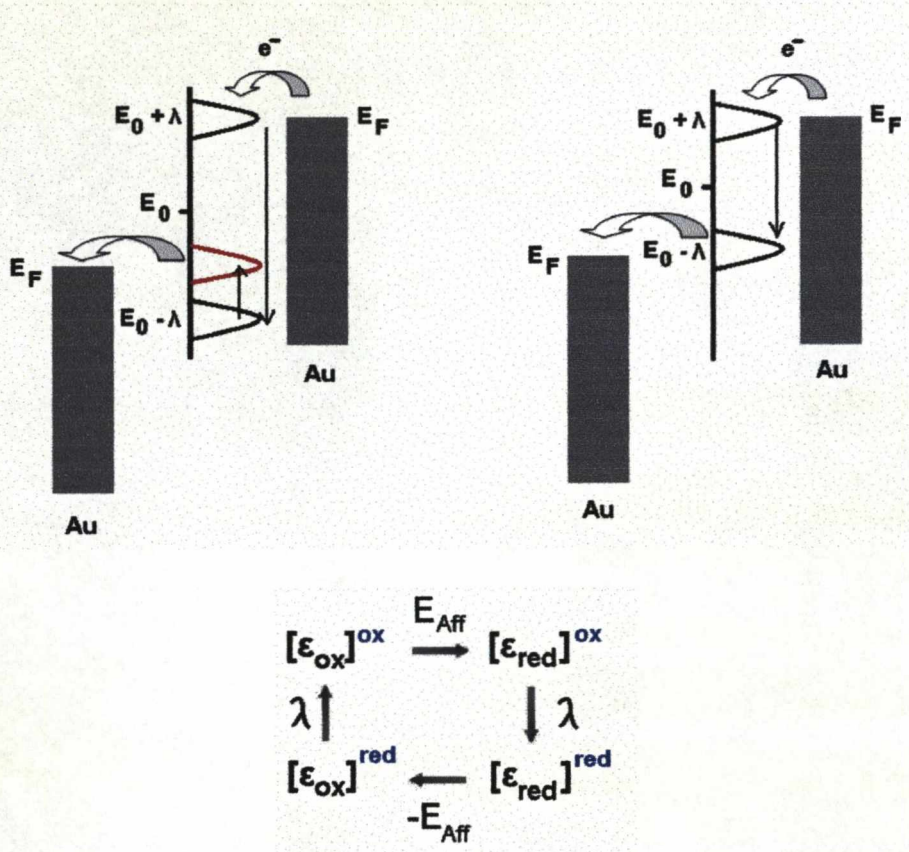

Figure 1.25. Energy level diagrams for the two-step sequential electron transfer mechanism in the case of small bias compared to the reorganisation energy, λ, left ($2\lambda > eV_{bias}$), and in the case of large bias, right ($2\lambda < eV_{bias}$). Below is the derivation of the energy separation between ε_{ox} ($\varepsilon_0 + \lambda$) and ε_{red} ($\varepsilon_0 - \lambda$) (= 2 λ). E_{Aff} is the electron affinity for ε_{ox}.

In the above, more advanced, picture of the two step process when substrate and tip potentials are tuned close to resonance (by adjustment of the electrochemical overpotential towards the unoccupied levels) with the molecular level an electron transfers to the oxidised level ($\varepsilon_0 + \lambda$) (which is brought closer to the Fermi level of the electrode by solvent and thermal fluctuations). This level can subsequently relax to a new value ε_{red} ($\varepsilon_0 - \lambda$).

It is possible to define the difference between the reduced and the oxidised levels (2λ) as shown below. (see also figure 1.25).

$$[\varepsilon_{ox}]^{ox} \rightarrow [\varepsilon_{red}]^{red} = E_{Aff} + (-E_{Aff}) + \lambda + \lambda = 2\lambda$$

In a second, also thermally assisted electron transfer step the electron is transmitted from the occupied molecular redox level to the second electrode. As the overpotential is raised further, the occupied level is trapped deeper below the Fermi level of the positively biased electrode (the tip) and larger thermal activation is needed in the second electron transfer step. The current therefore drops at higher overpotentials giving a maximum in the tunnelling current-overpotential relation.

Depending on the strength of the coupling of the levels to the electrode subtle differences in mechanisms are possible in the strong and weak limits. The subtleties are possible through the differences in two quantities, one being the ''relaxation time'' for electron transfer given by $\tau_{ET} \approx \hbar/\Delta$ where Δ is the energy ''broadening'' caused by the interaction with the electrodes. The other one is the environmental nuclear relaxation time, τ_{rel}. In the limit of strong electronic interactions, $\tau_{ET} << \tau_{rel}$. A multitude of electrons is then transferred in a time window τ_{rel} (fully adiabatic regime). As discussed in 1.6.4, the exact location of the current rise depends on other details, particularly the drops of the substrate electrochemical

potential and bias voltage at the site of the redox centre in the tunnelling gap.

In the opposite limit of weak molecule-electrode interactions, the fully diabatic limit, $\tau_{ET} >> \tau_{rel}$. The occupied level relaxes fully after the first ET step. This is again followed by the second step but only a single electron is now transferred in the overall process, i.e. within τ_{rel}, and the tunnelling enhancement close to energy resonance is much weaker than in the fully adiabatic limit.

As mentioned, a maximum in the tunnelling current should arise when the level falls in the energy window between the Fermi levels of the two electrodes.[118] This effect has been demonstrated using the STM contrast of images of iron-containing porphyrin molecules on a graphite electrode in a paper by Tao,[120] (although a resonant tunnelling mechanism was proposed) and by the Ulstrup group with various transition metal complexes.[121] More recently, though, this effect has been demonstrated with molecules, such as viologens and perylene tetracarboxylic diimides (PTCDI),[58] connected via gold-thiol linkages at both ends of the molecule using STM based current-distance spectroscopies. The bis(thiahexyl) viologen compound 6V6, however, does not display a maximum in the tunnelling current versus overpotential plot,[15] rather a broad sigmoidal rise which begins at potentials well before the formal redox potential. This behaviour will be compared to a similar molecule

later in this thesis which does show a maximum in tunnel current versus overpotential, and the reasons for the difference will be discussed.

1.6.7 Single molecule redox active electrochemical switches

Only a handful of molecules have been investigated using single molecule electrochemical procedures. These include firstly a viologen derivative which was initially studied by isolating individual or small numbers of molecules in an insulating alkanethiol matrix and adsorbing a gold nanoparticle onto the redox molecule via the matrix isolation technique.[122] The results of this work showed that as the substrate-to-solution potential was varied, the bipyridinium group can be switched between its oxidized ($bipy^{2+}$) and reduced ($bipy^{1+}$) states with the bipyridinium in its $bipy^{1+}$ showing a higher barrier transparency than in the $bipy^{2+}$ state. Later this work was repeated with a similar viologen derivative using the I(s) molecular lifting technique which too showed that as the substrate-to-solution potential was brought close to and past the formal reduction potential for the viologen an increase in the transparency of the molecular barrier could be observed.[15] In this case the increase was of a factor 6-7 fold over the low bias conductance found under ambient air conditions and too when the substrate potential was tuned in the positive region. No maximum, however, in the conductance-overpotential relation was found, which contradicted recent theoretical

work on such systems[118] which did predict a maximum located close to the formal redox potential of the molecule. Instead a sigmoidal increase was observed in the current and this has since been largely understood in terms of a 'soft-gating' model which involves motions of the nuclear co-ordinates on timescales relevant to that of the electron transfer process. This results in an apparent strong coupling of the electron to the soft motions of the molecule such as vibrations and/or flexible linker motions. The conductance of a hepta-aniline oligomer attached to gold electrodes of an STM held under potential control in electrolyte displayed a fifteen-fold increase in conductivity upon oxidation from the leucoemeraldine form to the emeraldine salt.[101] The single-molecule current-voltage characteristic was linear in toluene, whilst displaying 'negative differential resistance' in an acidic electrolyte. The conductance-overpotential behaviour of the aniline oligomer displayed a modest peak centred close to the formal oxidation potential (c.a 0.15 V further positive in the overpotential). The results demonstrate how electron transfer in single molecules can be linked to the environment and also that different mechanisms may apply if the electron and/or molecular levels are coupled to the environment.

Some of the largest switching ratios observed in the field of single molecule electrochemistry have been with perylene tetracarboxylic diimide (PTCDI) compounds in the order of several orders of magnitude.[58] The conductivity was studied as a function of the spacer

group between the PTCDI centre and the gold electrodes. Although the absolute conductivity changed depending on the strength of binding to the electrodes, the groups shared similar switching behaviours, all showing a modest peak near the formal reduction potential. The temperature dependence measurements of the conductance-overpotential relation indicated that the electron transfer involves a thermally activated process. At potentials positive of the redox transition an increase in temperature caused an increase in the conductivity, whilst close to and at the redox potential little temperature dependence could be seen. Although a two-step model of the electron transfer is favoured rather than a resonant tunnelling process, the temperature dependence of the conductance could not be fully reconciled in the full mechanistics of such a two-step process as laid out by Ulstrup and Kuznetsov. This is mainly due to the lack of a maximum in the conductance, but also, as pointed out in the paper, the lack of knowledge of key experimental parameters like ionic screening and proximity of redox group to the electrodes. The fact that breakjunctions produce ill defined electrodes probably does not help either.

A recent theoretical paper addressed the temperature dependence issue and suggested that the hydration sphere around the molecules causes fluctuations in the molecular conductance, and increasing the temperature (and hence the random motions of the water sphere) results in a higher population of more conductive states of the molecule over the course of a

single measurement.[123] Interestingly, the activation energy extracted from the temperature measurements was found to be about 0.4 and 0.6 eV for benzenethiol-PTCDI and ethanethiol-PTCDI molecules respectively. These are reasonable values for the outer shell (solvent polarization) component of the reorganization energy found in electron-transfer phenomena and suggest a strong link between the polarised water around the molecules and the molecular redox levels.

The lack of temperature dependence at the redox potential (and hence close to where the maximum in conductance is expected) was not discussed in the experimental or theory papers and is an interesting point to consider as it is at the heart of the two step hopping mechanism. The theory would suggest that the polar water molecules broaden the molecular levels by constantly changing their orientation with respect to the molecule (in the PTCDI case the water molecules are believed to interact strongly with the oxygen atoms of the four carboxyl groups). This constant change in electrostatic field strength shifts the molecular energy levels up and down in energy broadening the equilibrium energy level. It has been shown in DNA that such an effect can shift the molecular levels by substantial fractions of an electron volt[124]. When the level is off-resonant with the Fermi Level, a change in the temperature changes the broadness of the level so as to increase the density of states at the Fermi level, increasing the conductance. This effect is greatest when the level is off-resonant and diminishes the closer to resonance the level

becomes, although there will probably be different temperature responses in the fully adiabatic and diabatic limits. In any case, the observed experimental results point clearly to a strong coupling of the solvent to the single molecule conductance, which, as shall be seen, is a strong theme in this thesis.

Bibliography

[1] Y. N. Xia, G. M. Whitesides, *Annu. Rev. Mater. Sci.* **1998**, *28*, 153-184.

[2] G. S. Higashi, Y. J. Chabal, G. W. Trucks, K. Raghavachari, *Appl. Phys. Lett.* **1990**, *56*, 656-658.

[3] J. R. Heath, M. A. Ratner, *Phys. Today* **2003**, *56*, 43-49.

[4] X. G. Peng, L. Manna, W. D. Yang, J. Wickham, E. Scher, A. Kadavanich, A. P. Alivisatos, *Nature* **2000**, *404*, 59-61.

[5] M. S. Gudiksen, L. J. Lauhon, J. Wang, D. C. Smith, C. M. Lieber, *Nature* **2002**, *415*, 617-620.

[6] Electronics, Volume 38, Number 8, April 19, 1965

[7] S. Datta, *Nanotechnology* **2004**, *15*, S433-S451.

[8] Y. Q. Xue, M. A. Ratner, *Int. J. Quantum Chem.* **2005**, *102*, 911-924.

[9] A. Nitzan, *Annu. Rev. Phys. Chem.* **2001**, *52*, 681-750.

[10] www.its.caltech.edu/~feynman/plenty

[11] G. Binning, H. Rohrer, C. Gerber, E. Weibel, *Phys. Rev. Lett.* **1982**, *49*, 57-61.

[12] N. J. Tao, J. A. Derose, S. M. Lindsay, *J. Phys. Chem.* **1993**, *97*, 910-919.

[13] PROPERTIES OF SINGLE ORGANIC MOLECULES ON CRYSTAL SURFACES. Werner Hofer, Federico Rosei & Peter Grütter. IPC, ISBN 978-1-86094-628-8

[14] B. Q. Xu, N. J. J. Tao, *Science* **2003**, *301*, 1221-1223.

[15] W. Haiss, H. van Zalinge, S. J. Higgins, D. Bethell, H. Hobenreich, D. J. Schiffrin, R. J. Nichols, *J. Am. Chem. Soc.* **2003**, *125*, 15294-15295.

[16] J. M. Beebe, V. B. Engelkes, L. L. Miller, C. D. Frisbie, *J. Am. Chem. Soc.* **2002**, *124*, 11268-11269.

[17] K. W. Hipps, *Science* **2001**, *294*, 536-537.

[18] X. L. Li, J. He, J. Hihath, B. Q. Xu, S. M. Lindsay, N. J. Tao, *J. Am. Chem. Soc.* **2006**, *128*, 2135-2141.

[19] A. Aviram, M. A. Ratner, *Chem. Phys. Lett.* **1974**, *29*, 277-283.

[20] R. M. Metzger, B. Chen, U. Hopfner, M. V. Lakshmikantham, D. Vuillaume, T. Kawai, X. L. Wu, H. Tachibana, T. V. Hughes, H. Sakurai, J. W. Baldwin, C. Hosch, M. P. Cava, L. Brehmer, G. J. Ashwell, *J. Am. Chem. Soc.* **1997**, *119*, 10455-10466.

[21] A. Broo, M. C. Zerner, *Chem. Phys.* **1995**, *196*, 423-436.

[22] A. S. Martin, J. R. Sambles, G. J. Ashwell, *Phys. Rev. Lett.* **1993**, *70*, 218-221.

[23] G. L. Fisher, A. V. Walker, A. E. Hooper, T. B. Tighe, K. B. Bahnck, H. T. Skriba, M. D. Reinard, B. C. Haynie, R. L. Opila, N. Winograd, D. L. Allara, *J. Am. Chem. Soc.* **2002**, *124*, 5528-5541.

[24] W. Deng, L. Yang, D. Fujita, H. Nejoh, C. Bai, *Appl. Phys. A-Mater. Sci. Process.* **2000**, *71*, 639-642.

[25] D. Qu, K. Uosaki, *J. Phys. Chem. B* **2006**, *110*, 17570-17577.

[26] M. Epple, A. M. Bittner, A. Kuhnke, K. Kern, W. Q. Zheng, A. Tadjeddine, *Langmuir* **2002**, *18*, 773-784.

[27] K. Slowinski, R. V. Chamberlain, C. J. Miller, M. Majda, *J. Am. Chem. Soc.* **1997**, *119*, 11910-11919.

[28] E. Tran, M. A. Rampi, G. M. Whitesides, *Angew. Chem.-Int. Edit.* **2004**, *43*, 3835-3839.

[29] Y. J. Liu, H. Z. Yu, *J. Phys. Chem. B* **2003**, *107*, 7803-7811.

[30] M. Manolova, V. Ivanova, D. M. Kolb, H. G. Boyen, P. Ziemann, M. Buttner, A. Romanyuk, P. Oelhafen, *Surf. Sci.* **2005**, *590*, 146-153.

[31] J. G. Kushmerick, D. B. Holt, J. C. Yang, J. Naciri, M. H. Moore, R. Shashidhar, *Phys. Rev. Lett.* **2002**, *89*, 4.

[32] D. R. Stewart, D. A. A. Ohlberg, P. A. Beck, Y. Chen, R. S. Williams, J. O. Jeppesen, K. A. Nielsen, J. F. Stoddart, *Nano Lett.* **2004**, *4*, 133-136.

[33] J. Moreland, J. W. Ekin, *J. Appl. Phys.* **1985**, *58*, 3888-3895.

[34] X. D. Cui, A. Primak, X. Zarate, J. Tomfohr, O. F. Sankey, A. L. Moore, T. A. Moore, D. Gust, G. Harris, S. M. Lindsay, *Science* **2001**, *294*, 571-574.

[35] P. D. Jadzinsky, G. Calero, C. J. Ackerson, D. A. Bushnell, R. D. Kornberg, *Science* **2007**, *318*, 430-433.

[36] C. Li, I. Pobelov, T. Wandlowski, A. Bagrets, A. Arnold, F. Evers, *J. Am. Chem. Soc.* **2008**, *130*, 318-326.

[37] S. Ciraci, A. Baratoff, I. P. Batra, *Phys. Rev. B* **1990**, *41*, 2763-2775.

[38] J. M. Beebe, B. Kim, J. W. Gadzuk, C. D. Frisbie, J. G. Kushmerick, *Phys. Rev. Lett.* **2006**, *97*, 4.

[39] P. R. Emtage, W. Tantraporn, *Phys. Rev. Lett.* **1962**, *8*, 267-&.

[40] S. C. Meepagala, F. Real, *Phys. Rev. B* **1994**, *49*, 10761-10763.

[41] M. Mundschau, *Ultramicroscopy* **1991**, *36*, 29-51.

[42] B. Ren, G. Picardi, B. Pettinger, *Rev. Sci. Instrum.* **2004**, *75*, 837-841.

[43] J. Garnaes, F. Kragh, K. A. Morch, A. R. Tholen, *J. Vac. Sci. Technol. A-Vac. Surf. Films* **1990**, *8*, 441-444.

[44] S. N. Magonov, *Appl. Spectrosc. Rev.* **1993**, *28*, 1-121.

[45] R. M. Feenstra, W. A. Thompson, A. P. Fein, *Phys. Rev. Lett.* **1986**, *56*, 608-611.

[46] F. O. Goodman, N. Garcia, *Phys. Rev. B* **1991**, *43*, 4728-4731.

[47] E. M. Lifshitz, *Soviet Physics Jetp-Ussr* **1956**, *2*, 73-83.

[48] J. N. Israelachvili, *Surf. Sci. Rep.* **1992**, *14*, 109-159.

[49] R. M. Pashley, *J. Colloid Interface Sci.* **1981**, *83*, 531-546.

[50] U. Hartmann, *Phys. Rev. B* **1991**, *43*, 2404-2407.

[51] H. J. Butt, *Biophys. J.* **1991**, *60*, 777-785.

[52] M. Buttiker, Y. Imry, R. Landauer, S. Pinhas, *Phys. Rev. B* **1985**, *31*, 6207-6215.

[53] Y. Kurui, Y. Oshima, M. Okamoto, K. Takayanagi, *Phys. Rev. B* **2008**, *77*, 4.

[54] E. Scheer, N. Agrait, J. C. Cuevas, A. L. Yeyati, B. Ludoph, A. Martin-Rodero, G. R. Bollinger, J. M. van Ruitenbeek, C. Urbina, *Nature* **1998**, *394*, 154-157.

[55] B. Kim, J. M. Beebe, Y. Jun, X. Y. Zhu, C. D. Frisbie, *J. Am. Chem. Soc.* **2006**, *128*, 4970-4971.

[56] J. Heurich, J. C. Cuevas, W. Wenzel, G. Schon, *Phys. Rev. Lett.* **2002**, *88*, 4.

[57] N. J. Tao, *Nat. Nanotechnol.* **2006**, *1*, 173-181.

[58] X. L. Li, J. Hihath, F. Chen, T. Masuda, L. Zang, N. J. Tao, *J. Am. Chem. Soc.* **2007**, *129*, 11535-11542.

[59] R. Beckman, K. Beverly, A. Boukai, Y. Bunimovich, J. W. Choi, E. DeIonno, J. Green, E. Johnston-Halperin, Y. Luo, B. Sheriff, J. F. Stoddart, J. R. Heath, *Faraday Discuss.* **2006**, *131*, 9-22.

[60] N. Jlidat, M. Hliwa, C. Joachim, *Chem. Phys. Lett.* **2008**, *451*, 270-275.

[61] C. S. Wang, A. S. Batsanov, M. R. Bryce, G. J. Ashwell, B. Urasinska, I. Grace, C. J. Lambert, *Nanotechnology* **2007**, *18*, 8.

[62] A. H. Flood, J. F. Stoddart, D. W. Steuerman, J. R. Heath, *Science* **2004**, *306*, 2055-2056.

[63] L. L. Chang, L. Esaki, R. Tsu, *Appl. Phys. Lett.* **1974**, *24*, 593-595.

[64] P. E. Kornilovitch, A. M. Bratkovsky, R. S. Williams, *Phys. Rev. B* **2002**, *66*, 11.

[65] J. Bai, T. Wang, S. Sakai, *J. Appl. Phys.* **2000**, *88*, 4729-4733.

[66] A. R. Rocha, S. Sanvito, *Phys. Rev. B* **2004**, *70*, 7.

[67] J. M. Seminario, L. M. Yan, *Int. J. Quantum Chem.* **2005**, *102*, 711-723.

[68] A. Troisi, M. A. Ratner, *Phys. Chem. Chem. Phys.* **2007**, *9*, 2421-2427.

[69] A. R. Rocha, V. M. Garcia-Suarez, S. W. Bailey, C. J. Lambert, J. Ferrer, S. Sanvito, *Nat. Mater.* **2005**, *4*, 335-339.

[70] W. Haiss, R. J. Nichols, H. van Zalinge, S. J. Higgins, D. Bethell, D. J. Schiffrin, *Phys. Chem. Chem. Phys.* **2004**, *6*, 4330-4337.

[71] H. B. Akkerman, B. de Boer, *J. Phys.-Condes. Matter* **2008**, *20*, 20.

[72] F. Chen, X. L. Li, J. Hihath, Z. F. Huang, N. J. Tao, *J. Am. Chem. Soc.* **2006**, *128*, 15874-15881.

[73] S. Martin, W. Haiss, S. Higgins, P. Cea, M. C. Lopez, R. J. Nichols, *J. Phys. Chem. C* **2008**, *112*, 3941-3948.

[74] L. Venkataraman, J. E. Klare, I. W. Tam, C. Nuckolls, M. S. Hybertsen, M. L. Steigerwald, *Nano Lett.* **2006**, *6*, 458-462.

[75] M. D. Fu, W. P. Chen, H. C. Lu, C. T. Kuo, W. H. Tseng, C. H. Chen, *J. Phys. Chem. C* **2007**, *111*, 11450-11455.

[76] X. Li, A. A. Gewirth, *J. Am. Chem. Soc.* **2003**, *125*, 11674-11683.

[77] W. Haiss, H. van Zalinge, D. Bethell, J. Ulstrup, D. J. Schiffrin, R. J. Nichols, *Faraday Discuss.* **2006**, *131*, 253-264.

[78] W. Haiss, T. Albrecht, H. van Zalinge, S. J. Higgins, D. Bethell, H. Hobenreich, D. J. Schiffrin, R. J. Nichols, A. M. Kuznetsov, J. Zhang, Q. Chi, J. Ulstrup, *J. Phys. Chem. B* **2007**, *111*, 6703-6712.

[79] J. He, F. Chen, J. Li, O. F. Sankey, Y. Terazono, C. Herrero, D. Gust, T. A. Moore, A. L. Moore, S. M. Lindsay, *J. Am. Chem. Soc.* **2005**, *127*, 1384-1385.

[80] M. Tsutsui, Y. Teramae, S. Kurokawa, A. Sakai, *Appl. Phys. Lett.* **2006**, *89*, 3.

[81] X. Y. Xiao, B. Q. Xu, N. J. Tao, *Nano Lett.* **2004**, *4*, 267-271.

[82] P. Reddy, S. Y. Jang, R. A. Segalman, A. Majumdar, *Science* **2007**, *315*, 1568-1571.

[83] A. S. Duwez, S. DiPaolo, J. Ghijsen, J. Riga, M. Deleuze, J. Delhalle, *J. Phys. Chem. B* **1997**, *101*, 884-890.

[84] S. Kera, H. Setoyama, K. Kimura, A. Iwasaki, K. K. Okudaira, Y. Harada, N. Ueno, *Surf. Sci.* **2001**, *482*, 1192-1198.

[85] W. D. Tian, S. Datta, S. H. Hong, R. Reifenberger, J. I. Henderson, C. P. Kubiak, *J. Chem. Phys.* **1998**, *109*, 2874-2882.

[86] Y. Q. Xue, S. Datta, M. A. Ratner, *J. Chem. Phys.* **2001**, *115*, 4292-4299.

[87] J. G. Simmons, *J. Appl. Phys.* **1963**, *34*, 1793-&.

[88] J. R. Quinn, F. W. Foss, L. Venkataraman, M. S. Hybertsen, R. Breslow, *J. Am. Chem. Soc.* **2007**, *129*, 6714-+.

[89] J. R. Quinn, F. W. Foss, L. Venkataraman, R. Breslow, *J. Am. Chem. Soc.* **2007**, *129*, 12376-+.

[90] M. Mayor, H. B. Weber, J. Reichert, M. Elbing, C. von Hanisch, D. Beckmann, M. Fischer, *Angew. Chem.-Int. Edit.* **2003**, *42*, 5834-5838.

[91] A. Berlin, B. Vercelli, G. Zotti, *Polym. Rev.* **2008**, *48*, 493-530.

[92] C. Kergueris, J. P. Bourgoin, S. Palacin, D. Esteve, C. Urbina, M. Magoga, C. Joachim, *Phys. Rev. B* **1999**, *59*, 12505-12513.

[93] S. I. Taniguchi, M. Minamoto, M. M. Matsushita, T. Sugawara, Y. Kawada, D. Bethell, *J. Mater. Chem.* **2006**, *16*, 3459-3465.

[94] B. Q. Q. Xu, X. L. L. Li, X. Y. Y. Xiao, H. Sakaguchi, N. J. J. Tao, *Nano Lett.* **2005**, *5*, 1491-1495.

[95] H. Sakaguchi, A. Hirai, F. Iwata, A. Sasaki, T. Nagamura, E. Kawata, S. Nakabayashi, *Appl. Phys. Lett.* **2001**, *79*, 3708-3710.

[96] A. T. Hubbard, *Accounts Chem. Res.* **1980**, *13*, 177-184.

[97] W. Haiss, H. van Zalinge, H. Hobenreich, D. Bethell, D. J. Schiffrin, S. J. Higgins, R. J. Nichols, *Langmuir* **2004**, *20*, 7694-7702.

[98] Z. Li, B. Han, G. Meszaros, I. Pobelov, T. Wandlowski, A. Blaszczyk, M. Mayor, *Faraday Discuss.* **2006**, *131*, 121-143.

[99] X. Y. Xiao, L. A. Nagahara, A. M. Rawlett, N. J. Tao, *J. Am. Chem. Soc.* **2005**, *127*, 9235-9240.

[100] X. L. Li, B. Q. Xu, X. Y. Xiao, X. M. Yang, L. Zang, N. J. Tao, *Faraday Discuss.* **2006**, *131*, 111-120.

[101] J. He, F. Chen, S. Lindsay, C. Nuckolls, *Appl. Phys. Lett.* **2007**, *90*, 3.

[102] F. Giacalone, M. A. Herranz, L. Gruter, M. T. Gonzalez, M. Calame, C. Schonenberger, C. R. Arroyo, G. Rubio-Bollinger, M. Velez, N. Agrait, N. Martin, *Chem. Commun.* **2007**, 4854-4856.

[103] T. Albrecht, A. Guckian, J. Ulstrup, J. G. Vos, *IEEE Trans. Nanotechnol.* **2005**, *4*, 430-434.

[104] P. Damle, T. Rakshit, M. Paulsson, S. Datta, *IEEE Trans. Nanotechnol.* **2002**, *1*, 145-153.

[105] S. Datta, W. D. Tian, S. H. Hong, R. Reifenberger, J. I. Henderson, C. P. Kubiak, *Phys. Rev. Lett.* **1997**, *79*, 2530-2533.

[106] IUPAC Compendium of Chemical Terminology 2nd Edition (1997) 1972, 31, 619

[107] J. M. Saveant, *J. Phys. Chem. B* **2001**, *105*, 8995-9001.

[108] A. Kornyshev, A. Kuznetsov, J. Ulstrup, *PNAS* **2006**, *103*, 6799-6804.

[109] A. Kornyshev, A. M. Kuznetsov, *ChemPhysChem* **2006**, *7*, 1036-1040.

[110] S. Corni, *IEEE Trans. Nanotechnol.* **2007**, *6*, 561-570.

[111] A. Alessandrini, M. Gerunda, G. W. Canters, M. P. Verbeet, P. Facci, *Chem. Phys. Lett.* **2003**, *376*, 625-630.

[112] C. Boulas, J. Davidovits, F. Rondelez, D. Vuillaume, *Phys. Rev. Lett.* **1996**, *76*, 4797-4800.

[113] F. Remacle, R. Levine, *Faraday Discuss.* **2006**, *131*, 45-67.

[114] V. Mujica, M. Kemp, M. A. Ratner, *J. Chem. Phys.* **1994**, *101*, 6849-6855.

[115] F. Chen, J. Hihath, Z. F. Huang, X. L. Li, N. J. Tao, *Annu. Rev. Phys. Chem.* **2007**, *58*, 535-564.

[116] W. Wang, T. Lee, M. Reed, *Proceedings of the IEEE* **2005**, *93*, 1815-1824.

[117] W. Haiss, S Martin, E. Leary, H. van Zalinge, S. J. Higgins, L. Bouffier, R. J. Nichols. J. Am. Chem. Soc. submitted

[118] A. M. Kuznetsov, J. Ulstrup, *J. Phys. Chem. A* **2000**, *104*, 11531-11540.

[119] R. A. Marcus, *J. Chem. Phys.* **1956**, *24*, 966-978.

[120] N. J. Tao, *Phys. Rev. Lett.* **1996**, *76*, 4066-4069.

[121] T. Albrecht, K. Moth-Poulsen, J. B. Christensen, A. Guckian, T. Bjornholm, J. G. Vos, J. Ulstrup, *Faraday Discuss.* **2006**, *131*, 265-279.

[122] D. I. Gittins, D. Bethell, D. J. Schiffrin, R. J. Nichols, *Nature* **2000**, *408*, 67-69.

[123] H. Cao, J. Jiang, J. Ma, Y. Luo, *J. Am. Chem. Soc.* **2008**, *130*, 6674

[124] A. A. Voityuk, K. Siriwong, N. Rosch, *Angew. Chem.-Int. Edit.* **2004**, *43*, 624-627.

Chapter 2

Methods Overview

Chapter 2. Methods Overview

2.1 X-ray Photoelectron Spectroscopy (XPS)

Surface analysis by XPS is accomplished by irradiating the sample with monoenergetic soft x-rays and analyzing the energy of the ejected electrons (Fig.1). Mg Kα (1253.6 eV) x-rays were used in the experiments presented here. These photons have limited penetrating power in the solid of only a few hundred Angström. As illustrated in Fig.1 photons interact with atoms in the surface and cause electron emission by the photoelectric effect. Energy is conserved when a photon ionizes a sample and the energy of the photoelectron must be equal to the difference between the photon energy $h\nu$ and the atomic level binding energy.

$$E_K = h\nu - E_B$$

E_B = binding energy; $h\nu$ = photon Energy; E_K = photoelectron kinetic energy;

By measuring the kinetic energy of the emitted electrons the binding energy of the atomic orbital from which the electron originates can be calculated. In this way information which can be used to identify

chemical species and their environments is obtained. Structural and electronic information may also be derived from energy distribution spectra.

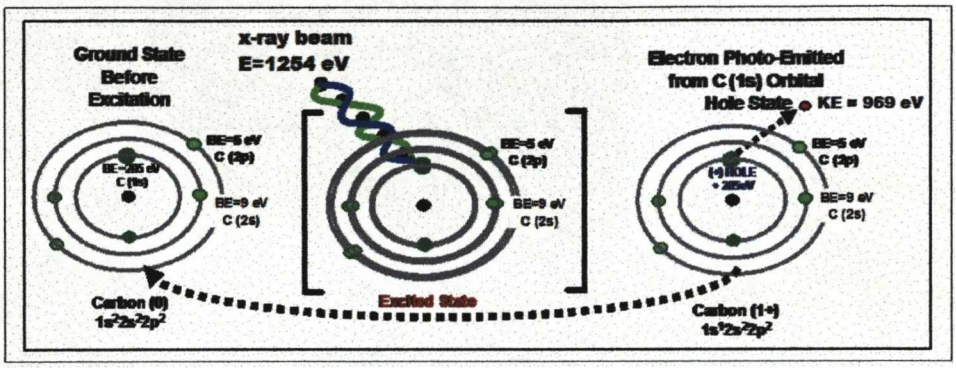

Figure 2.1. Schematic illustration showing the energy loss of a photon of energy 1254 eV interacting with an electron in the C1s core orbital resulting in the electron being ejected with $E_K = h\nu - E_B$

2.2 Angle resolved XPS

Angle resolved XPS allows non destructive depth information (up to 10 nm) by comparing spectra at various take off angles. Increasing the photoelectron takeoff angle by rotating the sample in the energy dispersive plane of the analyser (Fig.2.2) reduces the sampling depth of the technique. As a result the depth from which photoelectrons are detected is changed and the technique becomes surface sensitive. Comparing relative intensities at low and high take off angles, indicates whether a species is enriched or depleted in the surface region. This is useful for the analysis of thin films on surfaces where it is possible to determine the molecular orientation with

respect to the surface.

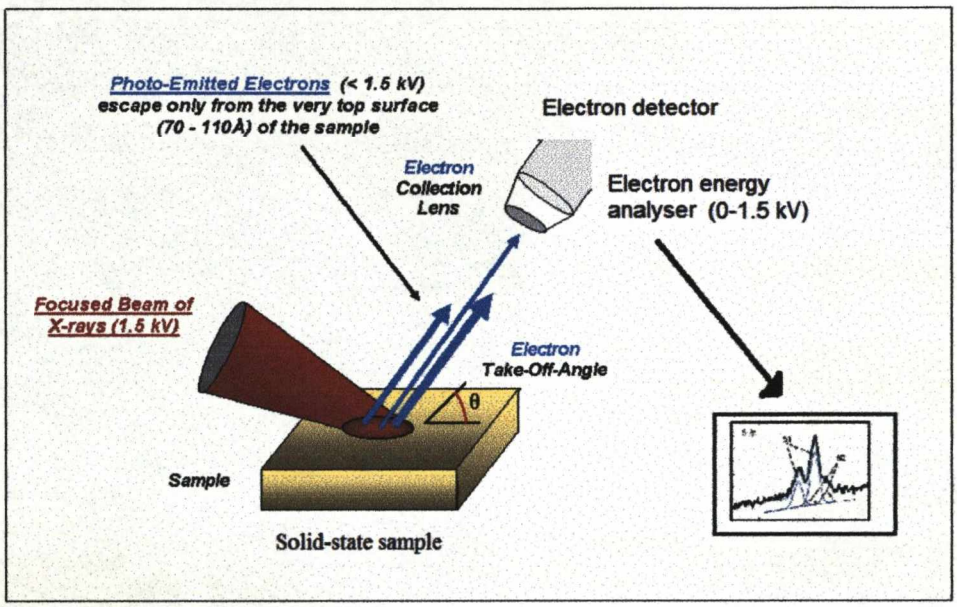

Figure 2.2. Illustration of an XPS spectrometer.

Spectra were acquired using a Scienta ESCA 300 spectrometer (NCESS, Daresbury Laboratory, UK) at 90^0 and 10^0 take-off angles. The spectra were referenced to the Au 4d 5/2 line positioned at 335.0 eV and Au 4f 7/2 line positioned at 84.1 eV. All molecules were adsorbed onto a gold-on-glass substrate from a 1×10^{-4} M dry DCM solution. The adsorption times were 30 seconds and 24 hours for low and high coverages respectively. The gold substrate was flame annealed in a butane flame just prior to adsorption.

2.3 Electrochemical studies - Cyclic Voltammetry

Cyclic voltammetry is a potential sweep technique where the potential is a linear triangular function of time (Figure 2.3). The potential time waveform shows that the potential is swept linearly between two potentials E_1 and E_2. Upon reaching the point E_2 the potential sweep is reversed. Current is monitored during the cyclic voltammetric sweep.

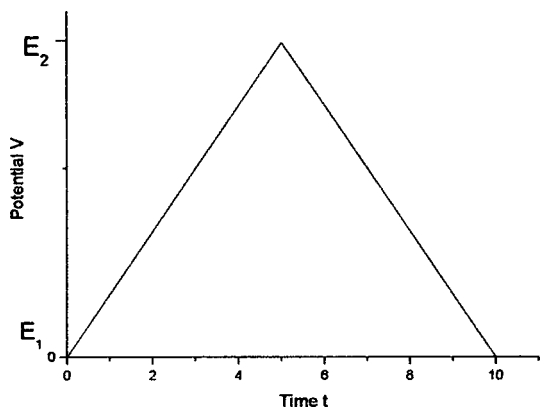

Figure 2.3. Potential time waveform for cyclic voltammetry.

The potential is usually applied to the working electrode in a sawtooth manner. A cyclic voltammogram is thus the plot of the current through this electrode as the potential is changed in a linear fashion, then returned in the opposite direction linearly and so on.

2.4 I(s) and I(t) methods

Experiments were performed using a Pico2000 (Molecular Imaging) STM. We employed the scanning tunnelling microscopy (STM) based I(*t*) and I(s) techniques to determine the single molecule conductances of all molecules studied in this thesis. The general procedure followed for each method is as follows. A gold-coated glass slide was flame-annealed (to red heat) using a butane flame for 10-15 seconds, allowed to cool, and then flame-annealed a second time. This procedure is known to produce atomically flat surfaces. The gold-coated glass slide was then immersed in a dilute (10^{-4} –10^{-5} M) solution of the appropriate dithioacetate for one minute to allow the formation of a low coverage monolayer. It was not necessary to remove the thioacetate groups prior to adsorption as they are found to cleave on gold forming the Au-S bond in the traditional manner in ambient air, as determined by our XPS studies.

After fixing the gold slide onto the sample plate and inserting it into the STM, a gold tip is brought to a 'fixed' distance above the gold surface - controlled using the set point current. The distance will vary slightly due to the differently conducting areas of the sample, especially in the presence of molecules.

I(t) method - For the I(t) measurements the feedback loop is switched off and the current is monitored as a function of time. Molecules which

spontaneously form and unform bridges between tip and surface cause jumps in the tunnelling current. The jumps are interpreted as the additional current due to conductance through the molecule(s). These jumps are analysed statistically and figure 2.4 shows a typical histogram for such an experiment. For a jump to be considered it must show two fairly level plateaus on either side. The absolute difference between plateaus is what is recorded in the histogram.

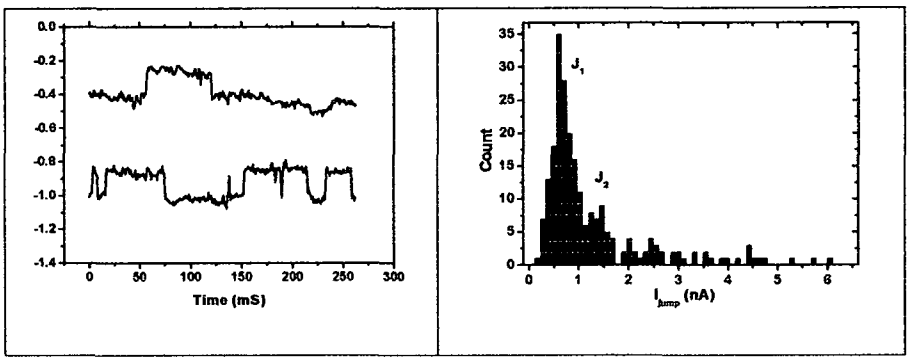

Figure 2.4. a) Example of I(t) current jumps observed for molecule 6Ph6 under perfluorononane. I_{set} = 1 nA, U_{bias} = 0.2 V. b) Histogram of the recorded jump sizes obtained at I_{set} = 3 nA, U_{bias} = 0.6 V for molecule 6Ph(OMe)$_2$6.

The experiment is repeated at different tip–substrate bias potentials, and the mean single molecule current is then plotted against the bias potential. The slope gives the molecular conductance.

An alternative way of analysing I(t) data is to set the baseline current in each trace to zero. Then all the data points can be summed together producing a histogram of the different plateaus in the current. Both methods have been used in this work and this is mentioned where appropriate.

I(s) method – For the I(s) measurements the tip is withdrawn a certain distance, while maintaining a constant x–y position, from the initial set point current, with the feedback loop disabled, to a pre set distance approximately twice the molecular length. A current–distance, I(*s*) curve is collected, where s is the relative tip–sample distance. We typically observe current–distance behaviour characteristic of the formation of molecular wires with a plateau in the current (I_M) due to conductance through the fully extended molecule in its lowest-energy conformation. As the tip is withdrawn further, the molecule then detaches at a distance characteristic of its length.

Again, the experiment is repeated many times, and the results are analysed in a statistical manner. The data points in I(s) scans containing molecular plateaus are added together into one histogram, which gives a peak at the value of the average plateau. This method of analysis lends weight to the longer, therefore more reliable, current plateau as these contain a large number of data points. Data which displays only exponential background tunnelling or very 'noisy' curves are rejected. This is, admittedly, arbitrary. However, sometimes molecules seem to be very unstable in the junction and give erratic signals which cannot be trusted. In these cases the current increases and decreases wildly over the scan, giving the appearance of 'noise'. Only those which contain well defined plateaus are considered valid, as shown in figure 2.5.

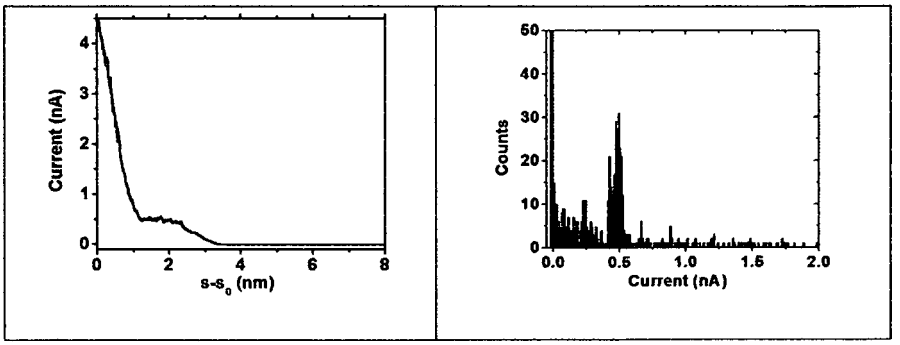

Figure 2.5. Example *I*(*s*) curve and the corresponding histogram of the data points. The 'counts' correspond to the number of points at a particular current value.

Chapter 3

Redox active molecular wires. Pyrrolotetrathiafulvalene (PTTF) versus viologen

Chapter 3

Redox active molecular wires.

Pyrrolotetrathiafulvalene (PTTF) versus viologen

3.1 Tetrathiafulvalene

Tetrathiafulvalene (TTF) and its derivatives are an interesting class of molecules in the field of organic electronics. Their electronic and magnetic properties arise from the ability to show reversible, stable, redox behaviour under ambient conditions, a high lying HOMO level and their rigid structure. TTF undergoes two reversible single electron oxidation processes resulting in the formation of a radical cation followed by a dication species. The transitions are achieved under mild conditions (+0.34 V and 0.78 V versus SCE)[1] and the species formed are highly stabilised due to the aromaticity of the 1,3-dithiolium rings (figure 3.1). The radical cation also benefits from being a planar structure which allows a high degree of delocalisation across the moiety.[2]

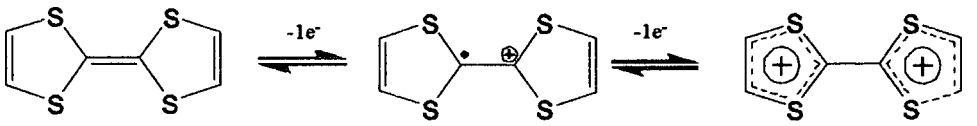

Figure 3.1. The three oxidation states of TTF. Neutral (left) radical cation (middle) and dication (right).

Initially efforts were focused on improving the conductivity of TTF salts and charge transfer (CT) complexes, after the discovery of the first metallic CT complex,[3] by improving the electron donating ability of the TTF group. Recent developments in the organic synthetic chemistry of TTF derivatives[1] have, however, increased the scope of the compound as a core building block in many areas of organic electronics, especially molecular electronics. In particular is the development of a class of compounds known as pyrrolo-TTFs (or PyTTFs) which consist of two pyrrol rings fused to the 3,4 and 3',4' positions of a central TTF.

3.2 Pyrrolo-Tetrathiafulvalene (PTTF)

For single molecule conductance measurements, a TTF would need two appended thiaalkyl group substituents, one on each ring. However, synthetic routes used inevitably make TTF compounds in a cis/trans mixture (owing to is D_{2h} symmetry). These isomers are often almost impossible to separate. TTF also isomerises between cis and trans in the presence of light[4] or the presence of acid[5]. This makes the use of TTF

unsuitable for single molecule work. PTTFs, on the other hand, can be functionalised via the terminal nitrogens into symmetric compounds whilst retaining the essential electrical properties of the parent TTF. We decided to study a PTTF derivative, HS-$(CH_2)_6$-PTTF-$(CH_2)_6$-SH – 6PTTF6, as it is a good candidate to display redox addressable conductance switching.

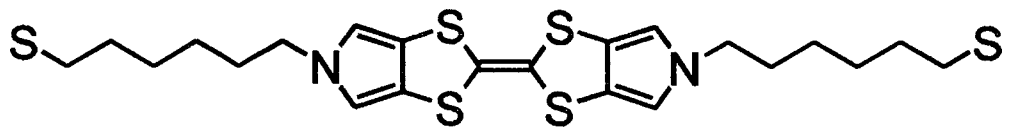

Figure 3.2. Structure of '6PTTF6'.

The design of the 6PTTF6, shown in figure 3.2, is such that the redox moiety is placed at the centre of two thiohexyl chains. In this configuration, the redox groups are electronically "decoupled" from the enclosing metal contacts by the $(CH_2)_6SH$ arms, giving double tunneling barriers. This is the same arrangement as in a molecule previously studied, and discussed here, namely 6V6, which has a viologen redox active core.

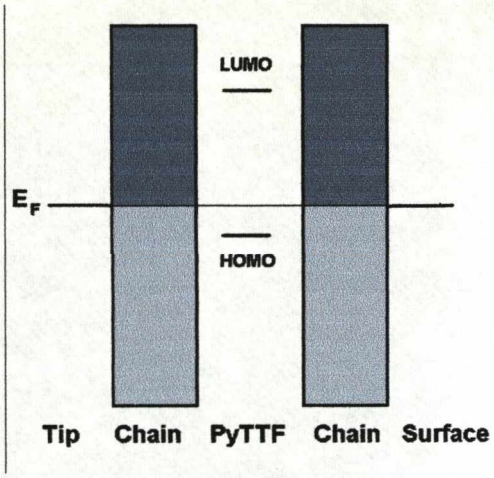

Figure 3.3. Double tunnel barrier representation of 6PTTF6.

The PTTF can be thought of as a quantum well in the middle of the two barriers, which can be shifted up or down in energy with respect to the electrodes by means of applying an overpotential (gating voltage). This is carried out using a four electrode electrochemical setup whereby two working electrodes are controlled through a reference electrode, and a counter electrode is present to balance Faradaic currents. There is a clear analogy in these experiments to a molecular transistor, with the tip and surface acting as source and drain, I_{SD} being the current flow between these two electrodes, while the counter electrode acts as a "gate". The gate voltage falls across the electrical double layers at the electrode/electrolyte interfaces.

3.3 Aims

The aim of the study is to compare the behaviour of the PTTF compound with two other similar structures, one also redox active and one redox inactive. The first is the viologen compound 6V6 previously reported[6, 7] which is redox active, and the second is the compound 6Ph6[8] which contains a central redox inactive benzene ring.

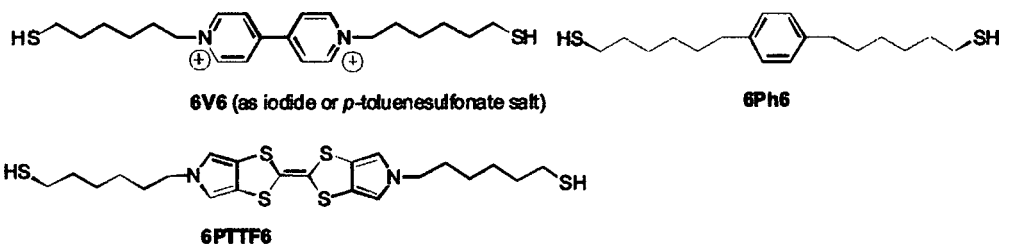

Figure 3.4. Structures of 6V6, 6Ph6 and 6PTTF6.

All three compounds (figure 3.4) contain the same thiahexyl groups on opposite side of the central aromatic group making them all symmetric and equally coupled to the gold electrodes. The benzene compound serves as a control experiment as we do not expect it to show any potential induced switching owing to its electrochemically inaccessible energy levels in an aqueous environment.

3.4 Synthesis

Synthesis of 6PTTF6

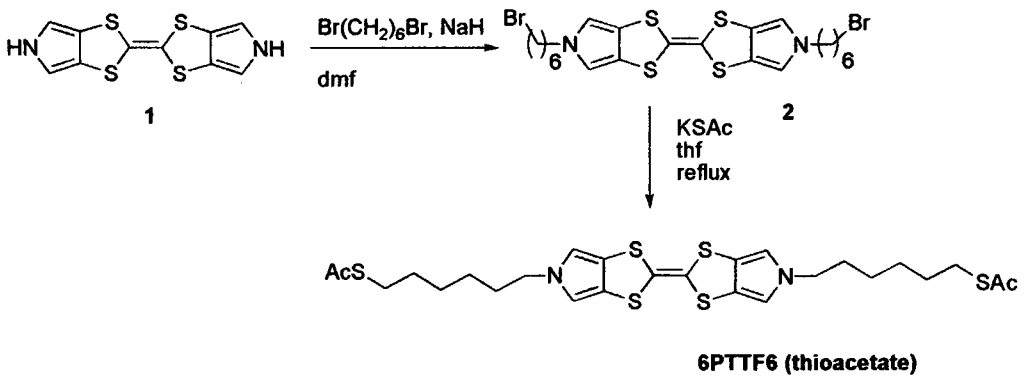

Figure 3.5. [9] **6PTTF6 was synthesised by the group at The University of Southern Denmark, Odense, Denmark by Sune Nygaard (see chapter 9 for full synthesis).**

Synthesis of 6V6[6]

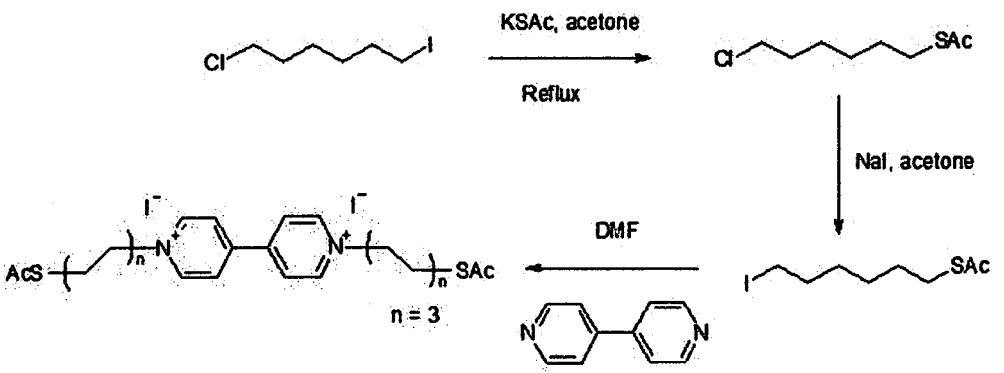

Figure 3.6.[10] **Potassium thioacetate and 1-chloro-6-iodohexane were refluxed in acetone overnight to yield 1-chloro-6-acetylsuphanylhexane, which was isolated using flash chromatography. This was treated with excess sodium iodide in acetone and refluxed over night. This resulted in 1-iodo-6-acetylsuphanylhexane, which was mixed with 4,4'-bipyridyl (4:1 molar ratio) and maintained at 80°C for 4 days. The N,N-di(6-thioacetohexyl)-4,4'-bipyridinium diiodide salt precipitated.**

Synthesis of 6Ph6

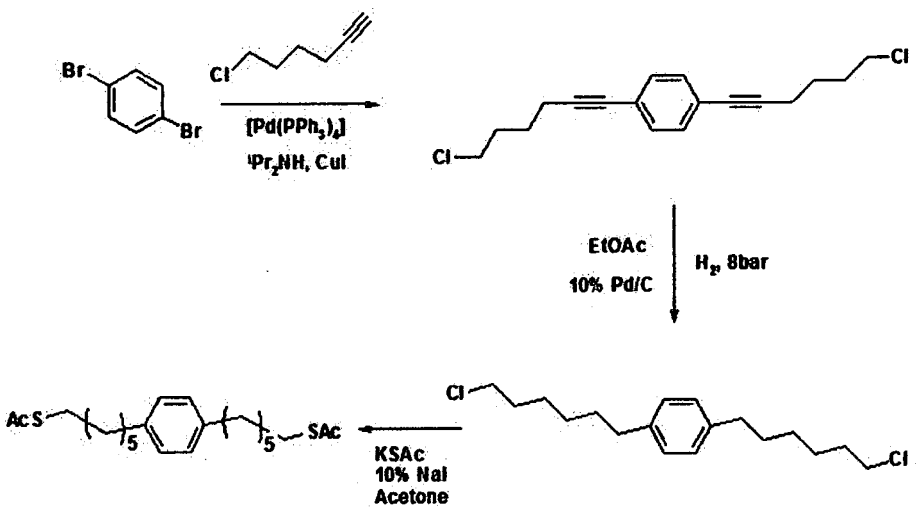

Figure 3.7. (see chapter 3)

3.5 X-Ray Photoelectron Spectroscopy of 6PTTF6 monolayers

Characterisation of 6V6 adsorption on Au(111) has been previously presented.[11] Spectra were acquired using a Scienta ESCA 300 spectrometer (NCESS, Daresbury Laboratory, UK) at 90^0 and 10^0 take-off angles; we present the 10^0 angle data here. The spectra were referenced to the Au 4d 5/2 line positioned at 335.0 eV. The molecule 6PTTF6 was adsorbed onto a gold-on-glass substrate from a 1 x 10^{-4} M dry DCM solution. The adsorption time was three minutes. The gold substrate was flame annealed in a butane flame just prior to adsorption.

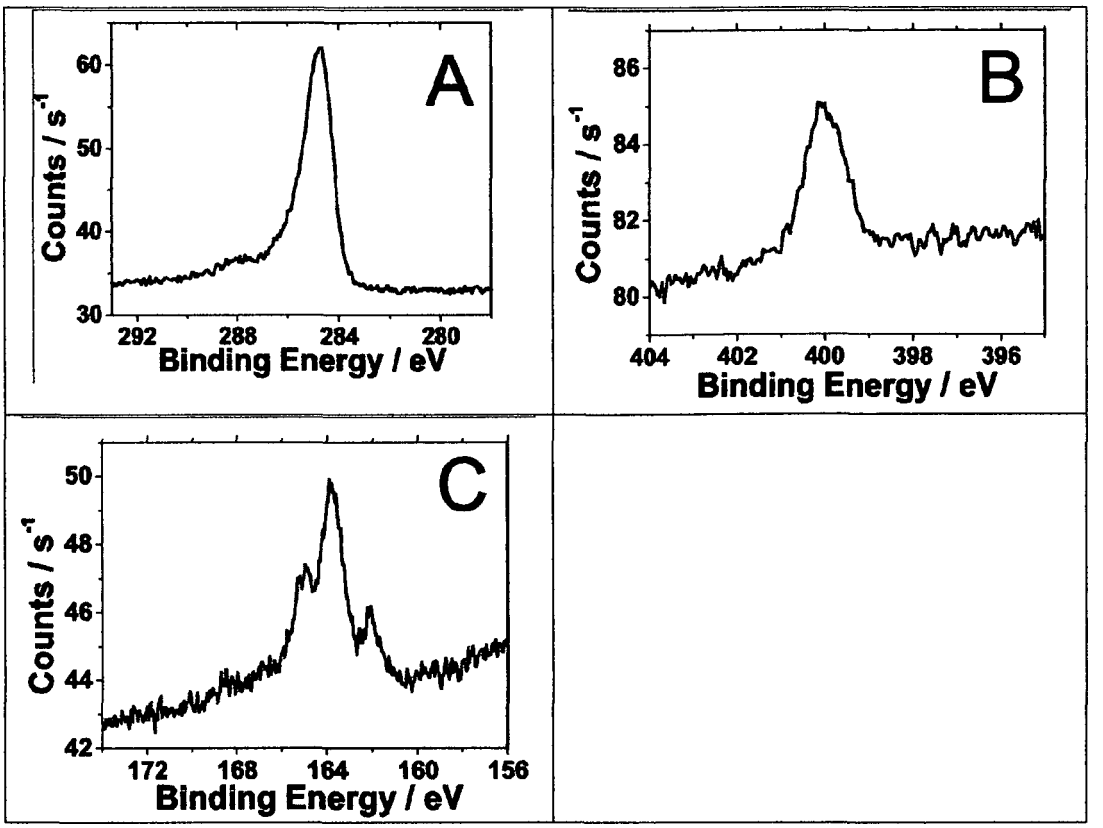

Figure 3.8. XPS spectra of 6PTTF6. A = C1s region; B = N1s region; C = S2p region.

Peaks due to carbon, nitrogen and sulphur were observed, consistent with the molecule adsorbed to the surface intact. Visible in the S2p spectrum is a peak due to sulphur bound to gold, at 161 eV[4] (i.e a full Au-S bond). The larger peaks at 164 eV and 164.5 eV are due to the sulphur in the TTF core, (plus some contribution from the second bound sulphur peak which will overlap with the peak at 164 eV).

3.6 Surface cyclic voltammetry

Cyclic voltammetry was used to measure the formal potential for the V^{2+} $\leftrightarrow$ $V^{+\cdot}$ / PTTF $\leftrightarrow$ $PTTF^{+\cdot}$ couples. Although the peak separation for both surface redox process depends strongly on sweep rate, the mean peak potential (E_0) = (E_{pa} + E_{pc})/2) remains almost constant (± 5 mV), and this mean peak potential is quoted. E_{pa} and E_{pc} are the anodic and cathodic peak potentials. All potentials are referred to the SCE electrode. All cyclic voltammetry (CV) experiments were carried out using an AutoLab PGSTAT 20 (Eco Chemie, The Netherlands) computer-controlled instrument. A Au(111) single-crystal electrode was employed as the working electrode with a surface area of 1.1 cm^2. 0.1 M phosphate buffer solution at pH 6.8 ($NaHPO_4/Na_2PO_4$ in water) was used as the electrolyte and was degassed with nitrogen prior to measurements.

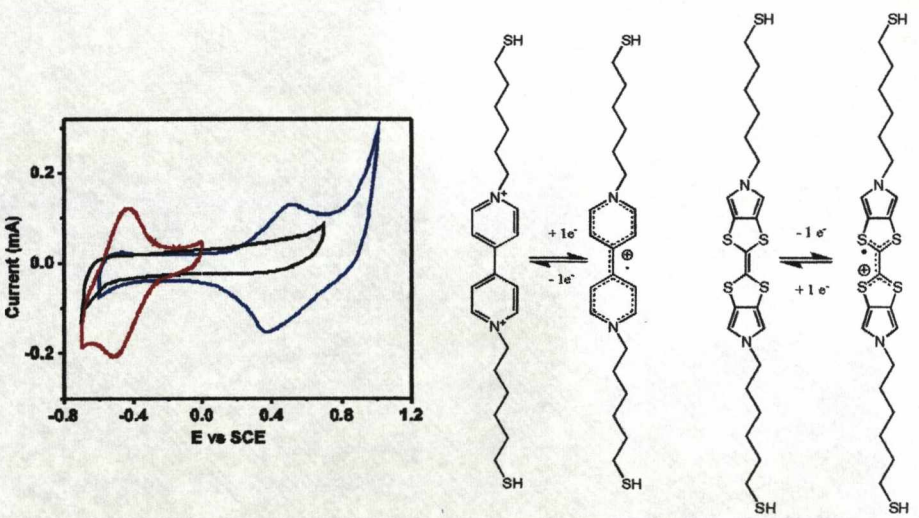

Figure 3.9. Surface cyclic voltammetry of monolayer coverages of 6V6 (red), 6PTTF6 (blue) and 6Ph6 (black).

E_0 = -0.42 V for 6V6

E_0 = 0.45 V for 6PTTF6

All cyclic voltammograms are shown to the same scale. Figure 3.9 shows the redox transitions for 6PTTF and 6V6. There is a second oxidation of 6PTTF6, to the dication state, which was not observed on gold due to gold oxidation which takes place between 0.8 and 1.0 V vs SCE, concomitant with the position of this process.

3.7 Scanning Tunnelling Spectroscopy

Gold STM tips and chromium-primed gold film on glass slides were used throughout. The tips were coated with Apiezon® wax to leave only the outermost apex in contact with the electrolyte.[12] Experiments were performed using a Pico2000 (Molecular Imaging) STM in 0.1 M phosphate buffer solution at pH 6.8 ($NaHPO_4/Na_2PO_4$ in water). Gold wires were used as the counter and reference electrodes (forming a gold oxide quasi reference electrode). Samples were flame-annealed prior to the experiments. The gold films were immersed in a 1 x 10^{-4} M solution of the relevant compound in dichloromethane (distilled from $CaCl_2$) for three minutes and after attachment, the samples were thoroughly washed

in pure DCM and blown dry with nitrogen. Cyclic voltammograms were recorded at the beginning and end of the experiments to check for drift in the reference electrode and the quality of the molecular layer. The single molecule measurements were carried out using the I(s) technique as previously described. 100 I(s) curves were recorded at each different gate potential. The gate potential was increased in steps of 100 mV from 0 to 0.6 V vs SCE.

3.8 I(s) – current-distance results – 6PTTF6

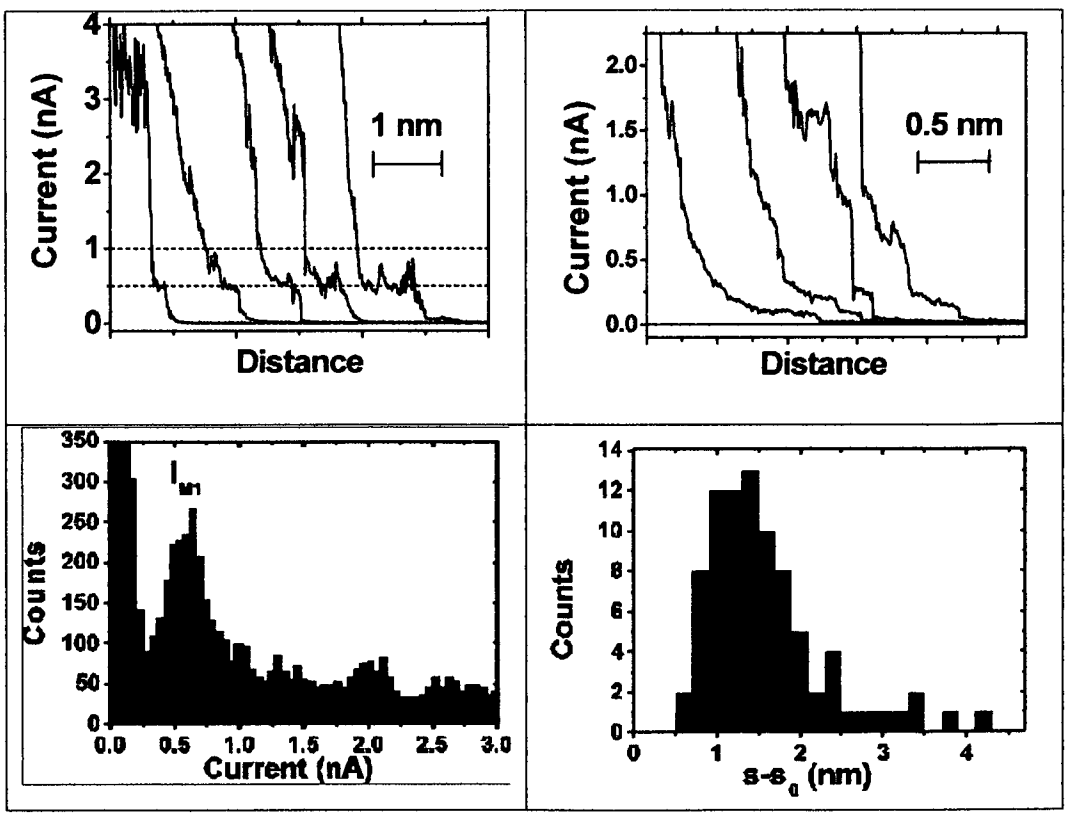

Figure 3.10. From top left: (1) I(s) spectroscopy examples for 6PTTF6. E_S = 0.46 V (vs SCE), U_{Bias} = -0.2 V and I_0 = 6 nA. (2) E_{Gate} = 0.66 V. (3) Histogram of I(s) curves at E_S = 0.46 V. (4) Histogram showing the break-off distance for each molecular wire measured at E_{Gate} = 0.46 V.

The S-S distance (determined from SPARTAN implementation of DFT (B3LYP/6-31G**) was 2.78 nm and s_0 was estimated to be 1 nm by extrapolation of the tunnelling current, in the absence of wire formation, back to G_0. Assuming that the conductance at the point where the tip would make mechanical contact with the surface is the conductance quantum G_0 ($G_0 = 2e^2/h$) provides the basis for an 'absolute' calibration of the gap separation at a given current according to Equation 1:

$$s(I) = \frac{\ln(G_0 \times U_0 / I)}{d\ln(I)/ds}$$

U_0 is the tip-sample bias voltage. As mentioned in chapter 2 the absolute distance depends on the conductivity of the sample, which changes from area to area with the surface quality and adlayer composition. Thus the absolute distance should be different with a molecule is inside the tunnel gap (although not necessarily bound to both electrodes) and without. Therefore this analysis gives an approximate break-off distance only.

For 6PTTF6 this method gave a mean wire break off distance of (2.34 ± 0.33) nm. Out of approximately 1000 I(s) scans about 70 to100 scans were saved which showed high quality discernable plateaus, characteristic of a molecule present between both electrodes. Those with no discernable current plateau were discarded and not included in the histograms. As described in the literature current plateau or steps have been related to

single or multiple molecules bridging the tip and substrate gap. Our histograms recorded for both 6PTTF6 and 6V6 showed a clear current peak marked as I_M in figure 3.10. Under this low coverage, low current set point conditions, higher current peaks are barely discernable. We tracked the position of this primary peak as a function of the overpotential.

3.9 Summary of conductance-overpotential relations for 6V6, 6PTTF6 and 6Ph6

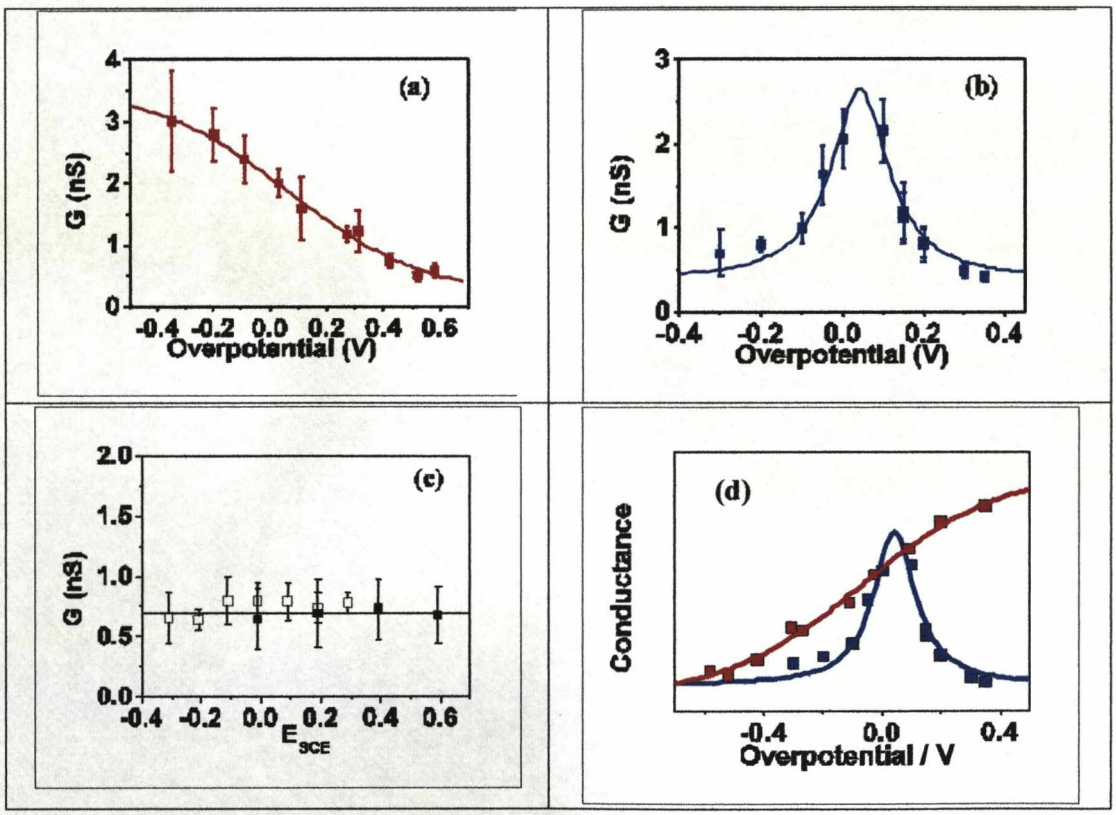

Figure 3.11. Single molecule conductance of (a) 6V6 (Red), (b) 6PTTF6 (Blue) and (c) 6Ph6 (Black), versus the overpotential (η) for the redox molecules and the electrode potential for 6Ph6. Data for filled symbols obtained using I(s) method; for open symbols using I(t) method. All fitting lines are guides for the eye only. (d) 6V6 plotted as overpotential multiplied by -1 (-η) and 6PTTF6 shown on the same axis.

The overpotential is taken as the potential experienced by the redox group, located in the middle of the junction. This is given by the equation,

$$\eta_{redox} = \eta + \tfrac{1}{2}V_{bias}$$

where η is the overpotential versus the saturated calomel electrode (i.e. the fraction of the substrate electrode-solution potential drop at the site of the molecular group is taken as 1. The fraction of the bias voltage at the molecular site is taken as 0.5). This is, at best, a guess as we do not consider the full nature of the electrolyte. However at low concentrations these should be reasonable assumptions.[7]

3.10 Theory

Figure 3.11 shows single molecule conductance data for each molecule as a function of the overpotential (redox active molecules) or electrode potential (6Ph6). For 6PTTF6, the data shows a conductance rise from ~0.5 nS in its neutral state to a maximum close to 2.5 nS, which falls again to the "off" conductance value of ~0.5 nS at positive overpotentials. The width of the conductance peak is ~0.2 V, in the range expected[12] for the tip-to-sample bias voltage of 0.2 V employed in these experiments. The conductance of the redox-inactive 6Ph6 is similar to that of the "off" states of 6V6 and 6PTTF6 but does not change as a function of potential; the frontier π–orbitals of the benzene ring are too far from the E_F of Au to be

brought into close proximity by gate potentials accessible in these experiments. The "classical" behavior of the gold|6PTTF6|gold single molecule junction, with a symmetrical peak close to the first oxidation potential for PTTF, can be rationalized both in terms of two-step (hopping) mechanisms and superexchange (tunneling) modes.[7, 13]

3.10.1 Two-step electron hopping theory

In the two step hopping mechanism the oxidized ($PTTF^{\cdot+}$) and reduced ($PTTF^{0}$) forms contribute comparably at the equilibrium redox potential to the tunneling current across the molecular junction[14]. A maximum would then result in the conductance vs. overpotential relationship, as is experimentally observed.

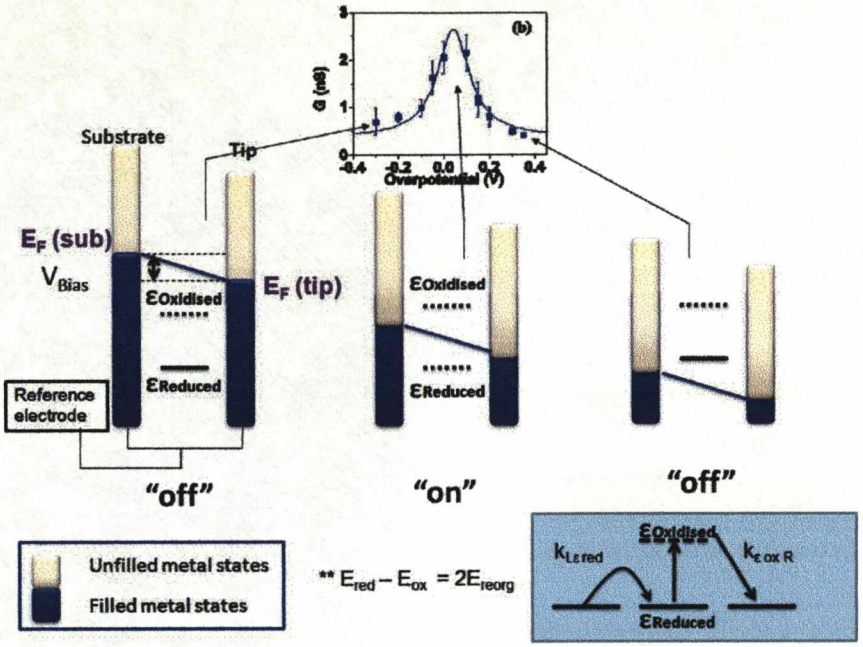

Figure 3.12. Energy level diagram of tip, substrate and redox level in the in situ STM configuration. See page 88 for explanation concerning the separation between ε_{ox} and ε_{red}.

Experimental investigations of single-molecule electrochemical redox switches were initiated by Tao's report[15] that showed tunnelling current features of a single redox molecule (iron protoporphyrin IX) with a maximum in the apparent height vs overpotential dependence at the equilibrium potential. The theoretical explanation given of these data used concepts of resonant tunnelling.[16, 17] Electron tunnelling through a single, i.e., the oxidized state of the redox group was thus considered, with emphasis on the inverted free energy region.

Further studies[18] and later reports [19-21] have shown that the inclusion of both valence states in the theoretical understanding is of prime importance for the dynamic nature of the process. This is because the charge resides in

the redox level for some period of time during the transfer between one electrode and the other (figure 3.12). This causes the redox level to relax to a new energetic position. The redox level can exist in an oxidized, ε_{ox}, and a reduced state, ε_{red}, the equilibrium positions of which are separated by twice the environmental reorganization free energy, λ, i.e. $\varepsilon_{ox} - \varepsilon_{red} = 2\lambda$. In terms of whether the molecule possesses a low lying LUMO level, or a high lying HOMO level, tunnelling will take place with electrons or holes respectively. In the case of electron tunnelling the level is initially empty (oxidized) and located above both Fermi levels. In the case of hole tunnelling the level is initially filled (reduced) and located below both Fermi levels. In this configuration tunnelling may proceed in a superexchange manner via non-localisation of charge on the redox centre in which the intermediate, molecular, levels are not populated but couple purely electronically the 'donor' and 'acceptor' states, i.e. with 'virtual' population. This is favoured relative to direct tunnelling because of the much shorter nearest-neighbour distances in the superexchange mode. This corresponds to the first 'off' state of the molecule (at potentials negative of the redox peak). With the application of a potential such that the redox level now lies close to, or inside the Fermi window of the electrodes, with the level position also assisted by thermal fluctuations, interfacial charge transfer from one electrode to the molecular level occurs. In the case of the PTTF this involves hole transfer to ε_{red} thus transforming the level to ε_{ox}. Electronic relaxation then occurs primarily as the solvation shell must now

accommodate the change in charge of the molecule by reorganising itself. When V_{bias} is small (less than a few hundred mV) this relaxation places the level outside the Fermi window (common values for the outer-shell (solvent polarization) component of the reorganization energy found in electron-transfer phenomena are between 0.4 and 0.6 eV). The next step in the charge transfer process involves tunnelling of the charge through the second barrier between the redox centre and the second metal electrode which completes the cycle. This is a thermally activated process due to the level now lying outside the Fermi window. The equilibrium value between the oxidised and the reduced state does not in general coincide with the standard redox potential and differs from the latter because of, in particular, changes in potential at the site of the redox group when inside the tunnel junction. However, the maximum value of the tunnelling current will occur when the rates of both interfacial charge transfer processes are equal, when the equilibrium position of the redox level lies level within the Fermi window, corresponding to the "on" state of 6PTTF6.

3.10.2 Two-step electron transfer model in relation to Marcus theory of inner-sphere electron transfer[22, 23]

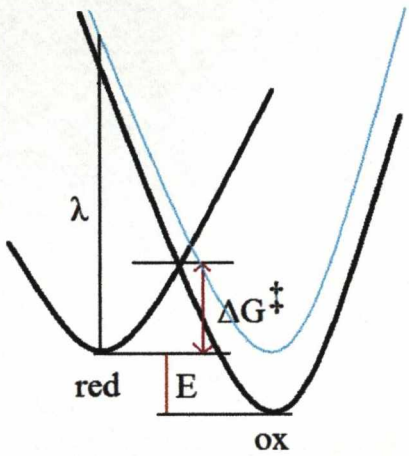

Figure 3.13. ET transitions along the nuclear reaction coordinate *q* from the initial to the final equilibrium configuration in the "normal" overvoltage region.

In the parabola representation of an electron transfer event the vertical axis is the free energy and the horizontal axis is the 'reaction coordinate' – a simplified axis representing the motion of the atomic nuclei being reorganised. The left hand parabola represents the free-energy surface for the nuclear motion of the reduced level (where the electron is on the molecule or group), and the right hand parabola represents the potential energy surface for the nuclear motion of the oxidised level (after the electron has transferred from the molecule to the acceptor electrode). The dependence of the electron transfer rate on the free energy change is

expressed in terms of a quadratic equation, hence the parabola shape of the potential energy surfaces,

$$\Delta G^{\ddagger} = (\lambda + e\eta)^2 / 4\lambda$$

This is a slightly modified form of the general Marcus equation, which correlates the Gibbs energy of activation ($\Delta G^{\ddagger}$) with the driving force ($\Delta_r G^{0'} = e\eta$) of the reaction. ¼ λ is the intrinsic barrier of the reaction. The driving force for electron transfer in our situation is given by the magnitude of the overpotential, η. The difference in energy between the oxidised and the reduced states amounts to the fraction of the overpotential and the fraction of the bias voltages experienced by the redox centre ($e\xi\eta + e\gamma V_{bias}$, $0 < \xi$ *and* $\gamma < 1$), and can be equated to the energy, E, liberated in an exothermic reaction. Crucially, if the liberated energy E, or $e\xi\eta + e\gamma V_{bias}$, is equal to λ, then $\Delta G^{\ddagger}$ will be equal to zero and the reaction is very fast, corresponding to the maximum in electron transfer and the onset of activationless behaviour. This corresponds to the "on" state in the conductance-overpotential relation of 6PTTF6.

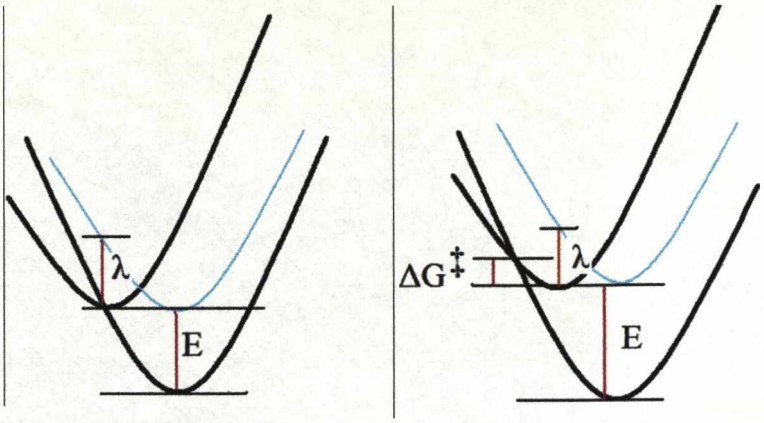

Figure 3.14. ET transitions along the nuclear reaction coordinate *q* from the initial to the final equilibrium configuration in the "activationless" (left) and "inverted" (right) overvoltage regions.

For E, or $e\xi\eta + e\gamma V_{bias,} > \lambda$ the so called inverted region is reached (figure 3.14) where the activation energy Gibbs energy of activation ($\Delta G^{\ddagger}$) increases with the driving force (essentially the overpotential, η, in the case of electrochemical STM). The reaction is thus slower the greater the driving force, or η. This was the prediction of Marcus which was verified by numerous experiments[24] much later. The "inverted" overpotential range is reached when the overpotential is high enough for the vacant molecular level to be initially above (in the case of shifting to positive values of η for 6PTTF6) both Fermi levels. As the molecular level is, however, rapidly converted to the relaxed *oxidised* form, a small steady-state current from the negatively biased electrode to the oxidised level ("electron transfer") still flows. This process becomes more difficult the higher η becomes and corresponds to the second "off" state of the molecule.

3.11 Discussion

The question now becomes: why does the PTTF moiety show classical two step transfer behaviour, whilst the viologen moiety does not? We can draw upon the similarities, which are that both contain the same thiahexyl linker groups, both are roughly the same length and both form a radical cationic state at their redox transitions. Different self-exchange rates between the two molecules at electrochemical interfaces or in homogeneous solution would give different absolute tunnelling currents. There are small difference in electron self-exchange rate constants (k_{se}) between viologens (e.g. $MV^{2+/\cdot+}$; k_{se} $8.1\cdot10^{8}$ $M^{-1}s^{-1}$ [25]) and TTFs (e.g. $Me_4TTF^{0/\cdot+}$; k_{se} $3.3\cdot10^{9}$ $M^{-1}s^{-1}$ [26]). This, however, cannot account for the different *forms* of the current-overpotential relations for 6V6 and 6PTTF6. This is illustrated by the different behaviour of a pair of structurally identical Os and Co complexes; self-assembled monolayers incorporating $[Co(terpy)_2]^{2+/3+}$ and $[Os(2,2'\text{-bpy})_2(4,4'\text{-bpy})Cl]^{2+/3+}$ units both show current-overpotential relations in scanning tunneling spectroscopy experiments similar in form to 6PTTF6, yet they have very different interfacial electron transfer rates, $>10^{6}$ s^{-1} (M = Os) and ca. 10^{3} s^{-1} (M = Co).[27] The similar self-exchange rate constants for the viologen and PTTF systems can qualitatively explain the similar values of the conductance at the formal zero overpotential value (close to 2.5 nS)

The conductance of both 6V6 and 6PTTF6 in the 'off' state, and the factor by which the conductance changes on reduction (6V6) or oxidation (6PTTF6), are similar. The difference clearly must lie in the properties of the central redox moiety, because the flexible alkyl spacers are present in all three molecules. Both the neutral PTTF moiety[28] and structurally-characterized $TTF^{\cdot+}$ derivatives[29] are planar in the solid state. DFT calculations [30] show that the PTTF core of an isolated molecule (as found in metal-molecule-metal junctions) is also planar for both states. Viologen dications can be planar or twisted about the inter-ring C-C bond, depending upon the anion, suggesting that inter-ring twisting is a low-energy process.[31] Strong π-π interactions in the solid state mean that the sole crystal structure of a $V^{\cdot+}$ salt [32] can tell us little about the likely configuration of an isolated molecule, but greater coplanarization upon reduction and increased inter-ring C-C double bond character is predicted.[33] There are therefore significant configurational differences between V^{2+} and $V^{\cdot+}$ that are not apparent in the PTTF system, demonstrated in figure 3.15.

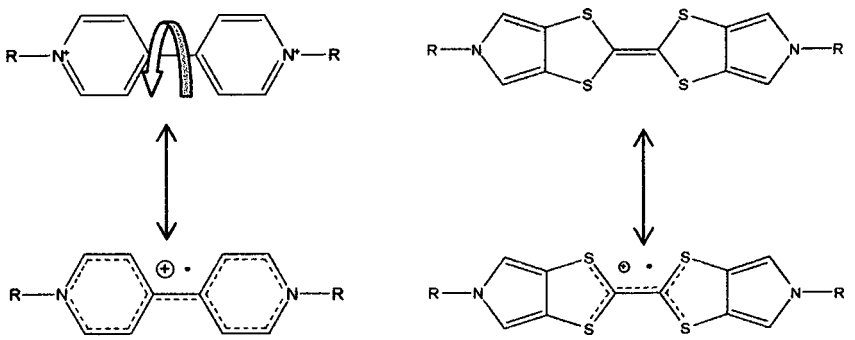

Figure 3.15. Viologen dication and radical cation states (left) and PTTF neutral and radical cation states (right).

It was demonstrated recently that the conductance for a series of diamino-biphenyl derivatives decreases with increasing torsion angle between the two phenyl rings,[34] consistent with a cosine-squared relation predicted for transport through *p*-conjugated biphenyl systems.[35] The magnitude of change between the ring locked fluorene molecule ($\theta = 0^0$) and the completely out of phase 3,6-3',6'-tetramethyl-biphenyl molecule ($\theta = 88^0$) was slightly over a factor 3. Whilst this is not a huge effect, the results suggest that tunnelling is non-resonant for this particular system. In the case of the viologen, the energy levels are much more closely aligned to the metal Fermi levels of the electrodes so that the influence of the torsion angle could become magnified. However, if resonant tunnelling was operative in the viologen/PTTF junctions, a conductance much closer to G_0 would be predicted due to resonant tunnelling predicting transmissions of near unity.

Closer inspection of the overpotential relation reveals that the conductance of the viologen proceeds to increase further even after the formal reduction potential has been attained. There is very little reason to believe that the dication dominates in the molecular junction after this potential has been reached, due to the overall similarity to the 6PTTF6 molecule. Hence, we propose that a competing effect is present in the viologen system, which is absent in the PTTF, namely that as the potential is raised closer to the second reduction point (~0.9 V)[36] that the molecule in the junction has progressively more planar character. This comes naturally out of the two step formalism of the electron transfer as once the position of the molecular level (ε_{ox}) is below the Fermi level of the electrodes (in the case of the viologen) and the first step in the cycle, reduction of the oxidised level, is facile and is not a rate limiting step. Therefore, the difference between the behaviour on opposite sides of the formal redox potential in the case of the viologen is down to the rate determining step either involving the planar molecule or ring twisted molecule. The less conductive rotational V^{2+} state dominates in the first rate determining step at potentials positive of -0.42 V, whilst the $V^{\cdot+}$ dominates in the second, rate determining, step at potentials negative of -0.42 V. This probably indicates that the reorganisation energy is substantially greater for the viologen than for the PTTF due to this large rearrangement of the two pyridinium rings.

A further, interesting, consideration is how would the conductance behave upon the second redox transition in both molecules? One could postulate that the total behaviour for both molecules would be the two individual molecule's behaviours joined together. This is because the two processes of reducing the viologen and oxidising the PTTF essentially mirror each other. However, this cannot be so as the viologen conductance still appears to increase up to almost the second reduction. By purging our liquid cell with argon we were able to reach a potential of -0.8 V before moving into the hydrogen evolution and thiol desorption regions. This is only 0.1 V lower than the second reduction process. It must be pointed out that the neutral viologen species is extremely sensitive to any trace of oxygen, and as the process is concomitant with H_2 evolution, we were unable to detect its presence. However, the confinement of the molecule in the junction, combined with the fact that at the resonance position equal amounts of oxidised (now the radical cation species) and reduced (neutral species) are present, one could assume that the influence of oxygen on the neutral species is negligible. Thus, the conduction at 0.1 V below the second reduction of the viologen should correspond to the conduction at 0.1 V after the first oxidation of the PTTF. The situations are, however, clearly different as the conductance returns quickly to the "off" value of 0.5 nS for the PTTF, whilst the viologen in still in the "on" state. This leads to the conclusion that hysteresis must be present in the two systems, and that the observed conductance-overpotential relation depends upon the starting

point in both systems, i.e. the structurally rigid neutral state, or the more flexible dicationic state. Also, no rise is seen approaching the second oxidation of the PTTF, which unfortunately coincides with the gold oxidation process at 0.7 – 1.0 V versus SCE. Why this is the case is unclear at this stage as alignment of the next molecular level should bring about another rise in the conductance.

3.12 Summary

In summary, we have shown that archetypical redox switching can be obtained in gold|6PTTF6|gold single molecule junctions. We have achieved defined *off-on-off* switching in these junctions which is controlled by the redox electrochemistry of the PTTF group. Differences between the conductance-overpotential behavior of 6V6 and 6PTTF6 are rationalized in terms of conformational dynamics of the respective systems which arise from the presence of a facile ring rotation between the two pyridyl rings of the viologen. This highlights the need to consider structural effects in single molecule electron transfer processes, not just electronic diferences, with such effects adding an extra layer of complexity to the phenomenon. Future work will involve the study of molecules with differing degrees of inter-ring rotational freedom to determine, perhaps, a transition between the classical and non-classical responses. Another line

of investigation will be aimed at studying systems over two full redox transitions (see the work of Albrecht et.al[37]) . This is more difficult as systems with such stable processes in range of our experiments are rare. However, changing the experimental conditions to extend the window of measurement could be one possible route to studying further both viologen and PTTF systems further. Ionic liquids, for example, have stability ranges of several volts and therefore offer the potential to access higher molecular redox states.

Bibliography

[1] J. O. Jeppesen, J. Becher, *Eur. J. Org. Chem.* **2003**, 3245-3266.

[2] M. A. Herranz, L. Sanchez, N. Martin, *Phosphorus Sulfur Silicon Relat. Elem.* **2005**, *180*, 1133-1148.

[3] J. Ferraris, V. Walatka, Perlstei.Jh, D. O. Cowan, *J. Am. Chem. Soc.* **1973**, *95*, 948-949.

[4] Y. N. Kreitsberga, E. E. Liepinsh, I. B. Mazheika, O. Y. Neiland, *Zhurnal Org. Khimii* **1986**, *22*, 416-420.

[5] A. Souizi, A. Robert, P. Batail, L. Ouahab, *J. Org. Chem.* **1987**, *52*, 1610-1611.

[6] W. Haiss, H. van Zalinge, S. J. Higgins, D. Bethell, H. Hobenreich, D. J. Schiffrin, R. J. Nichols, *J. Am. Chem. Soc.* **2003**, *125*, 15294-15295.

[7] W. Haiss, T. Albrecht, H. van Zalinge, S. J. Higgins, D. Bethell, H. Hobenreich, D. J. Schiffrin, R. J. Nichols, A. M. Kuznetsov, J. Zhang, Q. Chi, J. Ulstrup, *J. Phys. Chem. B* **2007**, *111*, 6703-6712.

[8] E. Leary, S. J. Higgins, H. van Zalinge, W. Haiss, R. J. Nichols, *Chem. Commun.* **2007**, 3939-3941.

[9] E. Leary, S. J. Higgins, H. van Zalinge, W. Haiss, R. J. Nichols, S. Nygaard, J. O. Jeppesen, J. Ulstrup, *J. Am. Chem. Soc.* **2008**.

[10] D. I. Gittins, D. Bethell, R. J. Nichols, D. J. Schiffrin, *Adv. Mater.* **1999**, *11*, 737-740.

[11] W. Haiss, H. van Zalinge, H. Hobenreich, D. Bethell, D. J. Schiffrin, S. J. Higgins, R. J. Nichols, *Langmuir* **2004**, *20*, 7694-7702.

[12] R. J. Nichols, D. M. Kolb, R. J. Behm, *J. Electroanal. Chem.* **1991**, *313*, 109-119.

[13] A. A. Kornyshev, A. M. Kumetsov, J. Ulstrup, *ChemPhysChem* **2005**, *6*, 583-586.

[14] J. Zhang, Q. Chi, A. M. Kuznetsov, A. G. Hansen, H. Wackerbarth, H. E. M. Christensen, J. E. T. Andersen, J. Ulstrup, *J. Phys. Chem. B* **2002**, *106*, 1131-1152.

[15] N. J. Tao, *Phys. Rev. Lett.* **1996**, *76*, 4066-4069.

[16] W. Schmickler, *Surf. Sci.* **1993**, *295*, 43-56.

[17] W. Schmickler, N. J. Tao, *Electrochim. Acta* **1997**, *42*, 2809-2815.

[18] A. M. Kuznetsov, J. Ulstrup, *J. Phys. Chem. A* **2000**, *104*, 11531-11540.

[19] A. M. Kuznetsov, J. Ulstrup, *J. Electroanal. Chem.* **2004**, *564*, 209-222.

[20] E. P. Friis, J. E. T. Andersen, L. L. Madsen, P. Moller, J. Ulstrup, *J. Electroanal. Chem.* **1997**, *431*, 35-38.

[21] J. D. Zhang, A. M. Kuznetsov, J. Ulstrup, *J. Electroanal. Chem.* **2003**, *541*, 133-146.

[22] H. Taube, H. Myers, R. L. Rich, *J. Am. Chem. Soc.* **1953**, *75*, 4118-4119.

[23] G. L. Closs, L. T. Calcaterra, N. J. Green, K. W. Penfield, J. R. Miller, *J. Phys. Chem.* **1986**, *90*, 3673-3683.

[24] L. S. Fox, M. Kozik, J. R. Winkler, H. B. Gray, *Science* **1990**, *247*, 1069-1071.

[25] G. Grampp, B. Y. Mladenova, D. R. Kattnig, S. Landgraf, *Appl. Magn. Reson.* **2006**, *30*, 145-164.

[26] S. V. Rosokha, J. K. Kochi, *J. Am. Chem. Soc.* **2007**, *129*, 828-838.

[27] T. Albrecht, K. Moth-Poulsen, J. B. Christensen, A. Guckian, T. Bjornholm, J. G. Vos, J. Ulstrup, *Faraday Discuss.* **2006**, *131*, 265-279.

[28] I. Doi, E. Miyazaki, K. Takimiya, Y. Kunugi, *Chem. Mat.* **2007**, *19*, 5230-5237.

[29] K. Honda, S. Takasaki, J. Yamada, S. Nakatsuji, H. Anzai, *Acta Crystallogr. Sect. C-Cryst. Struct. Commun.* **1998**, *54*, 261-264.

[30] Spartan '04 DFT implementation, B3LYP at 6-31* level

[31] D. A. Fletcher, R. F. McMeeking, D. Parkin, *J. Chem. Inf. Comput. Sci.* **1996**, *36*, 746-749.

[32] T. M. Bockman, J. K. Kochi, *J. Org. Chem.* **1990**, *55*, 4127-4135.

[33] R. E. Hester, S. Suzuki, *J. Phys. Chem.* **1982**, *86*, 4626-4630.

[34] L. Venkataraman, J. E. Klare, C. Nuckolls, M. S. Hybertsen, M. L. Steigerwald, *Nature* **2006**, *442*, 904-907.

[35] S. Woitellier, J. P. Launay, C. Joachim, *Chem. Phys.* **1989**, *131*, 481-488.

[36] Z. Li, B. Han, G. Meszaros, I. Pobelov, T. Wandlowski, A. Blaszczyk, M. Mayor, *Faraday Discuss.* **2006**, *131*, 121-143.

[37] T. Albrecht, J. Ulstrup, S. Mertens, F,L., *J. Am. Chem. Soc.* **2007**, *129*, 9162-9167.

Chapter 4

Chemical control of double barrier tunnelling in α,ω-dithiaalkanes

Chapter 4

Chemical control of double barrier tunnelling in α,ω-dithiaalkanes

1. 4.1 Introduction

It is found that the current through alkane chains decreases exponentially with increasing molecule chain length, as discussed in section 1.5.7.1, indicating a superexchange mechanism of electron transfer. Using the breakjunction technique between 278 – 333 K, the conductance of metal-alkane-metal junctions has been shown to be temperature independent,[1] which is in agreement with simple 1-D barrier tunnelling theory. The I\V characteristics of alkane junctions are linear at low bias (± 0.5 V) and become non-linear outside this range, and have been described by the Simmons tunnelling model [2] as well as in a superexchange framework.[3]

It has been demonstrated that other types of molecules, apart from alkanes, can have a different conduction mechanism than superexchange. As seen in the previous chapter, if the molecule possesses a level which lies close to the Fermi level of the electrodes, the tunnelling mechanism is considered to proceed via a two-step hopping process involving that level.[3] Generally

this process is expected to facilitate charge transport across the molecular bridge, with examples being mainly of redox active molecules shown in figure 4.1 (viologen[3], PTCDIs[4], olioganilines[5]).

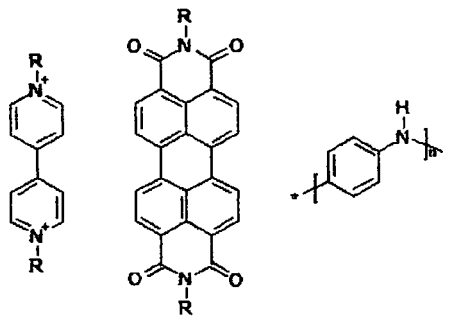

Figure 4.1. Generic structure of (from left to right) viologen, PTCDI and oligoaniline.

Using an electrochemical environment the Fermi level of the electrodes can be raised or lowered with respect to the molecular level, and monitoring the tunnelling current allows us to observe resonance type features in the current-overpotential relationship.

4.2 Aims

As a preliminary goal, we wished to examine whether it is possible to observe a transition from coherent superexchange tunnelling to hopping across a series of structurally similar compounds. For this, it is necessary to

design molecules with a well-defined 'hopping site' where there is a barrier for hopping. A suitable group of compounds is based on a modification of a symmetrically substituted bis-alkyl viologen compound, previously studied in the group. In order to draw a distinction between electrochemical and thermal mechanisms for activation, where the redox site lies close in energy to the electrodes, and the superexchange mechanism of alkanes, the hopping site has been chosen so that its redox levels are relatively far removed from the Fermi levels of the contacting metal electrodes. The suitable choice was a benzene ring, which is shown in figure 4.2 below.

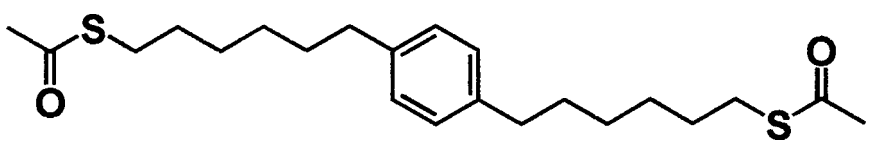

Figure 4.2. Structure of Thioacetic acid S-{6-[4-(6-acetylsulfanyl-hexyl)-phenyl]-hexyl} ester (6Ph6).

Benzene is a good choice as its levels should be intermediate between those of the alkanes and those of the viologen studied in the previous chapter. A further goal of this study was to investigate the effect of chemical substitution of the central site as it is well known in aromatic chemistry that chemical substituents substantially alter chemical reactivity

by changing the electronic structure of the ring π-system. The influence of a particular functional group on a parent molecule's chemistry may be predicted qualitatively by considering the electronic effect of the functional group. The choice of substituents was based on their electron donating or withdrawal capabilities, which may raise or lower the energy of the conducting orbital in the molecule. We chose methyl and methoxy groups to study the effect of σ and π electron donating substituents respectively, whilst tetrafluorobenzene was used in order to demonstrate the effects of electronegative groups. These are listed in Table 1 together with the HOMO and LUMO energies determined using the SPARTAN04 implementation of DFT (B3LYP/6-31G**). SPARTAN uses a hybrid DFT/Hatree-Fock code which seems to predict reliable HOMO-LUMO gaps, probably due to the underestimation and overestimation of DFT and HF respectively cancelling each other.

Molecule	Well structure	HOMO (eV)	LUMO (eV)
6Ph6	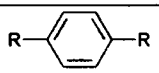	–6.23	+0.07
6Ph(F)$_4$6	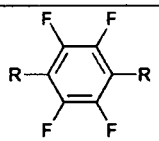	–6.63	–0.60
6Ph(OMe)$_2$6	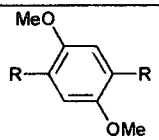	–5.24	+0.09
6Ph(Me)$_2$6	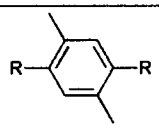	–5.98	+0.10
HS(CH$_2$)$_{12}$SH	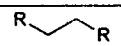	–8.05	+2.49

Table 1. Structures of the molecules studied and their frontier orbital energies (in eV) calculated using the SPARTAN quantum chemical program. R = HS(CH$_2$)$_6$ in all cases.

4.3 Synthesis

All compounds were prepared according to scheme 1 (showing the unsubstituted compound only).

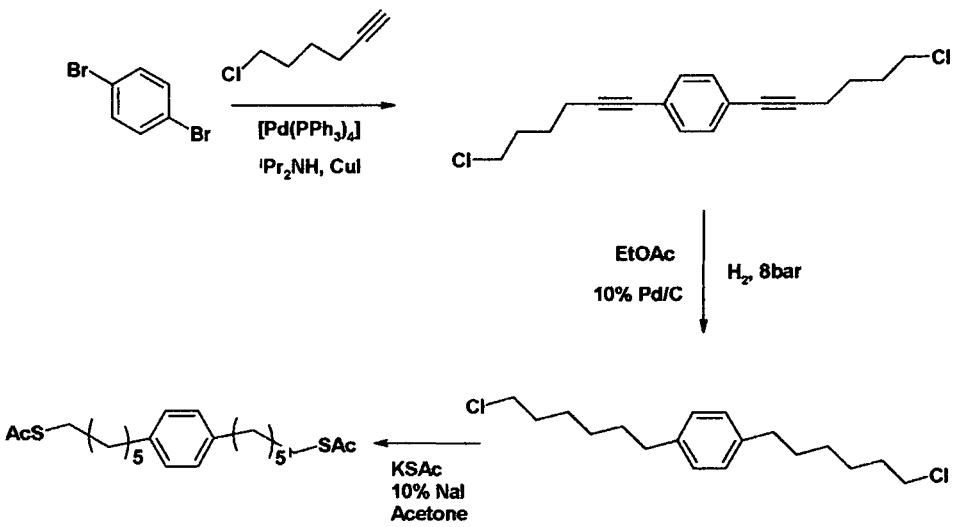

Figure 4.3. Synthesis of 6Ph6

The starting compound was the 1,4-dibromo species, which was treated with 1-chloro-hex-6-yne under Sonogashira conditions to yield the bis-chorohexyne species. Reduction of the triple bonds with H_2 followed by substitution of the chloro groups with potassium thioacetate gave the relevant thioacetic acid S-{6-[4-(6-acetylsulfanyl-hexyl)-phenyl]-hexyl} ester. Purification by column chromatography was performed after each step except the hydrogenation. The four molecules consisted of the following benzene groups:

Molecule 1, 6Ph6 = phenyl

Molecule 2, $6Ph(F)_46$ = 2,3,5,6-tetrafluoro-phenyl

Molecule 3, $6Ph(OMe)_26$ = 2,5-dimethoxy-phenyl

Molecule 4, $6Ph(Me)_26$ = 2,5-dimethyl-phenyl

4.4 Methods

Samples were prepared in the usual manner. It was not necessary to remove the thioacetate groups prior to adsorption as they are found to cleave on gold forming the Au-S bond in the traditional manner in ambient air, as determined by XPS studies (*vide infra*).

We employed the scanning tunnelling microscopy (STM) based I(t) and I(s) techniques to determine the single molecule conductances.

4.5 Results

Single molecule conductance measurements on 1,4-bis-(6-thiahexyl)-benzene derivatives reveal (i) that benzene rings serve as an effective indentation in the tunnelling barrier, and (ii) that more electron-rich benzene rings give higher conductances, consistent with hole conduction (i.e. via the benzene HOMOs). The conductance increase is rather weak however, with only a factor two difference between the most and the least conductive molecules.

4.5.1 Molecule 1, 6Ph6

4.5.1.1 Current-distance – I(s) results

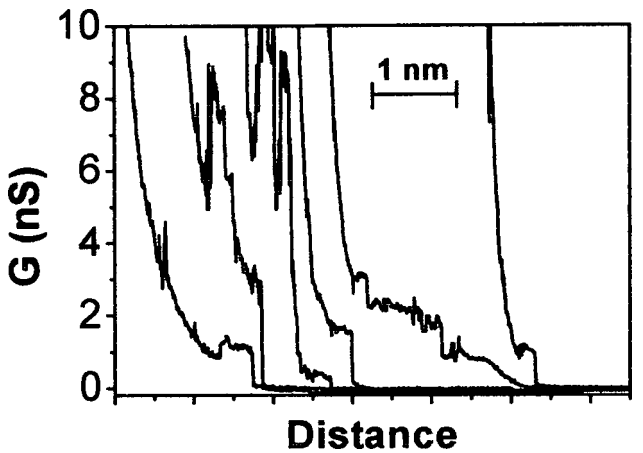

Figure 4.4. Typical low current jumps observed for 6Ph6 under perfluorononane liquid. I_{set} = 4 nA, U_{bias} = 0.2 V.

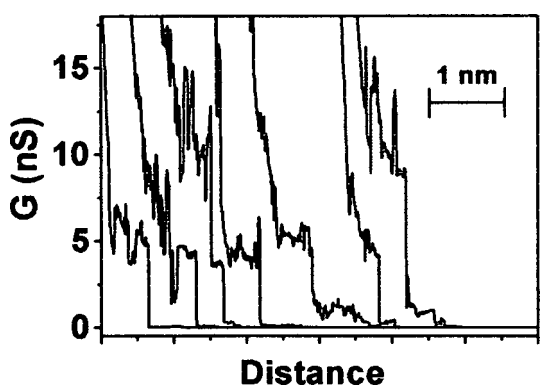

Figure 4.5. Typical high current jumps observed for 6Ph6 under perfluorononane liquid. I_{set} = 4 nA, U_{bias} = 0.2 V.

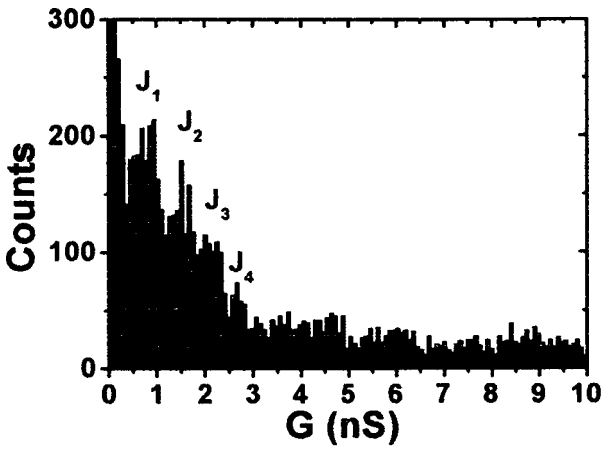

Figure 4.6. Histogram of 120 I(s) curves for 6Ph6. I_{set} = 4 nA, U_{bias} = 0.2 V.

A single molecule conductance of (0.72 ± 0.24) nS was measured for 6Ph6 using the I(s) method. The data for all 6Ph(x)$_n$6 molecules, however, displays significant evidence for *two* states of the molecular conductance. The majority of the data collected contained plateaus of the low type, however, 5 – 10 % of the data showed larger, high, plateaus which cannot be easily explained as multiple molecules in the lowest conductance state. The plateaus do not appear significantly in the histogram due to their low number and relatively short length. The average value of the high plateaus for 6Ph6 is roughly 4 - 5 nS, about a factor 5 – 6 times the low value. It has been very rare for us to observe more than four molecules in our junctions, especially because of the low coverage of molecules we employ on the gold surface, and thus to see plateaux consistent with six molecules in the junction, consistently, is quite unlikely.

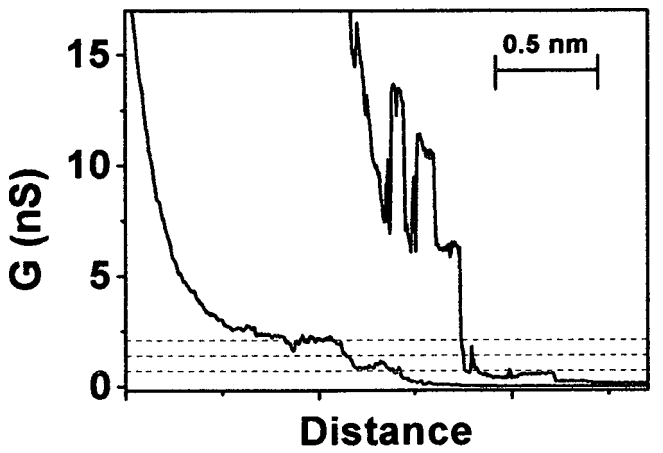

Figure 4.7. High and low conducting states of 6Ph6. The left curve shows three molecules in the low state followed by a single molecule. The right curve shows two molecules in the high conductance state followed by a single molecule which finally is pulled into the low conductance state. I_{set} = 4 nA, U_{bias} = 0.2 V.

Figure 4.7 for 6Ph6 gives an insight into the nature of the two distinct conductances. Initially we see the conductance of the junction jumping between two values, the upper being about twice the value of the lower (10 and 5 nS respectively). Finally we see that the conductance drops from the 5 nS level to precisely the lowest conductance observed, which in this case, is 0.8 nS. This behaviour is consistent with initially two molecules inside the tip-surface gap, one spontaneously attaching and detaching, and both in the high conductance state. As the tip-surface distance increases it becomes possible for only one molecule to exist inside the junction. At even greater tip-surface distances the single molecule becomes forced into the low conducting state which persists until the Au|molecule|Au junction finally

breaks with the full cleavage of a Au-Au or Au-S bond. This behaviour has been seen for alkanedithiols[6, 7]. The high conductance state was attributed to the sulphur head group binding in a three fold hollow gold site, whilst the low conductance state was attributed to binding on the atop site of a single gold atom – DFT calculations show such a change in adsorption site leads to a factor 4-5 times change in the conductance.[8] If we compare the two conductance curves in figure 4.7 again, then we can see that both molecular junctions persist over the same distance (about 1 nm from the starting set point distance), so we may expect both, and indeed all, junctions to show similar behaviour as the starting distance is the same for all measurements shown. On the other hand, the fact that only less than 10 % of the data show the high value could be explained by chance fluctuations of the initial tip-surface distance which result in molecules becoming able to adopt better bonding configurations between tip and surface. However, as most of the low series data show molecules remaining in the gap over a distance of 1 nm, this implies that the molecules are initially squashed into a gap of about half their length dimension (S...S distance is ~ 2 nm for molecules 1-4) and should, therefore, have enough freedom to adopt any preferred contact geometry. Therefore, the high and low states could be due to different conformer changes of the molecule itself inside the junction and could involve gauche to trans changes in the backbone of the molecule. However, two points

thus favour the contact theorem. Firstly, the ratio between the high and low conductance states changes with the binding group[1]. Secondly, high and low states have also been observed for rigid molecules like benzenedithiol[9] and 4,4'-bipyridine[10].

Other surface features could be responsible for the high and low conductance values apart from top and hollow adsorption site such as adatoms, step edges and other surface defect sites. Several recent studies have proposed new surface interactions between gold and thiols that involve sulphur bonding to gold adatoms on the surface, deduced from experimental measurements including X-ray standing wave experiments, electron and X-ray diffraction, and scanning tunneling microscopy.[11] Theoretical calculations (density functional theory and molecular dynamics) further support this notion.[12, 13] A recent STM based study has shown that removal of a SAM of octanethiol from a Au(111) surface, using a H_2 beam, leaves behind surface adatoms at a 1:2 gold adatom/alkanethiol ratio.[14] At the single molecule level it seems that only a few types of interaction are present for Au|dithiol|Au junctions, however, deducing these interactions is beyond the current scope of this work.

4.5.1.2 Time domain – I(t) results

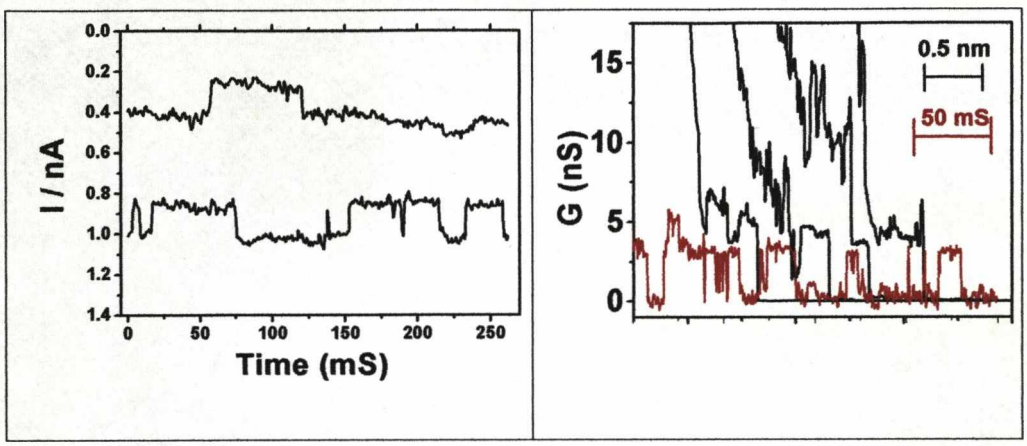

Figure 4.8. (left) Lowest current jumps for 6Ph6. I_{set} = 1 nA, U_{bias} = 0.2 V. (Right) Black lines are I(s) scans exhibiting high plateau. The red line is an I(t) scan, plotted as conductance, with the background normalised to zero for comparison. I_{set} = 4 nA, U_{bias} = 0.4 V.

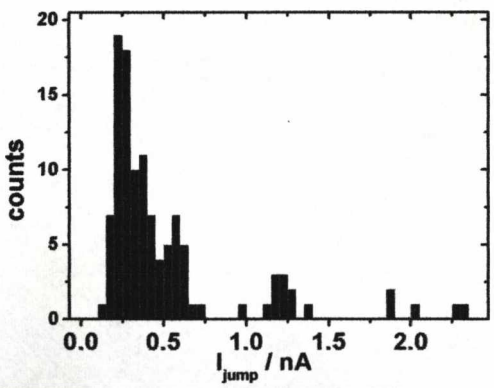

Figure 4.9. Current histogram of 6Ph6 under an argon atmosphere. I_{set} = 4 nA, U_{bias} = 0.4 V. G = 0.75 nS. Data set was selected through a labview analysis package, which records only high quality current jumps.

The red I(t) scan in figure 4.8 has been normalised to zero and plotted as a conductance jump (zero conductance represents thus the background current). The jumps in the I(t) compare well with the high plateau observed in the I(s) method. They are less frequent than the low jumps observed, as can be seen in the histogram of I(t) jumps observed under argon atmosphere (figure 4.9), however, they are still present.

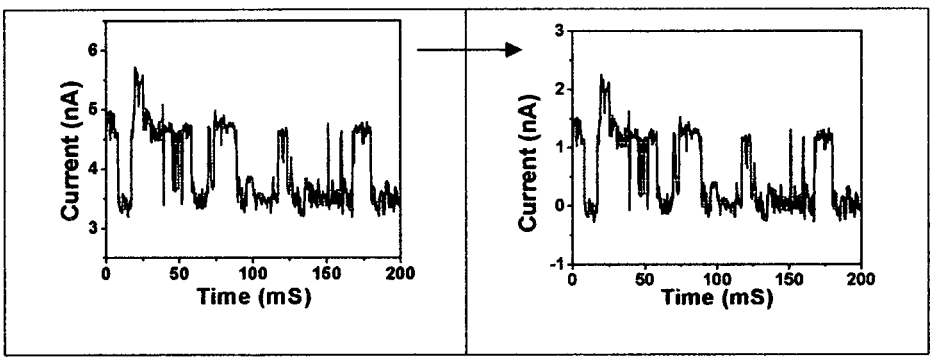

Figure 4.10. Example of large I(t) jumps for 6Ph6 (left) with the baseline corrected to zero (right). Data acquired at I_{set} = 4 nA, U_{bias} = 0.4 V under Ar. Data was hand selected.

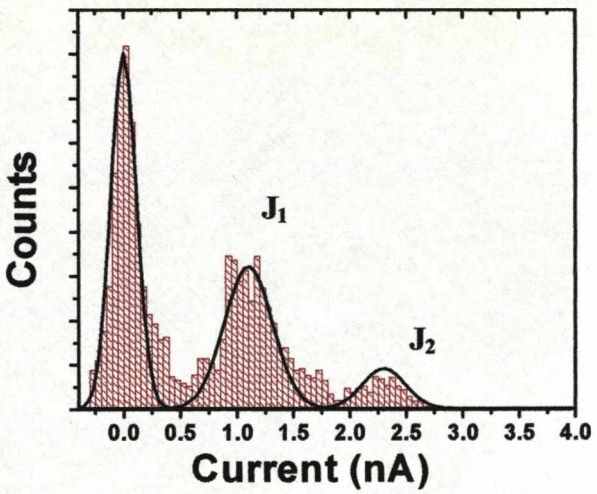

Figure 4.11. Histogram showing the sum of all data points for 30 current jumps, with their baselines normalised to zero. Data acquired at I_{set} = 4 nA, U_{bias} = 0.4 V under Ar. Data was hand selected.

The I(t) jumps in the histogram of figure 4.11 were first all normalised to zero by subtracting the background value of current from the whole data set. The Gaussian peaks fitted to the histogram peaks are separated by the amount equal to the jump between the background level of current and that when a molecule attaches, i.e. 1.2 nA which corresponds to a molecular conductance of (3 ± 0.6) nS. This value is approximately a factor four times larger than the low conductance peak and is consistent with the I(s) data (see figure 4.8).

4.5.1.3 I(s) under electrochemical potential control

We wished to investigate how the conductance of 6Ph6 responded to changing the electrochemical 'gating' potential. Prior to the STM measurements, a monolayer of 6Ph6 on gold (111) was characterised by ex-situ cyclic voltammetry. 6Ph6 was adsorbed on Au(111) single crystal, which had been manually polished and then flame annealed in a butane flame for 5 minutes prior to use. Within the window of potential control (determined mainly by the thiol desorption process and the oxidation of the gold) no redox processes were found using cyclic voltammetry (black trace, figure 4.12).

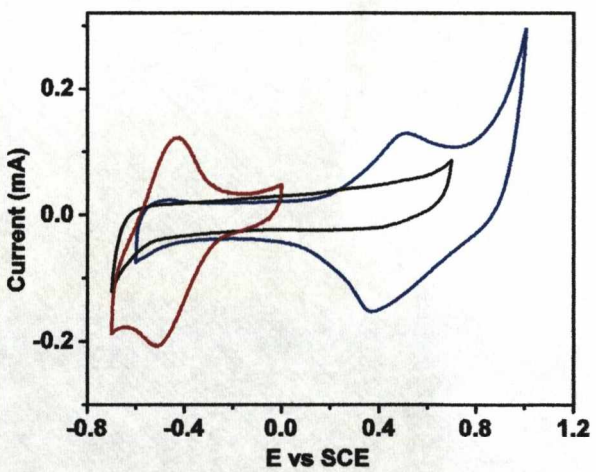

Figure 4.12. Cyclic voltammogram of a monolayer of 6Ph6 (black line) vs SCE. The CVs of a viologen (6V6) and a pyrrolotetrathiafulvalene (6PTTF6) compounds are shown for comparison (red and blue respectively). Conditions for all were 10 mM $NaHPO_4$ buffer solution (pH 7), Pt counter electrode, Au working electrode.

Using a gold on glass slide, a low coverage sub-monolayer of 6Ph6 was formed in the usual manner and placed under electrochemical potential control inside an STM cell. $NaHPO_4/Na_2PO_4$ buffer solution was used as the electrolyte and gold counter and quasi reference electrodes were employed. I(s) and I(t) measurements were then performed at different potentials of the working electrodes with respect to the reference.

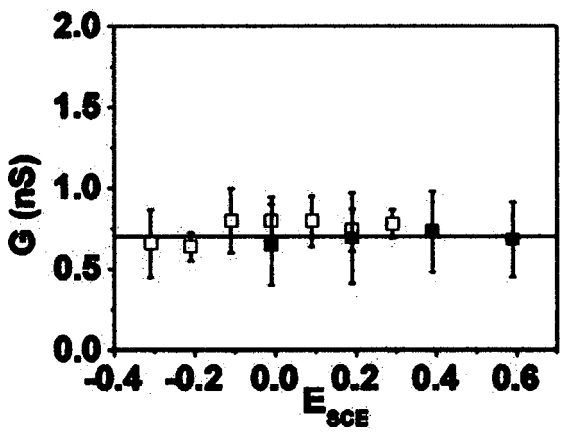

Figure 4.13. I(s), black squares, and I(t), white squares, data for 6Ph6. Each point represents the mean position of the primary histogram peak. $G_{average}$ = 0.75 nS.

No evidence of any dependence of the conductance on the gate potential was found, which suggest that electron transfer is via 'off-resonant' electron transport. The closest molecular orbitals are effectively too far away to be brought close enough to the gold Fermi level. Hence, no effect

of the overpotential takes place. Also the conductance remains the same as in ambient, non potential controlled, environments.

4.5.2 Molecule 2, 6Ph(F)$_4$6

4.5.2.1 XPS data

Spectra were acquired using a Scienta ESCA 300 spectrometer (NCESS, Daresbury Laboratory, UK) at 90^0 and 10^0 take-off angles. The spectra were referenced to the Au 4d 5/2 line positioned at 335.0 eV and Au 4f 7/2 line positioned at 84.1 eV. Molecule 2 was adsorbed onto a gold-on-glass substrate from a 1 x 10^{-4} M dry DCM solution. The adsorption times were 30 seconds and 24 hours for low and high coverage respectively. The gold substrate was flame annealed in a butane flame just prior to adsorption.

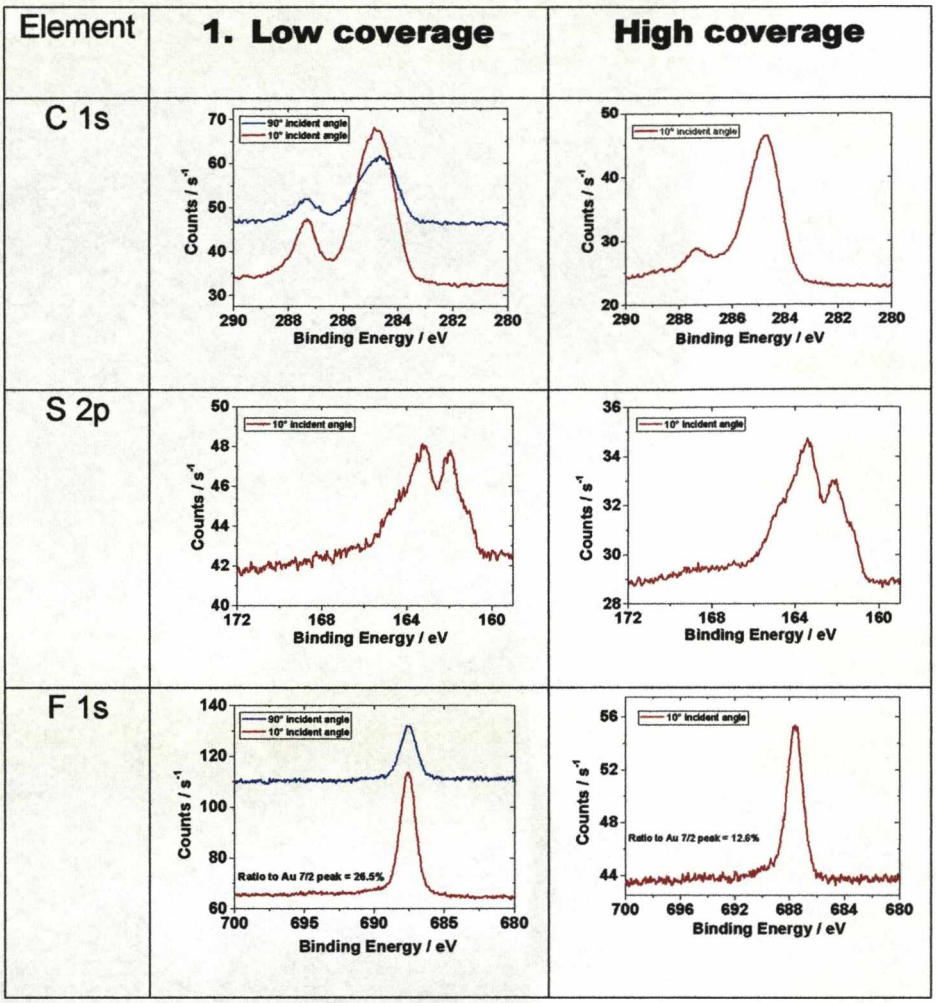

Figure 4.14. XPS data for 6Ph(F)$_4$6 on Au (111). Low coverage data was taken using a 30 second immersion time. High coverage data was taken using a 24 hour immersion time.

The carbon 1s region shows a clear peak at 287.4 eV, characteristic of a carbon bonded to a fluorine. The second peak at 285.0 eV is characteristic of the remaining carbon in the molecule. The ratio between the two peaks increases upon immersion of the gold sample in the solution for 24 hours. This can be interpreted as the molecules forming an upright standing self

assembled monolayer, which buries the tetrafluorobenzene unit, preventing the electrons from being ejected.

The S 2s region contains signals from Au-S bonds (162.1 eV) and S-H bonds (163.4) and the proportion of S-H increases upon long immersion times, again consistent with an upright standing monolayer. The presence of Au-S indicates that it is not necessary to employ thioacetate cleavage prior to monolayer formation.

The fluorine 1s region shows a clear single peak at 687.6 eV.

4.5.2.2 Current-distance – I(s) results

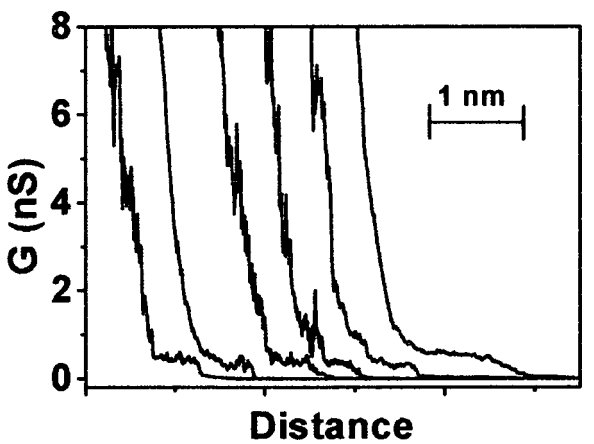

Figure 4.15. Lowest current plateaux observed for 6Ph(F)$_4$6. I_{set} = 3 nA, U_{bias} = 0.2 V.

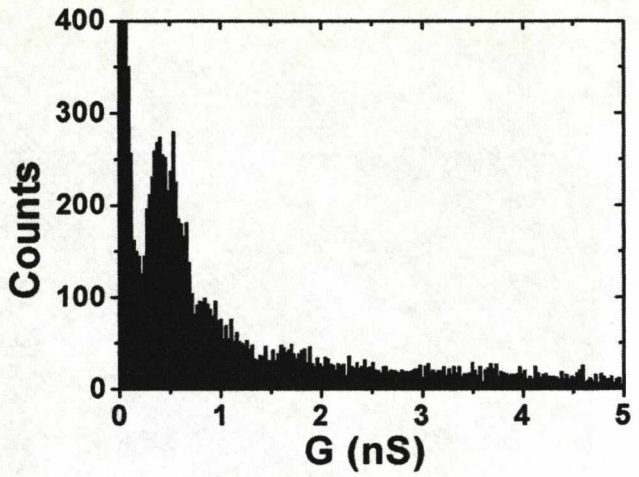

Figure 4.16. Histogram of 100 I(s) curves for 6Ph(F)$_4$6. I_{set} = 3 nA, U_{bias} = 0.2 V.

A single molecule conductance of (0.40 ± 0.09) nS was measured for 6Ph(F)$_4$6 using the I(s) method.

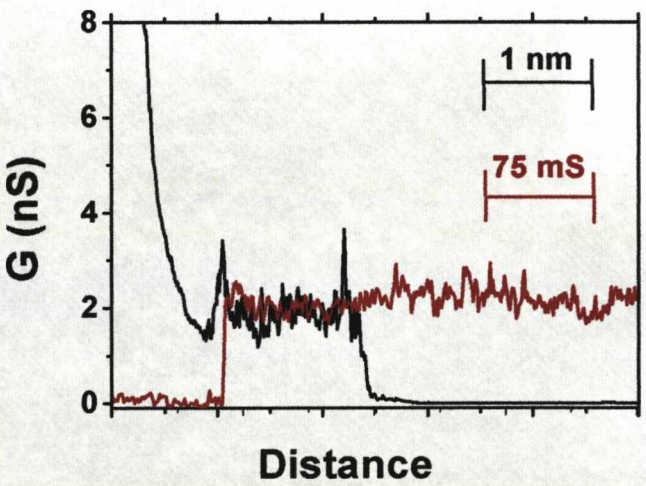

Figure 4.17. Examples of high conductance state of 6Ph(F)$_4$6 in the I(s), black line, and I(t), red line, methods. U_{bias} = 0.2 V.

4.5.2.3 Time domain – I(t) results

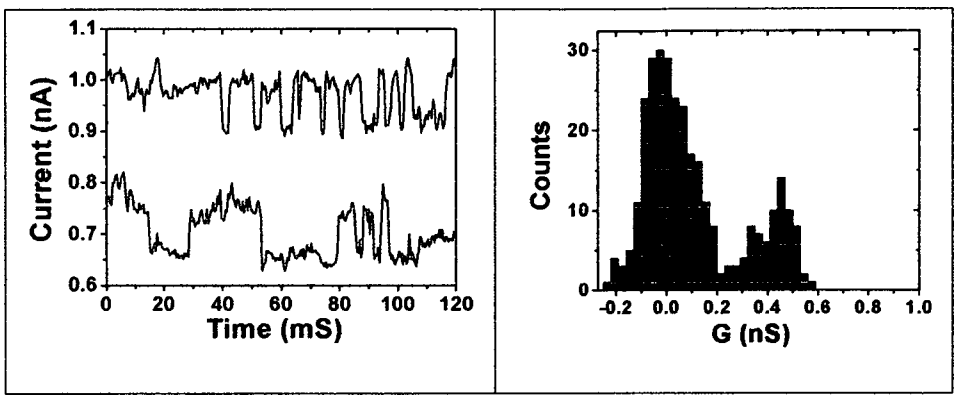

Figure 4.18. (left) Low jumps in the current vs time I(t) signals for 6Ph(F)$_4$6. I_{set} = 1 nA, U_{bias} = 0.2 V. Data was hand selected. (right) Histogram of the points contained in the top I(t) scan, with the data converted to conductance and the baseline set to zero (i.e. no molecule).

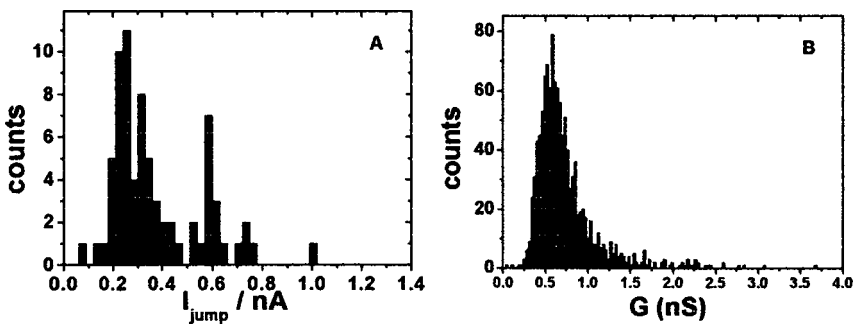

Figure 4.19. (A) Current histogram of 60 I(t) jumps of 6Ph(F)$_4$6 under perfluorononane, G = 0.45 nS). I_{set} = 3 nA, U_{bias} = -0.6 V. (B) Under E_S potential control, G = 0.57 nS, (0.01 M Na_2PO_4 buffer solution) U_{bias} = 0.2 V, I_{set} = 1 nA. Data sets were hand selected.

Figure 4.19 B shows all 1100 I(t) jumps recorded at E_S potentials varying between -0.35 to 0.60 V (vs Au quasi reference) summed together. About

100 jumps were recorded at each potential. There is no variation in conductance over these potentials.

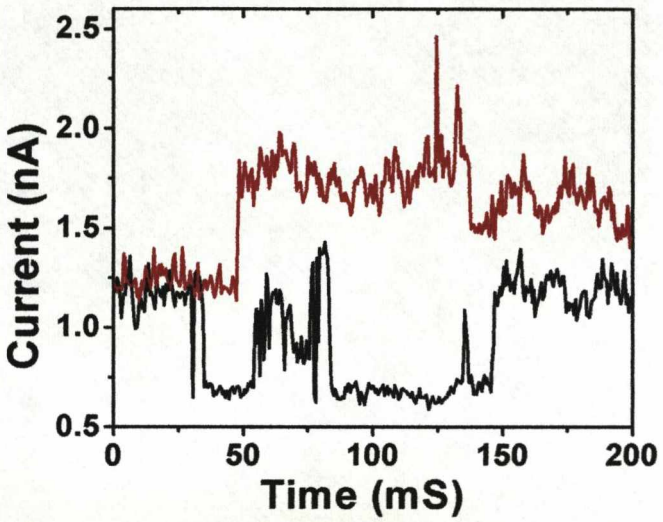

Figure 4.20. High current jumps in the I(t) signals for 6Ph(F)$_4$6. I_{set} = 1 nA, U_{bias} = 0.2 V. Data was hand selected.

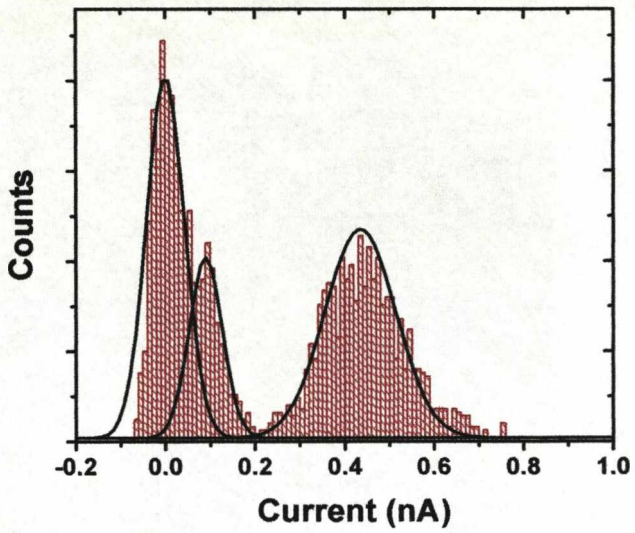

Figure 4.21. Histogram showing the sum of all data points for 18 high current jumps, with their baselines normalised to zero. Data acquired at I_{set} = 1 nA, U_{bias} = 0.2 V. Data was hand selected.

The I(t) scans which were selected contained jumps which were too large to be considered due to single or double molecular wires. From the 18 I(t) jumps considered, a conductance of (2.2 ± 0.5) nS was obtained for the larger events. This is again approximately a factor four to five times larger than the 0.4 nS measured as the lowest value, which agrees with the observations of the other molecules in the series, and with the alkanedithiol series. From the histogram in figure 4.21 the low jumps are still visible at 95 pA.

4.5.3 Molecule 3, 6Ph(OMe)$_2$6

4.5.3.1 Current-distance – I(s) results

The most prominent plateau found for 6Ph(OMe)$_2$6 in the I(s) method was around 1 nS. Occasionally, though, three distinct current plateaux could be seen, as shown in figure 4.22 below, which also contain the 1 nS plateau as the smallest step in the current.

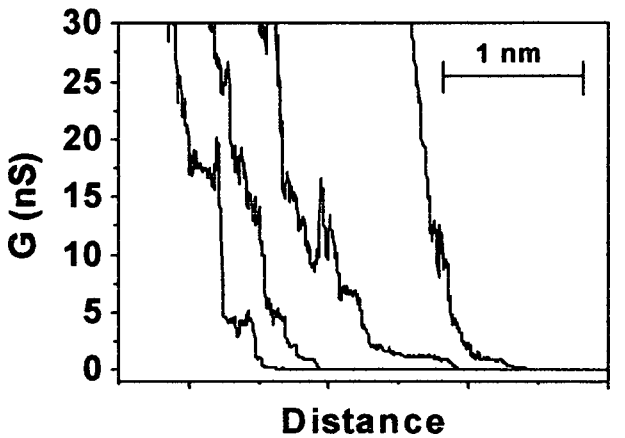

Figure 4.22. I(s) curves for 6Ph(OMe)$_2$6 under perfluorononane. U_{bias} = 0.15 V, I_{set} = 7 nA.

A few points stand out. Firstly, the larger plateaux always occur before the lower plateaux. Secondly, extending the junction does not cause a low plateau to jump to a high plateaux, rather only the high plateau to change to low plateau. This behaviour has been noted for alkanedithiols also, and could be due to the molecule adopting different binding configurations

within the gap. These differences could arise at the contact, where the thiol group can be located in different adsorption sites. Upon increasing the gap separation, the thiol group could move from one site to another, e.g hollow to top. It is also possible for a gold atom attached to the thiol to do the same. However, it is possible that the flexible alkyl linkers could adopt different geometries, and the plateaus represent changes in the gauche/trans ratio between methylene units.

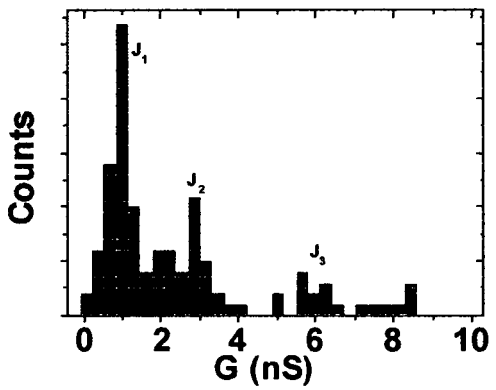

Figure 4.23. I(s) conductance histogram for 6Ph(OMe)$_2$6 under perfluorononane. U_{bias} = 0.15 V and I_{set} = 7 nA.

It is also possible that it is simply multiple wire junctions being broken. However, this would not lead to a clear peak which is substantially separated from the lowest group 1. Although these larger plateaus only account for approximately 10 % of the recorded data, we believe that more

measurements at smaller tip-sample distances should better highlight these different plateaus.

4.5.3.2 Time domain – I(t) results

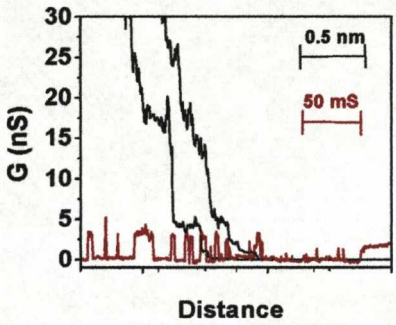

Figure 4.24. I(s) scans exhibiting high current plateau for 6Ph(OMe)$_2$6 (black traces). The red trace is an I(t) scan, plotted as conductance, with the background normalised to zero. I_{set} = 2.5 nA, U_{bias} = 0.4 V.

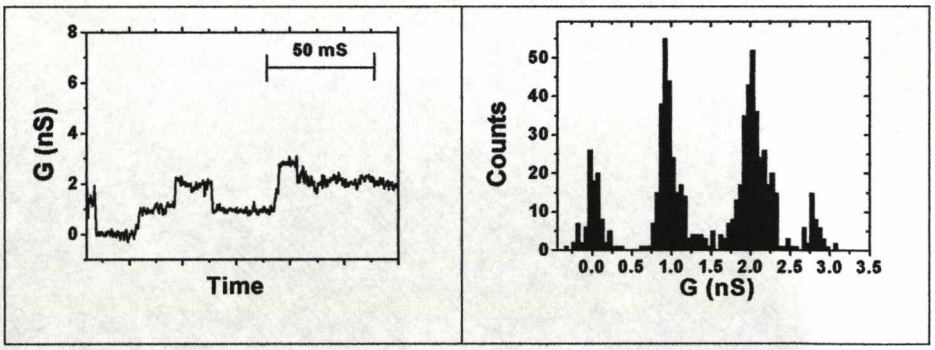

Figure 4.25. (left) I(t) scan of 6Ph(OMe)$_2$6. I_{set} = 4 nA, U_{bias} = 0.6 V. (right) Histogram of the points contained in the I(t) scan, with the data converted to conductance and the baseline set to zero (i.e. no molecule). Clearly one, two and three molecules attach during the course of the scan.

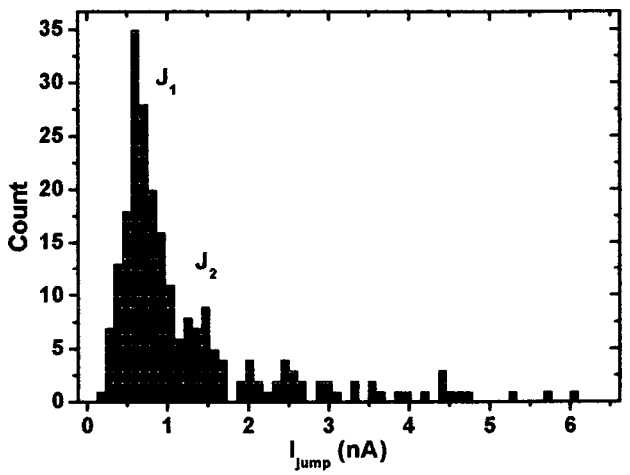

Figure 4.26. Histogram of ca. 200 I(t) jumps for 6Ph(OMe)$_2$6. I_{set} = 4 nA, U_{bias} = 0.6 V.

4.5.4 Molecule 4, 6Ph(Me)$_2$6

4.5.4.1 Current-distance – I(s) results

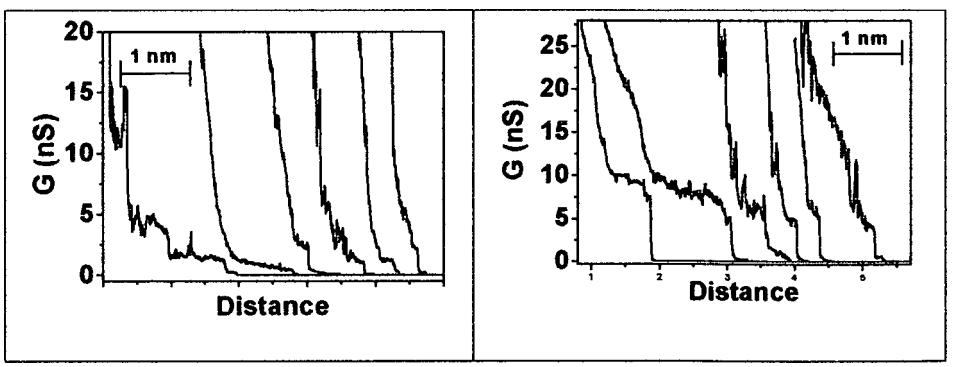

Figures 4.27. I(s) current-distance curves for 6Ph(Me)$_2$6. U_{bias} = 0.2 V, I_{set} = 6 nA.

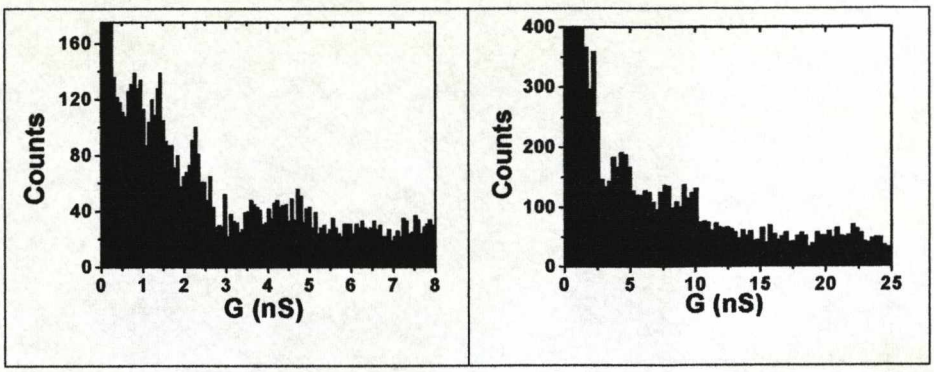

Figure 4.28. I(s) conductance histogram of 100 scans for 6Ph(Me)$_2$6 under perfluorononane. I_{set} = 7 nA, U_{bias} = 0.2 V. Both histograms are constructed from all the data, the right hand histogram is drawn at a different scale to emphasise the larger conductance value circa 4 nS.

4.5.4.2 Time domain – I(t) results

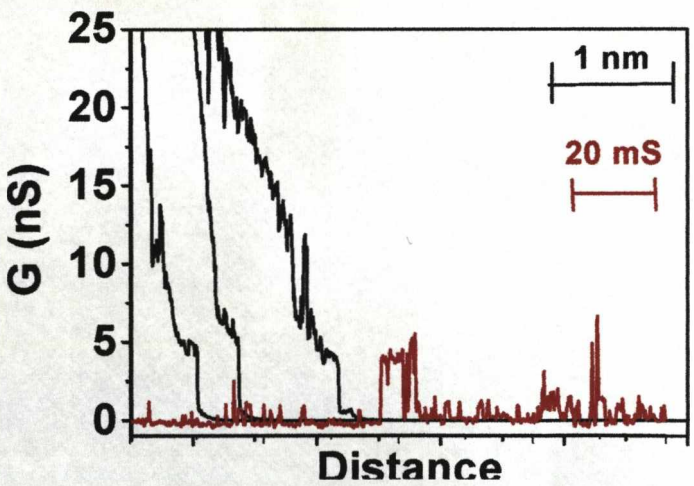

Figure 4.29. I(s) scans exhibiting high current plateau for 6Ph(Me)$_2$6 (black traces). The red trace is an I(t) scan, plotted as conductance, with the background normalised to zero for comparison. U_{bias} = 0.2 V, I_{set} = 5 nA.

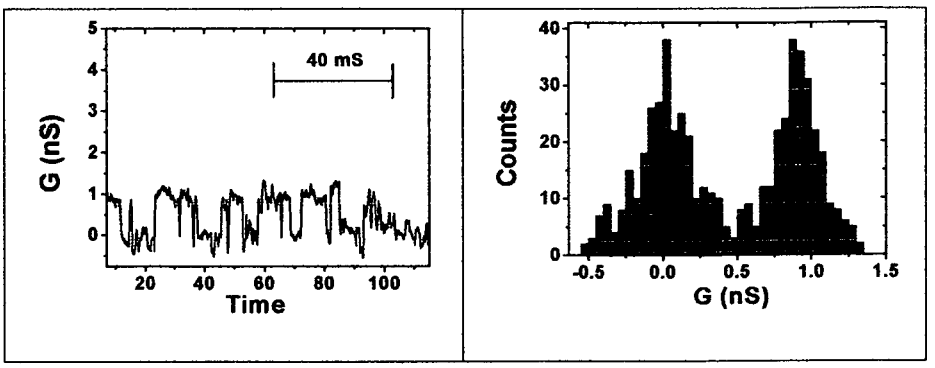

Figure 4.30. (left) I(t) scan of 6Ph(Me)$_2$6. I_{set} = 4 nA, U_{bias} = 0.6 V. (right) Histogram of the points contained in the I(t) scan, with the data converted to conductance and the baseline set to zero (i.e. no molecule).

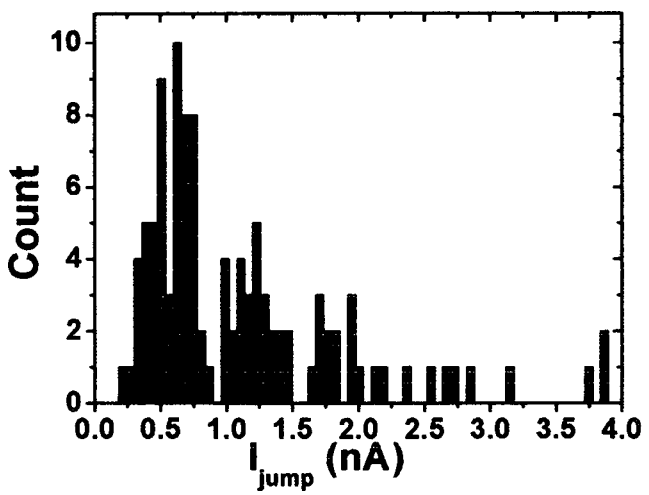

Figure 4.31. Histogram of ca. 70 I(t) jumps for 6Ph(Me)$_2$6. I_{set} = 4 nA, U_{bias} = 0.6 V. G = 1 nS.

4.5.5 I\V data for molecules 1-4

Molecules 1 to 4 behaved in an Ohmic manner between ± 0.6 V sample bias. I\V plots were constructed using the I(t) method at different potentials

and plotting the value of the lowest histogram peak. A representative I\V plot is shown below in figure 4.32.

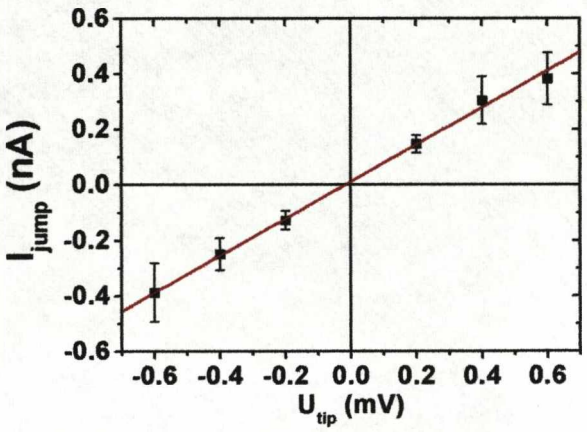

Figure 4.32. I\V plot constructed using the I(t) method for 6Ph6. G = (0.67 ± 0.07) at zero bias.

4.6 Discussion

The main aim of this chapter of work was to study a series of molecules, very similar to each other, but with different chemical substituent groups on a central benzene ring between two thiahexyl linkers. This sets it apart from the majority of experimental and theoretical work in this area which focuses on understanding the basic properties of molecular junctions.

We have determined the single molecule conductance of the molecule 6V6 and seen that when contacted to gold electrodes via the thiol groups, this

can be regarded as the single molecule equivalent of a double tunnelling barrier, figure 4.33.

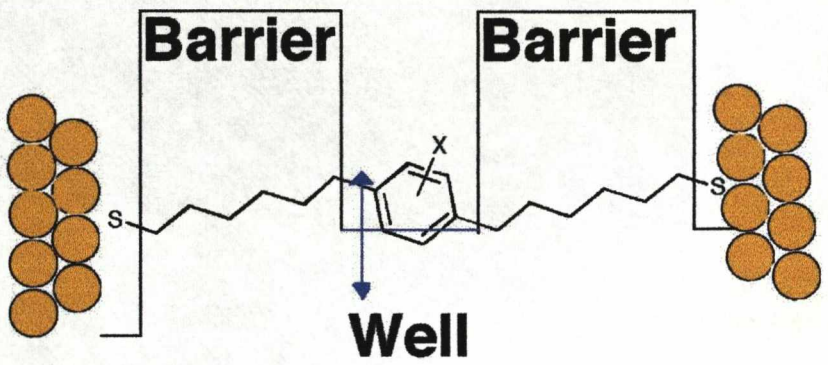

Figure 4.33. Structure of a single molecule double tunnel barrier.

This is apparent upon comparing the single molecule conductance of 6V6 (0.5 nS in air and 3 nS under potential control – E_S = -0.6V) with that of dodecane-1,12-dithiol (i.e. two back-to-back barriers with no well; 0.35 – 0.1 nS)[15]. Even though 6V6 is longer than dodecane-1,12-dithiol, it is more conductive due to the influence of the viologen acting as, presumably, a barrier indentation. The viologen group in 6V6 is redox-active. In this chapter, we have tried to address the following questions. Firstly, do smaller, non-redox-active moieties also act as ''wells''? Secondly, if so, can they be chemically tuned by altering the electronic structure of the well? Thirdly, is there a relationship between the frontier orbital energies of the well and the conductance of the whole junction?

We made a range of molecules, 1–4, in which the contacts and barriers are constant ($HS(CH_2)_6$–) and the wells are varied. Molecules 1–4 (Table 1) were synthesised (as dithioacetates) and fully characterised by microanalytical and spectroscopic methods. The results (Table 2) are valuable in two ways.

Molecule	I(*t*) (nS)	I(*s*) (nS)	$S_{1/2}$ (nm)
1	0.67 ± 0.07	0.72 ± 0.24	1.83 ± 0.19
2	0.48 ± 0.05	0.40 ± 0.09	2.35 ± 0.28
3	0.92 ± 0.14	0.9 ± 0.19	1.33 ± 0.14
4	0.77 ± 0.11	0.69 ± 0.27	1.38 ± 0.15

Table 2. Summary of single molecule conductance results for molecules 1-4. Only the lowest conductance values are shown with their corresponding break-off distance.

The results provide confirmation that we are dealing with molecular events, because the mean break-off distances are reasonably consistent with the lengths of the molecules (2nm S–S distances for the full extended, transoid conformers of all the molecules - as determined by molecular mechanics). Variations in the values of $s_{1/2}$ are probably due to difficulties in calibrating the absolute s_0 distance. For molecules 3 and 4 s_0 was calculated to be smaller than for 1 and 2. This probably reflects the larger conductance of a surface covered in molecules 3 and 4. All molecules gave

plateaus in the order of 0.5 to 1 nm. The results in Table 2 are interesting in several respects. Firstly, it is clear that the conductances are considerably greater than would be expected for an alkanedithiol of the same length as $6Ph(x)_n6$. This indicates that the aromatic units do indeed act as a ''well'' in the tunnelling barrier for $6Ph(x)_n6$ molecule. Secondly, it is clear that the conductance varies with substituent; electron-donating groups lead to higher conductances. However, the variation in the conductance is small, with only a factor two between the lowest and the highest conducting molecule. In figure 4.34 we plot the conductances against the HOMO energy for the aromatic unit, obtained from the Spartan04 implementation of DFT (B3LYP, 6-31G**; equilibrium geometry calculated for the transoid, extended form of 1–4 minimised using molecular mechanics). The energy of the HOMO in a benzene ring is sensitive to the electronic effects of substitution as evidenced by the change in ionisation potential for various substituted benzenes[16].

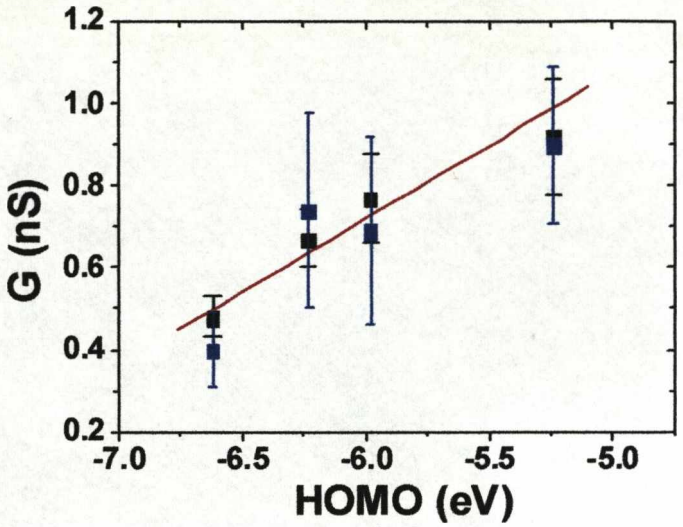

Figure 4.34. Plot of conductances determined by the I(*s*) (blue) and the I(*t*) (black) methods (with standard deviations) against HOMO energy calculated for molecules 1–4.

4.6.1 Attempt to Model the results using the Hammet equation

It is well understood that the chemistry of a particular parent compound can be modified by the attachment and / or change of substituent groups. The effects may be understood in terms of the substituent's electron donor / accepter capabilities. Efforts have been made to model the system in terms of the Hammett equation for systems of *p*-XC_6H_4Y:[16]

$$\log k/k_0 = \sigma\rho$$

where k_0 is the rate constant for X = H, k is the constant for the group X, ρ is a constant for a given reaction under a given set of conditions and σ is a constant characteristic of the group X. The σ values are numbers that sum together the total electrical effects (resonance and field) of a group X when attached to a benzene ring. k/k_0 were taken to represent the conductance of the substituted and unsubstituted benzene rings respectively. This form of analysis, however, is rather controversial in this manner as there is not a single 'reaction centre' in a molecular wire – current passes through the benzene ring on one side and leaves on the other. The authors used σ_p values (for para substituents), however, the substituents are either in the ortho or meta positions relative to the amine groups. σ_o / σ_m values would be more appropriate, however, as there is no clear way to label the groups as ortho or meta because there are, of course, two amine groups, neither values are really very appropriate and the method of analysis breaks down.

4.6.2 Conductance Mechanism

For molecules such as alkanedithiols in which superexchange is the accepted conductance mechanism, with the conductance G decreasing exponentially with the length of the molecule ($G = A\exp(-\beta_N N)$, equation 1) where A is characteristic of the metal–molecule coupling and is therefore

contact-dependent, β_N is a decay constant characteristic of the repeat unit (–CH_2–), and N is the number of repeat units. β_N for alkanes is generally seen to be 1.2 CH_2^{-1} (1 $Å^{-1}$). A superexchange mechanism is also expected to play a role for molecules 1–4, especially given that the central chemical group (the ''well'') is off-resonance.[3] However, simple barrier tunnelling (equation 1, where the decay constant β is proportional to the square root of barrier height) cannot adequately describe tunnelling across 1–4 since the ''well'' leads to a double tunnelling barrier with the barrier height only reduced at the well rather than across the entire molecule. Figure 4.34 is plotted in linear form since, *a priori*, the relationship between conductance and the HOMO position is not known and in any case is unlikely to follow the simple single barrier tunnelling model implicit in equation 1. The observation that a clearly apparent but rather weak (linear) relationship exists between conductance and HOMO position is noteworthy, and demonstrates that these molecular double tunnelling barriers are not represented adequately by equation 1, for which a reduction in barrier height across the whole molecular wire would lead to a non-linear relationship between conductance and frontier orbital position. Indeed, for a selection of conjugated molecular wires in which a single frontier orbital extends between the two sulphur terminal groups, we observe that *ln*(conductance) scales with the square root of the frontier orbital position, consistent with the general tunnelling model above.

A detailed theoretical description of the mechanism of conduction is outside the scope of this work. However we would suggest that a good starting point could be to model the system using the Gamow formula for the probability of elastic tunnelling under an arbitrary barrier:

$$\Gamma = \exp\left\{-\frac{2}{\hbar}\int_0^L dz\,\sqrt{2m(V(z)-E)}\right\} \quad \text{equation 2}$$

where L is the length of the molecule, and $V(z)$, defined in Equation (3), is the potential energy of the electron under the barrier. The latter is composed of: $V(z) = V_{min} + V_e(z) + V_{conf}(z)$ equation 3.

Here V_{min} is the height of the potential barrier at the conformation of molecular blocks optimal for tunneling in the absence of an external field

$V_e(z)$ is the electron energy in the external field and $V_{conf}(z)$ describes the deviations of the potential barrier height from the optimum value. Although not expected to predict accurate conductances, a comparison between single and double barrier (or barrier indentations) should be possible.

A very recent study of the single molecule conductances of a series of very short conjugated molecules (substituted 1,4-diaminobenzenes) using an

STM-based break junction technique found that electron donating substituents resulted in higher molecular conductances, and there was a (very approximate) correlation between the conductance and the Hammett σ parameter, consistent with hole transport (i.e. one could regard the molecule as being in a 'positive transition state' as it conducts).[16] Also, recent thermoelectric effect measurements on conjugated dithiols trapped between gold electrodes in the presence of a temperature gradient gave positive values for the junction Seebeck coefficients, indicating hole conduction (see page 63).[17] In our molecules, the presence of the alkyl tunnelling barriers means that the aryl substituents are far removed from the gold contacts during measurement, so that possible complications from steric effects, and consequent differences in contact geometry, are much less likely. It is interesting that although the conduction mechanism may well be different for short, conjugated molecules, the effect of substitution is the same.

4.6.2.1 Substituent effect

Next we shall discuss the rather weak effect the substituent group has on the single molecule conductance. This has been described in a recent theory paper concerning the short benzenediamine and dithiol molecules. The reason given for the weak influence of the substituents on the short

benzenediame molecules is that charge neutrality pins the HOMO/LUMO molecular levels, making it difficult to shift them relative to E_F.[18] However, in our case the benzene centre group is strongly decoupled from the metal electrodes, making Fermi level pinning unlikely. Instead our results may be explained by considering that the tunnelling current is dominated by the two hexyl chains. We have seen that molecules with redox active centre groups (viologen and pyrrolotetrathiafulvalene) only increase in conductance when the Fermi level is brought within a small fraction of an electronvolt from the molecular level (roughly ± 0.2 eV – see chapter 3). Thus, even though we change the frontier orbital energies of the centre group substantially, by more than 1 eV between the tetrafluoro-benzene and dimethoxy-benzene, the HOMO levels are still off-resonant with respect to the gold E_F and thus little effect on the molecular conductance can be seen. Away from resonance the 6V6, 6PTTF6 and 6Ph6 all have approximately the same conductance, which further illustrates this point.

4.6.2.2 Electrochemical results

The behaviour can be rationalised further by considering the lack of electrochemical potential dependence that 6Ph6 shows over the region of 0.8 V (figure 4.13). According to our Spartan calculations (see table 1) the

energies of the HOMOs for 6Ph6, $6Ph(F)_4 6$ and $6Ph(Me)_2$ all lie within 0.6 eV of each other, which is a similar energy range to that accessed by varying E_S. Thus we could have expected to see a small change under electrochemical potential control of some, if not all of the molecules. The fact that changing the substituents between fluorine and methoxy causes a factor two increase in the conductance whilst no change is observed by changing the potential of the substrate is a little surprising, taking into account that it is the relative change in the barrier between E_F and the molecular HOMO which is important. However, the absolute barrier height is unknown in both situations – electrochemical control and standard open-circuit. The same behaviour under electrochemical control is seen for octanedithiol[19] and benzenedithiol[20]. For short molecules about 1 nm in length, such as these examples, overlap of double layers on tip and surface are likely and could cause a lack of electrode field screening from the molecule. This should be less of an issue for 6Ph6, which is approximately 2.1 nm in length. What this could indicate is that the orbital energy change between benzene rings with different substituents is not strictly the cause for the observed effect. Instead, the electron density difference for each substituent may be a stronger factor. The higher the electron density the higher is the HOMO energy, so the dimethoxybenzene has the highest electron density on the ring and the tetrafluorobenzene the least. As we would expect hole tunnelling to dominate through alkane chains (based on

the relative orbital positions of the highest and the lowest chain orbitals to the gold Fermi level – see table 1) a quasi-intermediate involving hole localisation on the ring would be more stabilised by the strongest electron donating group, the dimethoxy. We suggest 'quasi-intermediate' rather than a full two-step mechanism, with full localisation and relaxation regarding the HOMO, as this should not be possible due to the strong energy mismatch between gold and benzene.

4.6.6.3 Influence of the alkyl chains on the conductivity

If we compare the conductance values we have obtained for our thiohexyl substituted benzene derivatives to those measured by Venkataraman[16] then the first thing to notice is that the values are much smaller, by 2-3 orders of magnitude. This can be simply explained by the presence of the saturated alkyl linker groups. Our compounds consist of 2 x 0.8 nm -$(CH_2)_6$- groups. However, based upon the generally observed value of the decay constant, β, for alkanedithiols (generally 1 $Å^{-1}$)[21] we calculate that the conductance should be in the region of 5 orders of magnitude less than Venkataraman's values for substituted diaminobenzene derivatives (1, 4-benzenediamine, G = 495 nS). This should also be the case when compared to 1,4-benzenedithiol, measured by Tao (G = 852 nS). As can be seen in figure 4.35 below, the predicted conductance for 6Ph6 based on a

decay of 1.3 CH_2^{-1} is more than 3 orders of magnitude lower than that actually measured.

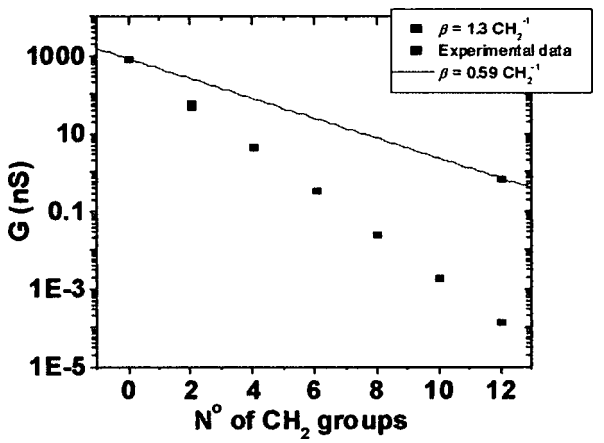

Figure 4.35. Predicted conductance values (black squares) for nPhn molecules with a $\beta = 1.3$ CH_2^{-1} - based on measurement of BDT, n = 0, (852 nS)[20]. Blue squares are experimental values of 1Ph1 and 6Ph6. The Black line is a fit line with $\beta = 0.59$ CH_2^{-1}.

The fact we only observe a 2-3 order of magnitude reduction in conductance for adding 12 CH_2 groups suggests that the conduction mechanism for 6Ph6 is different from either alkanedithiols or fully conjugated benzene ring systems without alkyl groups. If we look a little closer at the conductance values then we see that the conductance we measure for bis-thiohexyl-tetrafluorobenzene is a factor e^7 smaller than the 1,4-diamino tetrafluorobenzene, and bis-thiohexyl-dimethylbenzene is $e^{6.5}$ times smaller than 1,4-diamino-2,5-dimethylbenzene. A $\beta \approx 1$ CH_2^{-1}

implies that for each CH_2 group added the conductance should decrease by a factor e. Thus we see that the conductance is essentially reduced by an amount expected for adding about one thiohexyl chain, but not two. The question is how can we explain this unusual behaviour?

There are obvious differences between the two systems apart from the alkyl spacer units. Venkataraman studied diaminobenzenes, forming Au-NH_2 contacts rather than S-Au. Venkataraman and Tao have shown that different contact groups lead to a different absolute conductance for a molecule, but the same length dependence, at least in the case of X-$(CH_2)_n$-X where X can be SH, COOH or NH_2. So a β of 1 $Å^{-1}$ is found with all contact groups. The spread in conductances of alkane chains differing only by contact falls within the range of about one order of magnitude, so taking this and the previous observation into account makes it unlikely that the 2-3 orders of magnitude higher than expected conductance we see for compounds 1 – 4 could result purely from the Au-S bond. Wandlowski measured the β decay constant for different lengths of alkyl spacer on either side of a viologen moiety and found a value of 0.6 $Å^{-1}$ (0.74 CH_2^{-1}) for chain lengths between 5 and 8 CH_2 groups on each side (10 and 16 CH_2 groups in total) with the viologen in the 2+ state. By extrapolation of the conductance to the contact distance the contact conductance was estimated as 10μS, which is the same as that found for alkanedithiols. The β value for the bisalkylviologen series is similar to the 0.5 $Å^{-1}$ (0.6 CH_2^{-1}) we

extract from our measurements for 6Ph6. Incidentally, for the viologen compound 6V6 Wandlowski measures a conductance of 1 nS,[22] which is very close to the values we measure for our analogous benzene systems, although still a factor 2 larger than we measure for the same compound.[23] The similar value of conductance lends weight to our measurements and we can see that 1 nS is about the correct conductance for the generic system C_6-Ar-C_6.

4.6.6.4 Conductance of 6Ph6 compared to equivalent length alkanedithiols

The presence of an aromatic group between two alkyl linkers greatly facilitates charge transport through the molecule as can be seen by the much lower β factor, which is approximately half the value when compared to pure alkanes. For 6Ph6 the conductance is (0.72 ± 0.24) nS, as determined by the I(s) method. This is greater than any conductance measured for dodecanedithiol (HS-$(CH_2)_{12}$-SH), which is between 0.03[24] and 0.4 nS[15]. Dodecanedithiol is also considerably shorter that 6Ph6, at 1.6 nm S-S distance compared to 2.1 nm for 6Ph6. Hexadecanedithiol would be the equivalent alkanedithiol, which would have a conductance of circa 4×10^{-4} and 5×10^{-5} nS (based on extrapolation of data from

reference 15), which is very much lower than the conductance of 6Ph6. How can we explain this? Sufficiently strong interaction between a tunneling electron and its environment can lead to loss of coherence and to a different mechanism of transport. Such an interaction depends on the contact time, the time the tunneling electron is in contact with the medium with which it will interact. Landauer & Buttiker originally developed this concept[25], and when their treatment is modified for a molecule, the resulting contact time is;

$$\tau \approx N\hbar / \Delta E$$

where ΔE is the gap energy separating the electrostatic potential of the electrode with the appropriate frontier orbital energy on the molecule, and N is the number of subunits within the molecule. It can be seen from this equation that for short molecules with a large ΔE between the frontier orbitals and metal electrode Fermi level, that the contact time for the electron is shorter than for longer molecules with a lower ΔE. In other words inelastic events become more likely for longer molecules. In particular it has been shown that for DNA molecules coherent tunnelling dominates for short oligomers less than 2nm, giving a characteristic exponential decay in conductance. Incoherent hopping dominates over distances greater than 2nm.[26]

Our SPARTAN calculations place the HOMO, which is localised on the benzene ring in 6Ph6, 1 eV below the Fermi level of the gold electrodes (-6.23 versus -5.2 eV). This is much closer than the highest occupied alkyl chain orbital, which we calculate as being -8.05 eV – indicating the contact time is greater for 6Ph6 than its C_{16} analogue. If the contact time becomes comparable with the timescale of some of the molecular motions (vibrations or rotations for example), then inelastic events become more important, whereas coherent tunnelling becomes less probable. Indeed, the inelastic spectra of single alkanedithiol molecules have been recently reported, showing that electrons can couple to molecular vibrations even in high barrier compounds[27]. If the vibrations of the benzene ring cause the electron to 'acquire' energy as it passes through the molecule, this would result in an overall increase in the observed current when compared to coherent transport only.

4.7 Summary

The aim of this work was to assess the properties of a non-redox active aromatic group on the conduction of bis-alkyl, double tunnel barrier, compounds. Initially we wished to see a change from a superexchange to a hopping mechanism. Single molecule conductance measurements on 1,4-

bis-(6-thiahexyl)- benzene derivatives have revealed firstly that benzene rings serve as an effective indentation in the tunnelling barrier of two thiahexyl alkane chains and secondly that the more electron-rich benzene rings give higher conductances, consistent with hole conduction (i.e. via the benzene HOMO). The conductance measured for all the compounds measured lies between 0.4 and 1 nS, and are essentially very close values to that measured for the redox-active compound 6V6 in its so called 'off state', i.e. in the 2+ oxidation state. This means that the conduction mechanism is most likely universal for any system of two highly insulating barriers (alkane chains) on either side of a (less insulating) aromatic system. Benzene is the simplest aromatic ring system, with the closest lying orbitals still more than 1 eV off-resonant from the gold Fermi level. Hence, we expect the electron tunnelling still applies as the conductance mechanism across the molecule. However, if a purely superexchange mechanism were to operate, then a lower conductance should be observed as two thiahexyl chains together makes a molecule of dodecanedithiol which has reported conductances of between 0.08 and 0.35 nS. As we have observed, consistently, larger conductance groups for most of the benzene compounds studied (at roughly 4 – 5 times the main value and likely to correspond to the high conductance state) we can tentatively suggest that the main values we report here are related to a different (lower) conduction

group than that of the 0.35 nS for dodecanedithiol. This makes the effect due to the presence of the benzene group rather significant.

One the one hand the benzene group must contribute to the total resistance of the molecule as it is a tunnel barrier with height and length. On the other, the conductance for 6Ph6 seems to suggest an enhancement as compared to dodecanedithiol. Hence, a conduction process different to that in pure alkanes seems to be at work in this 'double barrier' molecules. At the present stage a detailed theoretical description of the mechanism of conduction is outside the scope of this work. This series of molecules likely represents an intermediate situation between a superexchange and hopping mechanism. Our results show that electronic properties of single molecule wires can be tuned by applying relatively straight forward chemical principles, but it also emphasizes some of the counter intuitive properties of charge transport in single molecule tunnelling wires.

BIBLIOGRAPHY

[1] X. L. Li, J. He, J. Hihath, B. Q. Xu, S. M. Lindsay, N. J. Tao, *J. Am. Chem. Soc.* **2006**, *128*, 2135-2141.

[2] V. B. Engelkes, J. M. Beebe, C. D. Frisbie, *J. Am. Chem. Soc.* **2004**, *126*, 14287-14296.

[3] W. Haiss, T. Albrecht, H. van Zalinge, S. J. Higgins, D. Bethell, H. Hobenreich, D. J. Schiffrin, R. J. Nichols, A. M. Kuznetsov, J. Zhang, Q. Chi, J. Ulstrup, *J. Phys. Chem. B* **2007**, *111*, 6703-6712.

[4] X. L. Li, J. Hihath, F. Chen, T. Masuda, L. Zang, N. J. Tao, *J. Am. Chem. Soc.* **2007**, *129*, 11535-11542.

[5] J. He, F. Chen, S. Lindsay, C. Nuckolls, *Appl. Phys. Lett.* **2007**, *90*, 3.

[6] N. J. Tao, *Nat. Nanotechnol.* **2006**, *1*, 173-181.

[7] C. Li, I. Pobelov, T. Wandlowski, A. Bagrets, A. Arnold, F. Evers, *J. Am. Chem. Soc.* **2008**, *130*, 318-326.

[8] M. H. Lee, G. Speyer, O. F. Sankey, *Phys. Status Solidi B-Basic Solid State Phys.* **2006**, *243*, 2021-2029.

[9] M. Tsutsui, Y. Teramae, S. Kurokawa, A. Sakai, *Appl. Phys. Lett.* **2006**, *89*, 3.

[10] X. S. Zhou, Z. B. Chen, S. H. Liu, S. Jin, L. Liu, H. M. Zhang, Z. X. Xie, Y. B. Jiang, B. W. Mao, *J. Phys. Chem. C* **2008**, *112*, 3935-3940.

[11] P. D. Jadzinsky, G. Calero, C. J. Ackerson, D. A. Bushnell, R. D. Kornberg, *Science* **2007**, *318*, 430-433.

[12] D. P. Woodruff, *Appl. Surf. Sci.* **2007**, *254*, 76-81.

[13] M. Yu, N. Bovet, C. J. Satterley, S. Bengio, K. R. J. Lovelock, P. K. Milligan, R. G. Jones, D. P. Woodruff, V. Dhanak, *Phys. Rev. Lett.* **2006**, *97*, 4.

[14] N. A. Kautz, S. A. Kandel, *J. Am. Chem. Soc.* **2008**, *130*, 6908-+.

[15] T. Morita, S. Lindsay, *J. Am. Chem. Soc.* **2007**, *129*, 7262-+.

[16] L. Venkataraman, Y. S. Park, A. C. Whalley, C. Nuckolls, M. S. Hybertsen, M. L. Steigerwald, *Nano Lett.* **2007**, *7*, 502-506.

[17] P. Reddy, S. Y. Jang, R. A. Segalman, A. Majumdar, *Science* **2007**, *315*, 1568-1571.

[18] D. J. Mowbray, G. Jones, K. S. Thygesen, *J. Chem. Phys.* **2008**, *128*, 5.

[19] N. J. Tao, *J. Mater. Chem.* **2005**, *15*, 3260-3263.

[20] X. Y. Xiao, B. Q. Xu, N. J. Tao, *Nano Lett.* **2004**, *4*, 267-271.

[21] R. W. Murray, *Chem. Rev.* **2008**, *108*, 2688-2720.

[22] Z. H. Li, I. Pobelov, B. Han, T. Wandlowski, A. Blaszczyk, M. Mayor, *Nanotechnology* **2007**, *18*, 8.

[23] W. Haiss, H. van Zalinge, S. J. Higgins, D. Bethell, H. Hobenreich, D. J. Schiffrin, R. J. Nichols, *J. Am. Chem. Soc.* **2003**, *125*, 15294-15295.

[24] Haiss et.al. Journal of the American Chemical Society. Submitted

[25] A. Nitzan, J. Jortner, J. Wilkie, A. L. Burin, M. A. Ratner, *J. Phys. Chem. B* **2000**, *104*, 5661-5665.

[26] A. Berlin, A. Burin, L., M. A. Ratner, *Chem. Phys.* **2002**, *275*, 61.

[27] J. Hihath, C. R. Arroyo, G. Rubio-Bollinger, N. J. Tao, N. Agrait, *Nano Lett.* **2008**, *8*, 1673-1678.

Chapter 5

Oligothiophene molecular wires

Chapter 5

Oligothiophene molecular wires

5.1 Introduction

Oligothiophenes, polythiophenes and their derivatives have been extensively investigated as semiconductors in organic thin film transistors and photovoltaic devices[1]; self-organised thin films of regioregular polyalkylthiophene derivatives have the highest field effect mobilities found to date for polymeric semiconductors[2]. They have a structure akin to polyacetylene, with an alternating double and single bond motif, stabilised by the presence of an electronegative element, sulphur. In general they are known for their hole transporting ability, that is to say their ability to carry a formal positive charge, and this ability increases as the number of monomer units increases in the oligomer series. Terthiophene, for instance, has a lower oxidation potential than bithiophene, which in turn has a lower oxidation potential than thiophene, since the longer the oligomer, the better the stabilisation of a formal charge due to the increase in conjugation across the oligomer's backbone. In general, changes in the energies of the highest occupied and lowest

unoccupied molecular obitals (HOMO and LUMO) and the difference between them (H/L gap), due to the changes in degree of conjugation, begin to lessen above six or seven monomer units. Thus, sexithiophene (T6) has almost the same HOMO/LUMO gap and energies as polythiophene.

We have examined the electrical properties of molecular junctions in which a pi-conjugated, and often redox-active, unit (*e.g.* 4,4'-bipyridinium, pyrrolotetrathiafulvalene, substituted benzene) is sandwiched between two thiahexyl 'spacers', with gold contacts. We showed that the single molecule conductance of the viologen di-thiol 6V6, in which the aromatic unit is a viologen redox group, is 0.5 nS, a value which is significantly greater than that measured for dodecane-1,12-dithiol itself (*i.e.* the equivalent single tunnelling barrier). We found that we could exert electrochemical control over the conductance. When measured under potential control in aqueous electrolyte, the conductance of 6V6 increased approximately six-fold as the potential was swept negative to approach the viologen cation radical redox state. The conductance of the pyrrolotetrathiafulvalene derivative also showed an approximately six fold increase as the electrochemical gate potential was swept past the oxidation redox state. We have since also demonstrated that, with substituted benzenes as the central aromatic unit, we can exert chemical control over the conductance, since for such molecules the conductance is higher for

electron–donating substituents and lower for electron withdrawing substituents.

5.2 Aims

We wanted to explore a system in which we could look at how the degree of conjugation of the well could affect conductance in double tunnel barrier molecules, and to examine the effect of varying the length (and hence degree of conjugation) of the pi-conjugated unit. We therefore synthesised and carried out single molecule conductance studies on a series of *a,a'*–bis(6–mercaptohexyl)-oligothiophenes, oligothiophenes, ranging from n=1 to n=5 (figure 5.1), n being number of thiophene rings. The quaterthiophene (n=4) was not synthesised due to time constraints.

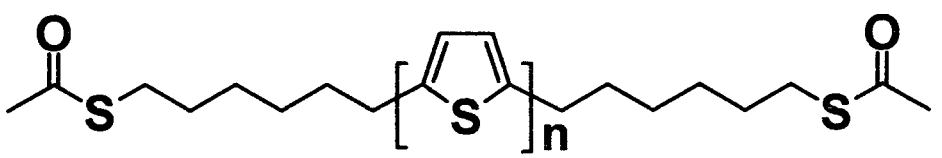

Figure 5.1. Generic structure of oligothiophene molecules, n = 1, 2, 3 and 5.

5.3 Physical properties of oliogothiophenes

Thiophene and its oligomers have attracted considerable theoretical investigation mainly due to their significance in organic electronics. The theoretical work is directed at understanding and modelling their electronic properties, of which perhaps the most important are the HOMO – LUMO positions and their separation (H/L gap). All the properties of an oligothiophene, such as conductivity, absorbance, emission, fluorescence, are determined by these parameters. It is well known that increasing the number of thiophene rings in an oligomer (where each thiophene is connected at the 2,5 positions) decreases the H/L gap by increasing the extent of electron delocalisation[3, 4]. Thus, the HOMO is raised in energy relative to the vacuum, due to increased electron richness, whilst the LUMO is lowered in energy. As an approximation, the conjugated backbone can be considered as a real-world example of the "electron-in-a-box" solution to the Schrödinger equation; however, the development of refined models to predict accurately absorption and fluorescence spectra of well-defined oligo(thiophene) systems is ongoing[5]. Conjugation relies upon overlap of the π-orbitals of the aromatic rings, and the number of (coplanar) rings determines the conjugation length—the longer the conjugation length, the lower the separation between adjacent energy levels, and the lower the H/L gap / longer the absorption wavelength.

Specifically in terms of molecular conductance, two parameters are fundamental in understanding the transport properties. One is the height of the barrier (Φ) which the electron must overcome to transfer across the molecule. The barrier height is determined by the position of the HOMO or the LUMO with respect to the Fermi level of the source electrode. The second is the length of the molecule, which dictates the distance over which the electron must travel in order to get from source to drain electrode. If the oligothiophene unit is higher in energy than the source's Fermi level, then the electron must tunnel across the molecule. Generally, a tunnelling mechanism implies that there is an exponential dependence of the current to the distance it has to travel[6, 7]. Counterbalancing this, however, is the decrease in the H/L gap with increase in length of oligomer, due to the conjugation effect, which means the barrier height becomes lower for each increase in oligomer length.

5.4 Synthesis

Molecules 1 to 3 were synthesised from the relevant dibrominated thiophene by performing a Sonogashira coupling with 1-chloro-hex-6-yne. Reduction of the triple bonds using H_2 and Pd/C was followed by substitution of the chloro groups using potassium thioacetate and a catalytic amount of potassium iodide.

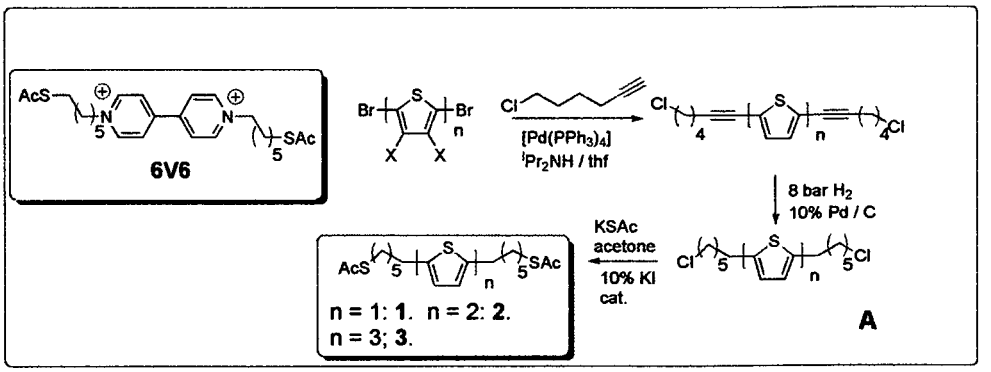

Figure 5.2. Synthesis of molecules 1 to 3.

Synthesis of the n = 5 compound has been previously published.[8] Samples of **1–3** (Figure 5.2) were synthesised and fully characterised by standard chemical techniques. We employed the scanning tunnelling microscopy (STM)-based I(s) technique to determine the single molecule conductances of the n = 1 to n = 5 compounds.

5.5 Experimental methods

5.5.1 Single molecule conductance determination by the I(s) method: additional details

A flame–annealed gold–coated glass slide is dipped into a dilute (10^{-4} – 10^{-5} M) CH_2Cl_2 solution of the appropriate dithioacetate for one minute to allow the formation of a low coverage monolayer. It was not nescesary to

remove the thioacetate groups prior to adsorption as they were found to cleave on gold forming the Au-S bond in the traditional manner in ambient air, as determined by XPS studies. We observe current–distance behaviour characteristic of the formation of molecular wires (gold|6Th$_n$6|gold junctions). We interpret the plateau in the current (*I(w)*) as characteristic of the fully–extended molecule. Moreover, as the tip is withdrawn further, the molecules detach at distances characteristic of their length, providing us with an additional confirmation that we are dealing with molecular events corresponding to the desired molecule, and we record this 'break-off' distance in the form of a histogram. The degree of uncertainty in this measurement is larger than in the determination of conductance because of the range of contact geometries and the difficulty of maintaining a constant starting–point in the measurements.

5.5.2 Experiments in the absence of water

For the argon purging experiments, we used an open STM cell to allow maximum exposure of surface to the atmosphere in the chamber. A diagram of the cell is shown in figure 5.3.

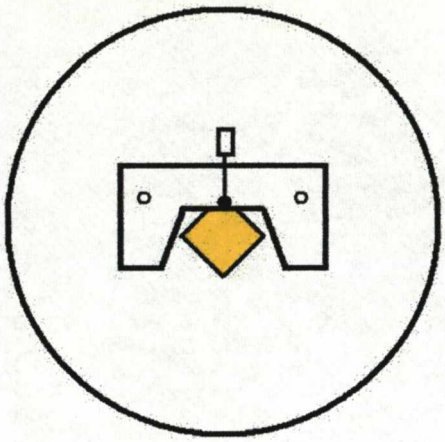

Figure 5.3. Diagram of the open STM cell used in the experiments. The yellow square represents the gold sample. This is only covered slightly at one corner where electrical contact is made.

The environmental chamber employed in the measurements was the PicoAPEX Environmental Control chamber to fit the Agilent PicoPlus system. The tubing connecting the cylinder of BOC Purashield argon was double lined with an inner rubber tube and an outer polyvinylacetate tube. This was to ensure no atmospheric water was picked up by the argon between the cylinder and the chamber. The flow of argon during the purging period of the experiments was monitored using a Dreschel bottle with a 4 mm tube connected to the outflow from the chamber. The rate was kept at 1 bubble per second. Then during the measurements a slight overpressure was maintained by ensuring the level of the meniscus inside the tube was just below the level of the liquid. This kept the chamber air free for the duration of the measurements.

5.5.3 UHV measurements

For measurements under vacuum, data were collected using a commercial Omicron UHV variable-temperature STM (VT-STM) with a base pressure of 3×10^{-11} mbar.

5.5.4 Data treatment and interpretation: histogram analysis

For each I(s) experiment, out of approximately 1000 I(s) scans *ca.* 100–150 scans showed discernable plateaux characteristic of a molecular event, and were therefore saved. Those with no discernable current plateau were not included in the histograms. As described in the literature, current plateaux or steps have been related to single or multiple molecules bridging the tip and substrate gap. Our histograms recorded for **1–4** showed a clear, primary, current peak, marked as I_M (average molecular current). Under such conditions (low coverage, low current set point), higher current peaks than those attributed to two or three molecules are barely discernable. In the case of simpler alkanedithiols, higher current peaks have been attributed to multiple molecular bridges and/or higher co-ordination contacts. For the oligothiophene wires we do not see such multiple primary current plateaus.

5.6 Results

We have studied the conductance as a function of varying the number of thiophene units and found this to be practically independent of the length of the molecule. We have also compared our results[9] with a detailed theoretical investigation of electron transport through these molecules, carried out using the recently–developed *ab initio* nonequilibrium Green's function (SMEAGOL) method[10, 11]. The experimental conductance is found to be almost length independent (indeed, the conductance *increases* from n = 1 to n = 2) and furthermore, no resonances are observed by carrying out I\V spectroscopy. On the contrary, the theoretical calculation predicted a length dependence and negative differential resistance in the I\V spectra, as the HOMO and LUMO levels were calculated as below and 'off-resonant' with the gold Fermi levels for all molecules. It was found that this discrepancy between theory and experiment could be explained not from changes in HOMO energy due to increased conjugation, but from the presence of water molecules surrounding the molecular wires, which not only yields an almost length independent conductance, but also removes transport resonances through continual changes in the polar environment around the thiophene core, which cause fluctuations in the molecular levels. This effect became larger the longer the thiophene

oligomer. As a consequence, for the longest molecular wires considered here, we find that the presence of water can increase the conductance by over *two* orders of magnitude compared with a water-free environment and therefore the presence or absence of water seems a crucial factor to be taking into account when designing future single molecule electronic devices.

5.6.1 Molecule 1: 6-Monothiophene-6 (6Th6)

6Th6 was the shortest in the family of thiophene molecules studied. We tested this compound in three different environments, namely air, under argon and under ultra high vacuum (UHV). The measurements performed in air were very reproducible, yielding the same results (within the error of the experiment of about ± 25 %) on several separate occasions. The conductance in air was found to be (0.61 ± 0.09) nS. This is comparable to the conductance of a similar molecule containing a benzene ring at the centre instead (6Ph6), which gave a conductance in air of (0.74 ± 0.24) nS, indicating that the conductance mechanism could be very similar in these two cases, although it could be coincidental. The conductance of the 6-Monothiophene-6 did not change when the STM chamber was purged with

argon for 24 hours in order to exclude as much air contamination as possible.

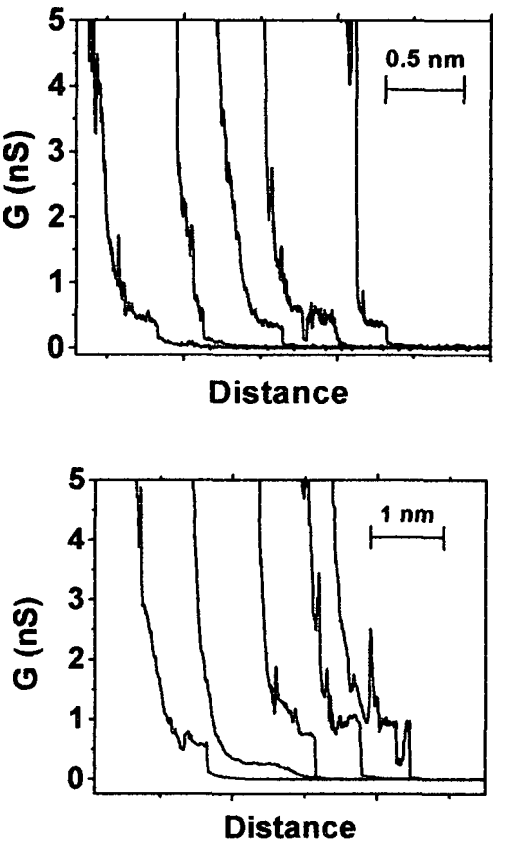

Figure 5.4. I(s) curves for 6Th6 (1) under argon after a 24 h purge (bottom) and in air (top). Both set were recorded at U_{bias} = 0.2 V

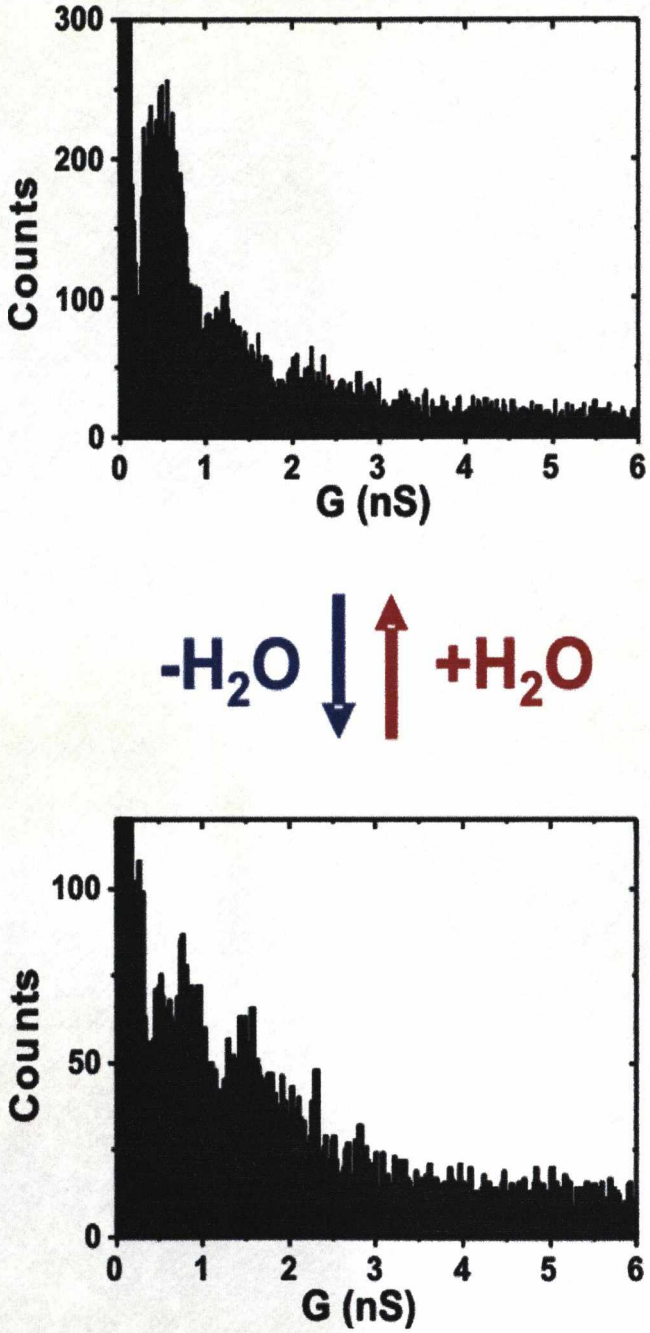

Figure 5.5. I(s) conductance histograms for 6Th6 (1) under argon after a 24 h purge (bottom) and in air (top). Both set were recorded at U_{bias} = 0.2 V

It is, however, worth pointing out that the quality of the histogram (lower in figure 5.5) deteriorated under an atmosphere of argon. Whilst still observable, the number of observed plateau decreases. This may be linked with the process of formation of the Au-S bond in the experiments, in which water may be necessary in the deprotonation of the terminal thiol group. However, the data that was collected was very clear, showing well extended and stable plateaux. This was also true under UHV conditions, where the amount of data showing convincing I(s) plateau was less than in air. Under these conditions, however, the conductance was measured at (0.67 ± 0.13) nS. Two of the best examples are shown below in figure 5.6,

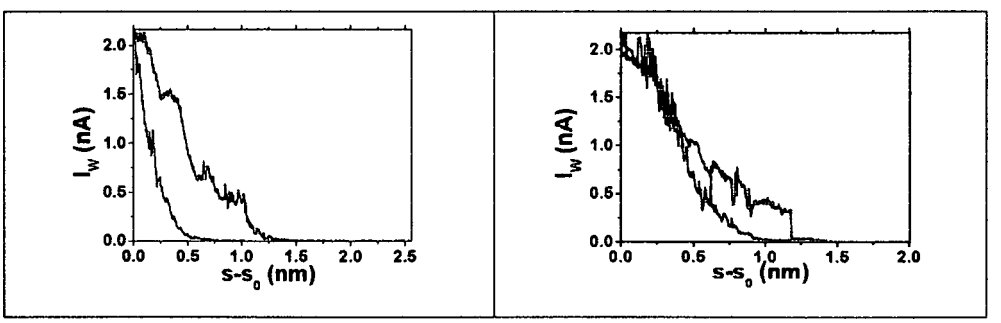

Figure 5.6. I(s) curves recorded at U_{bias} = 0.6 V under UHV. I_{set} = 2 nA. Background traces are also shown for comparison.

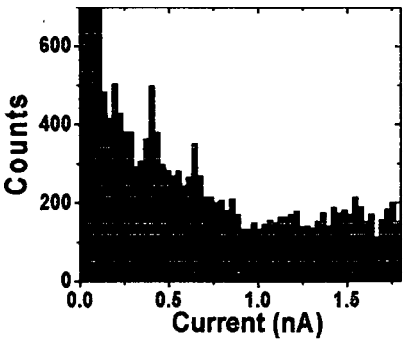

Figure 5.7. Current histogram constructed from circa 30 individual I(s) traces of 6-Th-6 under UHV at 0.6 V, I_{set} = 2 nA.

5.6.2 Molecule 2: 6-Bithiophene-6 ($6Th_26$)

$6Th_26$ was measured in ambient air, under an atmosphere of argon and under a water saturated argon atmosphere. In ambient air a conductance of (1.2 ± 0.17) nS was recorded at a tip-sample bias of 0.2 V and a setpoint current of 4 nA.

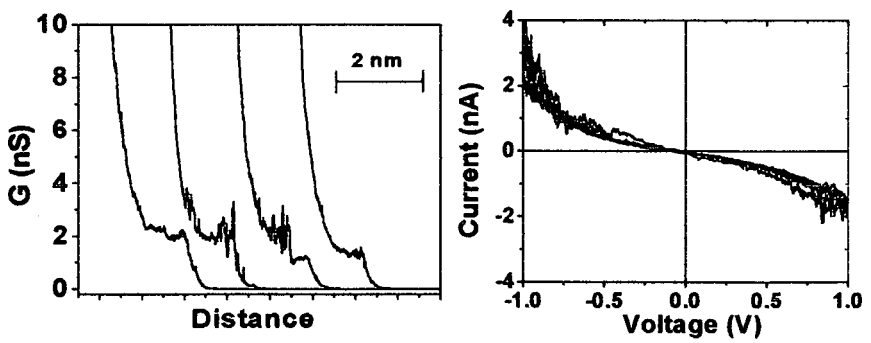

Figure 5.8. I(s) curves for $6Th_26$ (2) in air. U_{bias} = 0.2 V, I_{set} = 4 nA. (left) I\V spectra taken in a Ar/H_2O environment. G ≈ 1nS.

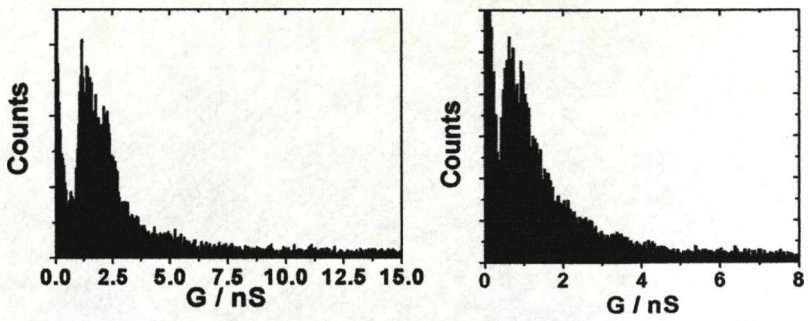

Figure 5.9. (left) I(s) conductance histogram for $6Th_26$ (2) in air. U_{bias} = 0.2 V and I_{set} = 4 nA. (right) $6Th_26$ (2) in Ar/H_2O U_{bias} = 0.6 V and I_{set} = 20 nA

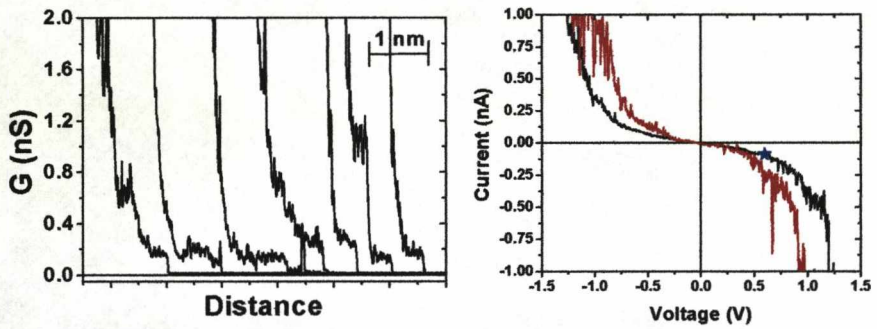

Figure 5.10. I(s) curves for $6Th_26$ (2) under Ar. U_{bias} = 0.6 V, I_{set} = 20 nA. (left) I\V spectra taken under Ar. Black and red traces are one and two molecules respectively. The blue star represents the conductance as measured using the I(s) method (0.12 nS).

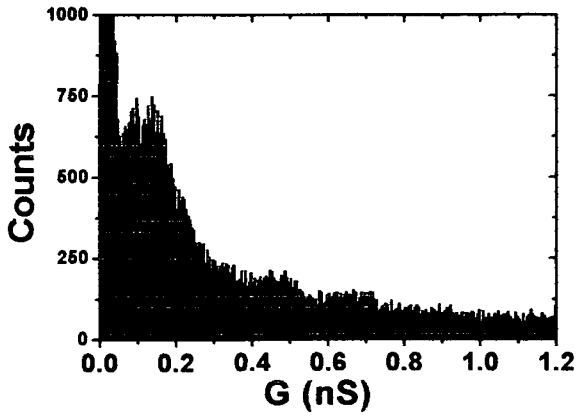

Figure 5.11. I(s) conductance histogram for $6Th_26$ (2) under Ar. U_{bias} = 0.6 V and I_{set} = 20 nA.

5.6.3 Molecule 3: 6-Terthiophene-6 ($6Th_36$)

$6Th_36$ was measured under the same three environments as 6Th6, in air, argon and under UHV. This compound showed a different conductance under argon and under UHV than it did in ambient air. The conductance in air is slightly larger than 6Th6, at (1.0 ± 0.2) nS and the I\V dependence is linear up to 0.6 V. Figure 5.10 shows, however, that when the experiment was performed under an atmosphere of dry argon the conductance diminished to just (0.012 ± 0.006) nS, almost a factor 100 times smaller than in air. Purging for 24 hours was necessary to achieve this low value, and an experiment performed with a shorter purging time of just 15 hours only resulted in a conductance drop by a factor 10 to between 0.1 and 0.2 nS. Under argon it was necessary to use a large bias voltage in order to see

the I(s) plateau because of the intrinsic noise of our system. We used a voltage of 1.0 V which gave a signal to noise ratio of about 3:1 / 4:1.

A reduction in the conductance, when compared to ambient air, was also observed when the molecule was measured under UHV. Under these conditions the conductance fell 25 times to 0.04 nS.

The conclusion which can be drawn from these results is that a component present in the ambient atmosphere is responsible for the large conductance difference observed in ambient air as opposed to the more defined argon and UHV environments.

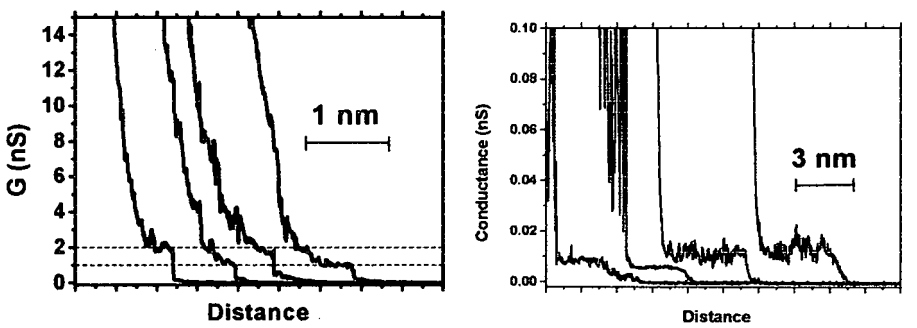

Figure 5.12. I(s) curves for 3 in air U_{bias} = 0.2 V and I_{set} = 7 nA (left) and under argon, U_{bias} = 1.0 V and I_{set} = 7 nA (right).

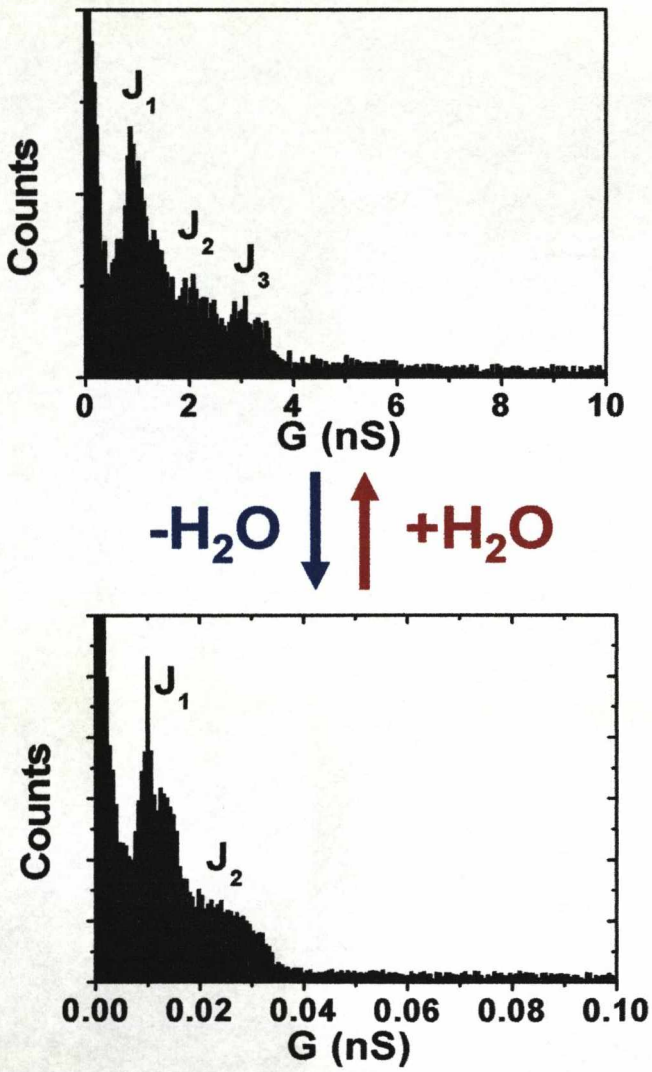

Figure 5.13. I(s) conductance histograms for $6Th_36$ (3) under argon, U_{bias} = 1.0 V and I_{set} = 7 nA (bottom) and in air U_{bias} = 0.4 V and I_{set} = 7 nA (top).

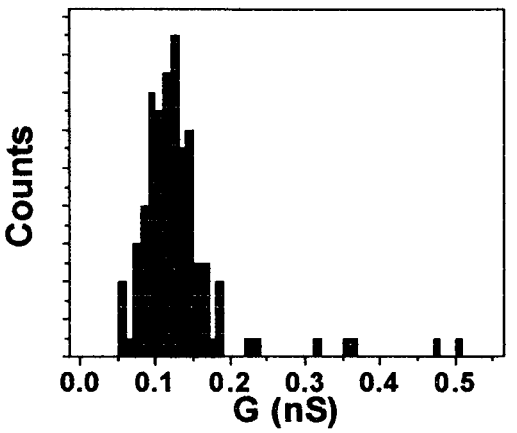

Figure 5.14. I(s) conductance histogram for 3 under argon after a 15 h purge. This was recorded at U_{bias} = 0.4 V and I_{set} = 7 nA

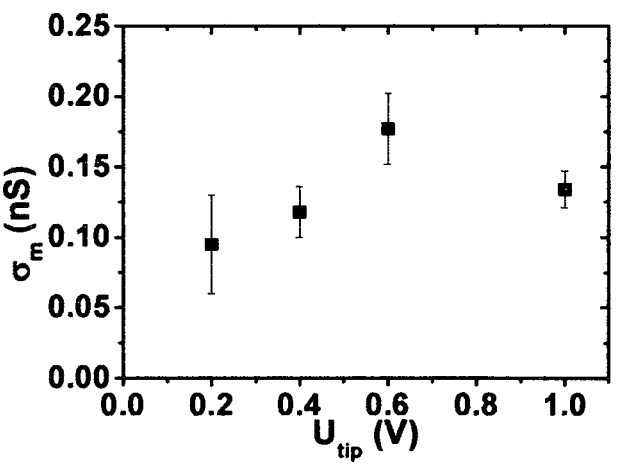

Figure 5.15. Conductance-bias voltage overview of the I(s) results from the 15 h purge with argon.

It was possible to record an I\V spectrum for $6Th_36$ after the 15 hour purge. The conductance after the 15 h purge was between a factor 5 and 10 lower than in air, and a small peak in the I\V at 0.6 V was seen. Confusingly, we

failed to record any I(s) plateau at 0.8 V. One explanation for this is that the molecule may become very conductive at this potential if the HOMO becomes very close in energy to the metal fermi level. We may have been unable to detect this due to the set point current chosen being too low. We use a low set point current in the I(s) technique so as not to crash the tip into the substrate surface. However, this limits our plateau detection to, in this case, 7 / 0.2 = 35 nS, which is equal to 5 x 10^{-5} G_0 and it is likely that at a bias of 0.8 V the gold Fermi level is aligned with the thiophene HOMO, which could cause the molecule to become very conductive. Considering the DFT calculations (see figure 5.22), this could be a substantial fraction of G_0.

An I\V plot was not possible, however, after the system had been purged for 24 h as the current plateaus at 1.0 V were only just visible within the resolution of our microscope. At lower potentials no plateaux were distinguishable above the level of noise on the system, which was about 2-3 pA.

5.6.4 Molecule 4. 6-quinquethiophene-6 ($6Th_56$)

$6Th_56$ was measured in ambient air and under an atmosphere of argon. In ambient air a conductance of (1.2 ± 0.17) nS was recorded at a tip-sample bias of 0.2 V and a setpoint current of 4 nA.

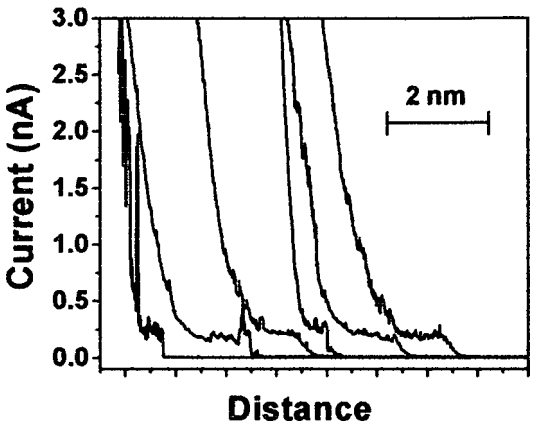

Figure 5.16. I(s) conductance traces for $6Th_56$ in ambient air. These were recorded at U_{bias} = 0.2 V and I_{set} = 4 nA

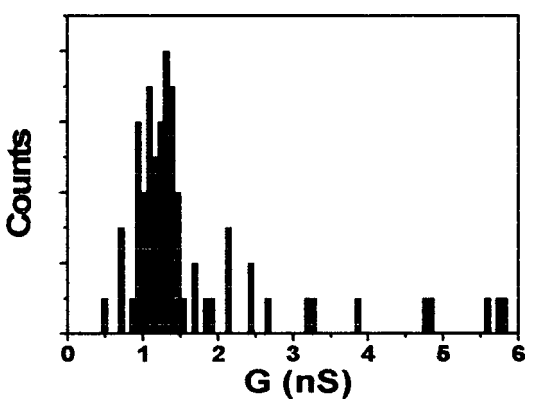

Figure 5.17. I(s) conductance histogram for $6Th_56$ (4) in ambient air. This was recorded at U_{bias} = 0.2 V and I_{set} = 4 nA

When molecule $6Th_56$ was probed under an atmosphere of argon (the same conditions apply as previously used for $6Th_36$, 24 hours of purging the system with pure argon gas) it was impossible to observe any current

plateaux in the I(s) experiment, even at a bias of 1.0 V, possible due to irreversible changes in the adlayer.

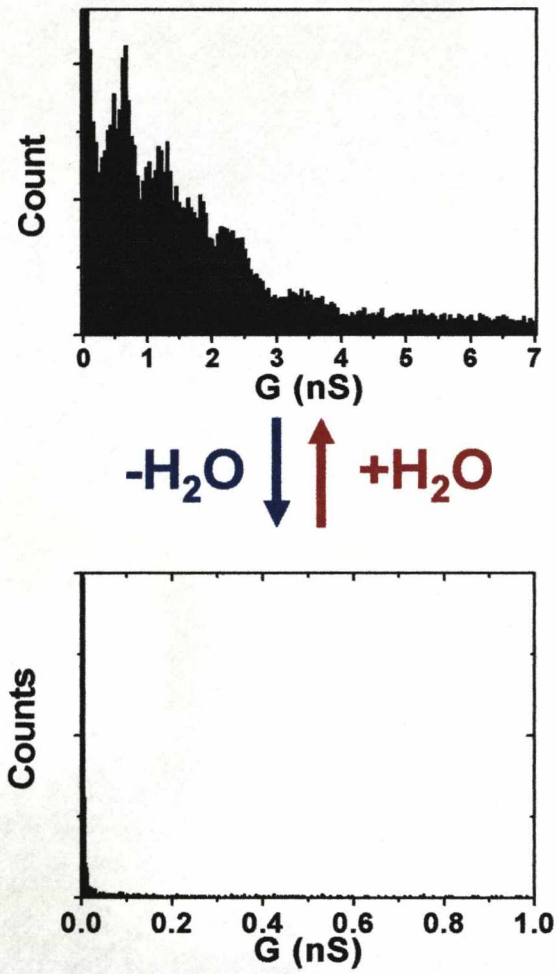

Figure 5.18. I(s) conductance histograms for $6Th_56$ under argon, U_{bias} = -1.0 V and I_{set} = 7 nA (bottom) and in air U_{bias} = -1.0 V and I_{set} = 7 nA (top).

Figure 5.16 shows the data for molecule $6Th_56$ in air (top) and under argon (bottom). The lower histogram of figure 5.16 emphasises that only bare

exponential decay curves were seen after purging with argon for 24 hours, indicating that the single molecule junction conductance for $6Th_56$ has an upper limit of about 6×10^{-3} nS in the absence of water. This was determined from the noise on the instrument on the day of performing the experiment. The noise was ± 3 pA (as measured from the centre of the baseline at zero current) and a signal to noise ratio of at least two is required for a discernible current plateau. At $U_{tip} = \pm 1.0$ V, a 6 pA plateau would correspond to a conductance upper limit of 6×10^{-3} nS.

We also performed measurements on molecule $6Th_56$ under argon atmosphere whilst in the presence of water vapour, by means of a Petri dish containing water placed inside the STM environmental chamber. Firstly the chamber was purged for one hour and a set of 150 measurements were recorded. Some current plateaus were visible close to the baseline at 30 pA after one hour purging - giving a conductance of (0.047 ± 0.010) nS. No larger current plateaux were seen. Although this conductance is larger than that recorded for molecule $6Th_36$ after a 24 hour argon, we only purged the chamber for one hour and are unlikely, therefore, to have removed all the water. We therefore purged for longer until gradually the current plateaus fell below the level of detection on our system.

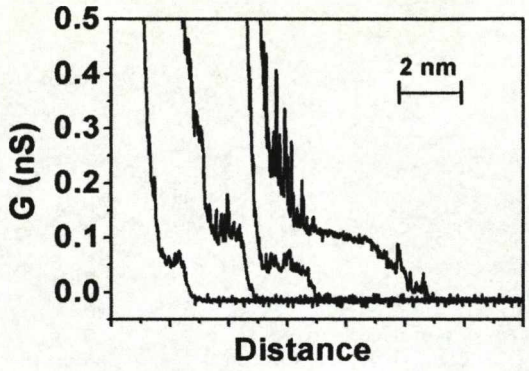

Figure 5.19. I(s) conductance traces for $6Th_56$ after argon purging for 1 hour. U_{bias} = 0.6 V and I_{set} = 5 nA

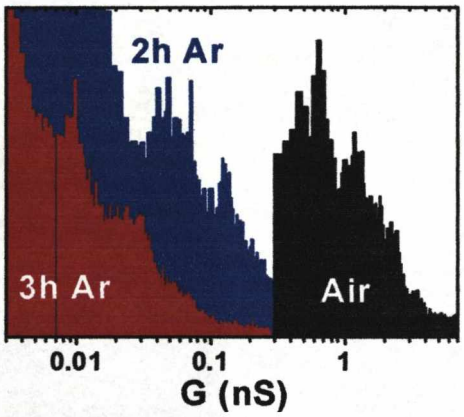

Figure 5.20. Histograms of the I(s) traces obtained at various times of argon purging. U_{bias} = 0.6 V and I_{set} = 5 nA. Conductance (x) axis is shown on a $\log_{10}$ scale (data points from the baseline of the 'air' data have been removed for clarity).

Then a Petri dish containing approximately 25 ml of milliQ water was placed inside the STM chamber, and the system was purged for a further hour with argon gas. The results are shown in figures 5.19/20 below.

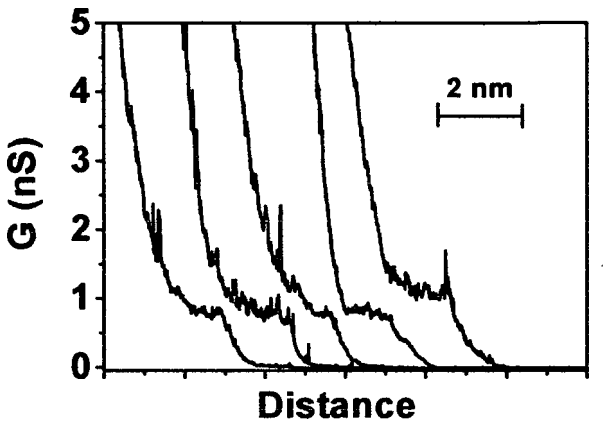

Figure 5.21. I(s) conductance traces for $6Th_56$ in the presence of water vapour and after argon purging for 1 hour. U_{bias} = 0.6 V and I_{set} = 5 nA

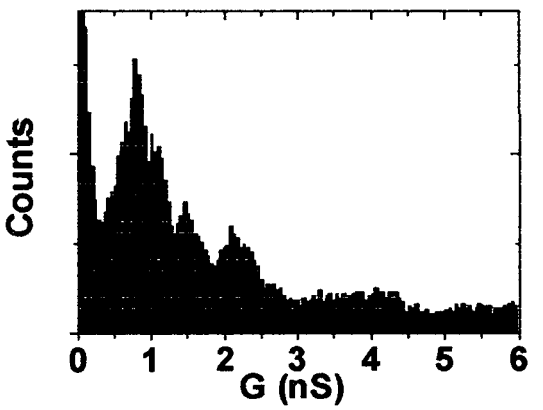

Figure 5.22. I(s) conductance histogram for $6Th_56$ under argon in the presence of water vapour, U_{bias} = 0.6 V and I_{set} = 5 nA

Clearly the conductance of the molecule in the presence of water has returned to the same value as in ambient air, leading to the conclusion that water causes the change in conductance between air and argon environments. Indeed, as molecular plateaux were not visible after purging for 24 hours, but remain visible, albeit at a low value, after just one hour of

purging, indicates that these compounds actually behave as sensors to the *amount* of water in the system. The water sensitivity is such that it may be possible to be able to detect not only the presence of water, but actually how much there is.

5.6.5 Test study. Octanedithiol under argon atmosphere.

As a control experiment we tested the conductance of octanedithiol using the same methods as with the oligothiophene compounds. Firstly a low coverage of ODT was prepared on a gold on glass substrate in from a dry DCM solution (distilled over calcium hydride) using an immersion time of 30 seconds. The substrate was mounted in the STM chamber using the open cell and the chamber was purged with dry argon for 24 hours. The results are shown below in figure 5.21 below.

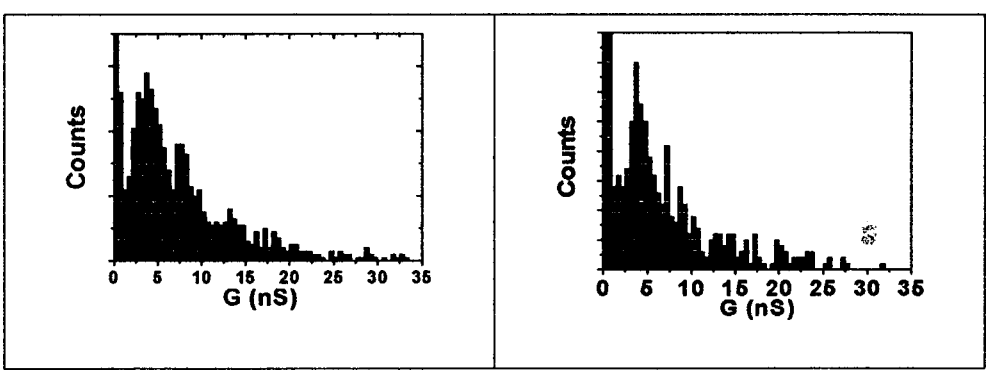

Figure 5.23. I(s) conductance histogram for ODT under argon (left) and in ambient air (right), U_{bias} = 0.6 V and I_{set} = 20 nA

Both data sets were recorded on different areas of the sample. Apart from a slightly broader first peak, both histograms are essentially identical within experimental error, giving a single molecule conductance of octane dithiol of (3.7 ± 0.9) nS under argon, and (4.2 ± 0.9) nS in air.

5.6.6 6EDOT6

We have shown in chapter four that modifying the electron density on the central benzene ring of a molecular wire can 'fine tune' the molecular conductance. We shall now show, briefly, that this is also possible with another type of aromatic group. We have studied the compound 6EDOT6 (EDOT = ethylene-dioxy-thiophene) which, compared to 6Thiophene6, has the structural difference of an ethylenedioxy moiety attached to the central thiophene group.

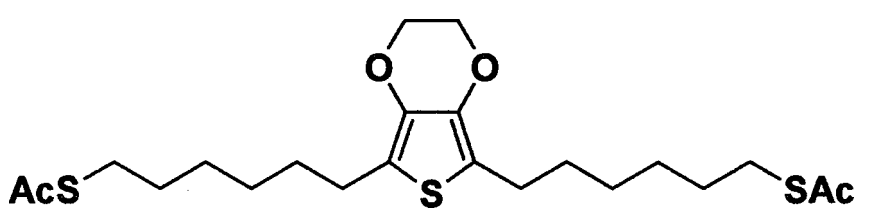

Figure 5.24. Structure of 6EDOT6.

This is a strong electron releasing group, raising the HOMO energy and increasing the electron density on the ring.

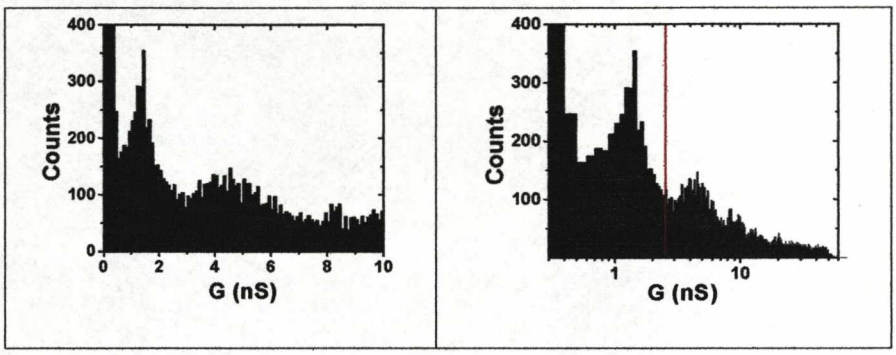

Figure 5.25. Histograms of the stacked I(s) conductance plateaus recorded at U_{bias} = 0.2 V, I_{set} = 10 nA. Number of plateaus stacked was 120. Left and right histograms are linear and log representations respectively. The red line in the right histogram represents the position of the expected 'two' molecule peak at 2.6 nS.

The molecule has a lowest conductance of (1.32 ± 0.33) nS. However, the next highest conductance peak comes at a value of (4.5 ± 0.8) nS, which is not consistent with two molecules of the lowest group. We should, therefore, consider this conductance that of a different fundamental group. The magnitude of difference between the two groups (a factor 3.5) is similar to that found with the benzene compounds.

The value of 1.3 nS for 6EDOT6 most likely corresponds to 0.6 nS conductance group of 6Th6. This is because we have seen that adding two methoxy groups to a benzene ring results in a 30% increase in conductance. The ethylenedioxy group gives a 100% increase in the conductance when compared to the thiophene parent compound.

5.6.7 Summary of results for $6Th_n6$ compounds

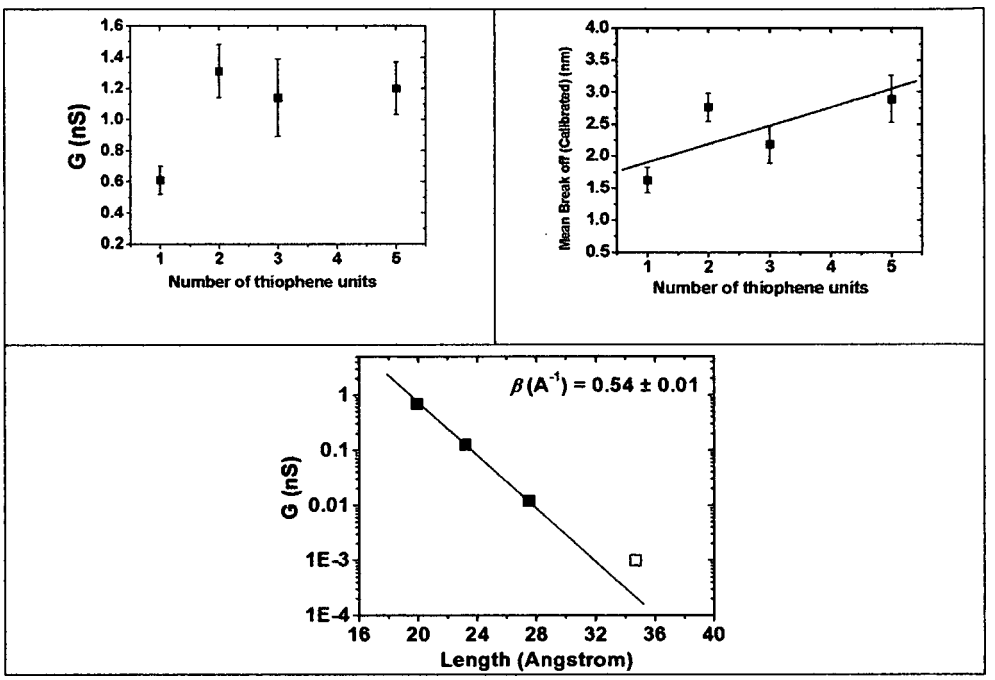

Figure 5.26. (Top left); Summary of the conductivities of molecules 1-4 in air. (Top right); Summary of the mean plateau break-off distance for 1-4 with line of best fit. (Bottom); Summary of molecules 1 - 4 under Ar atmosphere. Molecule 4 is an upper limit only. Based on the β factor of 0.54 $Å^{-1}$ – $G_{mol4} \rightarrow 2 \times 10^{-4}$ nS.

5.7 Polar interactions with aromatic rings

It has been shown experimentally, fifteen years ago in 1992, that water can form hydrogen bonds with benzene[12], although it had even been speculated for some time before that aromatic rings can behave as hydrogen bond acceptors[13]. Recent compelling, yet indirect, evidence for the hydrogen-bonding character of aromatic rings to water and other

biologically significant materials has been found using a number of experiments. These range from low-resolution ultraviolet (UV) and infrared (IR) spectroscopy of molecular clusters in supersonic jets[14] and in matrices[15] to x-ray crystallographic structures of a variety of proteins[13] as well as specifically designed synthetic materials[16]. Although the hydrogen positions were not directly located in these studies, they provided strong support for an interaction of hydrogen bond donors with the high electron density of the aromatic π-cloud. However, by studying the vibration-rotation-tunnelling (VRT) spectra of supersonic jets of water and benzene saturated argon gas the spectral patterns and moments of inertia have shown that water is bound to the face of the benzene ring in a π-complex, the hydrogens pointing towards the ring.[12]

In many respects this is a counter intuitive phenomenon. Benzene is normally assumed to be hydrophobic, which is a reasonable assumption based on the separation of water and benzene in a separation flask. However, the macroscopic properties of bulk water and bulk benzene do not simply translate down to the molecular nano scale. Closer inspection of the partition coefficients of benzene in water shows that benzene is slightly more soluble than purely saturated hydrocarbons – due to a strong quadrupole moment. The character of the water–benzene interaction could explain this higher solubility[17] as reflected by the $\lg(P_{ow})$ values (the

partition coefficients, P, between octanol and water) for benzene and cyclohexane (2.13 and 3.44, respectively)[18].

Noncovalent interactions involving aromatic rings are pivotal to protein–ligand recognition. Indeed, the vast majority of X-ray crystal structures of protein complexes with small molecules reveal bonding interactions involving aromatic amino acid side chains of the receptor and/or aromatic and heteroaromatic rings of the ligand. The complex of the enzyme acetylcholinesterase (AChE) with the drug E2020 (Aricept), which was developed to treat symptoms of Alzheimer's disease, is one example of the diversity of these interactions[19]. The X-ray crystal structure analysis reveals pi–pi stacking, O-H/π, and cation–π interactions as major forces that stabilize the association.

5.8 McConnell Model[20] for donor-acceptor coupling strengths

The relation derived by H. McConnell gives the through bond donor-acceptor interaction for a chain of *m* identical units with nearest neighbour interactions *v* and energy gaps Δ between the relevant donor and bridge localised states. For weakly coupled systems it is shown that the length dependence of the donor – acceptor coupling is exponentially distance

dependent[6]. In donor-bridge-acceptor systems with π-conjugated bridges, however, it is more difficult to split the bridge into well defined chain elements, as opposed to saturated σ-bonded systems, due to the extensive delocalisation, and the validity of the McConnell analysis falls into question.

A number of possibilities exist for the distance dependence through π-conjugated systems and they have been described theoretically by Eng and Albinsson[6]. In their work the natures of the bridges were studied as a function of the number of repeat units in the bridge, and different chemical groups making up the bridge were studied. The results showed that some groups followed an exponential distance rule, whilst other groups showed a non-exponential distance behaviour. For some groups, at a certain bridge length, the transmission began to increase. The critical issue is by how much the energy levels change with increase in bridge length. If the increase is small, then the increase in length dominates the transmission, and an exponential decrease in the transmission is observed. If, on the other hand, the change in energy is large upon increase of bridge conjugation length, then it becomes the energy barrier height which determines the transmission function, causing the transmission to increase with length.

For the groups OPE (oligophenylene ethylene), OPV (oligophenylene vinylene) and OTP (oligothiophene) all of these gave an exponential distance dependence (between n = 2 and n = 5 units), the oligothiophenes

having the lowest β value of 0.37 $Å^{-1}$. However, OE (oligoethylene), Ph-OE (phenyl end capped oligoethylene, OV (oligovinylene) and Ph-OV (phenyl end capped oligo(vinylene) all show non-exponential donor-acceptor coupling strength, according to their calculations. In these bridges the repeat unit is the vinylene or ethylene group, which are the smallest repeat units, involving adding only two carbon atoms per unit. The groups which show exponential bridge length dependence involve longer conjugated units containing, for example, ring twists which lead to poorer extended π-overlap.

The McConnell model therefore predicts that the trend in conductance over the series n = 1 to n = 5 thiophenes should be a decrease with length with an, albeit, low beta decay value. We see, essentially, a beta decay value of zero as there is no decrease in conductance across the series and so simple tunnelling bridge theory breaks down in this case. Another model is required to explain the non-decreasing conductance.

5.9 Modelling the effect of a real environment on single molecule conductance

There are numerous unknown factors in the modelling of molecular junctions, which are usually attributed to causing differences between

theoretical calculations and experimental measurements. Some examples of these factors often neglected are the contact geometry, i.e. the atomistics of the gold-thiol interaction, or more generally the geometry of the molecule in the junction. Molecular tilting effects in junctions was recently explored[21], however, the measured break-off lengths in our study correlate well with the lengths of the fully extended (all-trans) molecules. Hence, we considered the effect the environment could play on single molecule conductance. Here, due to the fact that the experiments are performed in an environment with water present (i.e. ambient air), we considered the influence of water molecules on the junction properties in our study. Ambient air also contains other molecules, such as CO_2, N_2, Ar and O_2. The first three of these are not expected to have a significant effect on single molecule conductance as N_2 and Ar are chemically inert, and do not possess dipole moments, making chemical interactions negligible. Oxygen is known to form singlet oxygen by electron transfer from photoexcited oligothiophenes[22]. It is also known to oxidise slowly polythiophenes, and by forming charge transfer complexes with even short oligomers. This could affect single molecular conductance. However, the DFT calculations suggested that this behaviour would not remove the length dependency in our molecules, so seems unlikely to be a primary cause of the length independency.

According to the ab initio DFT calculations performed on the n = 1 to n = 5 molecules the conduction mechanism of such junctions in a vacuum environment should be by superexchange, and thus the molecular conductance was expected to decrease exponentially with the length of the molecule. Remarkably, however, the experimental molecular conductances we measured are quite large and almost length-independent (Figure 5.24). It is clear from the experimental data in Figure 5.24 that all of the oligothiophene units are acting as tunnelling barrier indentations in air, because the conductances are all similar to that of a much shorter alkanedithiol, like $HS(CH_2)_7SH$ for example, although the oligothiophenes are all much longer than $HS(CH_2)_7SH$ (S...S = 1.06 nm). Even under water free environments, the conductance of $6Th_36$ after argon purging for 24 h is much larger than would be predicted for an α,ω–dithiaalkane of length (2.74 nm) comparable with $6Th_36$ (*i.e.* $HS(CH_2)_{20}SH$, S...S distance 2.69 nm; calculated conductance 1.37×10^{-5} nS), and that therefore, the terthiophene unit is still acting as an indentation in the tunnelling barrier under these conditions.

5.10 Ab-initio non-equilibrium Green's function using the SMEAGOL code

To understand this remarkable behaviour of length independence, detailed theoretical investigation of electron transport through these molecules were carried out using the recently–developed *ab initio* non-equilibrium Green's function (SMEAGOL) method[10, 11]. The calculations were all carried out by the group in Lancaster University, England lead by Colin J Lambert. The relaxed geometry of the oligothiophenes was found using the density functional code SIESTA[23]. A double-zeta plus polarisation basis set, Troullier-Martins pseudopotentials[24] to remove core electrons and the Ceperley-Alder[25] Local Density Approximation description of the exchange correlation, were used and the atomic positions were relaxed until all force components were smaller than 0.02 eV/Å. The molecule was then extended to include the surface layers of the gold leads; a layer comprising 14 atoms was chosen and the extended region included 8 layers of gold to allow a suitable representation of charge transfer effects at a molecule-gold interface. The flexible alkane chains were taken to have a fixed geometry corresponding to the fully-extended, all–*trans* molecule in the junction. The location of the thiol groups was taken to be a top site (*i.e.* directly above a surface gold atom), although the presence of the insulating

alkane chains was believed to limit any dependence on the contact geometry.

First molecular dynamics simulations were performed to find the optimum location of a water molecule in the vicinity of the thiophene units. For 6Th6, figure 5.25 shows the location of two local minima corresponding to positions, which we call "side" and "bottom". The "side" position is the lowest energy position (in qualitative agreement with previous work[20]) and it also produces the most dramatic change in the conductance, and therefore we initially recalculated the conductance in the presence of "side" molecules alone.

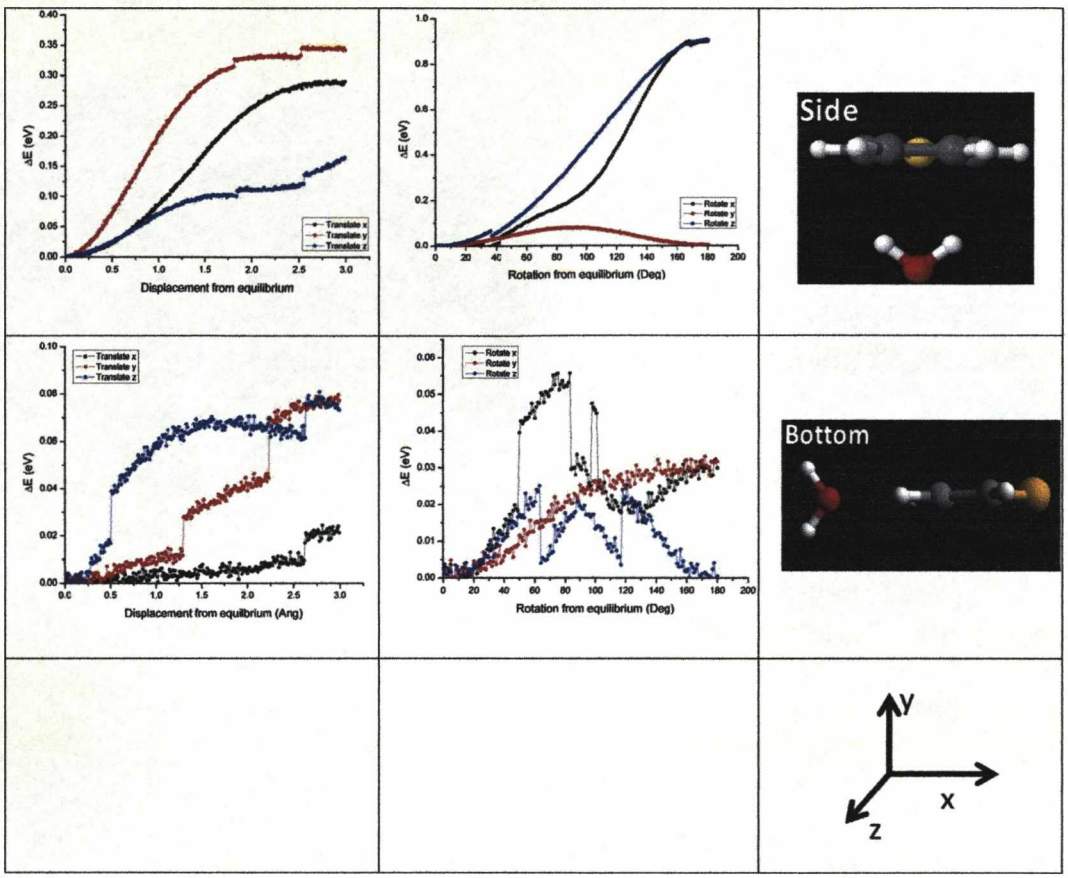

Figure 5.27. Energetics of the water association with the isolated thiophene ring.

The lines describing the translation in the y-axis (side configuration) and x-axis (bottom configuration) tell us the binding energy of the two interactions, with the side being 0.3 eV, and the bottom, 0.02 eV.

5.10.1 DFT Results

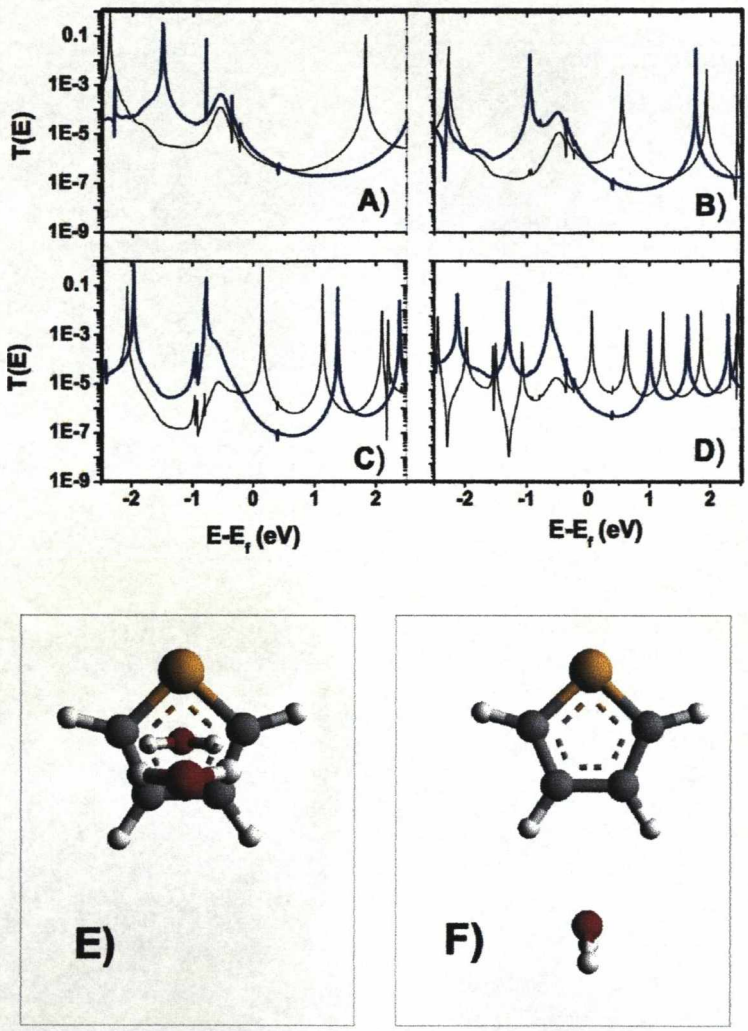

Figure 5.28. Zero bias transmission coefficient versus energy for 1 (A), 2 (B), 3 (C) and 4 (D). The blue curves are obtained in the absence of water and the black curves in the presence of two water molecules located at the lowest energy "side" positions as illustrated in (E). Water can also interact as shown in the "bottom" site (F), although the binding energy is lower.

Some general points to not about the theory are that the SMEAGOL code assumes very little apart from that transport is phase-coherent and that ET

could be ballistic, diffusive or tunnelling. The precise regime of the system is an output of the theory, not an input. It is well known that DFT underestimates the HOMO-LUMO gap[26] and it is not expected that the measured distance dependence is weaker if water has no effect. It is also consistent that in a water free environment the distance dependence is stronger than theory predicts.

In the absence of water, the black curves in Figure 5.24(A-D) shows the electron transmission coefficient T(E) for electrons of energy E for the oligothiophenes. These molecules exhibit the expected behaviour of a decrease in the gap between the HOMO and LUMO resonances as the molecule becomes longer. Figure 5.27 (black squares) shows a plot of the theoretical vacuum conductance at the Fermi energy against the molecular length. It shows that the conductance of the oligothiophenes decreases exponentially with length, in spite of the decrease in HOMO-LUMO gap with increasing number of thiophene rings. The calculated β decay constant is 0.18 $Å^{-1}$. The apparent discrepancy between theory and experiment was resolved by realising that the calculations leading to Figure 5.27 (black squares) assume a vacuum environment, whereas the experiments were conducted in ambient air, containing water vapour, and gold electrodes under such conditions are coated with a film of water.

It is known that electron transport in a conductance gap can be increased by the presence of random scatterers[19]. We therefore examined both the

relative effects of water molecules in the first solvation shell of the oligothiophene units, occupying favoured local energy minima positions, and the effects of randomly-positioned water molecules beyond the first solvation shell.

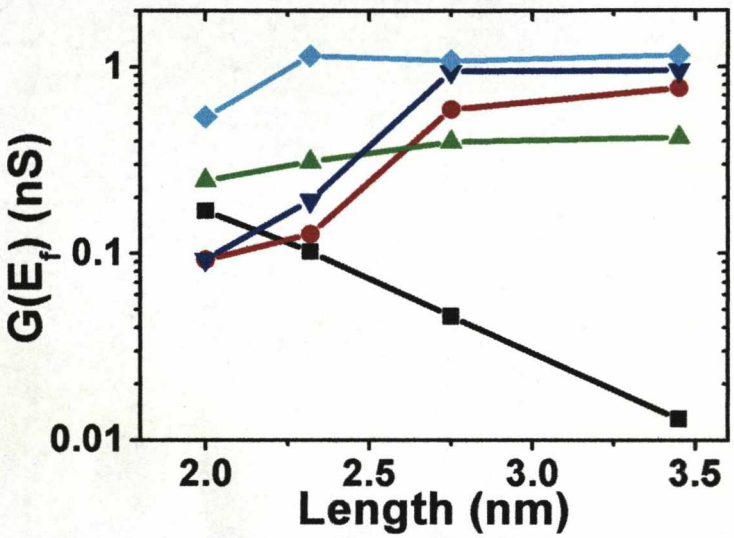

Figure 5.29. Results from the SMEGOL calculations on molecules 1-4 (n = 1 to n = 5). Black squares are with no water; Red circles are water in the side position; Blue triangles are water in the side position plus a random background of water molecules; Green triangles are water in the top position; The blue diamonds are the experimental results.

For all oligothiophenes, two "side" water molecules per thiophene ring were included. Figure 5.27 (blue line) shows that in the presence of these "side" molecules, the transmission resonances are significantly shifted with respect to their vacuum positions (black line). In particular, the LUMO resonance shifts towards the Fermi energy in all molecules, thus causing an increase in the zero-bias conductances. Crucially, the longer molecules

exhibit greater shifts, due to the presence of a larger number of water molecules, which in turn compensates for the reduction in conductance as a function of length. Figure 5.27 (red circles) shows the theoretical zero-bias conductance in the presence of water molecules in the "side" configuration. Clearly, the exponential length dependence is removed and, in agreement with experiment, after an initial rise between n = 1 and n = 2 rings the conductance is predicted to be almost independent of length. It is interesting to note that the same picture is obtained for water in the 'bottom' position (not shown here), except that, in this instance, the transmission resonances are shifted from the vacuum position in the opposite direction, so that the HOMO resonances are nearer to the Fermi energy.

5.10.2 Effect of random water molecules

The effect of a homogeneously-disordered cloud of water molecules surrounding the molecules was examined, and it was found that this alone does not remove the exponential length dependence. However, when included together with the "side"-bound water, additional homogeneously-disordered water does have a small but significant additional effect upon the calculated conductances (figure 5.27, blue triangles). Briefly, in addition to water in the side energy minima, a random distribution of water

molecules were included around the wire using the same density of water in all cases, which is about 10-15 waters. Then 50 different distributions were complied and plotted against the transmission functions together as shown in figure 5.28 and 5.29. Random water also leads to a smearing of transmission resonances, due to random shifts up and down of the energy levels, so that negative differential resistance behaviour (which might be expected from a brief inspection of figure 5.27C or D, for example) is not observed.

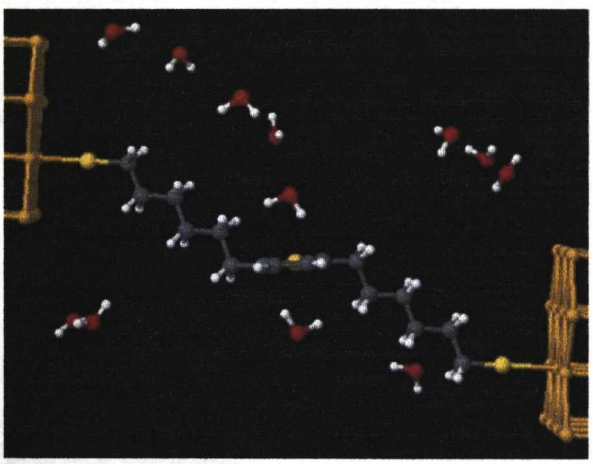

Figure 5.30. Molecule 1 with relaxed side water molecules and 10 additional random waters.

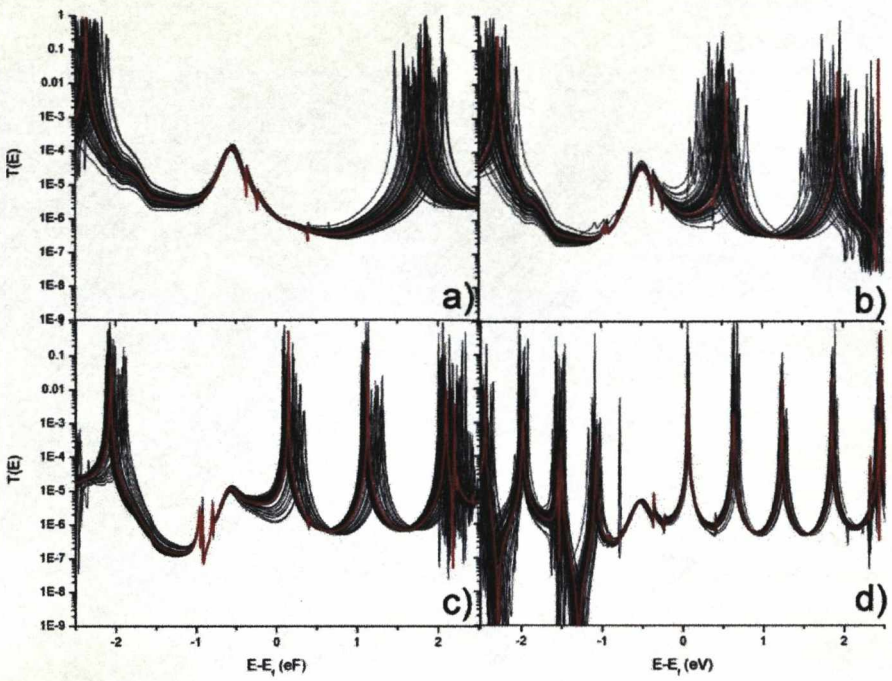

Figure 5.31. Overlaid transmission curves showing the effect of adding a random water background in addition to the relaxed waters in the side configuration for molecules 1-4.

5.11 Discussion

5.11.1 Extent of conjugation

There are two ways to investigate the effect of increasing the conjugation extent upon the single molecule conductance. The first is to change the degree of conjugation whilst keeping the distance between the chemical anchor groups constant. This method was demonstrated whilst our work was underway by the Columbia University group, New York. They

measured 9,10-diaminoanthracene (a), 1,4-diaminonapthalene (b) and 1,4-diaminobenzene (c) (see chapter 3, page 64). They found the order of conductance was a > b > c, the anthracene compound has the highest degree of conjugation and the highest conductance.

Conversely, when the amino groups were positioned at the ends of the molecule, like in 2,6-diaminonaphlathene (d) and 2,7-diaminanthracene (e), the conductance decreased in the order c > d > e. This is the trend we find with the oligothiophenes (measured under argon) and highlights that electron transfer mechanism involves tunnelling, which is sensitive to *distance* as well as energetic barrier height.

5.11.2 Water interaction with thiophene rings

Water may seem like an innocuous substance in which to perform single molecule electrical measurements. However, we have shown that a seemingly inert background can actually play a crucial role in determining the the molecular conductivity. Even though much progress has been made in the understanding of electron transport through molecular junctions, there continues to be a significant difference between results from different methods of measuring single molecule junctions. This is mainly between the breakjunction variations and the I(s) technique. The discrepancies threaten the effort to elucidate the intrinsic electronic properties of

molecular junctions. Hence, to take the field to higher levels, we need to understand what causes such inconsistencies. They are beginning to be explained in terms of the nature of the molecule-electrode contacts, however, there have been surprisingly few reports of significant solvent effects upon single molecule conductance, and in general, far less attention has been paid to the environment in which measurements are performed and to the implications any environmental effects could have on molecular conductance. However, see Albrecht et.al[27] for an account of the behaviour of small gold nanoparticles which suggests that solvent reorganization and dielectric saturation are important for their spectroscopic properties.

Conductance measurements are generally carried out under different environments depending on the choice of the group performing the measurements. These can include: ambient air[28], nitrogen[29], argon or under vacuum[30]. Also, a solvent can be used such as toluene[31], mesitylene or an aqueous electrolyte[32, 33]. It is well known that solvents can strongly affect the rates of chemical reactions through specific solute-solvent interactions which include, amongst others, hydrogen-bonding and dipole-dipole induced interactions. In particular, such interactions have been shown in α-oligothiophenes to cause a red-shift in the absorbance spectra upon increasing the polarity of the solvent[34].

Simple alkanedithiols have been shown to exhibit the same molecular conductance whether measured in air, under vacuum or under liquids of different polarity – at least the same conductance group can be seen under all these conditions.[35] We have performed our own control experiment using octanedithiol in an argon purged environment and found the same conductance reported by Tao in a variety of conditions (circa 3.7 nS). Indeed, reintroduction of ambient air into our STM chamber had no effect on the measured conductance. Some studies have, however, shown that water has a negative effect on the conductance of SAMs of alkanedithiols and conjugated OPE molecules between nanosphere junctions[36, 37]. By introducing specifically water vapour into the system, the conductivity of the junctions decreased, and when the water was removed the conductance increased again. The reversibility of this affect suggests the deterioration in conductance of these junctions is due to an interaction between water and molecules in the SAM, perhaps co-adsorbing on the surface. It is unlikely that there is competitive adsorption between water and strongly adsorbing thiols whereby water molecules would replace thiol molecules on the surface reducing the number of conducting molecules in the gap. However, studies have shown that the presence of hydrogen bonding partners next to metal-sulphur bonds substantial affects the strength of the metal to sulphur bond. For example N-H groups near the Fe-S bond in

Fe^{III}(octaethylporphyrinato)benzene-(2-trifluoroacetamido)thiolate substantially lower the covalency of the metal-sulphur bond[38].

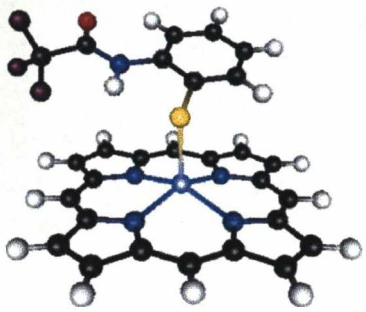

Figure 5.32. Structure of Fe(OEP)L (L = 2-trifluoroacetamide)

DFT modelling of this effect with water molecules confirmed the reduced covalency of the bond. Metal-sulfur-based active sites are abundant in nature, performing a wide variety of functions. Many of these sites feature multiple H-bonding interactions between the ligated sulphur atoms and the protein backbone NH groups. H-bonding interactions are thought to make a significant contribution to the large observed difference between the redox potentials of the active sites and structurally similar inorganic model complexes of electron transfer proteins[39]. H-bonding reduces the Fe-S bond covalency which would localize charge on the donor thiolate/sulfide atom and lower the stabilization of the oxidized state, raising the redox potentials. Further studies on square-planar Ni(II)-thiolate complexes such as Ni^{II}[*N*,*N*'-bis(2-mercaptoethyl)-1,5-diazacyclooctanato] (Ni(DACO))[40]

have revealed that H-bonding effects on M-S bond covalency are different in such systems with respect to the high-spin Fe(III) in the (porphyrinato)thiolates. Although in both cases the H-bonds are oriented along the π donor orbitals, in the case of Fe(III), this orbital is involved in bonding to the half-occupied Fe3d orbitals, while in the case of Ni(II) square planar complex, the thiolate π orbital is nonbonding as the d-π orbitals are filled. Therefore, H-bonding to the π donor orbital of a thiolate weakens the π bonding in Fe(III) but has no effect on the σ bonding in square planar Ni(II).

As the precise nature of the gold-thiol interaction is still not very well understood, especially for individual molecules on surface which move around on the surface quickly like alkanethiols or molecules in breakjunctions, then it is necessary to keep such an interaction in mind as a possible cause, perhaps, for the multiple conduction groups observed for alkanedithiols. However, as the sulphur p-orbitals are involved in the delocalised π-system of thiophene, such an interaction is crucial in modelling the behaviour of these molecules in a real environment.

5.11.3 Comparison with other thiophene molecular wires

We begin by noting that another group has also observed a conductance increase upon increasing the length of an oligothiophene molecular

wire[41]. This observation has been made by the Tao group who use the STM-breakjunction technique. They investigated two compounds, a ter and a quater thiophene both possessing thiomethyl groups in the two α ring positions, shown in figure 5.31.

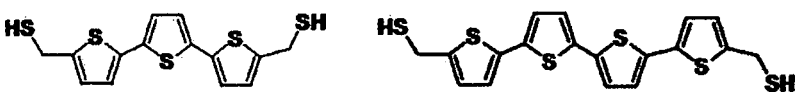

Figure 5.33. Structures of 5,5'-dimethanethiol-2,2':5',2''–terthiophene (left) and 5,5'-dimethanethiol- 2,2':5',2'':5'',2''' –quaterthiophene (right) from ref 38.

They found that the longer of the two compounds, the quaterthiophene, was more conductive than the shorter terthiophene compound. In their analysis, however, they only considered the change in the HOMO-LUMO gap between the two molecules as the cause of the behaviour. In the case of oligothiophenes, our theory predicts that although there is a reduction in the size of the H/L gap with length, the increase in length, and hence tunnelling distance, of the oligomer dominates the properties of the transmission curve, giving an exponential decrease in conductance with length. This is in agreement with the theoretical study carried out by Eng on thiophene bridges[6]. Interestingly, in Tao's results, there is also a medium dependency apparent for the quaterthiophene between the toluene

environment and the aqueous electrolyte. Although this is not explicitly mentioned, it can be deduced from the histograms that in toluene the conductance is 7.5 x 10^{-5} G_0, whilst in aqueous electrolyte it increases to 6.7 x 10^{-4} G_0. This behaviour agrees very well with our observations that the presence of water induces a higher conductance in oligothiophenes.

On the other hand, another set of measurements on oligothiophenes using a scanning probe microscope have shown the predicted exponential decrease in conductance with longer oligothiophenes[42]. In this study the oligothiophenes, having a methanethiol anchor group and numbering between one and four thiophene rings, were fabricated into a self assembled monolayer (SAM) on a gold (111) substrate. Electrical measurements were then performed using a AFM equipped with a Pt coated cantilever. The experiments were performed under an atmosphere of nitrogen using a force of 1 nN. At the low bias of 0.1 V the current measured across the oligothiophene layers falls off exponentially with a β decay factor of 0.41 $Å^{-1}$. This experiment is different to our single molecule measurements in that many molecules will be contacted between the tip (of 20 nm radius) and the substrate. Also, the molecules are asymmetric, having a thiol group only at one end of the molecule, making the contact resistance between the tip and the thiophene an unknown parameter. However, the behaviour falls into line with the expectations of our theoretical calculations in the absence of water, having almost the same

β decay factor. It is reasonable to assume in this study that, due to the densely packed nature of the thiophene film on the surface, coupled with the fact that the experiments were performed under an atmosphere of nitrogen, no water is present around the thiophene rings.

It has emerged recently that different conductance values can be seen in one set of current-distance experiments, especially using the breakjunction method. This has been shown for various head groups including thiol, carboxyl and amine. If the thiol sits in a 3 fold hollow site it has been shown to have a better coupling, and therefore lower contact resistance, to the metal than when sitting on top of an individual gold atom. This has been predicted theoretically, and inferred from experimental data by the distance a current plateau extends before the current jumps to another, usually lower, plateau. It is assumed that this is due to a transition from a hollow to a top site. For thiols the ratio between the two high and low plateaux is generally between 4:1 and 5:1. The difference between the highest and the lowest conductance we measure for molecule 3 is near a factor 100, which puts the difference outside the boundary of a contact effect. Also, we see very few transitions from the high conductance plateaux to a lower plateau in the presence of air. We seem to observe mostly the final plateau. Conversely, under argon we see no plateaus that are larger than 0.01 nS, even starting from a set point of 7 nA, which

indicates that the environmental effect we observe is not a consequence of changes at the Au-S bond.

5.11.4 Water effects on other types of molecule – PTCDI

In another series of measurements by the Tao group it has been shown that there is a temperature effect on the single molecule conductance of a particular redox active compound, namely a derivative of perylene tetracarboxylic diimide (PTCDI)[43] (see figure 4.2). This effect, however, is only manifest in an aqueous environment, and there is no temperature dependence in the non polar solvent toluene. This leads one to believe that water has a different interaction with these molecules as compared to non-polar solvents. A theoretical study which sought to provide a model for this behaviour suggested that the temperature-dependency of the PTCDI compounds could be attributed to the statistical behaviour of elastic electron transport induced by the temperature-dependent thermal motions of the surrounding water molecules[44] – the theory makes very similar arguments as Ulstrup and Kuznetsov.[45] Indeed, it was noted by the authors of the experimental work that there must exist a strong coupling of the redox states of the PTCDIs to the polarized water molecules of the solution. They further concluded that the results suggest the electron transport in these redox molecules is a thermally activated two-step

sequential process, in which electrons, assisted by thermal fluctuations, tunnel into the molecule from one electrode and out of the molecule to the second electrode. Whilst there is still doubt as to whether a two step mechanism applies, it seems very probable that the temperature-dependency arises from thermal fluctuations of the surrounding water molecules, and not from an increase in the energy of the electrons at the Fermi level, as this then would presumably be independent of the solvent. Furthermore, the authors fitted their results to a modified Marcus equation in order to determine an activation energy for the process. It is well understood that the coupling of redox states to the polarization of solvent molecules plays a critical role in the electron-transfer phenomena as described by Marcus theory, which informs us that there is an associated reorganization energy to the electron transfer process, due to the polarization of the surrounding polar solvent molecules and the structural relaxation of the molecule. By linear fitting the activation energy, E_a, vs $(V_g - V_0)2\lambda$, (where V_g and V_0 are the gate potential and the redox potential, respectively, and λ is the reorganisation energy) E_a was found to be 0.4 and 0.6 eV for thiophenyl-PTCDI and thioethyl-PTCDI, respectively. In the side configuration, when the δ^+ dipole moment of the water interacts with the δ^- charge of the aromatic π-cloud, the interaction should be stronger the more electron-rich the π-system is. Thus the activation energy is larger for the more electron rich PTCDI. This seems in good notional agreement with

the idea that the activation energy corresponds to the process of water molecules dissociating from the molecular wire in order to reorganise itself within the new electrostatic field they experience during electron transfer. What the theoretical model does not endeavour to explain is why there is a decrease in the temperature-dependence approaching the redox transition of the PTCDI, whereupon there ceases to be any dependence to the temperature. Let us consider the matter in terms of our own theoretical model for water gated transport. In our model the inner solvation shell is static, and causes a rigid shift of the HOMO and the LUMO in one direction. The outer solvation sphere is not fixed and is allowed to move relative to the thiophene molecule. This, we have found, causes a smearing and broadening of the transmission resonances, leading to loss of sharp steps in the I\V dependence of these compounds. If we can increase the energy of the outer sphere waters molecules, by increasing the temperature, then their thermal motions will increase and blur/broaden the resonances. In the experiments, this will be more noticeable the further off-resonance the level is, and should completely disappear when fully on-resonance as a broadening of the transmission resonance does not change its relative position to E_F. Solvent broadening of spectral lines is a well known phenomenon in absorption and fluorescence spectroscopies. Various studies have noted the importance of the H-bonding capabilities of the solvent with the solute in causing inhomogeneous line broadening.

In summary, it is fair to say that perhaps our model, whilst including random water molecules, does not include enough to provide a realistic picture of the environment in our experiments. In the theoretical treatment of the PTCDI system, the author use 60 surrounding water molecules, which itself is cut down from 800 by choosing only the nearest 60 molecules for computational reasons. We may, therefore, underestimate the broadening effect of the random background of water in our system. We also make the assumption that the inner solvation shell is fixed. If this shell also fluctuates (which it will) then there would be a very pronounced effect on the position of the transmission resonances. So whilst we cannot be sure that water rigidly shifts the energy levels of the thiophene molecules, or whether a resonance broadening mechanism applies, or indeed both, we can be sure of the importance of water in understanding the transport behaviour in these types of junction.

5.12 Possible sensor applications

We suggest that the molecular conductance for $6Th_36$ and $6Th_56$ is sensitive to the *amount* of water present in the system when performing I(s) measurements. Depending of the time spent purging the STM chamber progressively lower conductivities were observed the longer the system was purged for. For $6Th_36$ a ten hour purge (figure 5.12) gave a tenfold

reduction in the conductance, whilst a longer 24 hour purge took the conductance down by a further factor of ten. The same trend was observed for $6Th_56$, although in this case only a 5 hour purge was required before we could no longer detect the molecule (see figure 5.18). Further measurements are required, with greater control of the amount of water present, to determine perhaps a calibration standard. However, these crude results suggest that a water sensor could be built out of just a single molecule. The larger sensitivity comes from the longer oligomer, $6Th_36$ has an 'on-off' ratio of about 100 whilst $6Th_56$ has a minimum of 170 - the true ratio will be larger, close to 5000 based on extrapolation (see figure 5.24)

5.13 Summary

In this chapter we have presented the synthesis, measurement and theoretical treatment of the single molecule results of a series of α-ω-mercaptohexyl-oligothiopenes. The initial aim was to see how a change of conjugation in a double tunnel barrier molecule would affect the conductivity. We initially found that making the oligothiophene unit longer had little effect on the conductance. However, when compared to DFT calculations we realised that the conductivity of the longer oligomers was

much higher than the theory predicted. Indeed the theory predicted that although the H/L gap does shrink for longer oligomers, the effect of the tunnelling distance was crucial, with an exponential distance dependence and attenuation factor close to 0.2 $Å^{-1}$ predicted.

We have presented arguments that support the notion that water, by weakly interacting with the π-system of a molecule, can drastically alter the molecular conductance of the gold|molecule|gold junction. By shifting the frontier energy levels closer to the gold Fermi level, water has the effect of increasing the molecular conductance, and the effect becomes stronger the longer the oligomers.

We also saw that the effect of water was not simply to switch the conductance between a high and a low value, but rather to shift the conductance gradually indicating that the molecules are sensitive to the *amount* of water present. This has wider implications in other important electron transfer processes. Water is known significantly to affect rates of electron transfer (ET) reactions in biological systems by mediating ET coupling pathways and changing activation free energies[46]. Unusual 'structured' water molecules near redox cofactors have been found to accelerate ET kinetics when the cofactors are close together; such water appears to show anomalously weak distance decay for electron tunnelling[47]. Similarly, in a family of covalently-linked azurin complexes,

it was found that a *longer* linkage between azurin units led to a *higher* rate constant for intramolecular ET, apparently because the longer linkers permitted a dimer pair of water molecules to play a structural role that allowed a better path for electron transfer[48]. In these two instances, it is believed that water is involved in the electron tunneling pathway, whereas in our thiophene oligomers it "gates" the electron tunnelling pathway through the molecule. It has been suggested that water could interact strongly with the thiol-gold contacts[36], leading to a length-independent lowering of the conductance of gold|molecule|gold junctions, for simple alkanethiols and alkanedithiols. Our results represent the first examples of a length-dependent water-induced "gating" of electron transport through a synthetic molecular wire. They will have implications for molecular electronics, and it may also provide a new paradigm for the construction of single molecule sensors. It also emphasizes that solvent effects must be taken into account in laboratory studies of single molecule electronics.

Bibliography

[1] Skotheim, T.A. & Reynolds, J.R. eds., Handbook of Conducting Polymers Thind Edition. (Taylor and Francis Group, Boca Raton, 2007).

[2] I. McCulloch, M. Heeney, C. Bailey, K. Genevicius, I. Macdonald, M. Shkunov, D. Sparrowe, S. Tierney, R. Wagner, W. M. Zhang, M. L. Chabinyc, R. J. Kline, M. D. McGehee, M. F. Toney, *Nat. Mater.* **2006**, *5*, 328-333.

[3] A. Chandekar, J. E. Whitten, *Synth. Met.* **2005**, *150*, 259-264.

[4] R. Telesca, H. Bolink, S. Yunoki, G. Hadziioannou, P. T. Van Duijnen, J. G. Snijders, H. T. Jonkman, G. A. Sawatzky, *Phys. Rev. B* **2001**, *6315*, 11.

[5] Bässler, H. Electronic Excitation. In Electronic Materials: The Oligomer Approach; Müllen, K.; Wegner, G., Eds.; Wiley-VCH: Weinheim, Germany 1998. ISBN 3-527-29438-4.

[6] M. P. Eng, B. Albinsson, *Angew. Chem.-Int. Edit.* **2006**, *45*, 5626-5629.

[7] H. M. Liu, N. Wang, J. W. Zhao, Y. Guo, X. Yin, F. Y. C. Boey, H. Zhang, *ChemPhysChem* **2008**, *9*, 1416-1424.

[8] W. Haiss, H. van Zalinge, H. Hobenreich, D. Bethell, D. J. Schiffrin, S. J. Higgins, R. J. Nichols, *Langmuir* **2004**, *20*, 7694-7702.

[9] Leary E. et. al. Physical Review Letters. (submitted)

[10] A. R. Rocha, V. M. Garcia-Suarez, S. Bailey, C. Lambert, J. Ferrer, S. Sanvito, *Phys. Rev. B* **2006**, *73*, 22.

[11] A. R. Rocha, V. M. Garcia-Suarez, S. W. Bailey, C. J. Lambert, J. Ferrer, S. Sanvito, *Nat. Mater.* **2005**, *4*, 335-339.

[12] S. Suzuki, P. G. Green, R. E. Bumgarner, S. Dasgupta, W. A. Goddard, G. A. Blake, *Science* **1992**, *257*, 942-944.

[13] M. Levitt, M. F. Perutz, *J. Mol. Biol.* **1988**, *201*, 751-754.

[14] A. J. Gotch, T. S. Zwier, *J. Chem. Phys.* **1992**, *96*, 3388-3401.

[15] A. Engdahl, B. Nelander, *J. Phys. Chem.* **1985**, *89*, 2860-2864.

[16] J. L. Atwood, F. Hamada, K. D. Robinson, G. W. Orr, R. L. Vincent, *Nature* **1991**, *349*, 683-684.

[17] P. Ruelle, M. Buchmann, H. Namtran, U. W. Kesselring, *J. Comput.-Aided Mol. Des.* **1992**, *6*, 431-448.

[18] M. P. Payne, L. C. Kenny, *J. Toxicol. Env. Health Pt A* **2002**, *65*, 897-931.

[19] G. Kryger, I. Silman, J. L. Sussman, *J. Physiol.-Paris* **1998**, *92*, 191-194.

[20] H. McConnell, *J. Chem. Phys.* **1961**, *35*, 508-&.

[21] W. Haiss, C. S. Wang, I. Grace, A. S. Batsanov, D. J. Schiffrin, S. J. Higgins, M. R. Bryce, C. J. Lambert, R. J. Nichols, *Nat. Mater.* **2006**, *5*, 995-1002.

[22] R. Boch, B. Mehta, T. Connolly, T. Durst, J. T. Arnason, R. W. Redmond, J. C. Scaiano, *J. Photochem. Photobiol. A-Chem.* **1996**, *93*, 39-47.

[23] J. M. Soler, E. Artacho, J. D. Gale, A. Garcia, J. Junquera, P. Ordejon, D. Sanchez-Portal, *J. Phys.-Condes. Matter* **2002**, *14*, 2745-2779.

[24] N. Troullier, J. L. Martins, *Phys. Rev. B* **1991**, *43*, 1993-2006.

[25] D. M. Ceperley, B. J. Alder, *Phys. Rev. Lett.* **1980**, *45*, 566-569.

[26] P. Bai, *Physica Status Solidi (A)* **2007**, *204*, 1876.

[27] T. Albrecht, J. Ulstrup, S. Mertens, F,L., *J. Am. Chem. Soc.* **2007**, *129*, 9162-9167.

[28] W. Haiss, R. J. Nichols, H. van Zalinge, S. J. Higgins, D. Bethell, D. J. Schiffrin, *Phys. Chem. Chem. Phys.* **2004**, *6*, 4330-4337.

[29] Z. H. Li, I. Pobelov, B. Han, T. Wandlowski, A. Blaszczyk, M. Mayor, *Nanotechnology* **2007**, *18*, 8.

[30] A. Nishikawa, J. Tobita, Y. Kato, S. Fujii, M. Suzuki, M. Fujihira, *Nanotechnology* **2007**, *18*, 10.

[31] B. Q. Xu, N. J. J. Tao, *Science* **2003**, *301*, 1221-1223.

[32] D. I. Gittins, D. Bethell, D. J. Schiffrin, R. J. Nichols, *Nature* **2000**, *408*, 67-69.

[33] J. D. Zhang, A. M. Kuznetsov, I. G. Medvedev, Q. J. Chi, T. Albrecht, P. S. Jensen, J. Ulstrup, *Chem. Rev.* **2008**, *108*, 2737-2791.

[34] S. C. Meng, J. Ma, Y. S. Jiang, *J. Phys. Chem. B* **2007**, *111*, 4128-4136.

[35] X. L. Li, J. He, J. Hihath, B. Q. Xu, S. M. Lindsay, N. J. Tao, *J. Am. Chem. Soc.* **2006**, *128*, 2135-2141.

[36] D. P. Long, J. L. Lazorcik, B. A. Mantooth, M. H. Moore, M. A. Ratner, A. Troisi, Y. Yao, J. W. Ciszek, J. M. Tour, R. Shashidhar, *Nat. Mater.* **2006**, *5*, 901-908.

[37] J. S. Na, J. Ayres, K. L. Chandra, C. B. Gorman, G. N. Parsons, *Nanotechnology* **2007**, *18*, 7.

[38] A. Dey, T. Okamura, N. Ueyama, B. Hedman, K. O. Hodgson, E. I. Solomon, *J. Am. Chem. Soc.* **2005**, *127*, 12046-12053.

[39] P. J. Stephens, D. R. Jollie, A. Warshel, *Chem. Rev.* **1996**, *96*, 2491-2513.

[40] A. Dey, K. N. Green, R. M. Jenkins, S. P. Jeffrey, M. Darensbourg, K. O. Hodgson, B. Hedman, E. I. Solomon, *Inorg. Chem.* **2007**, *46*, 9655-9660.

[41] B. Q. Q. Xu, X. L. L. Li, X. Y. Y. Xiao, H. Sakaguchi, N. J. J. Tao, *Nano Lett.* **2005**, *5*, 1491-1495.

[42] H. Sakaguchi, A. Hirai, F. Iwata, A. Sasaki, T. Nagamura, E. Kawata, S. Nakabayashi, *Appl. Phys. Lett.* **2001**, *79*, 3708-3710.

[43] X. L. Li, J. Hihath, F. Chen, T. Masuda, L. Zang, N. J. Tao, *J. Am. Chem. Soc.* **2007**, *129*, 11535-11542.

[44] H. Cao, J. Jiang, J. Ma, Y. Luo, *J. Am. Chem. Soc.* **2008**, *130*, 6674-+.

[45] A. M. Kuznetsov, J. Ulstrup, *J. Phys. Chem. A* **2000**, *104*, 11531-11540.

[46] H. B. Gray, J. R. Winkler, *Q. Rev. Biophys.* **2003**, *36*, 341-372.

[47] J. P. Lin, I. A. Balabin, D. N. Beratan, *Science* **2005**, *310*, 1311-1313.

[48] I. M. C. van Amsterdam, M. Ubbink, O. Einsle, A. Messerschmidt, A. Merli, D. Cavazzini, G. L. Rossi, G. W. Canters, *Nat. Struct. Biol.* **2002**, *9*, 48-52.

Chapter 6

Incorporating a hexanuclear platinum cluster into a molecular wire

Chapter 6

Incorporating a hexanuclear platinum cluster into a molecular wire

6.1 Introduction and aim

Molecules designed to act as molecular wires,[1] switches[2, 3] and diodes[4, 5] have recently been examined theoretically and/or experimentally. However, so far though the majority of reports on single molecule conductances[3, 6] have been concerned with purely organic compounds.[1] The conductance of a linear chain of metal atoms formed, for example, in breakjunction experiments[7, 8] is quantized in units of the fundamental value $G_0 = 77.4\ \mu S = 2e/\hbar$. The conductance of organic wires, however, is rather low for most compounds longer than 1.5 – 2 nm, usually 4-5 orders of magnitude lower than G_0. For example, the 2.3 nm long carotinoid compound measured by Lindsay et.al. has a low bias conductance of 2.6 nS ($3.4 \times 10^{-5}\ G_0$)[9], whilst the 2.4 nm long teraniline compound, also measured by Lindsay et. al, has a low bias value of 1.0 nS ($1.3 \times 10^{-5}\ G_0$)[10]. Both these compounds are highly conjugated wires. Recently porphyrin molecular wires have been reported with low β decay values

(the measure of electron attenuation), but still having low conductances ranging between 2 nS for the 2.3 nm long monomer, to 0.6 nS for the 5.0 nm long trimer[11]. Thus, whilst low β decay values can be achieved, it seems conductances close to G_0 are unfeasible for such long, purely organic, molecular wires.

Molecules which can transport charge over long distances such as 2nm or more would be very useful in molecular electronic applications. However, the data which has been published so far clearly demonstrates that carbon as the sole basis for electronic wires is far from ideal. A possible reason is the energy mismatch between electron energies on the metal electrodes and on the carbon based bridging molecule(s). Other, more complex, effects such as electron-phonon coupling may also take part in organic wires, which can lead to enhancement or reduction of conductance than expected on a purely energetic basis.

It is also becoming clear that even for molecules whose levels are aligned with the ensuing metal Fermi levels conductivities as high as G_0 are not apparent (see chapter 2). Therefore, it is would be desirable to incorporate metals or metal units into molecular wires in an attempt to improve the possible range of conducting wires available at nano-scale.

Metal containing molecular wires are good candidates for connector elements in nanoscale switchable molecular devices. Indeed, the utilization of metal-carbonyl clusters as single-electron tunnelling

transistors has been reported[12], and their employment as molecular capacitors is also under scrutiny[13]. However, well-documented examples of electron transfer in molecular frameworks containing cluster subunits are rare. As much work has been done in the areas of metal cluster and metal complex chemistry, there are many examples of *potential* wire molecules which could be tested in the future. We have investigated two such candidate wires based on a central hexanuclear platinum carbonyl cluster, henceforth {Pt_6}, thanks to their unique chemistry which allows the formation of well characterised wire-like molecules.

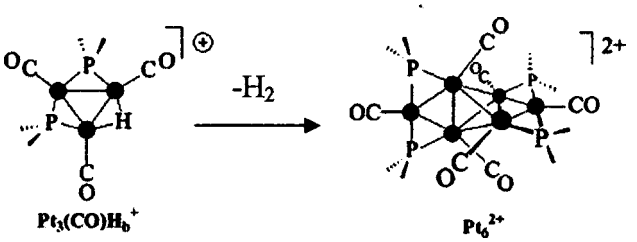

Figure 6.1. Formation of {Pt_6} from {Pt_3H}. Conditions: HOTf, $CHCl_3$, Pt_3H, CO.[14]

The bis-carbonyl Pt_6^{2+} in figure 6.1 above is reacted with two equivalents of butanedithiol to form the molecular wire. The hexanuclear core of the wires may be described as being obtained by the condensation of two "Pt_3" units through their un-bridged Pt-Pt bonds, resulting in two edges of the triangles at bonding distances in the range of 2.62–2.87 Å. This gives rise to a central tetrahedral unit with two edge bridging "PtP_2" moieties. -

This bonding arrangement is rare with the only other known examples being the hexanuclear gold clusters, $[\{(Me_3P)Au\}_6(\mu_3\text{-}O)_2](BF_4)_2$ [15] and $[Au_6(dppp)_4](NO_3)_2$.[16]

Small metal clusters have attractive size dependent electrical properties for applications in nanoscience and nanoelectronics.[17] They have already featured nicely in nanoscale electrical junctions as either contacts or active elements [18] displaying Coulomb charging. Electron transfer from, to, or across a cluster-containing spacer, triggered by external stimuli, would make these units promising candidates for the preparation of connector elements in nanoscale switchable molecular devices.[19] However, examples of molecular frameworks containing cluster subunits are uncommon,[20] and well-documented studies of the electron transfer activity in such systems are exceedingly rare.[21] Experimentally the junctions have been fabricated by adsorbing isolated metal clusters onto self assembled monolayers. The aim is to introduce a new approach in which the clusters are directly chemically fabricated into single molecular wires specifically designed to measure their electrical properties. A new molecular wire was developed containing the hexanuclear cluster fragment $Pt_6(\mu\text{-}PBu^t_2)_4(CO)_4$ (hereafter $\{Pt_6\}$), stabilized by bulky bridging phosphido ligands.[22] and we have used the scanning tunnelling microscopy (STM)-based I(s) technique to measure its properties.

6.1.1 Definition of a cluster

A cluster is an ensemble of chemically bonded atoms in an intermediate state between a molecule and a bulk material. Various elements are well known in forming cluster compounds, for instance carbon forms fullerenes, boron forms boranes and many transition metals form quite stable clusters. The term 'cluster' was introduced in the 1960s by F. A. Cotton[23] to describe small structures with metal-metal bonds. The simplest cluster can contain a single metal-metal bond (i.e. just two metal atoms). The largest clusters contain hundreds of individual atoms. There are essentially two broad categories of cluster, those without a ligand shell, termed 'naked', and those with a ligand shell. Certain types of ligands stabilize transition metal clusters well and include carbon monoxide, phosphines, halides, isocyanides, alkenes and hydrides.

Clusters are able to form from metals which possess diffuse d-orbitals, such as the refractory metals (W, Mo, Nb, Ta and Re). For the platinum group clusters, and in particular platinum and palladium carbonyl clusters, the metals are in low formal oxidation states (I and II generally), but the 'real' charges are usually an intermediate value. Electron counting rules exist to predict stabilities and reactivities. In cluster chemistry the 'polyhedral skeletal electron pair theory' provides electron counting rules

that can be used to predict the structure of electron deficient clusters. Originally developed by K. Wade[24], and later developed by others such as Mingos[25], they are commonly known as Wade's rules. The rules were originally developed to aid the prediction of the structures of borane and carborane cluster compounds, and only apply to clusters where every face is triangular. There is an alternative and more straightforward version of the rules that uses a total valence electron count. This approach can be applied to transition metal clusters. The total valence electrons are counted plus any charge electrons. Both approaches are formalisms and really should not be regarded as a true picture of electron sharing in clusters.

6.1.2 Electron transfer across metal clusters

It has been suggested that metal clusters stabilised in a ligand shell are valid candidates to assemble functional devices for data storage and could potentially represent the ultimate solution for miniaturisation in microelectronics and nanolithography[26-30]. Clusters, metallic and organometallic, display a wide variation in electronic behaviour. As mentioned earlier a lot of the properties of metal clusters are size dependent, although electronic properties can be ligand dependent also. Properties include, among others, the HOMO-LUMO gap and the redox

couple spacing. These are perhaps the two most important properties upon which to focus in relation to molecular electronics. The stability of the cluster (to air and to reduction/oxidation) is a key concern as any practical applications demand high stability of the componentry, and the reversibility of the redox transitions is critical too. The electrical properties of clusters are normally probed directly using cyclic voltammetry. This mode of transferring electrons is, however, different than electron transfer in the solid state (i.e through solid wires). Finally of issue would be how to actually connect a cluster into an electronic circuit as so far clusters are studied in a relatively un-tethered fashion. We hope to begin to address these issues in the rest of this chapter.

From a design point of view it is interesting to note the remarkable correspondence between the solution electrochemical response of monolayer-protected gold cluster (MPC) ensembles and the tip-based tunnelling spectroscopy of an individual MPC physisorbed on, for example, a gold-on-mica support. The STM tip experiment on these display a reversible coulombic staircase with six charging steps constantly separated by ca. 0.34V[31]. A coulomb staircase involves the sequential filling of discrete energy levels (MOs) and does not happen for bulk metals due to their continuous bands. It was speculated that electrochemical charging is an *ensemble coulomb staircase*. To explain briefly, Coulomb charging occurs when the contact resistance is larger than the resistance

of the nanostructure in question and when the total capacitance of the object is so small that adding a single electron requires significant *charging* energy. To add a single charge to a nanoparticle requires energy, since the electron can no longer be 'dissolved' into an effectively bulk material. For a nanoparticle surrounded by a dielectric with dielectric constant ε_r, the capacitance of the NP is dependent on its size as; $C(r) = 4\pi r\varepsilon_0\varepsilon_r$, where r is the radius of the NP and ε_0 is the permittivity of the vacuum. The energy required to add a single charge to the particle is given by the charging energy; $E_c = e^2 / 2\ C(r)$. Tunnelling of single charges to NPs can be seen at temperatures of $k_BT < E_c$ in the I\V characteristics.

It was believed that metal carbonyl clusters (MCC) should adopt 'closed shell' electronic configurations and could possibly exhibit an almost perfect correspondence between number of cluster valence electrons (CVE) and geometry of the metal frame, and vice versa. There are many examples of structurally characterised, low-nuclearity, MCC which add weight to the above view[32]. Rules for electron counting in MCC have been developed with the support of semiempirical calculations[33, 34], which rationalised the relationships between electron count and geometry of most clusters and proved to be extremely useful in designing and making new MCC. However, as the MCC gets bigger, deviations from the predicted electron count become apparent. This difference in the number of required

CVE is apparently due to the change in atomic properties of the involved metal atoms, which are less relevant in low-nuclearity clusters and become progressively more effective as the size and, consequently, the number of energy levels increase. Low nuclearity clusters display molecular properties whilst progressively higher nuclearity clusters show the more metallic property of electron sink behaviour. Thus controlling the size of the cluster could allow us to make either single electron transistors (small clusters) or electron sinks (large clusters).

6.1.3 Metal incorporating molecular wires

Linear chain metal-metal bond complexes have been synthesized for over 40 years[35]. Compounds with metal-metal bonds of various orders (from 1/2 to 4) have since been reported. The conductance of linear chains of metal atoms supported by pyridylamine ligands, and capped with isothiocyanate groups, has been reported recently [36] and are represented in figure 6.2. These represent to date the best examples of forming almost continuous metal bridges between metal contacts, using molecules, in the literature. These have been studied with nickel, cobalt and chromium metal chains mainly in the (II) to (III) metal oxidation states. For the 2.35 nm *hepta*chromium metal wire a conductance of 145 nS (1.8×10^{-3} G_0) was reported.

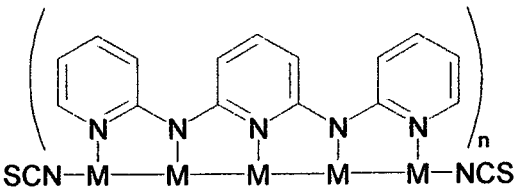

Figure 6.2. A pyridylamine supported metal wire. M = Ni, Co and Cr. n = 4.

The only report on platinum containing molecular wires which are capable of bridging metal contacts involves a square planar platinum(II) complex[37], where the presence of the platinum atom is shown to actually increase the resistance significantly by forming a conjugation break between the two *trans*-acetylide ligands. Figure 6.3 shows the chemical structure.

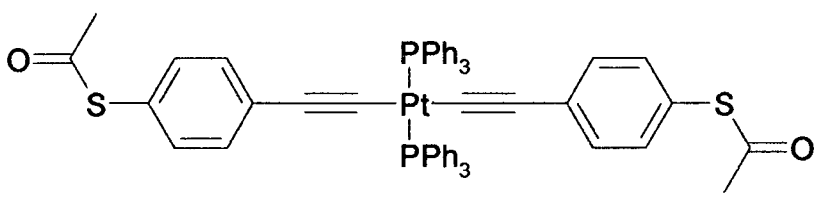

Figure 6.3. Structure of the platinum *trans*-acetylide compound.

When compared to compounds such as 1,4-diphenylethynyl benzene, the platinum acts to reduce the conductance by three orders of magnitude. This behaviour is ascribed to the Pt atom in this complex having little π-character, thus breaking the conjugation between the two acetylide

groups. The molecular conductance ranges from 0.02 nS to 0.2 nS between 0 and 4 V. Other examples of metal containing wires generally only contain single metal atoms isolated in complexes, and show properties more associated with molecular rather than metallic conduction. We demonstrate in this chapter that the inclusion of a platinum metal cluster into an organic framework may provide significant progress in the realisation and technological development of functional molecular devices.

6.1.4 Potential cluster containing molecular wires

There are many examples in the literature of suitable molecules which could be used as molecular wires. An example would be the compound $Mo_2Ir_2(\mu\text{-}CO)_3(CO)_7(\eta^5\text{-}C_5H_4CH_2CH_2OH)_2$ [38] shown below in figure 6.4.

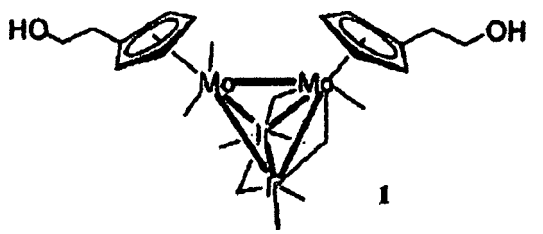

1

Figure 6.4 Structure of the Mo-Ir complex. The molybdenum containing compounds have a reversible oxidation process at ~ 0.8 V, whereas the tungsten analogues have slightly more accessible redox

states, with two reversible oxidations $E_{1/2}$ between 0.5 and 0.7 V (vs Ag/AgCl)[39]

Conversion of the terminal alcohol groups to thiols, for instance, could form a redox addressable switch in a similar manner to the viologen and pyrroloTTF compounds in chapter 3.

A series of linear chains of three Pt atoms have been formed in which the two terminal Pt atoms are capped with different isocyano groups. Represented in figure 6.5, these display potential for tunable molecular wires containing metal atoms. The linear tri-platinum compound is prepared by site-selective incorporation of a Pt^0 atom into the dpmp (bis(diphenylphosphinomethyl)phenylphosphine) bridged diplatinum complex $[Pt_2(\mu\text{-dpmp})_2(XylNC)_2]\text{-}(PF_6)_2$ (XylNC = 2,6-xylyl isocyanide), which contain Pt in the +1 oxidation state.[40]

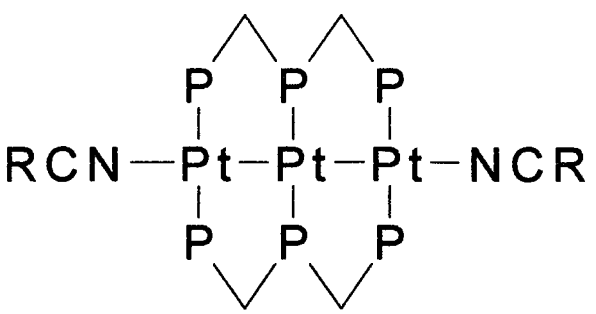

Figure 6.5. $[Pt_3(\mu\text{-dpmp})_2(RNC)_2](PF_6)_2$ (R = 2,4,6-mesityl, *tert*-butyl, 4-tolyl)

The Pt^0 atom occupies the terminal position, chelating to the free phosphine group in the dinuclear species. If $Pd(XylNC)_2$ is used as the metal fragment, then Pd^0 can be inserted into the Pt^I-Pt^I bond forming a Pt(I)-Pd(0)-Pt(I) chain. The isocyanide derivatives are formed through the reaction of $[Pt_3(\mu\text{-dpmp})_2(XylNC)_2](PF_6)_2$ with monoisocyanide compounds to form clusters with Pt-Pt bond lengths very sensitive to the π-acidity of the isocyanide ligands.

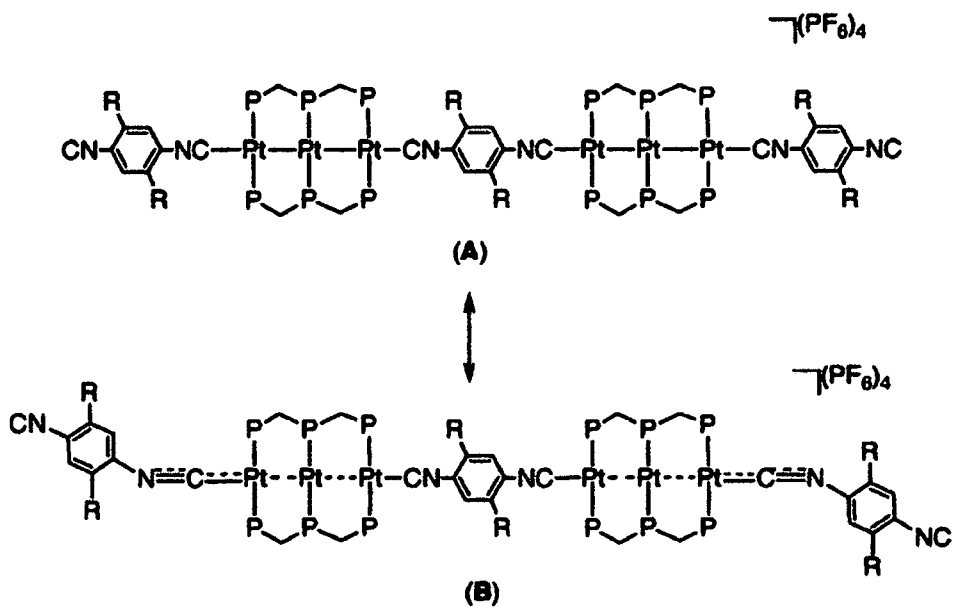

Figure 6.6. Resonance structure of the potential wire $[(bisNC_x)Pt_3(dpmp)_2(bisNC_x)Pt_3(dpmp)_2(bisNC_x)]$-$(PF_6)_4$

Reactions of the platinum trimer (figure 6.5) with phenylene-1,4-bisisocyanide or 2,5-dimethylphenylene-1,4-bisisocyanide resulted exclusively in the formation of green powders formulated as $[(bisNC_x)Pt_3(dpmp)_2(bisNC_x)Pt_3(dpmp)_2(bisNC_x)]$-$(PF_6)_4$ (R = H or Me)

(Figure 6.6)[41]. EXAFS analyses demonstrated that the compounds in figure 6.6 involved the linear $\{Pt_3(\mu\text{-dpmp})_2\}$ cores with significantly longer Pt-Pt distances (2.85(4) Å (R = H), 2.86(4) Å (R = Me)) compared to 2.73(4) Å for $[Pt_3(\mu\text{-dpmp})_2(XylNC)_2](PF_6)_2$, suggesting that an extensive migration of metal-metal bonding electrons into CN σ^* orbitals results in the longer Pt-Pt distances. This could be an interesting system for molecular conductance studies due to its high degree of conjugation combined with linear metal chains.

There are, in fact, many examples of metal-metal bonded compounds which could be investigated for their potential molecular electronic applications, too many to mention here. Further examples which merit a brief mention are a cage-type hexanuclear platinum(0) cluster which encapsulates two mercury(0) atoms[42]. Finally, an example of an organometallic polymer comprising a backbone of covalently bounded tin atoms has been reported[43]. Tin and indium are the only metallic elements reported to form organometallic polymers in such a way, forming a molecular metal wire encapsulated by organic ligands. This may be useful as a long, highly conductive, molecular wire.

6.1.5 Junction architecture

Serveral metal clusters have been investigated using STM techniques previously in which they are adsorbed onto a rigid substrate – HOPG[44] and alkanethiol SAMs[45] have been used. However, to the best of our knowledge, a cluster molecule has never been studied covalently attached between an STM tip and surface, or in any other 'source-drain' type configuration. The type of connection is crucial in terms of molecular electronic applications. Poor and ill-defined contacts do not allow us to reliably compare results from one device to other device structures. Such contacts are non-covalent, which is why we have used a cluster which can be tethered covalently at both ends for our study, as shown in figure 6.7 B.

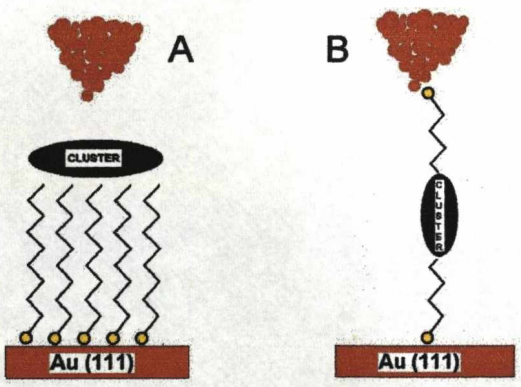

Figure 6.7. Schematic representations of two different ways of incorporating clusters into a nano-scale junction. *A* represents the cluster adsorbed onto a SAM. *B* represents the cluster chemically bound inside a single wire.

In configuration B, however, the junction simulates an important type of device architecture in the semi-conductor field - the double tunnel barrier (DTB) junction. Normally a DTB junction consists of a semi-conductor, e.g. GaAs, confined between two other semi-conductors with a larger band gap, e.g. GaAlAs ('barriers'). The GaAs region can also be thought of as an indentation in the larger total barrier. DTB junctions, in the form of Resonant Tunnelling Diodes (RTDs), use quantum effects to produce negative differential resistance (NDR). This property is based on the quantum mechanical principle that an electron or hole inside the barriers can have only a discrete energy. When the energy of the quantum well coincides with the energy of the incoming electrons a resonance occurs, facilitating transmission of charge across the double barrier. When the hexanuclear platinum core cluster is symmetrically placed between two alkanethiol linker ligands it can be regarded as an analogue to the purely inorganic DTBs as its energy is much closer to the gold E_F than the alkyl linkers.

We shall investigate whether the $\{Pt_6\}$ molecule behaves in a similar manner to that of purely inorganic DTBs, i.e. displaying resonant tunnelling and negative differential resistance phenomena, or whether for single molecules different conduction mechanisms apply.

6.2 Synthesis of HS-$(CH_2)_4$S-{Pt_6}-S$(CH_2)_4$-SH

The synthesis of this compound was carried out by the Leoni group, Pisa, Italy. However, we shall describe it briefly here.

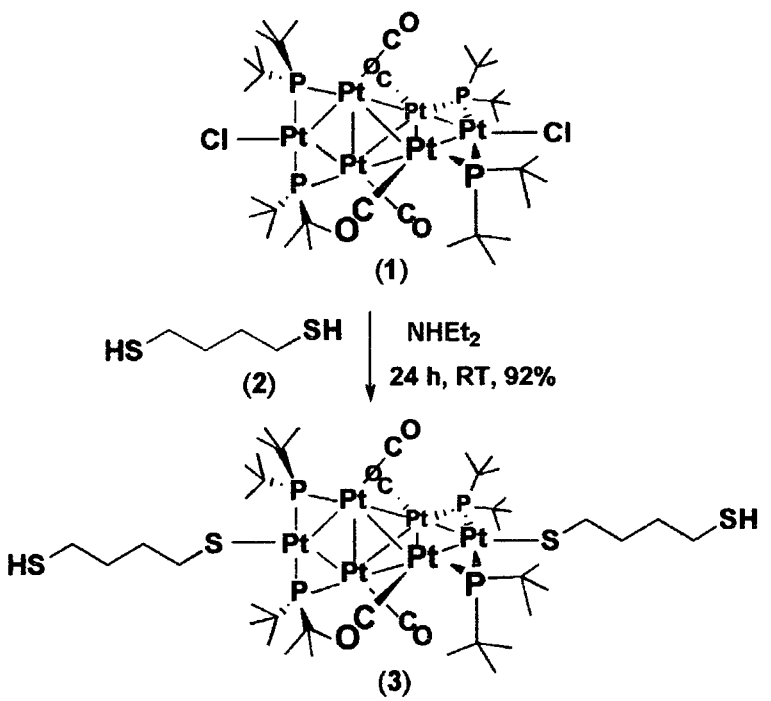

Scheme 6.8. Synthesis of 4{Pt_6}4, complex 3.

[$Pt_6(\mu$-$PBu^t_2)_4(CO)_4Cl_2$] (1) was prepared as previously described.[46] This compound undergoes nucleophilic substitution selectively at the Pt-Cl groups, due to the steric hindrance created by the bulky $^tBu_2P$- groups which block reactions at the centre of the complex. Complex 1 was reacted

with 10 equivalents of 1,4-butanedithiol in diethylamine as the solvent and the base. After 24 hours, complex 3 was isolated as a red-brown solid after removal of the solvent in 92% yield.

Significant IR and NMR parameters for 4{Pt_6}4 compare well with corresponding data for analogous derivatives characterized by x-ray diffraction,[47] and microanalytical data confirm the structure given in Scheme 5.8. As expected on the basis of the general redox behaviour of the family of clusters {Pt_6}X_2,[47] compound **3** undergoes a chemically-reversible one-electron reduction at E° = –1.49 V and a second, moderately reversible reduction at –1.64 V *vs.* saturated calomel electrode (SCE), in CH_2Cl_2 solution. Two irreversible oxidations (E_P^A = +0.58 and +0.75 V) are also apparent. The electronic spectrum shows several intense bands in the visible region. The lowest-energy band is at 503 nm (2.46 eV). This lowest energy transition is slightly larger than the voltammetric HOMO – LUMO gap (2.07 eV) which may be due to the HOMO-LUMO transition being forbidden.

6.2.1 NCS-{Pt_6}-SCN

This was prepared by metathesis of complex 1 with NaSCN. A solution of KSCN (10 mg, 0.103 mmol) in H_2O (2 mL) was added to a solution of [{Pt_6}$(CO)_2$]$(CF_3SO_3)_2$ (74 mg, 0.0334 mmol) in acetone (5 mL) with

constant stirring at 25°C. An orange solid precipitated out quickly and the solution was stirred further for ca. 15 min. $\{Pt_6\}(SCN)_2$ was filtered off, washed with water / acetone (1 / 1) and vacuum dried (microcrystalline orange solid, 56 mg, 85 % yield). Microanalyses; found: C, 23.0; H, 3.48; N, 1.42. Calcd for $C_{38}H_{72}N_2O_4P_4Pt_6S_2$: C, 23.1; H, 3.67; N, 1.41. ^1H NMR ($CDCl_3$, 25°C): d (ppm) = 1.52 (vt, $^3J_{HP} + {}^5J_{HP}$ = 7.6 Hz, CCH_3). $^{13}C\{^1H\}$ NMR ($CDCl_3$, 25°C): δ (ppm) = 207.1 (s, CO), 121.6 (s, CN), 45.2 (m, CCH_3), 31.7 (s, CH_3). $^{31}P\{^1H\}$ NMR ($CDCl_3$, 25°C): δ (ppm) = 331.1# (s) $^{195}Pt\{^1H\}$ NMR ($CDCl_3$, 25°C): δ (ppm) = - 4553 (m, 1 Pt), - 3284 (m, 2 Pt). IR (solid state): 2116, 2080 (ν_{CN}), 2014 cm^{-1} (ν_{CO}).

6.3 Methods

6.3.1 I(s) measurements

A flame–annealed gold–coated glass slide was dipped into a dilute (10^{-4} – 10^{-5} M) solution of 4{Pt_6}4 for one minute to allow the formation of a low coverage monolayer. We next employed the scanning tunnelling microscopy (STM) based I(s) technique to fabricate Au|{Pt_6}|Au molecular junctions and to measure their electrical properties. The STM was placed inside its environmental chamber and the system was purged with dry

argon gas overnight in order to remove oxygen and water. A gold STM tip was brought to a fixed distance above the sub-monolayer–modified gold surface under argon, controlled using the set point current (10-20 nA). The surface was imaged in order to find an area containing molecules (conditions of I_0 = 0.1 nA were used with bias voltages ranging between 0.2 and 1.2 V). Under these conditions wire formation was generally suppressed, although occasional molecular bridges were seen in images which looked like bright lines or streaks. Once an area of molecules had been identified the STM tip was placed above either a single molecule, or a cluster of molecules, and the feedback loop was then switched off, and the tip withdrawn while maintaining a constant x–y position. A current–distance (*I(s)* where s = relative tip–sample distance) curve was collected. We typically observe current–distance behaviour characteristic of the formation of molecular wires (Figure 6.17) with a plateau in the current (I_M) due to conductance through the fully–extended molecule in its lowest-energy conformation. As the tip was withdrawn further, the molecule detaches at a distance characteristic of its length (tunnelling current therefore diminishing sharply), and this break-off distance is also measured. The experiment was repeated many times, and the results are analysed statistically by adding together all the data points for each I(s) curve collected which contained a plateau or plateaus – bare exponential

and noisy scans were dismissed (refer to section 2.4, chapter 2 for more details.

We also performed I\V spectroscopy on 4{Pt_6}4. This was done in two manners. The first involved repeatedly scanning the bias voltage between ± 1.5 V and waiting for a molecule to bridge the junction and remain inside for the duration of the experiment. The second method was to perform the I(s) measurements at different bias voltages. For this method we used bias voltages of +0.2, +0.6 and +1.0 V. The time consumption of performing the measurements prevented us from collecting more data at negative bias using this method.

6.3.2 Polarization Modulation FTIR Reflection-Absorption Spectroscopy (PMIRRAS)

Due to the presence of four carbonyl groups in 4{Pt_6}4 PMIRRAS was used to characterise the layer deposited on the gold surface used in the I(s) measurements. PMIRRAS is a versatile technique for assessing layer quality and density in SAMs. PMIRRAS is commonly used for the characterization of thin films or monolayers on metal substrates as it has the advantage of high surface sensitivity.

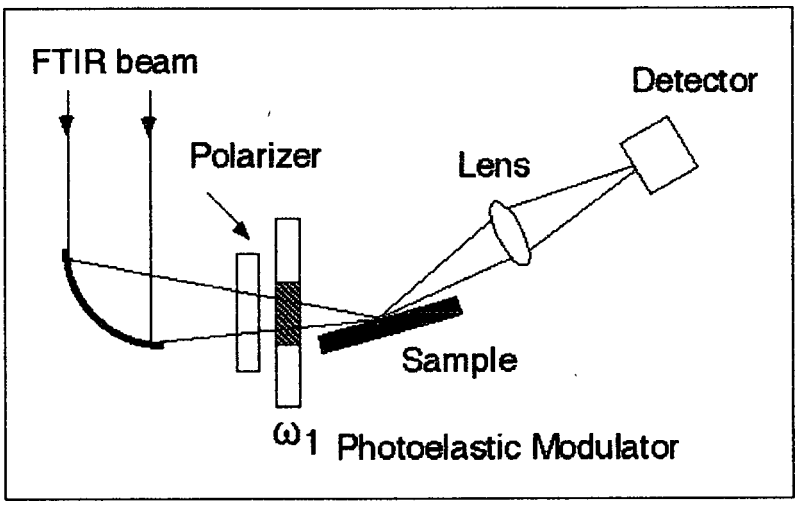

Figure 6.9. Schematic representation of the experimental setup in PMIRRAS

The light passes through a polarizer which can polarize the light in one of two ways. Only the p-component of light, which has a component perpendicular to the metal surface, can excite vibrations of the molecules of the monolayer[48] while s-polarized light which exhibits an electric vector parallel to the metal surface cannot excite adsorbate vibrations. We therefore concentrated on the p-polarized light spectrum.

Samples were prepared in the same manner as used in the I(s) measurements (1 x 10^{-4} M solution, 30 seconds immersion). The polariser was set to 0° (p-polarisation) and is modulated with a photoelastic modulator (Hinds Instruments PEM-90), and an LIA (Stanford Research Systems SR830 DSP) is used to demodulate the resulting signal. When the multiplexer (MUX) is selected on the PMA electronics panel the low pass

filtered detector signal (sum/dc signal) and the high pass filter (difference/ac signal) are sent to the spectrometers analog-to-digital converter. Both signals are combined in one interferogram.

6.4 Results – HS-$(CH_2)_4$S-{Pt_6}-S$(CH_2)_4$-SH (4{Pt_6}4)

6.4.1 XPS and PMIRRAS

The adsorbed complex was characterised by X-Ray photoelectron (XPS) and polarisation modulated infrared reflection absorption (PM–IRRAS) spectroscopies, and scanning tunnelling microscopy (STM) imaging. Complex 4{Pt_6}4 shows a single, rather broad CO stretching band at 2004 cm^{-1} in the solid state (2009 cm^{-1} in CH_2Cl_2 solution). The PM–IRRAS spectrum of the monolayer shows an intense band at 2014 cm^{-1} (Fig. 1a), ν(CO) = 1840-1875 cm^{-1} on the twofold (μ_2) bridge sites of a Pt (111) surface[49] indicating lower back-bonding in the {Pt_6} complex.

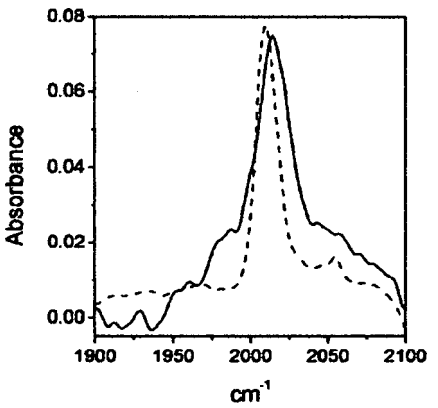

Figure 6.10. PM-IRRAS spectrum of 4{Pt_6}4 on Au (111) substrate (solid line) and solution IR spectrum (dash line).

The XPS spectrum shows Pt $4f_{5/2}$ and $4f_{7/2}$ spectral lines at 76.1 and 72.8 eV respectively (figure 6.11). The $4f_{7/2}$ peak position is similar to those of related Pt-Pt bonded species, such as $[Pt_3(\mu^3\text{–CO})(\mu\text{–dppm})_3]^{2+}$ [50](dppm = $Ph_2PCH_2PPh_2$; 72.9 eV) or $[Pt_2Cl_2(\mu\text{–dppm})_2]$ (72.4 eV[51]), and is notably different from Pt metal (70.9 eV[52]).

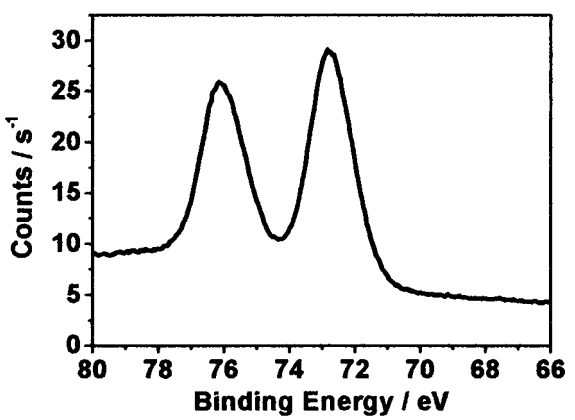

Figure 6.11. XPS spectrum of the Pt 4f region of 4{Pt_6}4 on Au (111) at 10^0 angle of incidence.

The P 2p peak occurs at 131.2 eV, figure 6.12, and compares very well with the complex $[Pt_3(\mu^2\text{-}CO)_3(C_6H_{11}PH_2)_3]$ (131.2 eV[53]). Free cyclohexylphosphine was determined as 130.7 eV. The Pt $4f_{7/2}$ peak position in this compound was 72.2 eV, also in good comparison with complex 3.

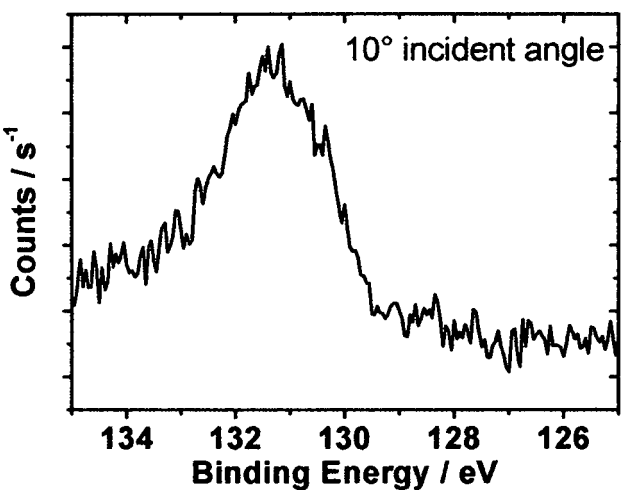

Figure 6.12. XPS spectrum of the P 2p region of 4{Pt_6}4 on Au (111).

The sulphur region of the XPS spectrum (figure 6.13) shows a doublet as the main peaks, characteristic of Au-S bonds, the Au-$Sp_{3/2}$ and the Au-$Sp_{1/2}$ (162.0 eV and 163.2 respectively). A minor doublet is detectable upon peak fitting which corresponds to free thiol SH, contributing about 10% to the spectrum. The Pt-S signal is almost identical to the Au-S signal, however, and for alkanethiols adsorbed on bulk Pt peaks are observed at 162.4 and 163.4 eV for the 2p doublet.[54]

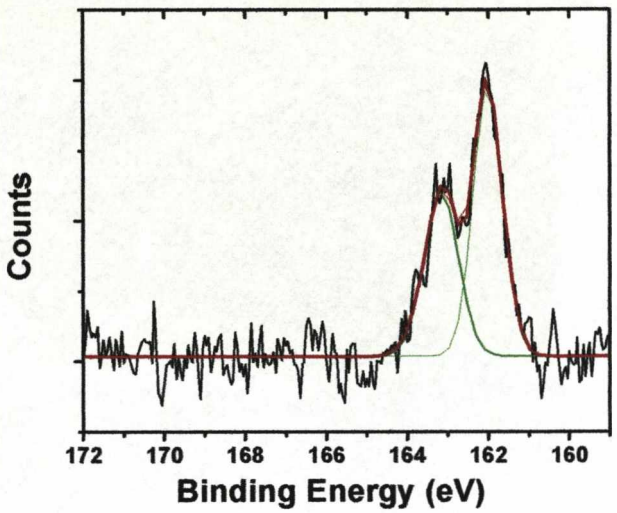

Figure 6.13. XPS spectrum of the S 2p region of 4{Pt_6}4 on Au (111).

6.4.2 STM Image analysis

In STM images of the low-coverage monolayer (figure 6.14), sub-molecular resolution was not achieved owing to the mobility of Au-S bonds on the timescale of STM imaging, but the molecules showed up as bright dots, and line scans across these dots showed that their size is consistent with intact 4{Pt_6}4.

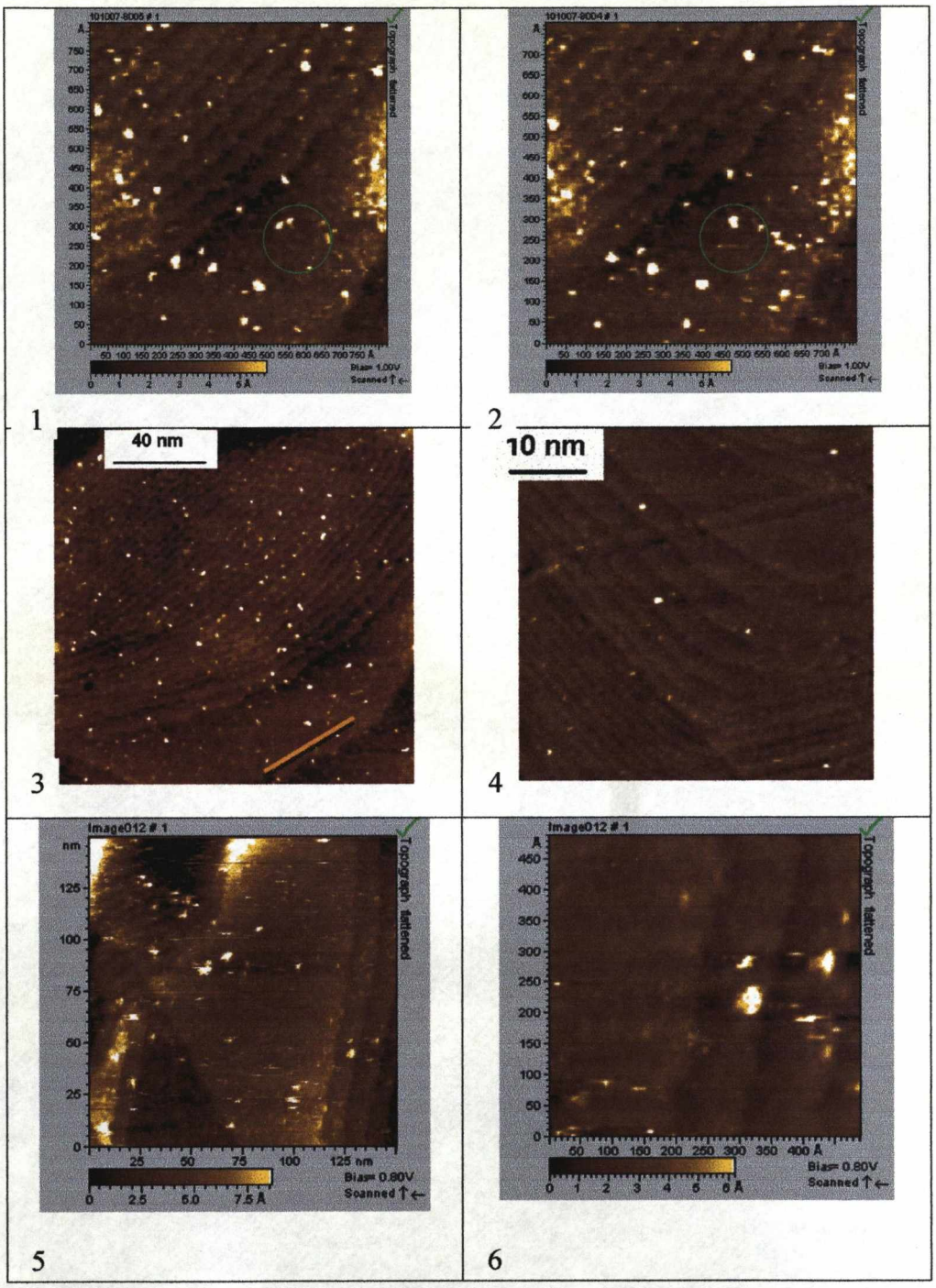

Figure 6.14. Images of low coverage monolayer of 4{Pt_6}4 on flame-annealed Au on glass slide under argon atmosphere. Images 1-2; V_b = 1.0 V, I_0 = 100 pA. Images 3-4; V_b = 1.2 V, I_0 = 100 pA. 5-6; V_b = 0.8 V, I_0 = 100 pA (scan speed = 1 line/sec, no. points per line = 512,

resolution was between 0.3 and 0.4 nm per image). The images show an area of Au(III) terraces. Note that the molecules, seen here as bright dots, show a tendency to adsorb at step edges, hence the lines of dots seen in image 1, however they also adsorb on terraces.

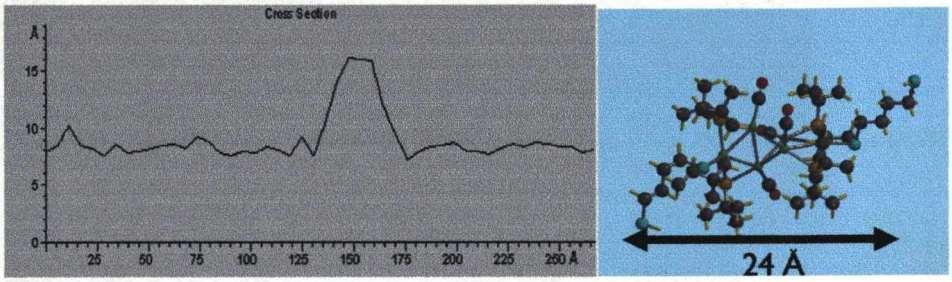

Figure 6.15. Line scan across one of the bright dots representing 4{Pt_6}4 (image 3) showing that the protrusion width is consistent with that of intact 4{Pt_6}4. Note the measured height is determined by the density of molecular states at the Fermi level and does not simply correspond to the true dimensions in the z scale.

6.4.3 Current-distance, I(s) results and I\V behaviour

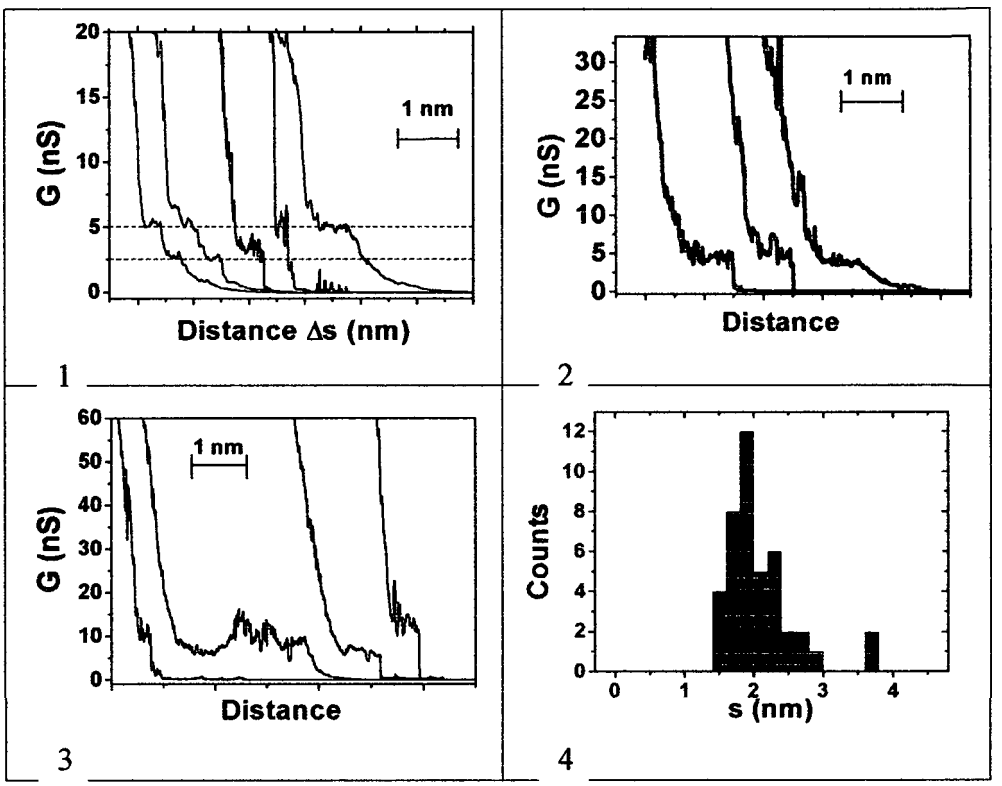

Figure 6.16. Example I(s) scans for $4\{Pt_6\}4$. 1: V_b = 0.2 V, I_{set} = 10 nA. 2: V_b = 0.6 V, I_{set} = 20 nA. 3: V_b = 1.0 V, I_{set} = 60 nA. 4: Histogram of the break-off distances at 0.2 V.

The mean break-off distance was 2 nm at the three measured potentials. However, some plateaus were much longer than this value and one example is shown in figure 6.16 above. We note that the Au-S bond is stronger than the Au-Au bond, so it may be possible to extrude a gold filament during junction cleavage. However, Au has a certain number of nearest neighbours in a flat surface, so this probably happens only on rough areas.

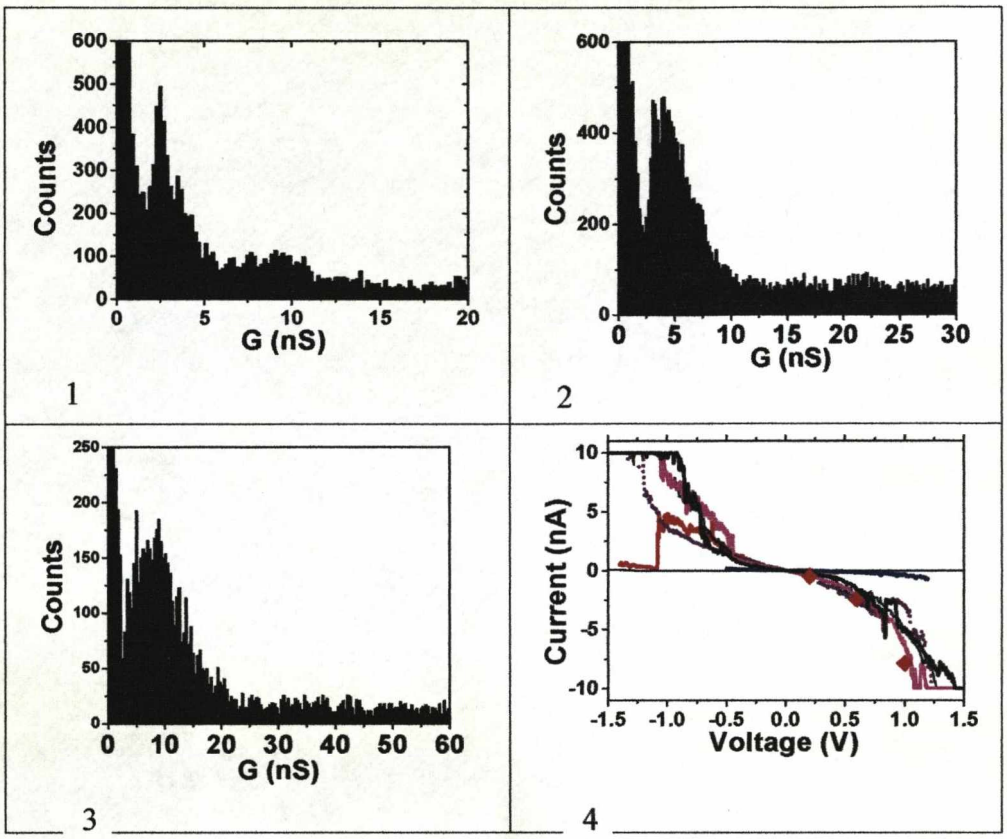

Figure 6.17. I(s) histograms for 4{Pt_6}4. 1: V_b = 0.2 V, I_{set} = 10 nA, number of scans = 50. 2: V_b = 0.6 V, I_{set} = 20 nA, number of scans = 75. 3: V_b = 1.0 V, I_{set} = 60 nA, number of scans = 30. 4 shows I\V traces recorded on single molecules by disabling the feedback loop and sweeping the bias potential.

As a control experiment, we determined the conductance of Au|1,8–octanedithiol|Au junctions under conditions identical to those for 4{Pt_6}4, *i.e.* under an argon atmosphere and with a similar set point current (although the absolute s_0 distance will vary). The primary peak in the conductance histogram is located at (3.7 ± 0.9_ nS (+0.6 V bias, I_{set} = 20 nA)

6.4.4 NCS-{Pt_6}-SCN

This compound has not been characterised by XPS or PMIRRAS, however, preliminary STM measurements have been performed and shown below. The molecule makes a good comparison to the previous as it has no resistive alkyl chains.

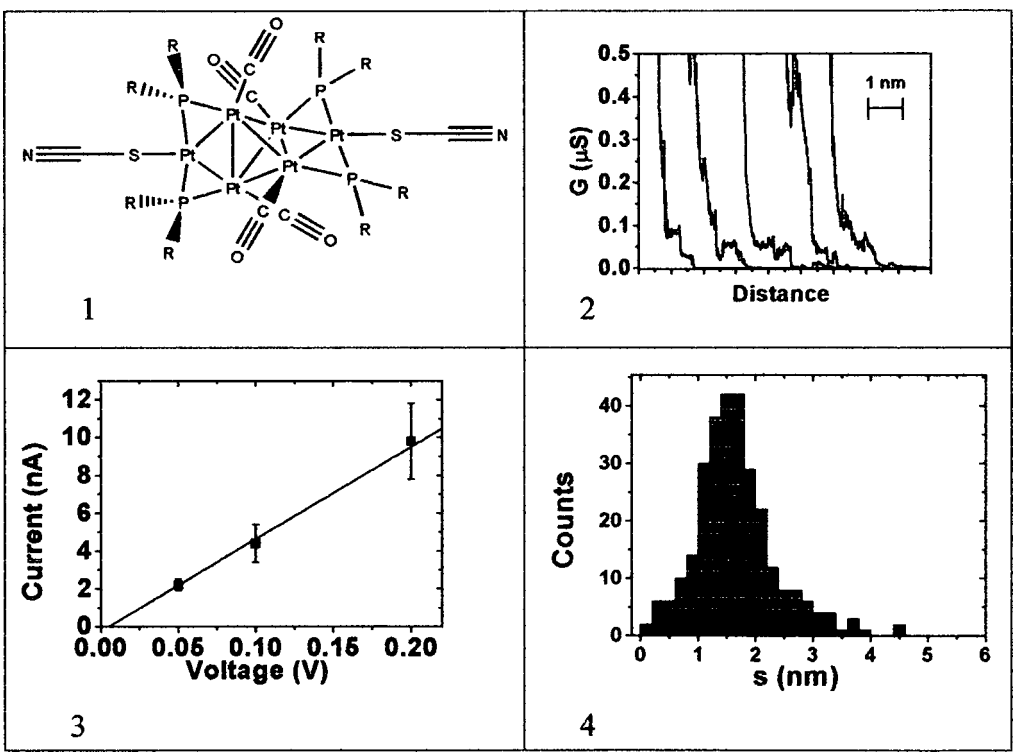

Figure 6.18. 1: Structure of NCS-{Pt_6}-SCN. 2: I(s) scans of 4 under Ar. V_b = 0.1 V, I_{set} = 50 nA, tip was moved down by 1 nm from I_{set} before the measurement so as to contact the molecules. 3: Plot of I(s) histogram peak currents for measurements on 4 plotted against bias potential. Error bars from width of histogram peaks at half maxima. G = 50 nS. 4: Calibrated break-off lengths at V_b = 0.1 V, I_{set} = 50 nA. The N..N distance in 4 is 15 Å.

6.5 Discussion

Firstly, let us compare the results of the conductance measurements on 4{Pt_6}4 and NCS-{Pt_6}-SCN with other compounds of a similar length in order to understand how these molecules fit into the general scheme of single molecule wires.

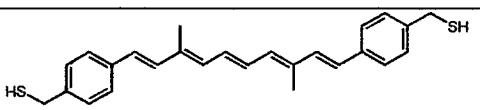	Carotinoid, G = 2.6 nS[9] (STM-BJ) (3.4 x 10^{-5} G_0, $d_{S..S}$ = 23 Å)
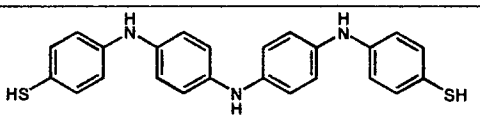	Teraniline, G = 1.0 nS[55] (STM-BJ) (1.3 x 10^{-5} G_0, $d_{S..S}$ = 24 Å)
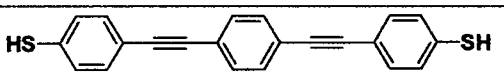	OPE, G = 9.3 nS[56] (MCBJ) (1.2 x 10^{-4} G_0, $d_{S..S}$ = 20.7 Å)
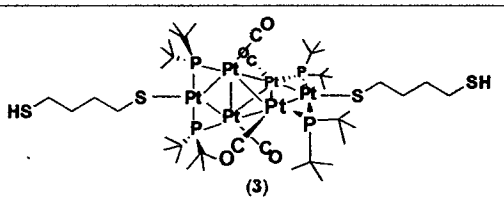	4{Pt_6}4, G = 2.4 nS (STM-I(s)) (3.1 x 10^{-5} G_0, $d_{S..S}$ = 24 Å)
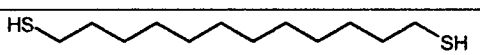	$HS(CH_2)_{12}SH$, G = 0.1 nS[57] (STM-BJ) (1.3 x 10^{-6} G_0, $d_{S..S}$ = 17 Å)

Figure 6.19. Comparison between different types of molecular wire of length close to 20 Å. The measurement method is also shown.

As can be seen in figure 6.19, even the highly conjugated organic compounds such as the carotinoid and aniline based molecules are not

conductive in comparison with the quantum value of 77.4 μS exhibited by metallic chains formed in break-junction experiments. Only a 100^{th} of a percent of the total charge impinging on the molecule passes through in the experiments, so clearly these molecules are non-metallic at low bias. However, the 4{Pt_6}4 complex is comparable with the highly conjugated compounds even though it consists of much larger tunnel barriers in the form of two butanedithiol ligands. This indicates the effect upon the charge transport behaviour of the molecule of the central platinum cluster, which greatly facilitates the charge transmission over a considerable distance. Indeed, the S...S distance in 4{Pt_6}4 of 2.4 nm is roughly equivalent to that of $HS(CH_2)_{18}SH$ (S...S = 2.45 nm). The single molecule conductance of $HS(CH_2)_{18}SH$ over the same bias range would be too small to measure with our available equipment. However, it can be estimated by extrapolation from published data on $HS(CH_2)_nSH$ (n = 6, 8, 10)[58, 59] and works out as 4.6×10^{-5} nS. Thus, length for length, the {Pt_6} cluster is markedly more conductive than an alkyl chain. This trend is also seen for other double tunnel barrier systems discussed in the other chapters. 6Ph6 also exhibits a larger conductance than even simply the two barriers (thiahexyl) combined as in dodecanedithiol, and this seems to be a special property of the double barrier system.

Molecule	Conductance , G (nS)	S-S distance (nm)[a]
HS-$(CH_2)_4$-S-Pt_6-S-$(CH_2)_4$-SH	2.4 ± 0.5	2.40
HS$(CH_2)_8$SH	3.7 ± 0.9	1.20
HS-$(CH_2)_6$-Ph-$(CH_2)_6$-SH	0.74 ± 0.24	2.11
HS$(CH_2)_{12}$SH	0.10	1.71

Table 1. A comparison of double tunnel barriers with their respective single barrier equivalents. [a] Spartan S-S distance.

As mentioned earlier, the model most commonly applied to organic single molecule conductance is superexchange. If a purely superexchange mechanism were operational then the conductance would depend exponentially on the number of repeat units in the wire, giving the dependence $G = A\exp(-\beta_N N)$. This model fits the single barrier alkanedithiols well, where only one repeat unit is present. The $\{Pt_6\}$ cluster has Pt atoms also in the molecular backbone, so the electronic decay can be expected to differ through the different regions of the molecule. The total transmission through the wire is commonly estimated as the product of the transmissions through the different regions (i.e. [alkane]-[S-Pt_6-S]-[alkane]); [60]

$T_{Wire} = T_{alkane}T_{\{Pt6\}}T_{alkane}$

As the six platinum atoms carry a formal single positive charge (leading to a lowering of the HOMO energy) we could have expected the conductance to be lower than a C_8 alkane chain as all the regions of the wire are tunnel barriers. What we observe is that there are almost identical conductances for the cluster compound and octanedithiol (ODT) under the same conditions at low bias, with G = (2.4 ± 0.5) nS and (3.7 ± 0.9) nS, however, at larger bias values up to 1.0 V the platinum complex becomes more conductive (G = 8 nS at U_{bias} = 1.0 V). This indicates that the Pt_6 core has a very low resistance, and electron transfer is facile across this group. However, in order to explain the larger conductance at 1.0 V one needs an alternative mechanism to simply adiabatic tunnelling and should consider the possibility that there is a non-adiabatic, possibly resonant tunnelling pathway across the molecule. Resonant tunnelling has been demonstrated in inorganic semi-conductor DTB junctions, notably in RTDs (resonant tunnelling diodes) and it may be a viable mechanism for charge transfer across metal|molecular organic/inorganic|metal interfaces.

Regarding the I\V behaviour of $4\{Pt_6\}4$ the slope cannot be modelled using a Simmons' fit, unlike alkanedithiols which are considered classic single tunnelling barriers. The slope of $4\{Pt_6\}4$ increases more sharply than predicted by a Simmons fit[61], and in order to replicate the low bias

conductance over a 2 nm barrier a very low barrier height of 0.2 eV must be used, which is unreasonable in this system.

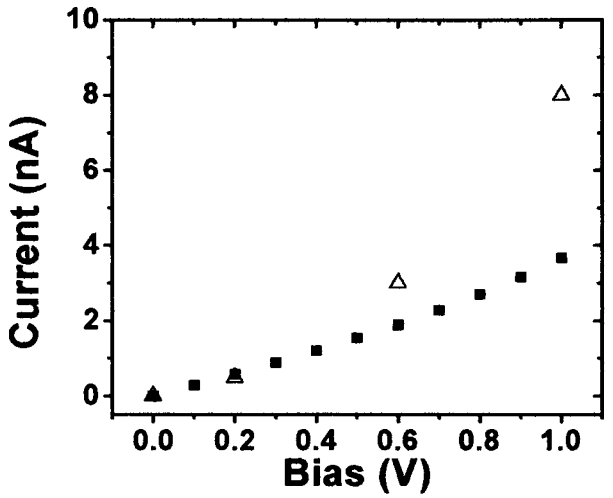

Figure 6.20. Simmons fit of the I\V dependence of 4{Pt_6}4 (black squares) using the parameters d = 1.2 nm, barrier height = 1.15 eV. Red triangles – experimental data for 4{Pt_6}4.

Using the parameters which fit octanedithiol (d = 1.2 nm and Φ = 1.15 eV) we can fit the low bias result, however the current still increases too rapidly at large bias and ultimately the model fails in this region. Clearly the molecule is not acting as a single barrier, and the results indicate that perhaps we should view the system as a real double barrier structure, which is approaching 'resonance' at the higher biases. Certainly the sharp increase in current at 1.0 V agrees with the measured electrochemical HOMO-LUMO gap of c.a. 2.1 eV if the Fermi level of the electrodes lies in the middle of the HOMO-LUMO gap, giving a barrier of about 1 eV. Also the current would agree more with that of ODT at low bias if the

'well' is substantially off-resonant at these potentials, which it does, as resonance effects would be small.

On the other hand, the I\V plot for the complex without any saturated linkers NCS-{Pt_6}-SCN can be modelled with a Simmons fit using reasonable parameters. If one takes the Pt-Pt of the two apical atoms (0.75 nm) and a barrier height of 0.8 eV one obtains the following plot:

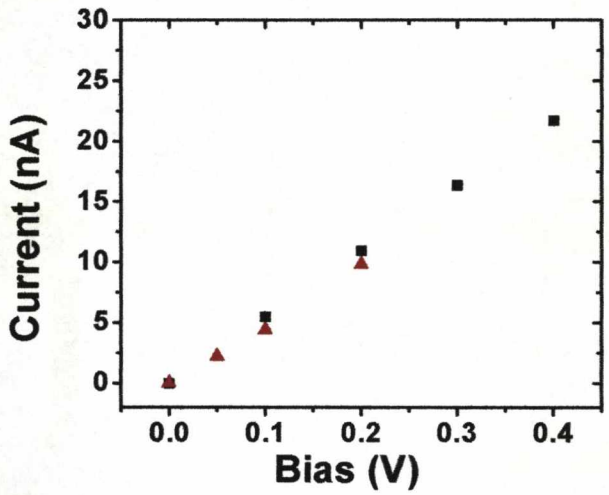

Figure 6.21. Simmons fit of the I\V dependence of 4{Pt_6}4 (black squares) using the parameters d = 0.75 nm, barrier height = 0.8 eV. Red triangles – experimental data for NCS{Pt_6}SCN.

The N..N distance in this complex is 1.4 nm, however there is a strong possibility that there is cleavage of the thiocyanate group on wet gold to produce the thiol/thiolate. This is due to the strong affinity gold has for the free cyanide (CN) group. Hence, 0.75 nm represents the distance between outer platinum atoms and is a sensible barrier length for this molecule.

In terms of its conductivity (50 nS) the dithiocyanate complex has a similar low bias conductance to the metal chain compounds supported by pyridylamine ligands. For the penta-chromium chain a conductance of 100 nS was measured and for the penta-nickel a conductance of 42 nS was found[36]. The penta-metal chains are a good comparison for the $\{Pt_6\}$ group as they are approximately the same length, even if the platinum atoms are not arranged in a linear fashion. Platinum in this complex has a low formal oxidation state of +1 compared to +2 and +4 for nickel in the metal string complex. The effect of oxidation state on metal conductivity is little understood, however the similarities in the conductance between these complexes suggests only a small influence at this stage. Evidently the conductance depends on the energy position of the transport channel, and oxidation state affects orbital energies (for d-orbitals the energy decreases as the oxidation state increases), however comparing different oxidation states in different metals could be misleading as different metals also have different energy levels.

The conductivities of the two platinum complexes investigated also demonstrate the inability to ascertain a particular group's resistance in a way that one could determine the resistance/conductance of any system by knowing the individual resistances of its component parts. If we attempt to predict the resistance of the dibutanethiol platinum complex from the resistance measured for the complex without saturated alkyl groups even

allowing for the different contact group (thiol versus thiocyanate) one obtains a resistance much larger than actually measured. Roughly the addition of a CH_2 group is expected to increase the resistance by a factor 3, implicit from the β factor measured for alkane chains, and so the addition of 8 methylene groups should result in a measured resistance that is around $3^8 = 6561$ times larger. As we measure 2×10^{-2} MΩ for the dithiocyanate we derive a value of 1.3×10^2 MΩ, which compared to the actual value of 4×10^{-1} MΩ from the experiment is much too large. The measured resistance increases by only an order of magnitude rather than by four which this simple theory would predict in an analogous manner as the dialkylbenzenes compounds in chapter 3. Clearly this is an indication of a different conduction mechanism at work than that which operates in simple alkanedithiols and requires further experimentation and theoretical insight in order to elucidate this phenomenon.

6.6 Summary

In summary we have shown that molecules incorporating metal clusters can be measured using the I(s) single molecule conductance measurement technique. The incorporation of a hexanuclear platinum cluster inside two butane chains gives almost the same low bias conductance as the two

chains joined together (i.e. an octanedthiol molecule) .The conductivity increases upon application of larger bias voltages.

This work has highlighted the great potential of such cluster compounds as, for instance, spacer units in functional organic molecular circuits. Indeed, types of cluster similar to those studied here could be used to produce long molecular wires with high conductance, and those with more accessible redox potentials could also behave as switches or diodes.

Further theoretical investigation is needed to ascertain the specific conductance mechanism, but the presence of a group with energetically low lying orbitals compared to the chain orbitals has a pronounced effect on the type of transport mechanism, which is probably different from pure tunnelling (i.e superexachange/hopping).

Many new and highly interesting metal containing low nuclearity clusters are discovered all the time, and an exhaustive review here is unfeasible. However, there is the scope for a wide ranging investigation of the electronic behaviour of not only metal cluster compounds, but also non-metallic clusters like carbon and boron compounds as two examples. Further collaborations between cluster chemists, physicists, electronic engineers and materials scientists will hopefully develop this area into a new and exciting field of research.

Bibliography

[1] N. J. Tao, *Nature Nanotechnology* **2006**, *1*, 173-181.

[2] X. L. Li, J. Hihath, F. Chen, T. Masuda, L. Zang, N. J. Tao, *Journal of the American Chemical Society* **2007**, *129*, 11535-11542.

[3] W. Haiss, H. van Zalinge, S. J. Higgins, D. Bethell, H. Hobenreich, D. J. Schiffrin, R. J. Nichols, *Journal of the American Chemical Society* **2003**, *125*, 15294-15295.

[4] P. Kornilovitch, A. Bratkovsky, S. Williams, in *Molecular Electronics III, Vol. 1006*, **2003**, pp. 198-211.

[5] N. Jlidat, M. Hliwa, C. Joachim, *Chemical Physics Letters* **2008**, *451*, 270-275.

[6] B. Q. Xu, N. J. Tao, *Science* **2003**, *301*, 1221-1223.

[7] N. Agrait, A. L. Yeyati, J. M. van Ruitenbeek, *Phys. Rep.-Rev. Sec. Phys. Lett.* **2003**, *377*, 81-279.

[8] J. M. Krans, J. M. Vanruitenbeek, V. V. Fisun, I. K. Yanson, L. J. Dejongh, *Nature* **1995**, *375*, 767-769.

[9] J. He, F. Chen, J. Li, O. F. Sankey, Y. Terazono, C. Herrero, D. Gust, T. A. Moore, A. L. Moore, S. M. Lindsay, *J. Am. Chem. Soc.* **2005**, *127*, 1384-1385.

[10] F. Chen, J. He, C. Nuckolls, T. Roberts, J. E. Klare, S. Lindsay, *Nano Lett.* **2005**, *5*, 503-506.

[11] G. Sedghi, K. Sawada, L. J. Esdaile, M. Hoffmann, H. L. Anderson, D. Bethell, W. Haiss, S. J. Higgins, R. J. Nichols, *J. Am. Chem. Soc.* **2008**, *130*, 8582-+.

[12] S. P. Gubin, Y. V. Gulayev, G. B. Khomutov, V. V. Kislov, V. V. Kolesov, E. S. Soldatov, K. S. Sulaimankulov, A. S. Trifonov, *Nanotechnology* **2002**, *13*, 185-194.

[13] C. Femoni, M. C. Iapalucci, G. Longoni, P. H. Svensson, P. Zanello, F. F. De Biani, *Chem.-Eur. J.* **2004**, *10*, 2318-2326.

[14] F. F. de Biani, A. Ienco, F. Laschi, P. Leoni, F. Marchetti, L. Marchetti, C. Mealli, P. Zanello, *J. Am. Chem. Soc.* **2005**, *127*, 3076-3089.

[15] K. Angermaier, H. Schmidbaur, *Inorg. Chem.* **1994**, *33*, 2069-2071.

[16] J. W. A. Vandervelden, J. J. Bour, J. J. Steggerda, P. T. Beurskens, M. Roseboom, J. H. Noordik, *Inorg. Chem.* **1982**, *21*, 4321-4324.

[17] T. Albrecht, S. F. L. Mertens, J. Ulstrup, *Journal of the American Chemical Society* **2007**, *129*, 9162-9167.

[18] N. Oncel, A. S. Hallback, H. J. W. Zandvliet, E. A. Speets, B. J. Ravoo, D. N. Reinhoudt, B. Poelsema, *Journal of Chemical Physics* **2005**, *123*, 044703.

[19] F. W. Vergeer, C. J. Kleverlaan, P. Matousek, M. Towrie, D. J. Stufkens, F. E. Hartl, *Inorganic Chemistry* **2005**, *44*, 1319-1331.

[20] A. Bernardi, C. Femoni, M. C. Iapalucci, G. Longoni, F. Ranuzzi, S. Zacchini, P. Zanello, S. Fedi, *Chem.-Eur. J.* **2008**, *14*, 1924-1934.

[21] A. Albinati, F. F. de Biani, P. Leoni, L. Marchetti, M. Pasquali, S. Rizzato, P. Zanello, *Angewandte Chemie-International Edition* **2005**, *44*, 5701-5705.

[22] P. Leoni, F. Marchetti, L. Marchetti, M. Pasquali, *Chemical Communications* **2003**, 2372-2373.

[23] F. A. Cotton, T. E. Haas, *Inorg. Chem.* **1964**, *3*, 10-&.

[24] K. Wade, *Inorganic & Nuclear Chemistry Letters* **1972**, *8*, 559-&.

[25] D. M. P. Mingos, *Accounts Chem. Res.* **1984**, *17*, 311-319.

[26] G. Schmid, Y. P. Liu, *Nano Lett.* **2001**, *1*, 405-407.

[27] S. Hoeppener, L. F. Chi, H. Fuchs, *Nano Lett.* **2002**, *2*, 459-463.

[28] M. H. V. Werts, M. Lambert, J. P. Bourgoin, M. Brust, *Nano Lett.* **2002**, *2*, 43-47.

[29] A. C. Templeton, M. P. Wuelfing, R. W. Murray, *Accounts Chem. Res.* **2000**, *33*, 27-36.

[30] L. F. Chi, M. Hartig, T. Drechsler, T. Schwaack, C. Seidel, H. Fuchs, G. Schmid, *Appl. Phys. A-Mater. Sci. Process.* **1998**, *66*, S187-S190.

[31] R. S. Ingram, M. J. Hostetler, R. W. Murray, T. G. Schaaff, J. T. Khoury, R. L. Whetten, T. P. Bigioni, D. K. Guthrie, P. N. First, *J. Am. Chem. Soc.* **1997**, *119*, 9279-9280.

[32] C. Femoni, M. C. Iapalucci, F. Kaswalder, G. Longoni, S. Zacchini, *Coord. Chem. Rev.* **2006**, *250*, 1580-1604.

[33] G. Ciani, A. Sironi, *J. Organomet. Chem.* **1983**, *241*, 385-393.

[34] B. K. Teo, *Inorg. Chem.* **1984**, *23*, 1251-1257.

[35] F. A. Cotton, *Inorg. Chem.* **1998**, *37*, 5710-5720.

[36] I. W. P. Chen, M. D. Fu, W. H. Tseng, J. Y. Yu, S. H. Wu, C. J. Ku, C. H. Chen, S. M. Peng, *Angew. Chem.-Int. Edit.* **2006**, *45*, 5814-5818.

[37] M. Mayor, C. von Hanisch, H. B. Weber, J. Reichert, D. Beckmann, *Angewandte Chemie-International Edition* **2002**, *41*, 1183.

[38] N. T. Lucas, M. G. Humphrey, A. D. Rae, *Macromolecules* **2001**, *34*, 6188-6195.

[39] N. T. Lucas, J. P. Blitz, S. Petrie, R. Stranger, M. G. Humphrey, G. A. Heath, V. Otieno-Alego, *J. Am. Chem. Soc.* **2002**, *124*, 5139-5153.

[40] T. Tanase, H. Ukaji, H. Takahata, H. Toda, T. Igoshi, Y. Yamamoto, *Organometallics* **1998**, *17*, 196-209.

[41] T. Tanase, E. Goto, R. A. Begum, M. Hamaguchi, S. Z. Zhan, M. Iida, K. Sakai, *Organometallics* **2004**, *23*, 5975-5988.

[42] T. Tanase, E. Goto, H. Takenaka, T. Horiuchi, Y. Yamamoto, J. Kuwabara, K. Osakada, *Organometallics* **2005**, *24*, 234-244.

[43] F. Choffat, P. Smith, W. Caseri, *Adv. Mater.* **2008**, *20*, 2225-+.

[44] A. Bettac, L. Koller, V. Rank, K. H. Meiwes-Broer, *Surf. Sci.* **1998**, *404*, 475-479.

[45] A. H. N Oncel , HJW Zandvliet , EA Speets , BJ Ravoo , DN Reinhoudt , B Poelsema *Journal of Chemical Physics* **2005**, *123*.

[46] A. Albinati, P. Leoni, L. Marchetti, S. Rizzato, *Angewandte Chemie-International Edition* **2003**, *42*, 5990-5993.

[47] C. Bonaccorsi, F. F. de Biani, P. Leoni, F. Marchetti, L. Marchetti, P. Zanello, *Chem.-Eur. J.* **2008**, *14*, 847-856.

[48] L.J. Bellamy, The Infrared Spectra of Complex Molecules; Chapman and Hall, London and New York, Second Edition, 1980.

[49] A. M. Baro, H. Ibach, *Surf. Sci.* **1981**, *103*, 248-256.

[50] G. Ferguson, B. R. Lloyd, R. J. Puddephatt, *Organometallics* **1986**, *5*, 344-348.

[51] M. C. Jennings, G. Schoettel, S. Roy, R. J. Puddephatt, G. Douglas, L. Manojlovicmuir, K. W. Muir, *Organometallics* **1991**, *10*, 580-586.

[52] B. C. Beard, P. N. Ross, *J. Phys. Chem.* **1986**, *90*, 6811-6817.

[53] M. Arfelli, C. Battistoni, G. Mattogno, *J. Electron Spectrosc. Relat. Phenom.* **1989**, *49*, 273-277.

[54] T. Laiho, J. Lukkari, M. Meretoja, K. Laajalehto, J. Kankare, J. A. Leiro, *Surf. Sci.* **2005**, *584*, 83-89.

[55] J. He, F. Chen, S. Lindsay, C. Nuckolls, *Appl. Phys. Lett.* **2007**, *90*, 3.

[56] S. Wu, M. T. Gonzalez, R. Huber, S. Grunder, M. Mayor, C. Schonenberger, M. Calame, *Nat Nano* **2008**, *3*, 569-574.

[57] T. Morita, S. Lindsay, *J. Am. Chem. Soc.* **2007**, *129*, 7262-+.

[58] X. L. Li, J. He, J. Hihath, B. Q. Xu, S. M. Lindsay, N. J. Tao, *J. Am. Chem. Soc.* **2006**, *128*, 2135-2141.

[59] C. Li, I. Pobelov, T. Wandlowski, A. Bagrets, A. Arnold, F. Evers, *J. Am. Chem. Soc.* **2008**, *130*, 318-326.

[60] Z. H. Li, I. Pobelov, B. Han, T. Wandlowski, A. Blaszczyk, M. Mayor, *Nanotechnology* **2007**, *18*, 8.

[61] W. Y. Wang, T. Lee, M. A. Reed, *Rep. Prog. Phys.* **2005**, *68*, 523-544.

Chapter 7

A study of 1,8-octanedithiol using the I(s) and I(t) techniques

Chapter 7

A study of 1,8-octanedithiol using the I(s) and I(t) techniques

7.1 Introduction

Molecular electronics has advanced significantly in recent years and a variety of interesting effects have been observed. Despite these advances, however, a detailed understanding of many of the mechanisms involved in molecular electronics has not yet been achieved. In 2003 Xu and Tao[1] and Haiss *et al.*[2] demonstrated that the electronic properties of single molecules can be studied by a statistical analysis of molecular junctions which were repeatedly formed in an STM, either in organic liquids[1] or under electrochemical conditions[2-5]. The method adopted by Tao involves making mechanical contact between the tip and the substrate, the so called break-junction technique. The I(s) method, on the other hand, relies on an initial separation between the tip and substrate, determined by the set-point current, and allowing the spontaneous formation of metal|molecule|metal junctions before withdrawing the tip and breaking the junction. The

conductance of alkanedithiols has been widely studied using these techniques[6-10]. Surprisingly, these two seemingly similar STM-based methods applied to the same system resulted in very different conductance values for identical molecules. For example the single molecule conductance values for a 1,8–octanedithiol molecule between gold electrodes determined with the break-junction method (~20 nS) were a factor of approximately 20 times larger than the values determined with the $I(s)$ method (~1nS). It is essential to be able to control efficiently and precisely electron transport through such molecular junctions and understand the details of the factors that affect the transport before such devices can be made practical.

This disagreement reflects our present poor insight into the atomistics of single molecule junctions. Two different fundamental conductance groups were observed for alkanedithiol compounds using the break-junction method, whilst a third group has been pointed out at a lower conductivity using the I(s) method. Peaks in the histograms of current plateaus seem to indicate the presence of preferred junction geometries. However, it is unclear how much the geometry varies within the spread of an individual peak corresponding to a single molecule. Recently an idea was put forward that the higher conductance groups are due to multiple molecule bridges based on observations made using a cantilever-type mechanically controlled break-junction. This is unlikely as peaks in the histograms

corresponding to integer values of the three conductance groups can readily be observed, indicating each group to be fundamental in its own right and not due to clusters of molecules.

Based on the results of alkanedithiol studies by the I(s), I(t)[11, 12] and break-junction methods,[13] the break-junction techniques gave the consistently larger conductance values. However, the reported conductance of 1,8-octanedioic ($HOOC-(CH_2)_6COOH$) acid is actually larger using the I(s) technique[14] than the break-junction.[13] Clearly the two techniques create different surface roughness conditions – the break-junction resulting in large mountainous surface structure after measurement,[15] whilst the I(s) technique results in flatter surfaces. Whilst rougher surfaces may be more favourable for thiol compounds, this may not be universal for all types of binding group.

7.2 Aims

The rationale for studying the precise origins of the different conduction values is that in order to make reliable comparisons between the results of different groups, and indeed between different compounds, we must know exactly which group we are observing in any particular case. As presented in this thesis, multiple conduction groups are now thought to be a generic property of thiol terminated compounds (see chapter 4). We

wish to gain an insight, when performing single molecule measurements, into the tendency of a metal|molecule|metal junction to adopt particular conductance regimes and what the physical origin of this phenomenon could be.

It has recently been shown that hydrating gold microsphere junctions which incorporate SAMs of alkanedithiol molecules lowers the current through such junctions[16]. Inelastic electron tunnelling spectroscopy on the hydrated junctions revealed the presence of free thiol (R-SH) groups suggesting that water hydrates the contacts between metal and molecule which results in a weakening of the gold-sulphur bond and hence a higher contact resistance. The effect has also been studied in real-time using an oligo phenylene ethynylene (OPE) compound[17]. Nanosphere junctions of these molecules were monitored over time under exposure to different environments and only when exposed to air or water vapour did the current across them drop significantly. The current also fluctuated much more in the presence of water than under vacuum conditions, suggesting an increased variability in the contacts between the molecules and the gold nanoparticles. We have studied the effect of hydration on a series of oligothiophene molecular wires (see chapter 4) and found that the conductivity of the longer oligomers increases in the presence of water. This effect was explained in terms of an electrostatic field gating mechanism in which the presence of water molecules around the

thiophene core shifted the energy levels closer to the gold electrode Fermi level. This mechanism cannot happen with alkanedithiols as they do not posses polarisable aromatic units, only saturated bonds. However, the question arises - can we observe a water induced effect on the conductance of a single alkanedithiol molecule? If so, could the presence of water in single molecule measurements play a role in the observation of the different fundamental conduction groups?

7.3 Methods

A gold-on-glass slide was coated with ODT (1×10^{-4} M concentration in distilled DCM). The sample was then rinsed with freshly distilled DCM and placed in an open STM cell – see methods, chapter 3). The STM chamber was purged with a flowing stream of dry argon for 24 hours. I(s) and I(t) measurements were then carried out on different areas of the sample after taking an image of the area and assessing drift of the system. For each measurement 1000 scans were taken and analysed using a labview automated analysis program. The program records only the value of the plateau and not the whole number of data points.

7.4 Results

7.4.1 I(s) method under argon atmosphere

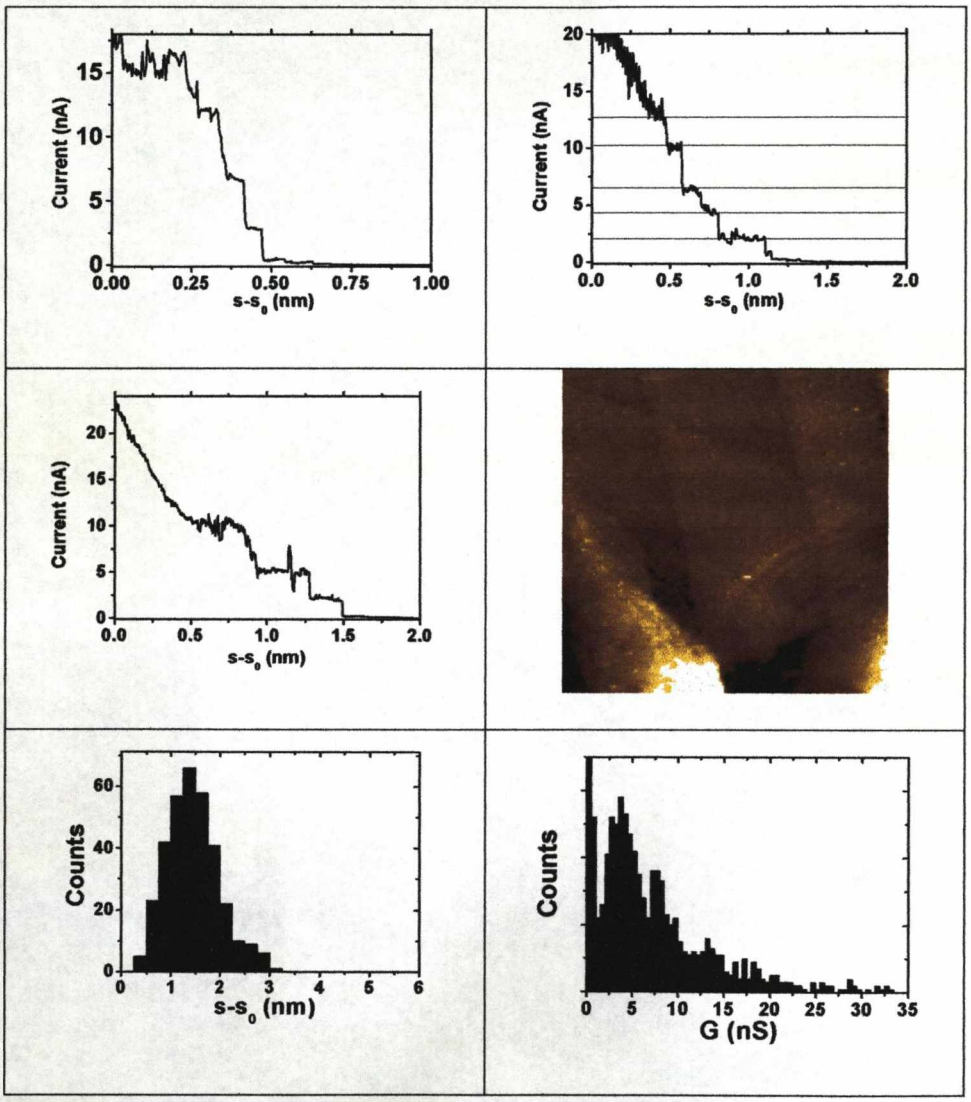

Figure 7.1. *I*(*s*) curves obtained on Au(111) in the presence of ODT under argon atmosphere at U_{bias} = 0.6 V and I_0 = 20 nA. The steps in the I(s) curves correspond to a fundamental conductance of (3.7 ± 0.9) nS. The mean break-off distance for the final plateau was 1.35 nm.

The image displays the area where the measurements were performed – dimensions 125x125 nm.

Figure 7.1 shows typical *I*(*s*) curves observed in the presence of octanedithiol (ODT). The image taken before the measurements shows that the surface was mostly flat with some monatomic steps. The I(s) results in this area indicate that the most prominent, fundamental, conduction group under such conditions is observed at (3.7 ± 0.9) nS. This value is in agreement with the break-junction results of Tao. The mean break-off distance is quoted without calibration - due to the large uncertainty in obtaining a constant s_0. However, the result seems to suggest that s_0 is quite small as the uncalibrated result is equal already to the fully extended molecule. One possibility is, however, that gold atoms are extruded from the surface and the tip prior to junction cleavage as it is known that the gold-sulphur bond is stronger than the gold-gold bond[18].

The final feature in some I(s) scans was sometimes much smaller than 3.7 nS however. An analysis of these features reveals that the mean extent is much longer than for the 3.7 nS plateau. There are also no distinct peaks as the features tend to be rather ill-defined. Some examples are shown in figure 7.2.

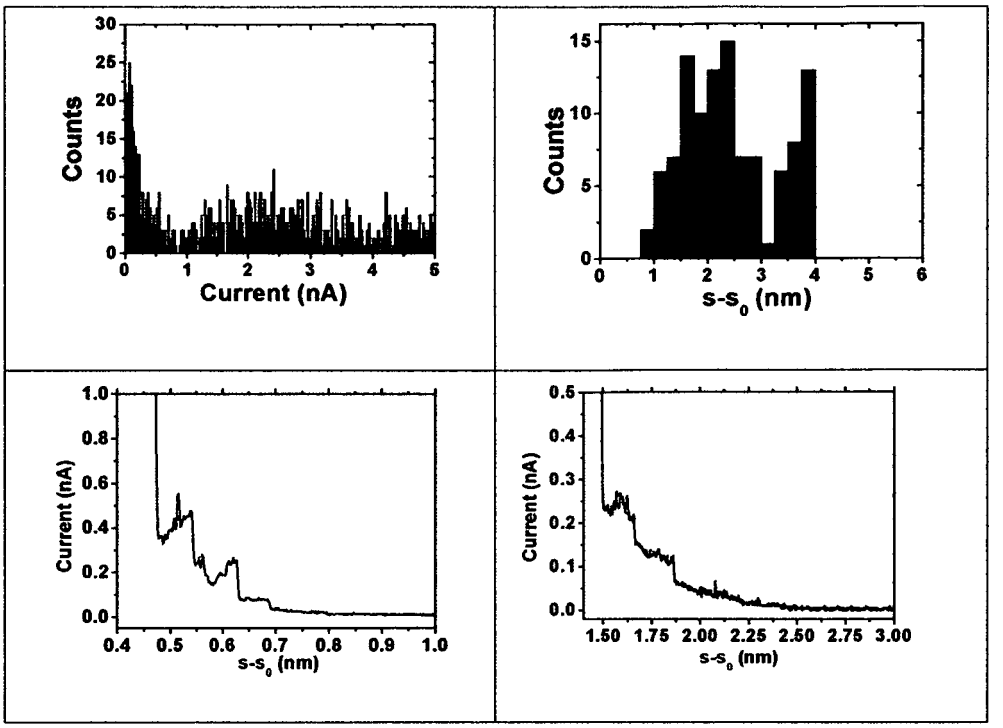

Figure 7.2. I(s) curves showing small features after the larger 3.7 nS plateau. U_{bias} = 0.6 V and I_0 = 20 nA.

These events could be due to non-bridged molecules which remain in the junction after cleavage. Plus, the process of breaking the junction causes instability in both electrodes, and this could manifest itself in the form of false-plateaus which correspond to atom, or molecule, movement.

7.4.2 I(s) method as a function of the set-point current, I_0

The I(s) histograms obtained at low I_0 (1-2 nA, U_{bias} = 0.6 V) gave very little in the way of current plateau. Some 3.7 nS plateau could be seen, however, only when a molecule attached after the feedback loop had been

disabled and the scan commenced. This is because the current which flows through a molecule at 0.6 V is greater than the set-point of 1-2 nA and so the feedback loop retracts the tip, breaking the junction.

At a set-point of 4 nA plateaus began to be regularly observed, and increasing the value of the set-point current resulted in progressively more and more plateaus recorded. The prominence of a group 2 peak, representing the current through two molecules, grew when I_0 was above 10 nA. At much higher set-points (between 25 and 50 nA) evidence of a new conductance group located at about 10 nA, with a double around 20 nA, was present. This group is in accordance with the 'high' conductance group observed by Tao[18], with a value of, in our case, approximately 17 nS.

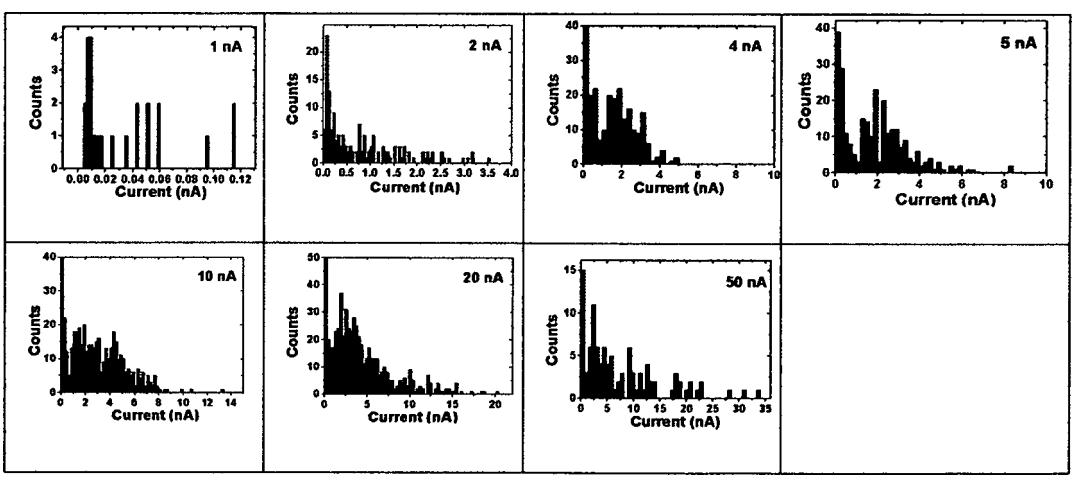

Figure 7.3. I(s) histograms, each from 1000 scans, at different set-point currents (shown in the figure). All the scans were taken from the same area of the sample. U_{bias} = 0.6 V.

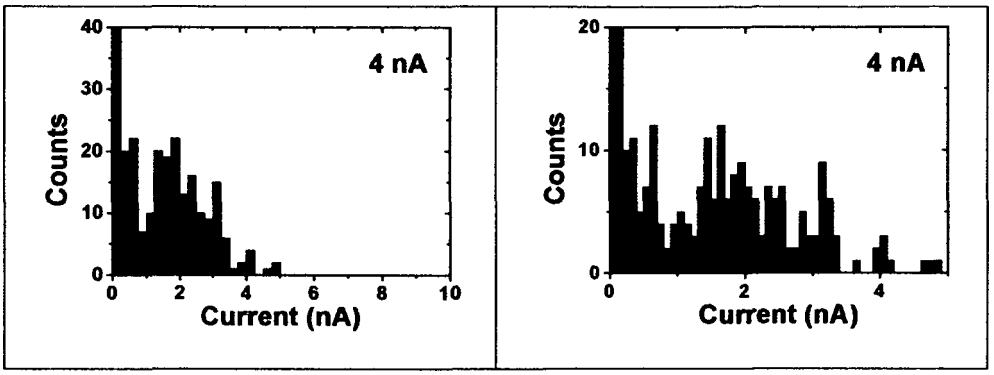

Figure 7.4. A comparison of the results at 4 nA presented using different bin sizes. The bin sizes are 0.3 (15% peak width @ 2 nA) for the left histogram and 0.1 (5% peak width @ 2 nA) for the right.

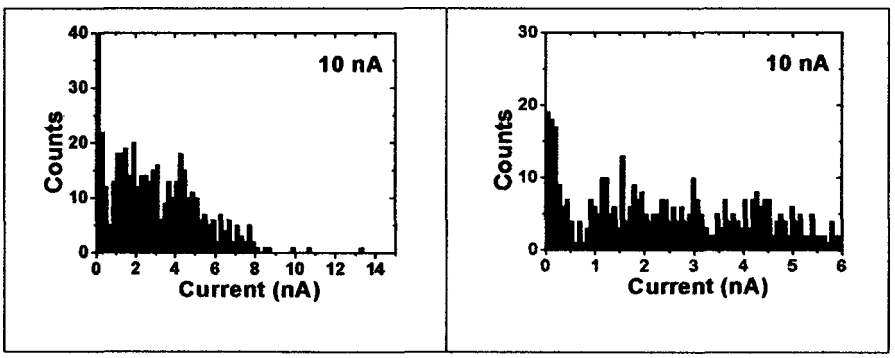

Figure 7.5. A comparison of the results at 10 nA presented using different bin sizes. The bin sizes are 0.2 (10% peak width @ 2 nA) for the left histogram and 0.08 (4% peak width @ 2 nA) for the right.

Clearly the left hand histogram representations in figures 7.4 and 7.5 display the data optimally for both sets of data. At 4 nA set-point there is some evidence of a group of plateau at circa 0.6 nA, however, the weighting of the data tends to the larger events about 2 nA. At 10 nA the right hand histogram shows evidence of only very small and sporadic

current events, indicating that as the set-point current is increased the dominant group measured is centred about 2 – 2.5 nA.

7.4.3 Reintroduction of ambient air

After the measurements were completed under argon, the STM chamber was re-open to the air and left to acclimatise for two hours. Then I(s) scans were taken at various locations around the sample keeping the set-point current and bias voltage constant. The set-point current in air may, however, correspond to a different absolute tip-sample separation.

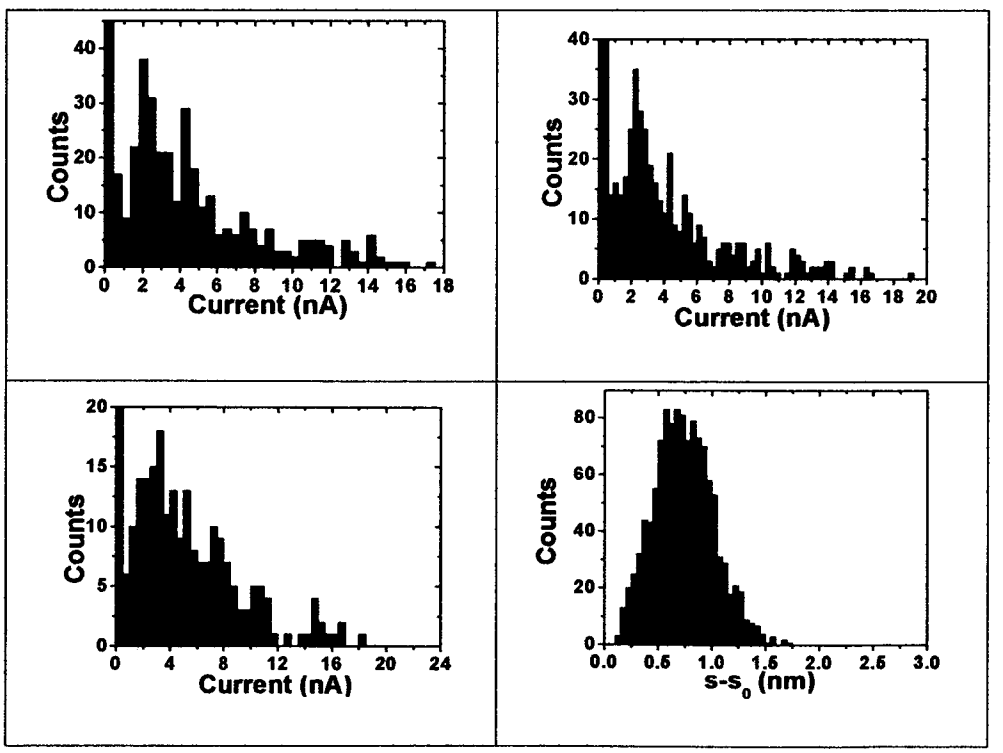

Figure 7.6. I(s) measurements taken under ambient air at different positions on the sample. U_{bias} = 0.6 V and I_0 = 20 nA.

Peaks in the histogram at 2.5 nA (3.7 nS) remained clearly visible after air was readmitted to the STM chamber (figure 7.6). The presence of ambient air seems, therefore, to have no effect on the single molecule conductance of ODT. The imaging resolution deteriorated somewhat from the dry, argon saturated, conditions as can be seen if we compare images taken under the different conditions:

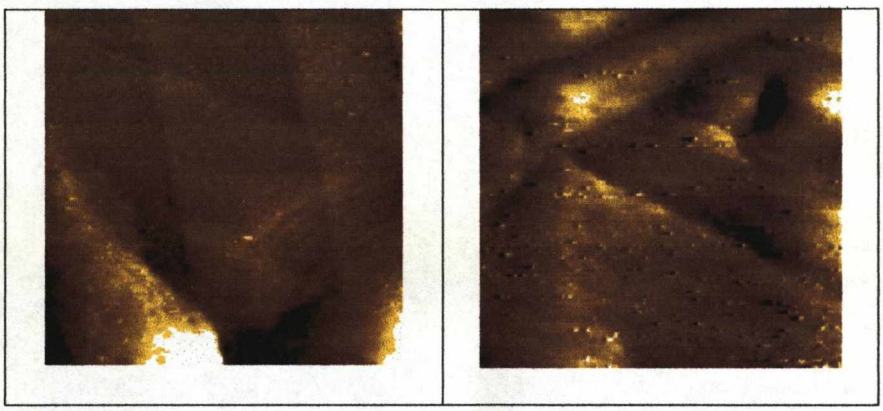

Figure 7.7. Images of ODT coated surfaces taken under argon atmosphere (left) and under ambient air (right) and are different areas of the sample. U_{bias} = 0.6 V, I_{set} = 0.5 nA. Both images are 125x125 nm.

The resolution of the step edges is lower under ambient air.

7.4.4 I(s) measurements after washing the sample with ethanol

Finally, the sample was removed from the STM and rinsed with 10-20 ml of absolute ethanol. Ethanol is normally used to wash excess or unbound

thiol from the gold surface, however it is known that ethanol adsorbs to gold quite strongly. The following measurements were made to assess any effect of ethanol on the conductance of ODT.

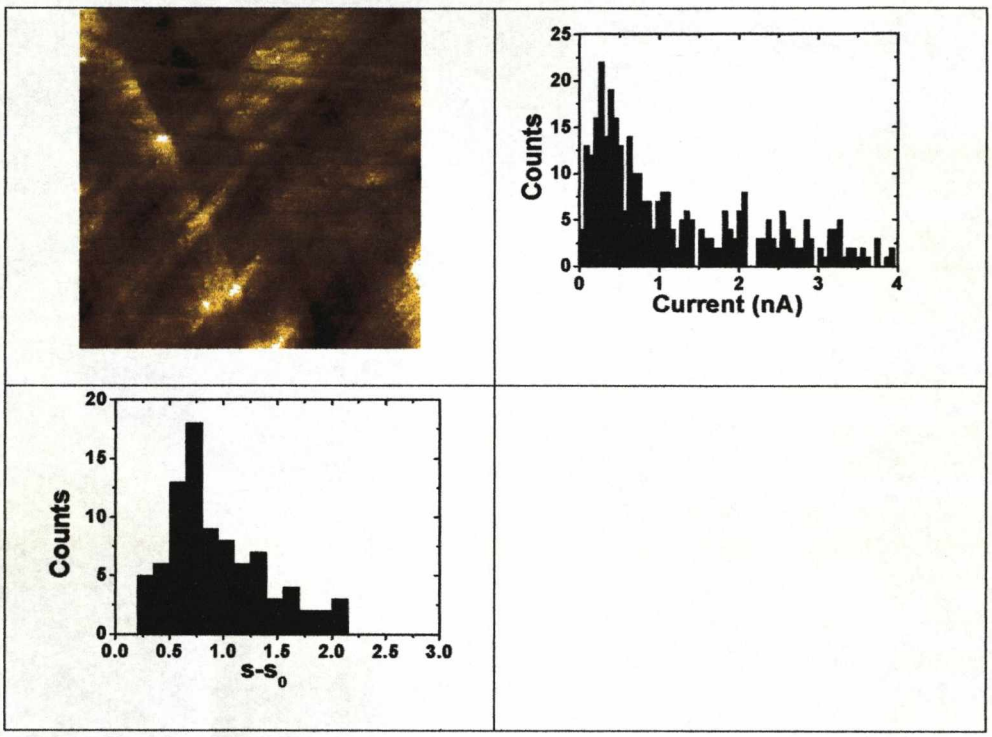

Figure 7.8. I(s) measurements taken under ambient air after washing the sample with EtOH. U_{bias} = 0.6 V and I_0 = 20 nA.

A dramatic reduction in the 4 nS jumps was observed after the process of washing the whole thiol-coated gold surface with ethonal, and the predominant conduction value is now found at (0.53 ± 0.19) nS. The mean break-off length of the current plateaus remained consistent with the length of the molecule (figure 7.8).

7.4.5 I(t) method under argon atmosphere

The second method of measuring single molecule conductivities we have used is the I(t) method[12]. It involves measuring the tunnelling current over a period of time (200 ms) with the feedback loop temporarily disabled. This results in the ability to observe current jumps which can be caused by individual, and sometimes more than one, molecule either spontaneously attaching or detaching from one of the STM electrodes (tip or surface). This method allows the junction size to be changed systematically by changing the initial set-point current. Generally, the lower the set-point current, the larger the tip-sample distance will be. However, as there is no control as to certain junction properties, namely the number of molecules inside the junction, and whether any molecules are already attached at the beginning of an I(t) measurement, the absolute separation of the electrodes remains uncertain in each case. It is clear as the set-point current is increased the chance of a molecule being attached at the start of the scan is greater. This makes the calibration of distances at higher set-point currents yet more uncertain.

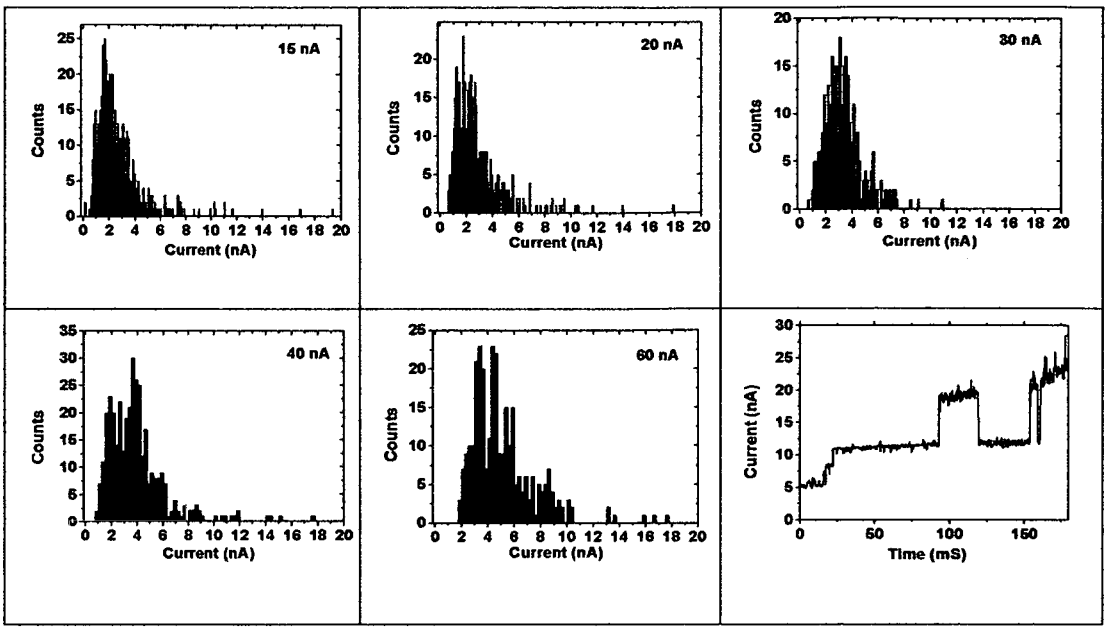

Figure 7.9. I(t) histograms at various set-point currents between 15 and 60 nA. U_{bias} = 0.6 V. Example of a double molecule attachment followed by a transition of one of the molecules to a higher conductive state.

Figure 7.9 shows the results of I(t) scans at different set-point current. Between 15 and 20 nA set-point currents the current jump size remained fairly constant at (2 ± 0.5) nA, which is consistent with the plateau values observed using the I(s) method (2.4 nA). Upon reaching a set-point current of 40 nA, however, a peak at roughly twice this value appears and dominates the histogram at 60 nA. At 40 nA the peak at 2 nA is still observable, whilst at 30 nA set-point current the result seems to be a convolution of the two peaks. The results can be interpreted as displaying the conductance of a single molecule between 15 and 20 nA, then two molecules between 40 and 60 nA. At 30 nA it was equally likely to

observe single and double molecule attachments/detachments, hence the intermediate vale of the histogram peak. Examples of the current jumps are shown in figure 7.10 below.

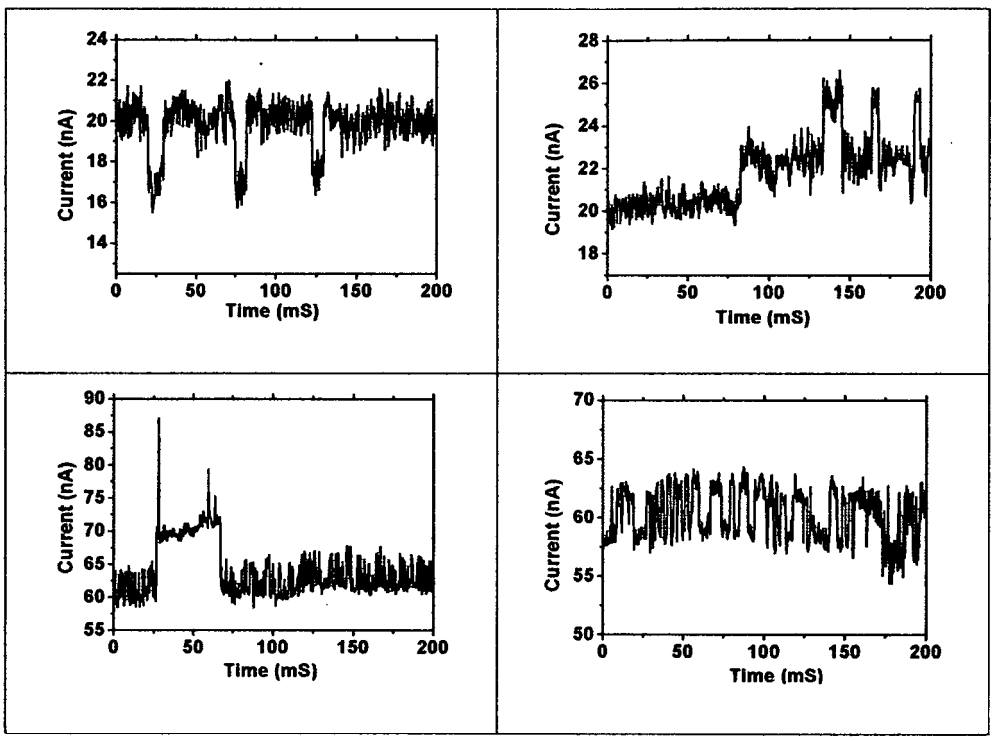

Figure 7.10. Examples of I(t) scans at 20 nA (top) and 60 nA (bottom). $U_{bias} = 0.6$ V.

7.5 Discussion

It is possible from the results from the analysis of the two techniques for measuring single molecule conductance draw several conclusions. The first is that, under relatively well defined condition such as those prepared here

with argon gas, the most probable conductance group to observe for octanedithol is found between 3.3 – 3.7 nS. The I(s) data is clear and well reproducible and many of the scans show multiple plateaus consistent with two or three molecules spanning the junction. The I(t) data under argon atmosphere agrees well with the I(s) data at the low set-point currents 15-20 nA, whilst at the higher set-points multiple molecule events became more common. This agrees with the observation of multiple plateaus in the I(s) at a set-point of 20 nA.

The I(s) measurements as a function of the set-point current show that, under the measured conditions, molecular wire formation was unlikely below a value of 4 nA. Above this critical value, the effect of increasing the set-point current was to increase the number of molecular junctions measured in a series, and also to increase the number of events due to multiple molecular bridges.

The introduction of air into the STM chamber seemed to have little effect on the observed value of the single molecule conductivity of ODT, however, the ethanol wash seems to have deteriorated the conductivity substantially. A value of 0.53 nS was found after this procedure, which agrees with the value published by Haiss et.al.[12] The implication of this is that, as ethanol is known to adsorb to gold, the presence of other adsorbates on the gold electrode surface (contaminants) has an effect on the conductivity of dithiol molecules. Ethanol has a much lower affinity for

gold than thiols[19]. However, as only a dilute monolayer of thiols is present in our system, adsorption of co-species is possible and could modify the surface in such a way that molecular conductivity is reduced. Speculatively, the thiols could adopt less conductive configurations on the surface, perhaps through the alterations to the specific binding of sulphur to gold.

Summary

In the final section on molecular wire measurements we studied the simple molecule octanedithiol under various conditions of the I(s) experiment. One of the clear outcomes of the study was to find multiple conduction groups, which is a feature also seen for other molecules in this thesis (especially the benzene containing wires). The predominant average value was 3.7 nS under a pure argon atmosphere. However, a larger group was visible at c.a. 17 nS in both I(s) and I(t) measurements. The best theory into the cause of the two groups is different bonding modes between the thiol groups and the gold surface/tip. We are unable to say why these two values in particular predominate. Theoretically it is possible to have many thiol-gold interactions, especially when in STM experiments the tip shape is hardly known and likely to be far from 'ideal'.

Exposure of the sample to ethanol caused the average conductivity to drop by a factor six to seven. The reason for this is not fully understood, however, evidence for weakening with the sulphur-gold bond in the presence of hydrogen-bonding compounds was discussed and the evidence for the interaction between water and thiophene was presented in chapter 5. This chapter highlights the problem which faces the field of single molecule conductivity – how to control the atomistics of molecule-electrode contacts.

Bibliography

[1] B. Q. Xu, N. J. J. Tao, *Science* **2003**, *301*, 1221-1223.

[2] W. Haiss, H. van Zalinge, S. J. Higgins, D. Bethell, H. Hobenreich, D. J. Schiffrin, R. J. Nichols, *J. Am. Chem. Soc.* **2003**, *125*, 15294-15295.

[3] Z. Li, B. Han, G. Meszaros, I. Pobelov, T. Wandlowski, A. Blaszczyk, M. Mayor, *Faraday Discuss.* **2006**, *131*, 121-143.

[4] X. Y. Xiao, L. A. Nagahara, A. M. Rawlett, N. J. Tao, *J. Am. Chem. Soc.* **2005**, *127*, 9235-9240.

[5] F. Chen, J. He, C. Nuckolls, T. Roberts, J. E. Klare, S. Lindsay, *Nano Lett.* **2005**, *5*, 503-506.

[6] X. L. Li, J. He, J. Hihath, B. Q. Xu, S. M. Lindsay, N. J. Tao, *J. Am. Chem. Soc.* **2006**, *128*, 2135-2141.

[7] C. Li, I. Pobelov, T. Wandlowski, A. Bagrets, A. Arnold, F. Evers, *J. Am. Chem. Soc.* **2008**, *130*, 318-326.

[8] B. Q. Xu, *Small* **2007**, *3*, 2061-2065.

[9] A. Nishikawa, J. Tobita, Y. Kato, S. Fujii, M. Suzuki, M. Fujihira, *Nanotechnology* **2007**, *18*, 10.

[10] M. T. Gonzalez, J. Brunner, R. Huber, S. M. Wu, C. Schonenberger, M. Calame, *New J. Phys.* **2008**, *10*, 9.

[11] W. Haiss, H. van Zalinge, D. Bethell, J. Ulstrup, D. J. Schiffrin, R. J. Nichols, *Faraday Discuss.* **2006**, *131*, 253-264.

[12] W. Haiss, R. J. Nichols, H. van Zalinge, S. J. Higgins, D. Bethell, D. J. Schiffrin, *Phys. Chem. Chem. Phys.* **2004**, *6*, 4330-4337.

[13] F. Chen, X. L. Li, J. Hihath, Z. F. Huang, N. J. Tao, *J. Am. Chem. Soc.* **2006**, *128*, 15874-15881.

[14] S. Martin, W. Haiss, S. Higgins, P. Cea, M. C. Lopez, R. J. Nichols, *J. Phys. Chem. C* **2008**, *112*, 3941-3948.

[15] J. He, O. Sankey, M. Lee, N. J. Tao, X. L. Li, S. Lindsay, *Faraday Discuss.* **2006**, *131*, 145-154.

[16] D. P. Long, J. L. Lazorcik, B. A. Mantooth, M. H. Moore, M. A. Ratner, A. Troisi, Y. Yao, J. W. Ciszek, J. M. Tour, R. Shashidhar, *Nat. Mater.* **2006**, *5*, 901-908.

[17] J. S. Na, J. Ayres, K. L. Chandra, C. B. Gorman, G. N. Parsons, *Nanotechnology* **2007**, *18*, 7.

[18] Z. F. Huang, F. Chen, P. A. Bennett, N. J. Tao, *J. Am. Chem. Soc.* **2007**, *129*, 13225-13231.

[19] R. P. S. Fartaria, F. F. M. Freitas, F. Fernandes, *Int. J. Quantum Chem.* **2007**, *107*, 2169-2177.

Chapter 8

Chemical synthesis section

Chapter 8

Experimental synthesis

Reagents were purchased from the Aldrich Chemical Company and used as received, except where otherwise stated. Solvents were dried by standard laboratory procedures and distilled under nitrogen or argon before use in the coupling reactions. Proton, ^{13}C and $^{13}C\{^{1}H\}$ NMR spectra were recorded using a Bruker Avance 400 MHz spectrometer, and were referenced to internal TMS. Mass spectra were recorded in CI positive ion mode using NH_3.

8.1. 1,4-Bis-(6-chloro-hexyl)-benzene:

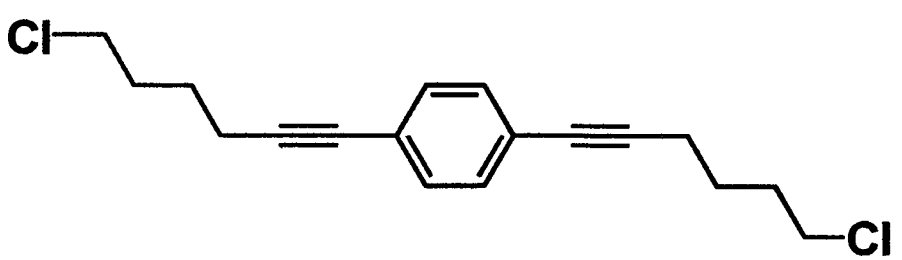

A mixture of 1,4–diiodobenzene (3.22 g, 9.75 mmol), $[PdCl_2(MeCN)_2]$ (0.13 g, 5 mol%), PPh_3 (0.256 g, 10 mol %) and CuI (0.056 g, 3 mol %) in $^{i}Pr_2NH$ (50 cm^3) was degassed for 20 min. by Ar bubbling. The 6–chloro–

hex–1–yne (3.07 g, 26.3 mmol) was added, and the mixture was refluxed for 5 h under N_2. It was allowed to cool to room temperature and then filtered, the precipitate was washed with CH_2Cl_2 (30 cm^3) and the combined solutions were evaporated to dryness. The residue was extracted with hexanes and filtered. The solution was evaporated to dryness, yielding the crude product. Since ^1H and ^{13}C NMR spectra and CIMS indicated the presence of some 1,12-dichloro-dodeca-5,7-diyne (from oxidative dimerisation of 6–chloro–hex–1–yne), and this proved impossible to remove using chromatography, the crude product (2.236 g, 7.28 mmol) was dissolved in EtOAc (60 cm^3), treated with 10% Pd on charcoal (1.01 g) and stirred for 24 h under H_2 (8 bar) at room temperature. The solution was filtered, the solids were washed with EtOAc (3 × 50 cm^3) and the solvent was evaporated under reduced pressure. The product was purified by column chromatography (95:5 hexanes: EtOAc) to remove 1,12–dichlorododecane, and afford the product (1.44 g, 47 %). CI MS (NH_3): m/z: 332 $[M+NH_4]^+$, 314 $[M]^+$. ^1H NMR data ($CDCl_3$) δ = 1.43, 1.77 (q's, 16H in total, $-CH_2CH_2-$), 2.58 (t, 4H, ^3J 7.7 Hz, Ar-CH_2), 3.52 (t, 4H, ^3J 6.7 Hz, -CH_2Cl), 7.08 (s, 4H, C_6H_4).

8.2. Thioacetic acid *S*-{6-[4-(6-acetylsulfanyl-hexyl)-phenyl]-hexyl} ester, 1:

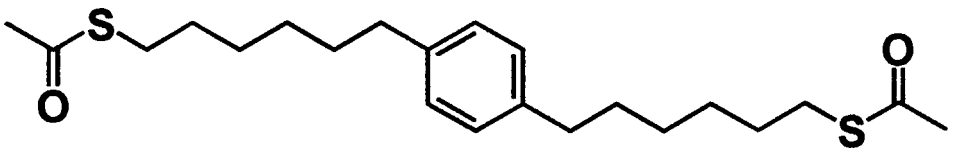

1,4-Bis-(6-chloro-hexyl)-benzene (1.38 g, 4.44 mmol) was treated with 20 eq. NaI (13.3 g) in refluxing acetone (60 cm^3) for 24 h. The solvent was removed in *vacuo* and the product was extracted into diethyl ether (100 cm^3), filtered from sodium salts and evaporated to dryness. Crude yield 2.00 g, 91 %. This was recrystallised from hexane (1.27 g, 58 %). A portion (1.05 g, 2.13 mmol) of the recrystallised di–iodide was added to a solution of KSAc (0.728 g, 6.39 mmol) in acetone (100 cm^3) and brought to reflux for 24 h, then allowed to cool to room temperature. The solution was filtered, the solvent was removed in *vacuo* and the crude product was recrystallised from hexane. Yield 0.661 g, 80 % (based on di–iodo compound). . Elemental analysis: found; C, 66.92; H, 8.72 %. $C_{22}H_{34}O_2S_2$ requires C, 66.96; H, 8.68 %. CI MS (NH_3): m/z: 412 $[M+NH_4]^+$, 395 $[M+H]^+$. ^1H NMR data ($CDCl_3$) δ = 1.39 (m, 8H, $-CH_2-$), 1.57 (m, 8H, $-CH_2-$), 2.32 (s, 6H, $-C(O)CH_3$), 2.56 (t, 4H, ^3J 7.7 Hz, $ArCH_2-$), 2.85 (t, 4H, ^3J 7.3 Hz, $-CH_2S$), 7.07 (s, 4H, C_6H_4). ^{13}C NMR data ($CDCl_3$) δ = 29.08, 29.20, 29.54, 29.84, 31.06, 31.77, 35.83, 128.65, 140.29, 196.46.

8.3. 1,4-Bis-(6-chloro-hex-1-ynyl)-2,3,5,6-tetrafluoro-benzene:

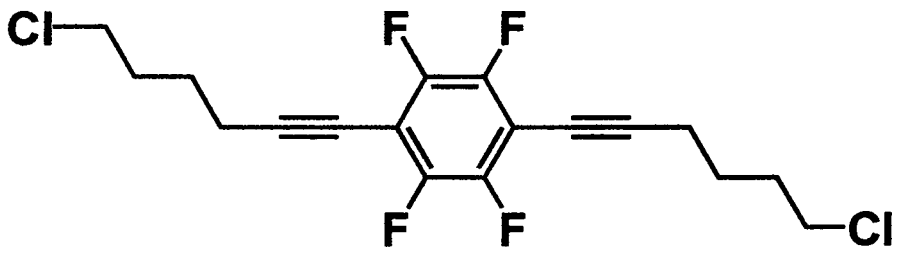

A mixture of 1,4–dibromo-2,3,5,6-tetrafluoro-benzene (3.00 g, 9.74 mmol), $[PdCl_2(MeCN)_2]$ (0.13 g, 5 mol %), PPh_3 (0.256 g, 10 mol %) and CuI (0.056 g, 3 mol %) in $^iPr_2NH$ (50 cm^3) was degassed for 30 min. by Ar bubbling. The 6–chloro–hex–1–yne (3.07 g, 26.3 mmol) was added, and the mixture was refluxed for 5 h under N_2. It was allowed to cool to room temperature, then filtered, the precipitate was washed with CH_2Cl_2 (30 cm^3) and the combined solutions were evaporated to dryness. The residue was extracted with hexanes and filtered. The solution was evaporated to one third volume and the precipitated product was filtered off. The mother liquor was evaporated to dryness, taken up in the minimum of hot hexane and cooled to –10 °C. The product was filtered off. Combined yield 1.39 g, 38 %. Elemental analysis: found; C, 57.12; H, 4.34 %. $C_{18}H_{16}F_4Cl_2$ requires C, 57.01; H, 4.25 %. CI MS (NH_3): m/z: 378 $[M]^+$. ^1H NMR ($CDCl_3$) δ = 1.81, 1.97 (m's, 8H, $-CH_2CH_2-$), 2.57 (t, 4H, ^3J 6.9 Hz, $C{\equiv}CCH_2$), 3.60 (t, 4H, ^3J 6.4 Hz, $-CH_2Cl$). ^{13}C NMR data ($CDCl_3$) δ =

19.6, 25.7, 31.8, 44.7, 67.2, 94.3; other resonances not resolved owing to ^{19}F-^{13}C coupling.

8.4. 1,4-Bis-(6-chloro-hexyl)-2,3,5,6-tetrafluoro-benzene:

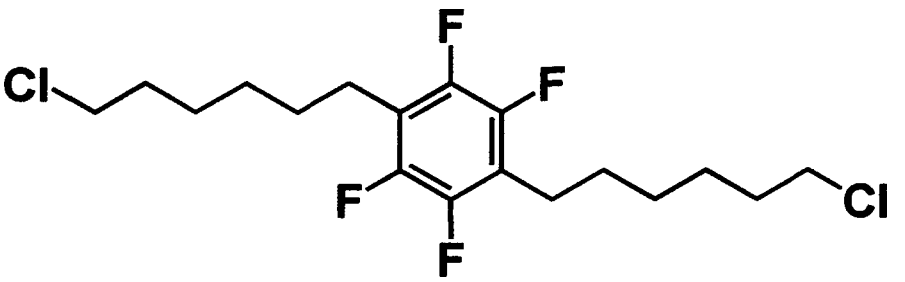

1,4-Bis-(6-chloro-hex-1-ynyl)-2,3,5,6-tetrafluoro-benzene (1.14 g, 3.01 mmol) was subjected to hydrogenation (60 cm^3 EtOAc, 0.52 g 10 % Pd/C, 8 bar H_2, 24 h, room temperature). The catalyst was filtered off and the solvent was removed in *vacuo*. The product was pure enough to use in the next step. Yield 1.06 g, 92 %. CI MS (NH_3): m/z: 404 $[M+NH_4]^+$, 386 $[M]^+$. ^1H NMR data ($CDCl_3$) δ = 1.38, 1.48 (m's, 8H, $-CH_2CH_2-$), 1.61 (m, 4H, $-CH_2-$), 1.78 (m, 4H, $-CH_2-$), 2.70 (t, 4H, ^3J 7.6 Hz, Ar-CH_2), 3.52 (t, 4H, ^3J 6.6 Hz, $-CH_2Cl$). ^{13}C NMR data ($CDCl_3$) δ =22.9, 26.9, 28.8, 29.5, 32.8, 45.3, 100.0; other resonances not resolved owing to ^{19}F-^{13}C coupling.

8.5. Thioacetic acid *S*-{6-[4-(6-acetylsulfanyl-hexyl)-2,3,5,6-tetrafluoro-phenyl]-hexyl} ester, 2:

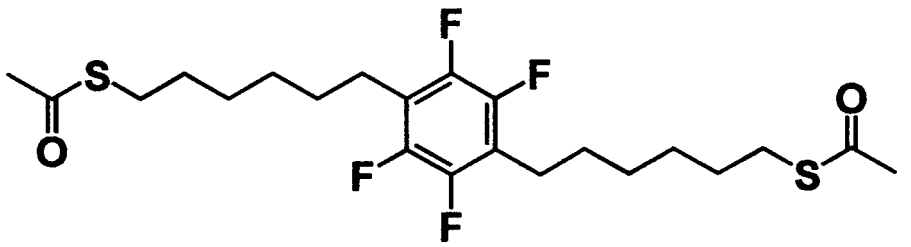

1,4-Bis-(6-chloro-hexyl)-2,3,5,6-tetrafluoro-benzene (0.95 g, 2.48 mmol)was treated with 20 eq. NaI (7.44 g) in refluxing acetone (60 cm^3) for 24 h. The solvent was removed in *vacuo* and the product was extracted into diethyl ether (2 × 100 cm^3), shaken with solid sodium thiosulfate, and evaporated to dryness. Crude yield 1.173 g, 84 %. It was added to a solution of KSAc (0.71 g, 6.2 mmol) in acetone (100 cm^3) and brought to reflux for 24 h, then allowed to cool to room temperature. The solution was filtered, the solvent was removed in *vacuo* and the crude product (0.911 g, 96 %) was recrystallised from hexane. Elemental analysis: found; C, 56.81; H, 6.53 %. $C_{22}H_{30}F_4O_2S_2$ requires C, 56.63; H, 6.48 %. CI MS (NH_3): m/z: 410 $[M]^+$. ^1H NMR data ($CDCl_3$) δ = 1.38 (m, 8H, $-CH_2-$), 1.57 (m, 8H, $-CH_2-$), 2.32 (s, 6H, $-C(O)CH_3$), 2.68 (t, ^3J 7.7 Hz, $ArCH_2-$), 2.86 (t, ^3J 7.2 Hz, $-CH_2S$). ^{13}C NMR data ($CDCl_3$) δ = 22.9, 28.8, 29.0, 29.4, 29.7, 31.0, 196.3; other resonances not resolved owing to ^{19}F-^{13}C coupling.

8.6. 1,4-Bis-(6-chloro-hex-1-ynyl)-2,5-dimethoxy-benzene:

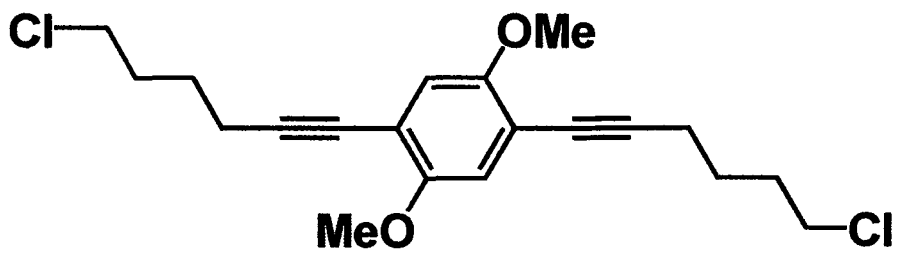

A mixture of 1,4–dibromo-2,5-dimethoxy-benzene (2.88 g, 9.75 mmol), $[PdCl_2(MeCN)_2]$ (0.13 g, 5 mol%), PPh_3 (0.256 g, 10 mol %) and CuI (0.056 g, 3 mol %) in $^iPr_2NH$ (40 cm^3) was degassed for 30 min. by Ar bubbling. The 6–chloro–hex–1–yne (3.07 g, 26.3 mmol) was added, and the mixture was refluxed for 24 h under N_2. It was allowed to cool to room temperature and then filtered, the precipitate was washed with CH_2Cl_2 (20 cm^3) and the combined solutions were evaporated to dryness. The residue was taken up in the minimum hot CH_2Cl_2:hexane (20:80) and cooled in the freezer (–20 °C). The product was filtered off. Yield 1.37 g, 39 %. Elemental analysis: found; C, 65.30; H, 6.62 %. $C_{20}H_{24}Cl_2O_2$ requires C, 65.40; H, 6.59 %. CI MS (NH_3): m/z: 384 $[M+NH_3]^+$, 367 $[M]^+$. ^1H NMR ($CDCl_3$) δ = 1.79, 1.99 (m's, 8H, –CH_2CH_2–), 2.53 (t, 4H, ^3J 6.9 Hz, C≡CCH_2), 3.61 (t, 4H, ^3J 6.6 Hz, -CH_2Cl), 3.82 (s, 6H, OMe), 6.85 (s, 2H, aromatic H). ^{13}C NMR data ($CDCl_3$) δ = 19.5, 26.3, 32.1, 44.9, 56.8, 95.3, 113.6, 116.2, 154.3.

8.7. Thioacetic acid *S*-{6-[4-(6-acetylsulfanyl-hexyl)-2,5-dimethoxy-phenyl]-hexyl} ester, 3:

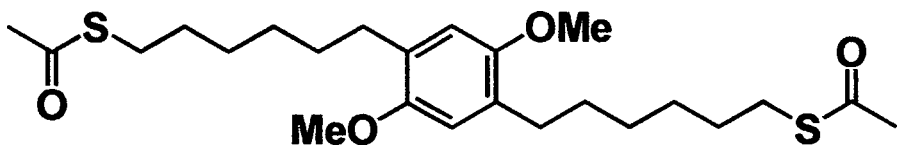

1,4-Bis-(6-chloro-hex-1-ynyl)-2,5-dimethoxy-benzene (0.721 g, 2.15 mmol) was subjected to hydrogenation (40 cm^3 EtOAc, 0.287 g 10 % Pd/C, 8 bar H_2, 24 h, room temperature). The catalyst was filtered off and the solvent was removed in *vacuo*. The product was purified by column chromatography (hexane), and used directly. Yield 0.553 g, 75 %. A 0.50 g portion (1.36 mmol) was dissolved in acetone (50 cm^3), and treated with a mixture of KSAc (0.47 g, 4.1 mmol) and catalytic NaI (0.02 g). The mixture was refluxed for 48 h, cooled to room temperature and evaporated to dryness. The residue was extracted with Et_2O (3 × 20 cm^3). The combined extracts were evaporated to dryness. Purification by chromatography (hexane) yielded the product (??? g, ??? %). Elemental analysis: found; C, 65.30; H, 9.42 %. $C_{24}H_{38}O_4S_2 \cdot 0.5$ hexane requires C, 65.15; H, 9.11 %. ES MS (MeOH, 10 V): m/z: found 477.2109. Calc for $[M+^{23}Na]^+$ 477.2109. ^1H NMR ($CDCl_3$) δ = 1.40, 1.58 (m's, 16H, –CH_2CH_2–), 2.31 (s, 6H, –C(O)CH_3), 2.55 (t, 4H, ^3J 7.7 Hz, -CH_2Ar), 2.86 (t, 4H, ^3J 7.3 Hz, -CH_2S), 3.77 (s, 6H, OMe), 6.63 (s, 2H, aromatic H). ^{13}C

NMR data ($CDCl_3$) δ = 29.1, 29.4, 29.6, 29.9, 30.4, 30.5, 31.0, 56.6, 113.5, 129.5, 151.7, 196.3.

8.8. 1,4-Bis-(6-chloro-hex-1-ynyl)-2,5-dimethyl-benzene:

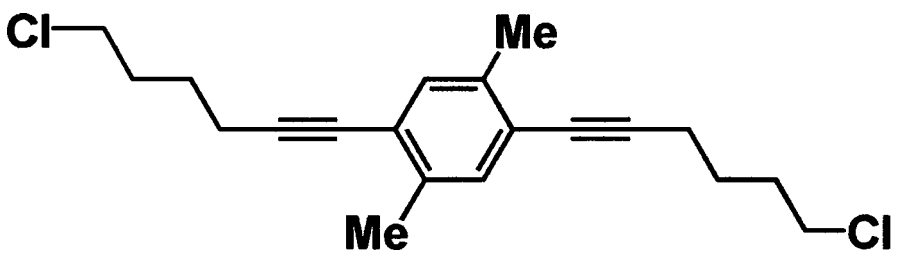

A mixture of 1,4–dibromo-2,5-dimethyl-benzene (2.57 g, 9.75 mmol), $[PdCl_2(MeCN)_2]$ (0.13 g, 5 mol%), PPh_3 (0.256 g, 10 mol %) and CuI (0.056 g, 3 mol %) in $^iPr_2NH$ (40 cm^3) was degassed for 30 min. by Ar bubbling. The 6–chloro–hex–1–yne (3.07 g, 26.3 mmol) was added, and the mixture was refluxed for 24 h under N_2. It was allowed to cool to room temperature and then filtered, the precipitate was washed with CH_2Cl_2 (20 cm^3) and the combined solutions were evaporated to dryness. The residue was taken up in hexane and purified by column chromatography (hexane). Cream solid. Yield 0.934 g, 29 %. Elemental analysis: found; C, 71.17; H, 7.15 %. $C_{20}H_{24}Cl_2$ requires C, 71.64; H, 7.21 %. CI MS (NH_3): m/z: 352 $[M+NH_3]^+$, 335 $[M]^+$. ^1H NMR ($CDCl_3$) δ = 1.76, 1.98 (m's, 8H, –CH_2CH_2–), 2.32 (s, 6H, ArMe), 2.50 (t, 4H, ^3J 7.0 Hz, C≡CCH_2), 3.60 (t,

4H, ^{3}J 6.5 Hz, -CH_2Cl), 7.17 (s, 2H, aromatic H). ^{13}C NMR data ($CDCl_3$) δ = 19.3, 20.35, 26.4, 32.0, 44.9, 80.5, 94.4, 123.3, 133.0, 137.3.

8.9. 1,4-Bis-(6-chloro-1-hexyl)-2,5-dimethyl-benzene:

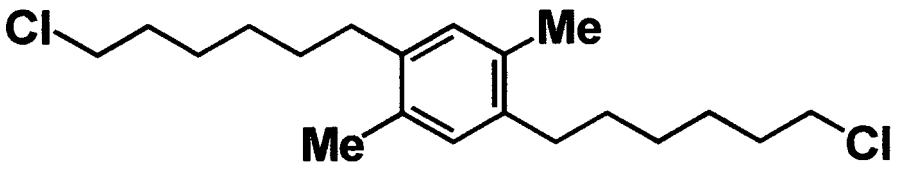

1,4-Bis-(6-chloro-hex-1-ynyl)-2,5-dimethyl-benzene (0.62 g, 1.85 mmol) was subjected to hydrogenation (40 cm^3 EtOAc, 0.24 g 10 % Pd/C, 8 bar H_2, 24 h, room temperature). The catalyst was filtered off and the solvent was removed in *vacuo*. The product was purified by column chromatography (hexane). Yield 0.52 g, 82 %. Elemental analysis: found; C, 69.33; H, 9.49 %. $C_{20}H_{32}Cl_2$ requires C, 69.96; H, 9.39 %. CI MS (NH_3): m/z: 360 $[M+NH_4]^+$, 342 $[M]^+$. ^{1}H NMR ($CDCl_3$) δ = 1.40, 1.44, 1.54 (m's, 12H, –CH_2CH_2CH_2–), 2.52 (t, 4H, ^{3}J 7.9 Hz, ArCH_2), 3.53 (t, 4H, ^{3}J 6.7 Hz, -CH_2Cl), 6.88 (s, 2H, aromatic H). ^{13}C NMR data ($CDCl_3$) δ = 19.1, 27.2, 29.4, 30.7, 33.0, 33.2, 45.5, 131.1, 133.4, 138.5.

8.10. Thioacetic acid *S*-{6-[4-(6-acetylsulfanyl-hexyl)-2,5–dimethyl-phenyl]-hexyl} ester:

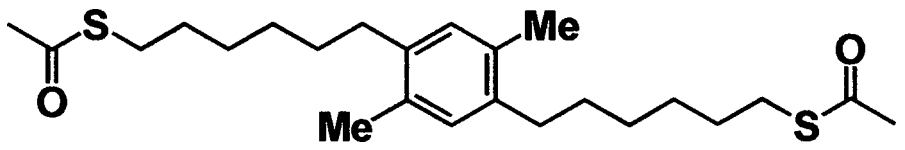

1,4-Bis-(6-chloro-1-hexyl)-2,5-dimethyl-benzene (0.50 g, 1.47 mmol) was dissolved in acetone (50 cm^3), and treated with a mixture of KSAc (0.50 g, 4.4 mmol) and catalytic NaI (0.02 g). The mixture was refluxed for 48 h, more KSAc (0.3 g) was added, and the mixture was refluxed for a further 16 h. It was then cooled to room temperature and evaporated to dryness. The residue was extracted with Et_2O (3 × 20 cm^3). The combined extracts were evaporated to dryness. Purification was by column chromatography (hexanes). Yield 0.405 g, 65 %. Elemental analysis: found; C, 67.80; H, 9.00 %. $C_{24}H_{38}O_2S_2$ requires C, 68.20; H, 9.06 %. CI MS (NH_3): m/z: 440 $[M+NH_4]^+$, 423 $[M]^+$. ^1H NMR ($CDCl_3$) δ = 1.41, 1.55 (m's, 16H, –CH_2CH_2–), 2.23 (s, 6H, $ArCH_3$), 2.32 (s, 6H, –$C(O)CH_3$), 2.50 (t, 4H, ^3J 7.8 Hz, -CH_2Ar), 2.87 (t, 4H, ^3J 7.3 Hz, -CH_2S), 6.87 (s, 2H, aromatic H). ^{13}C NMR data ($CDCl_3$) δ = 19.1, 29.1, 29.2, 29.6, 29.9, 30.7, 31.0, 131.0, 133.2, 133.4, 138.5, 196.3.

8.11. 2,5-Bis-(6-chloro-hex-1-ynyl)-thiophene:

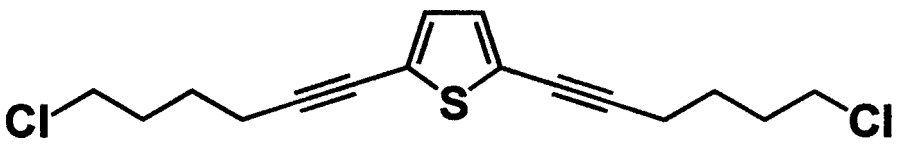

A mixture of 2,5–dibromothiophene (1.50 g, 6.20 mmol), $[PdCl_2(MeCN)_2]$ (0.08 g, 5 mol%), PPh_3 (0.16 g, 10 mol %) and CuI (0.035 g, 3 mol %) in $^{i}Pr_2NH$ (10 cm^3) was degassed for 20 min. by Ar bubbling. The 6–chloro–hex–1–yne (1.46 g, 12.5 mmol) was added, and the mixture was stirred for 24 h at room temperature. It was then filtered, the precipitate was washed with CH_2Cl_2 (5 cm^3) and the combined solutions were evaporated to dryness. The residue was extracted with hexanes and filtered. The solution was evaporated to dryness, yielding the crude product, which was purified by column chromatography (5 cm SiO_2, 100% hexanes). Yield 1.45 g, 75 %. Elemental analysis: found; C, 61.45; H, 5.84 %. $C_{16}H_{18}Cl_2S$ requires C, 61.34; H, 5.79 %. MS: m/z: 330 $[M+NH_3]^+$, 313 $[M]^+$. ^1H NMR ($CDCl_3$) δ = 1.76, 1.92 (m's, 8H), 2.47 (t, 4H, ^3J 6.9 Hz), 3.59 (t, 4H, ^3J 6.3 Hz), 6.93 (s, 2H). ^{13}C NMR data ($CDCl_3$) δ = 19.4, 26.1, 32.0, 44.8, 74.5, 94.3, 124.6, 131.2.

8.12. 2,5-Bis-(6-chloro-hexyl)-thiophene:

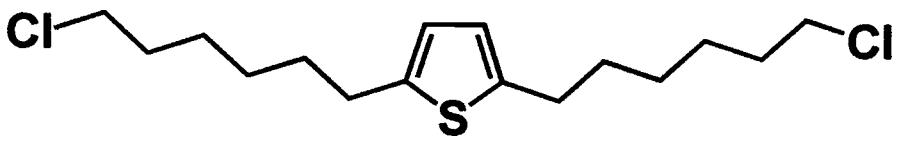

8.11 (0.45 g, 1.44 mmol) was subjected to hydrogenation (35 cm^3 EtOAc, 0.25 g 10 % Pd/C, 8 bar H_2, 5h, room temperature). The catalyst was filtered off and the solvent was removed in *vacuo*. The product was purified by column chromatography (hexanes/10% EtAc). Yield 0.40 g, 86 %. Elemental analysis: found; C, 60.19; H, 8.79 %. $C_{16}H_{26}Cl_2S_3$ requires C, 59.80; H, 8.15 %. MS: m/z: 338 $[M+NH_3]^+$, 321 $[M]^+$. ^1H NMR data ($CDCl_3$) δ = 1.25-1.55 (m, 8H), 1.66 (m, 4H), 1.76 (m, 4H), 2.75 (t, 4H, ^3J 7.4 Hz), 3.53 (t, 4H, ^3J 6.6 Hz), 6.56 (s, 2H). ^{13}C NMR data ($CDCl_3$) δ = 26.6, 28.3, 30.0, 31.5, 32.5, 45.0, 123.5, 143.0.

8.13. Thioacetic acid S-{6-[5-(6-acetylsulfanyl-hexyl)-thiophen-2-yl]-hexyl} ester (1):

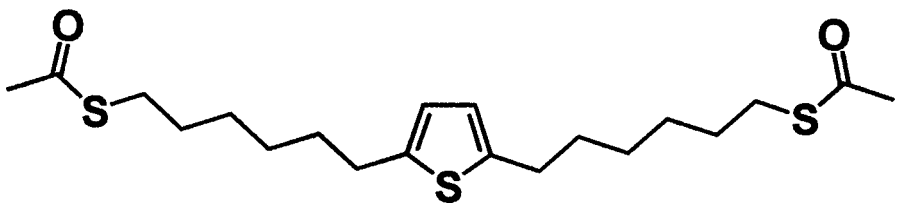

Compound **8.12** (0.40 g, 1.24 mmol) was treated with 10 eq. NaI in refluxing acetone for 15 h. The solvent was removed in *vacuo* and the product was extracted into hexanes, filtered from sodium salts and evaporated to dryness. It was then added to KSAc (0.314 g, 2.75 mmol) in acetone (40 cm^3) and refluxed for 16 h. The solution was allowed to cool to room temperature and the precipitated NaCl was then filtered off. The solvent was removed in *vacuo* and the product was extracted into Et_2O, filtered from sodium salts and evaporated to dryness. The crude product was purified by column chromatography (80:20 hexanes:CH_2Cl_2). Yield 0.274 g, 55 %. Elemental analysis: found; C, 64.03; H, 9.41 %. $C_{20}H_{32}O_2S_3$·hexane requires C, 64.14; H, 9.52 %. MS: m/z: 418 $[M+NH_3]^+$, 401 $[M]^+$, 325 $[M–SAc]^+$. Selected ^1H NMR data ($CDCl_3$) δ = 0.87 (t, hexane –CH_3) 2.32 (s, 6H, –C(O)CH_3), 2.73 (t, 4H, ^3J 7.4 Hz), 2.86 (t, 4H, ^3J 6.9 Hz), 6.54 (s, 2H). ^{13}C NMR data ($CDCl_3$) δ = 28.9, 29.5, 29.8, 30.4, 31.0, 31.9, 123.8, 143.4, 196.3.

8.14. 5,5'–dibromo–2,2'–bithiophene

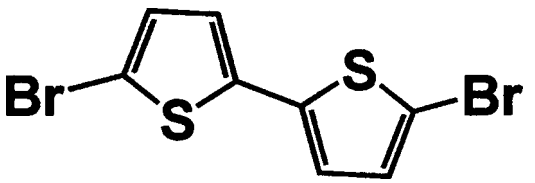

5,5'–dibromo–2,2'–bithiophene (2A) was prepared in 97 % yield by an adaptation of the method of Bäuerle *et al.*[1] Elemental analysis: found; C, 29.72; H, 1.20 %. $C_8H_4Br_4S_2$ requires C, 29.65; H, 1.24 %. MS (CI+, NH_3): m/z: 324 $[M]^+$. ^1H NMR ($CDCl_3$) δ = 6.85 (d, 2H, *J* 3.8), 6.96 (d, 2H). ^{13}C NMR data ($CDCl_3$) δ = 110.1, 122.8, 129.3, 136.4.

8.15. 5,5'–bis(6–chlorohex-1-ynyl)–2,2'–bithiophene:

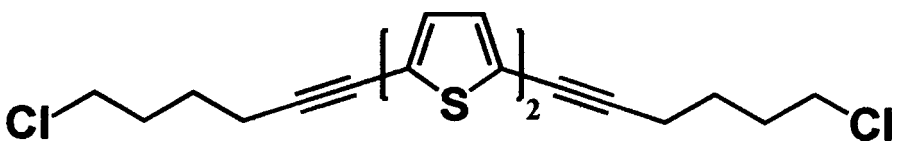

A mixture of **8.14** (1.89 g, 5.54 mmol), 6–chloro–hex–1–yne (1.74 g, 15 mmol), $[PdCl_2(MeCN)_2]$ (0.072 g, 0.278 mmol, 5 mol %), PPh_3 (0.145 g, 10 mol %) and CuI (0.032 g, 3 mol %) in $^iPr_2NH$ (50 cm^3) and CH_2Cl_2 (10 cm^3) was degassed for 20 min. by Ar bubbling. The mixture was heated to 80 °C under N_2 for 24 h and allowed to cool to room temperature. It was

filtered and the solids were washed with CH_2Cl_2 (20 cm^3). The combined filtrates were evaporated to dryness and the crude brown product was stirred with hexanes (20 cm^3). The hexane solution was decanted off, and evaporated to dryness. The residue was recrystallised from 30:70 CH_2Cl_2:hexanes (r.t. to –30 °C). The orange needles were filtered off and dried in *vacuo*. Yield 1.26 g, 57 %. Elemental analysis: found; C, 61.17; H, 5.17 %. $C_{20}H_{20}Cl_2S_2$ requires C, 60.75; H, 5.10 %. MS (CI, NH_3): m/z: 395 $[M]^+$. ^1H NMR ($CDCl_3$) δ = 1.77, 1.95 (m's, 8H), 2.49 (t, 4H, ^3J 6.9), 3.59 (t, 4H, ^3J 6.5), 6.98, 7.00 (AB, 4H, J_{AB} 3.8). ^{13}C NMR data ($CDCl_3$) δ = 19.5, 26.1, 32.0, 44.8, 74.7, 95.2, 123.5, 123.9, 132.4, 137.4.

8.16. 5,5'-Bis-(6-chloro-hexyl)- 2,2'–bithiophene:

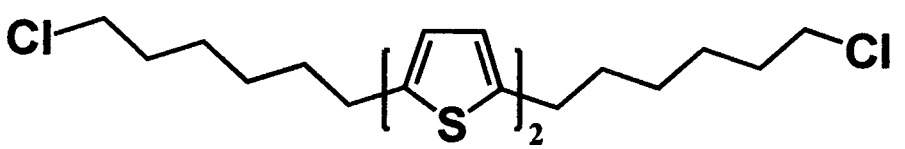

8.15 (0.834 g, 2.11 mmol) was subjected to hydrogenation (50 cm^3 EtOAc, 0.29 g 10 % Pd/C, 8 bar H_2, 15 h, room temperature). The catalyst was filtered off and the solvent was removed in *vacuo*. The product was purified by column chromatography (95:5 hexanes:ethyl acetate). Yield 0.63 g, 74 %. Elemental analysis: found; C, 59.76; H, 6.97 %. $C_{20}H_{28}Cl_2S_2$ requires C, 59.54; H, 6.99 %. MS (CI, NH_3): m/z: 403 $[M]^+$. ^1H NMR

($CDCl_3$) δ = 1.44, 1.75 (m's, 16H), 2.79 (t, 4H, ^3J 7.7), 3.54 (t, 4H, ^3J 6.6), 6.65, 6.89 (d's, 4H, J 3.6). ^{13}C NMR data ($CDCl_3$) δ = 27.0, 28.6, 30.4, 31.7, 32.9, 45.4, 123.1, 125.1, 135.8, 144.7.

8.17. Thioacetic acid S-{6-[5'-(6-acetylsulfanyl-hexyl)-[2,2']bithiophenyl-5-yl]-hexyl} ester:

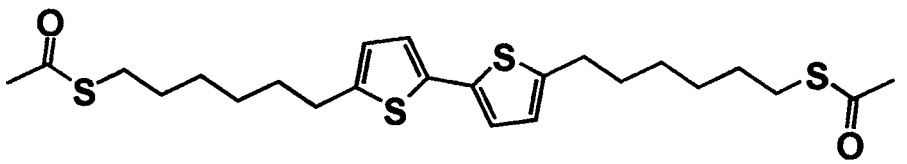

To 5,5'-bis-(6-chloro-hexyl)- 2,2'–bithiophene (8.16) (0.118 g, 0.293 mmol) in acetone (50 cm^3) was added NaI (0.67 g, 4.47 mmol). The solution was refluxed for 24 h and evaporated in *vacuo*. The product was extracted into CH_2Cl_2 and the solution was evaporated to dryness. The residue was recrystallised from hot MeOH as a yellow solid (yield 0.083 g, 46 %). The 5,5'-bis-(6-iodo-hexyl)- 2,2'–bithiophene (75.2 mg, 0.129 mmol) was then treated with KSAc (33 mg, 0.284 mmol) in acetone (35 cm^3). The mixture was refluxed for 8 h, the solvent was removed in *vacuo* and the residue was stirred with CH_2Cl_2 (20 cm^3) for 20 mins and filtered. The product was purified by column chromatography (95:5 hexanes:ethyl acetate). Yield 36.5 mg, 59 %. Elemental analysis: found; C, 63.99; H, 9.01 %. $C_{24}H_{34}O_2S_4 \cdot$hexane requires C, 63.33; H, 8.50 %. MS (CI, NH_3):

m/z: 500 $[M+NH_3]^+$, 483 $[M]^+$. Selected ^1H NMR ($CDCl_3$) δ = 0.85 (t, 6H, hexane $-CH_3$), 1.37, 1.65 (m's, 16H), 2.33 (s, 6H, $-C(O)CH_3$), 2.77 (t, 4H, ^3J 7.6), 2.87 (t, 4H, ^3J 7.2), 6.64, 6.89 (d's, 4H, J 3.6). ^{13}C NMR data ($CDCl_3$) δ = 27.0, 28.6, 30.4, 31.7, 32.9, 45.4, 123.1, 125.1, 135.8, 144.7.

8.18. 5,5''–dibromo–2,2':5',2''–terthiophene:

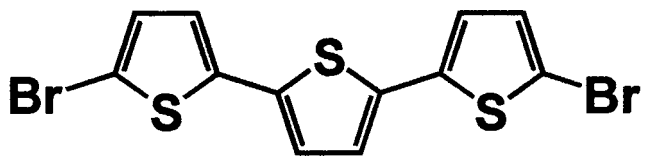

5,5''–dibromo–2,2':5',2''–terthiophene was prepared by *N*-bromosuccinimide bromination of 2,2'-bithiophene in dmf by the method of Bäuerle *et al.*[1] Yield 74 %. Elemental analysis: found; C, 35.89; H, 1.45 %. $C_{12}H_6Br_2S_3$ requires C, 35.48; H, 1.49 %. MS (CI, NH_3): m/z: 407 $[M]^+$. ^1H NMR ($CDCl_3$) δ = 6.90, 6.97 (AB, 4H, J_{AB} 3.8), 7.00 (s, 2H). ^{13}C NMR data ($CDCl_3$) δ = 111.7, 124.4, 125.0, 131.1, 136.0, 138.7.

8.19. 5,5''–bis(6–chlorohex-1-ynyl)–2,2':5',2''–terthiophene:

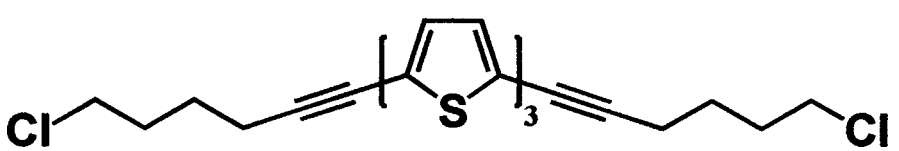

A mixture of **8.18** (1.50 g, 3.69 mmol), 6–chloro–hex–1–yne (1.21 cm^3, 2.7 eq.) $[PdCl_2(MeCN)_2]$ (0.048 g, 5 mol %), PPh_3 (0.097 g, 10 mol %) and CuI (0.021 g, 3 mol %) in $^iPr_2NH$ (50 cm^3) was degassed for 20 min. by Ar bubbling. The mixture was heated to 80 °C under N_2 for 24 h and allowed to cool to room temperature. It was filtered and the solids were triturated with hexanes (20 cm^3). The orange solid was filtered, washed with water and dried in *vacuo*. It was judged pure enough for use in the next stage. Yield 1.12 g, 64 %. Elemental analysis: found; C, 60.03; H, 4.60 %. $C_{24}H_{22}Cl_2S_3$ requires C, 60.36; H, 4.64 %. MS (CI, NH_3): m/z: 477 $[M]^+$. ^1H NMR ($CDCl_3$) δ = 1.78, 1.94 (m's, 8H), 2.50 (t, 4H, ^3J 7.0), 3.60 (t, 4H, ^3J 6.5), 6.985, 7.009 (AB, 4H, J_{AB} 3.8), 7.03 (s, 2H). ^{13}C NMR data ($CDCl_3$) δ = 19.1, 25.7, 31.7, 44.5, 74.3, 94.9, 123.0, 123.4, 124.6, 132.0, 136.0, 137.2.

8.20. 5,5''-Bis-(6-chloro-hexyl)- 2,2':5',2''–terthiophene:

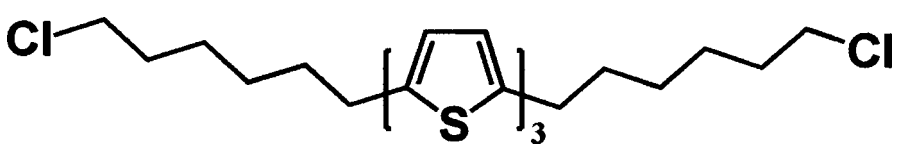

8.19 (0.630 g, 1.32 mmol) was subjected to hydrogenation (50 cm^3 EtOAc, 0.18 g 10 % Pd/C, 8 bar H_2, 15 h, room temperature). The catalyst was filtered off and the solvent was removed in *vacuo*. The product was

purified by column chromatography (95:5 hexanes:ethyl acetate). Yield 0.43 g, 67 %. Elemental analysis: found; C, 59.66; H, 6.10 %. $C_{24}H_{30}Cl_2S_3$ requires C, 59.36; H, 6.23 %. MS (CI, NH_3): m/z: 485 $[M]^+$. ^1H NMR ($CDCl_3$) δ = 1.37–1.52 (m's, 8H), 1.70 and 1.79 (m's, 8H), 2.80 (t, 4H, *J* 7.6), 3.53 (t, 4H, ^3J 6.7), 6.67 (d, 2H, *J* 3.4), 6.96 (d, 2H), 6.97 (s, 2H).

8.21. Thioacetic acid S-{6-[5''-(6-acetylsulfanyl-hexyl)-[2,2';5',2'']terthiophen-5-yl]-hexyl} ester:

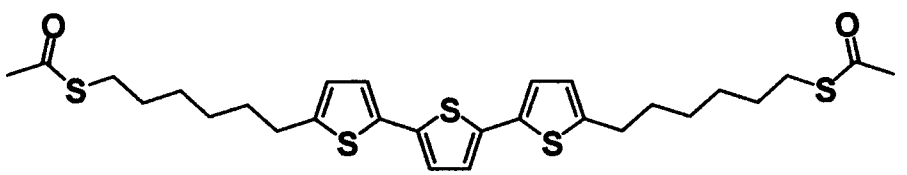

To **8.20** (0.363 g, 0.767 mmol) in acetone (50 cm^3) was added NaI (0.012 g, 10 mol %) and KSAc (0.263 g, 2.3 mmol). The mixture was refluxed for 48 h then evaporated to dryness. The product was extracted into CH_2Cl_2 (30 cm^3), filtered and evaporated to dryness. The residue was recrystallised from 30:70 CH_2Cl_2:hexanes. Yield (1st crop) 0.12 g. MS (CI, NH_3): m/z: 582 $[M+NH_3]^+$, 565 $[M]^+$. ^1H NMR ($CDCl_3$) δ = 1.38, 1.62 (m's, 16H), 2.32 (s, 6H), 2.78 (t, 4H, ^3J 7.4), 2.87 (t, 4H, ^3J 6.5), 6.66, 6.95 (d's, 4H, J_{AB} 3.5), 6.96 (s, 2H). ^{13}C NMR data ($CDCl_3$) δ = 28.87, 28.89, 29.5, 29.8, 30.4, 31.0, 31.7, 123.6, 123.9, 125.3, 135.1, 136.5, 145.4, 196.3.

8.22. 2,5-Bis-(6-chloro-hex-1-ynyl)-3,4-ethylenedioxythiophene:

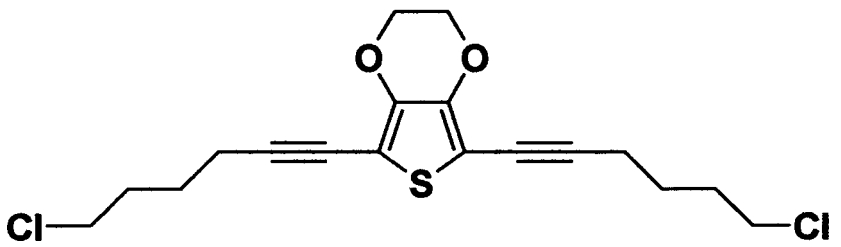

A mixture of 2,5–dibromo-3,4-ethylenedioxythiophene (1.39 g, 4.63 mmol), $[PdCl_2(MeCN)_2]$ (0.132 g, 5 mol%), PPh_3 (0.267 g, 10 mol %) and CuI (0.058 g, 3 mol %) in $^iPr_2NH$ (40 cm^3) was degassed for 20 min. by Ar bubbling. The 6–chloro–hex–1–yne (1.19 g, 10.2 mmol) was added, and the mixture was stirred for 24 h at 60^0C. It was then filtered, the precipitate was washed with CH_2Cl_2 (20 cm^3) and the combined solutions were evaporated to dryness. The residue was extracted with hexanes and filtered. The solution was evaporated to dryness, yielding the crude product, which was purified by column chromatography (5 cm SiO_2, 95% hexane, 5% ethyl acetate). Yield 0.6 g, 35.3 %. Elemental analysis: found; C, 58.23; H, 5.39 %. $C_{18}H_{20}O_2Cl_2S$ requires C, 58.22; H, 5.43 %. MS: m/z: 373 $[M]^+$. ^1H NMR ($CDCl_3$) δ = 1.75, 1.92 (m's, 8H), 2.50 (t, 4H, ^3J 7.0 Hz), 3.58 (t, 4H, ^3J 6.5 Hz), 4.24 (s, 4H). ^{13}C NMR data ($CDCl_3$) δ = 19.7, 26.2, 32.0, 44.9, 65.2, 71.8, 97.1, 99.3, 143.0.

8.23. 2,5-Bis-(6-chloro-hexyl)-3,4-ethylenedioxythiophene

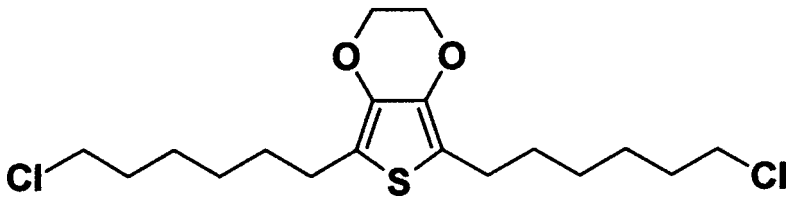

2,5-Bis-(6-chloro-hexyl)-3,4-ethylenedioxythiophene (0.396 g, 1.06 mmol) was subjected to hydrogenation (30 cm^3 EtOAc, 0.15 g 10 % Pd/C, 8 bar H_2, 15h, room temperature). The catalyst was filtered off and the solvent was removed in *vacuo*. The product was purified by column chromatography (hexanes/10% EtAc). Yield 0.372 g, 91 %. Elemental analysis: found; C, 57.43; H, 7.65 %. $C_{18}H_{28}O_2Cl_2S_3$ requires C, 56.99; H, 7.44 %. ^1H NMR data ($CDCl_3$) δ = 1.38-1.45 (m, 8H), 1.58 (m, 4H), 1.76 (m, 4H), 2.59 (t, 4H, ^3J 7.5 Hz), 3.53 (t, 4H, ^3J 6.8 Hz), 4.14 (s, 4H). ^{13}C NMR data ($CDCl_3$) δ = 25.9, 27.0, 28.7, 30.7, 33.0, 45.4, 113.8, 137.5.

8.24. Thioacetic acid S-{6-[5-(6-acetylsulfanyl-hexyl)-3,4-ethylenedioxythiophen-2-yl]-hexyl} ester:

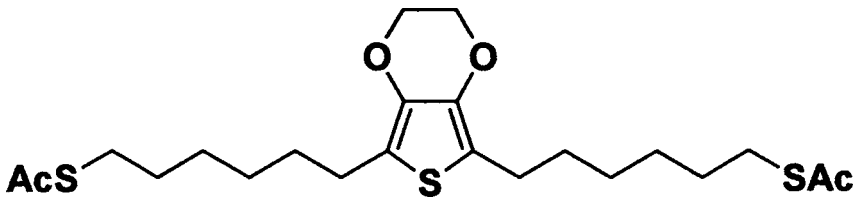

2,5-Bis-(6-chloro-hexyl)-3,4-ethylenedioxythiophene (0.27 g, 0.72 mmol) was treated with 20 eq. NaI in refluxing acetone (30 cm^3) for 24 h. The solvent was removed in *vacuo* and the product was extracted into hexanes, filtered from sodium salts and evaporated to dryness. It was then added to KSAc (0.246 g, 2.15 mmol, 3 eq) in acetone (35 cm^3) and refluxed for 24 h. The solution was allowed to cool to room temperature and the precipitated NaCl was then filtered off. The solvent was removed in *vacuo* and the product was extracted into Et_2O, filtered from sodium salts and evaporated to dryness. The crude product was purified by column chromatography (80:20 hexanes:CH_2Cl_2). Yield 0.11 g, 32 %. Elemental analysis: found; C, 58.03; H, 7.56 %. $C_{22}H_{33}O_4S_3$ requires C, 57.61; H, 7.47 %. MS: m/z: 481 $[M+Na]^+$, 459 $[M+H]^+$. ^1H NMR data ($CDCl_3$) δ = 1.34-1.38 (m, 8H), 1.58 (m, 8H), 2.57 (t, 4H, ^3J 7.0 Hz), 2.32 (s, 6H) 2.86 (t, 4H, ^3J 6.8 Hz), 4.15 (s, 4H). ^{13}C NMR data ($CDCl_3$) δ = 25.9, 28.9, 29.5, 29.8, 31.0, 65.1, 113.8, 137.5, 196.3.

8.25. Bis(pyrrolo)-TTF 1:

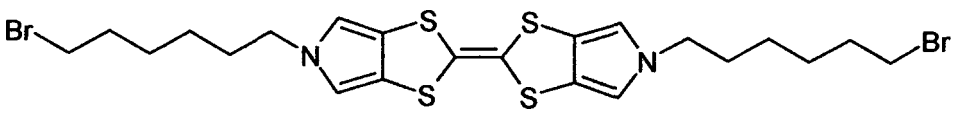

Both PTTF compounds were synthesis and characterised by Sune Nygaard, University of Southern Denmark, Campusvej 55, DK-5230 Odense M, Denmark.

A solution of bispyrrolotetrathiafulvalene **1** (0.50 g, 1.77 mmol)1 and 1,6-dibromohexane (1.83 g, 7.5 mmol) in anhydrous DMF (25 mL) was cooled to 273 K and purged with N_2 for 15 min. NaH 55% in mineral oil (0.35 g, 8.0 mmol) was added in one portion which resulted in a color change from yellow to brown. The reaction mixture was stirred for 2.5 hours before the reaction was quenched by the addition of CH_2Cl_2 (100 mL). The combined organic phase was washed with H_2O (2 × 100 mL), dried ($MgSO_4$) and evaporated to dryness. The resulting black oil was subjected to column chromatography (SiO_2, CH_2Cl_2:pet.ether v/v 1:1) which afforded pure 2 as a yellow solid (0.41 g, 38 %): mp 152_154 °C; ^{1}H NMR ($CDCl_3$, 300 MHz) _ 1.26–1.48 (m, 8H), 1.70–1.87 (m, 8H), 3.87 (t, 4H), 3.81 (bs, 4H), 6.43 (s, 4H); ^{13}C NMR ($CDCl_3$, 75 MHz) _ 37.7, 68.0, 69.0, 69.3, 69.9, 70.65, 70.71, 115.5, 153.1. MS (ESI) *m/z* 608

([M]$^+$, 80), 528 (100); Anal. Calcd. for $C_{22}H_{28}Br_2N_2S_4$: C, 43.42; H, 4.64; N, 4.60; S, 21.08. Found: C, 43.55; H, 4.78; N, 4.31; S, 19.92.

8.26. Bis(pyrrolo)-TTF 2:

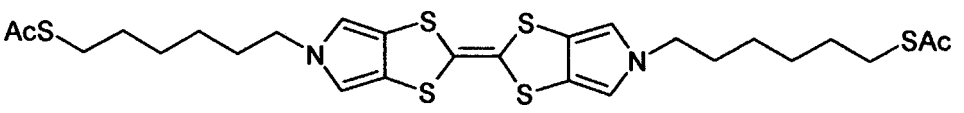

To a clear yellow solution of **2** (0.40 g, 0.66 mmol) in anhydrous THF (25 mL) was added $KSC(O)CH_3$ (0.37 g, 3.3 mmol) in one portion. The reaction mixture was refluxed for 3 hours. The reaction mixture was cooled to room temperature and the solvent was removed, whereafter the yellow residue was redissolved in CH_2Cl_2. The organic phase was washed with H_2O (2 × 100 mL), dried ($MgSO_4$) and evaporated to dryness. The resulting yellow solid was subjected to column chromatography (SiO_2, CH_2Cl_2) which afforded the pure product as a yellow solid (0.33 g, 83 %): mp 139_140 °C; ^{1}H NMR ($CDCl_3$, 200 MHz) _ 1.26–1.36 (m, 8H), 1.50–1.56 (m, 4H), 1.66–1.72 (m, 4H), 2.30 (s, 6H), 2.82 (t, J = 5 Hz, 4H), 3.8 (bs, 4H), 6.40 (s, 4H). ^{13}C NMR ($CDCl_3$, 75 MHz) _ 26.1, 28.2, 29.0, 29.3, 30.6, 31.3, 50.3, 112.4, 118.7, 195.9. MS (ESI) *m/z* 598 ([M]$^+$, 100), 522 (60). Anal. Calcd. for $C_{26}H_{34}N_2O_2S_6$: C, 52.14; H, 5.72; N, 4.68; S, 32.12. Found: C, 52.19; H, 5.89; N, 4.65; S, 31.99.

Chapter 9

Overall conclusions

Overall conclusions

The major focus of this thesis was to investigate how it is possible to link the atomic structure of molecular wires to their conductance properties. By measuring molecules in groups we have attempted to uncover the underlying mechanism of electron transfer across the molecular wires in each chapter. By making small changes to the structure of molecular wires it is possible to alter their conduction properties quite significantly. This was demonstrated in chapter one where pyrrolo-TTF and viologen based molecular wires were compared. It was found that if the wire has a significant amount of conformational (in this case rotational) freedom about inter-ring bonds then the type of switching behaviour seen at the redox transition is notably different than that for a more rigid wire. In particular the more rigid PTTF displayed a peak in the conductance-overpotential relation close to the formal redox potential However, the conformational more free viologen displayed a broad increase about the redox transition, with no peak observable. Both observations fit into the 'two step' model of electron transfer, which involves residence of the electron/hole on the centre group during transfer. In fact, if a single step mechanism was operational then the difference in behaviour would be much harder to explain.

The work carried out on the benzene containing molecular wires showed that the conductance could be finely tuned by altering the substituent groups attached to the central ring. Interestingly, however, when the conductance of 6Ph6 was measured as a function of the electrochemical 'gate' potential, no fine tuning of the conductance was seen. This leads to the conclusion that the amount of electron density on the benzene ring is the most important factor for hole transfer than the relative position of the molecular level compared to the electrode Fermi level.

The effect of the extent of conjugation across a series of oligothiophene molecular wires was explored in chapter three (oligomers contained between one and five thiophene rings). It was found however, that the increase in the length of the wire, associated with the increase in conjugation, was the dominant factor in determining the conductivity. Though the HOMO-LUMO gap was lower for the longer oligomers, the thiophene units remained 'off-resonant' with respect to the gold electrodes meaning that the conductivity dropped with increasing number of thiophene rings. However, it was discovered that in the presence of water the length dependency disappeared, and the conductance of even the quinquethiophene wire was larger than the monothiophene wire. DFT modelling (in collaboration with Lancaster University) revealed that water, by weakly interacting with the dipole moment of oligothiophenes, shifted the transport resonances (HOMOs or LUMOs) of the central thiophene

units closer to the gold Fermi level. The effect becomes more pronounced the longer the oligomer, hence removing the length dependency across the series. This work has implications for the way in which single molecule conductivity measurements will be performed in the future, emphasizing that solvent/environmental effects must be taken into account. Also it may also provide a new paradigm for the construction of single molecule sensors.

Conductivity measurement on a hexanuclear platinum cluster (which was synthesised in Pisa, Italy) demonstrated that molecular wires containing significant numbers of metal atoms could be successfully measured using the I(s) technique. Their stability on gold(111) was checked using XPS and PMIRRAS. The conductivity of 4{Pt_6}4 was comparable to highly conjugated wires of similar length. This is noteworthy as the cluster wire contains eight fully saturated methylene groups in its backbone. Without the alkyl groups the conductance was considerably higher (by a factor 20) than the equivalent length alkanedithiol, demonstrating the lower barrier of the {Pt_6} group.

The use of metal containing wires in nano-circuits has a promising future. We would like to make larger cluster compounds with more metallic character with the view of seeing conductances approaching the quantum conductance, G_0. This achievement probably isn't possible with metal string compounds as they involve metal atoms in certain oxidation states,

which removes the metallic character and makes the bonding more molecular.

In the final section on molecular wire measurements we studied the simple molecule octanedithiol under various conditions of the I(s) experiment. One of the clear outcomes of the study was to find multiple conduction groups, which is a feature also seen for other molecules in this thesis (especially the benzene containing wires). The predominant average value was 3.7 nS under a pure argon atmosphere. However, a larger group was visible at c.a. 17 nS in both I(s) and I(t) measurements. The best theory into the cause of the two groups is different bonding modes between the thiol groups and the gold surface/tip. We are unable to say why these two values in particular predominate. Theoretically it is possible to have many thiol-gold interactions, especially when in STM experiments the tip shape is hardly known and likely to be far from 'ideal'.

Exposure of the sample to ethanol caused the average conductivity to drop by a factor six to seven. The reason for this is not fully understood, however, evidence for weakening with the sulphur-gold bond in the presence of hydrogen-bonding compounds was discussed and the evidence for the interaction between water and thiophene was presented in chapter 5. This chapter highlights the problem which faces the field of single molecule conductivity – how to control the atomistics of molecule-electrode contacts.

From this thesis we can also conclude some further remarks. Firstly, the I(s) technique is a very reliable way to measure single molecule conductance. In particular we have seen that this technique strongly favours single molecule events. This is probably a reflection of the way in which the junctions must form, i.e. by molecules spontaneously attaching from one electrode to both electrodes. This is unlike the breakjunction method which forces many molecules to attach. We note that our histograms generally show a width of about 25% the peak position, whereas measurements with breakjunctions of the cantilever type can give peaks which span a whole order of magnitude. This reflects the number of possible ways in which junctions can form under such conditions, with the I(s) technique favouring a much better defined type of junction.

Secondly, most organic molecules are not very good conductors! We have shown in the chapter 3 that even the most conjugated wires have conductance channels in which there is less than a tenth of a percent probability for an electron to tunnel through. When we studied 6PTTF6 we aligned the molecular HOMO with the gold Fermi level and still only saw a conductance of 3.3×10^{-5} G_0. For long molecules the problem may be the result of the electron hopping across the molecule, forcing it to energetically relax after each hop. In the future, we believe that shorter molecules, coupled by metallic clusters or nanoparticles, may be the best way to engineer nano-circuits.

As a final point of consideration, the understanding gained of electron transfer at the fundamental level of single molecules will enable a better understanding of natural processes involving electron transfer. The most significant electron transfer process in nature is photosynthesis; the process which traps solar energy in the leaves of plants, converting water and carbon dioxide into carbohydrates and oxygen. Photosynthesis involves a highly complex sequence of electron transfer steps, particularly between Photosystem II and Photosystem I (the two light harvesting regions containing chlorophyll *a*) and subsequently away from these reaction centres into other parts of the cell membrane. Photosynthesis is a highly controlled redox reaction, and in particular results in the oxidation of water (to oxygen). Splitting water into H_2 and O_2 is, however, a very desirable reaction for the future viability of hydrogen fuel cells. The problem at the moment is generating enough hydrogen without resorting to burning fossil fuels. The knowledge acquired now in single molecule electron transfer may help the construction of devices which operate using the same principles as photosynthesis, but tuned to the production of hydrogen from solar radiation. Already, ruthenium complexes are being investigated as catalysts for this process. However, as the process is carried out in solution, success has been low because of the inability to stop back-reactions inherent in solution based chemistry. In plants, the electrons are transferred rapidly away from the reaction centres, to prevent any back-reactions, in a

process which involves electron transfer across many organic molecules. The challenge for chemists now is to use our knowledge of electron transfer in organic molecules to create devices which mimic the chain of electron transfer steps which plants use so well in photosynthesis. The development of this technology could provide the much needed counterpart to the hydrogen fuel cell, making its use completely sustainable and non-polluting.

Appendix

Appendix

Control measurements for the I(t) technique

We performed control experiments for the I(t) technique in the absence of dithiol molecules. The substrate was prepared in the usual manner by flame annealing several times in a butane flame for 20 second periods. Initially measurements were conducted in ambient air. Whilst monitoring the current as a function of time over periods between 0.2 and one second distinct jumps in the current could be readily observed. The appeared identical to those attributed to the spontaneous formation of metal|molecule|metal bridges in the presence of dithiol compounds. Examples are shown below in figure App. 1:

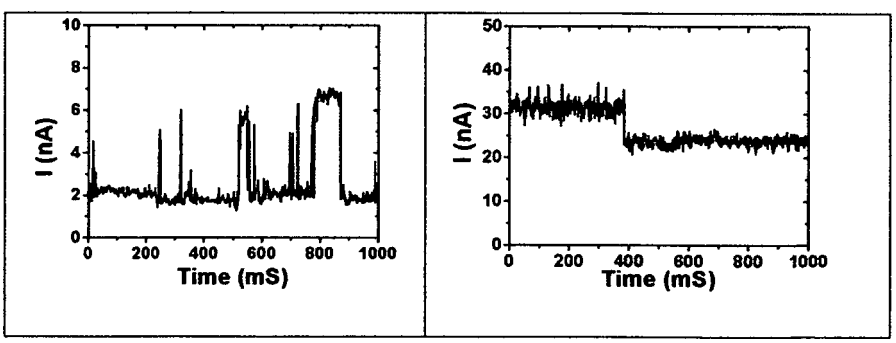

Figure App. 1. Examples of 'I(t) jumps' observed on an unmodified surface.

The size of the jumps depends upon the setpoint current, I_0, and therefore the distance between tip and surface. This is demonstrated in figure App. 02 which plots the size of jump against I_1 – the level of the current prior to the jump.

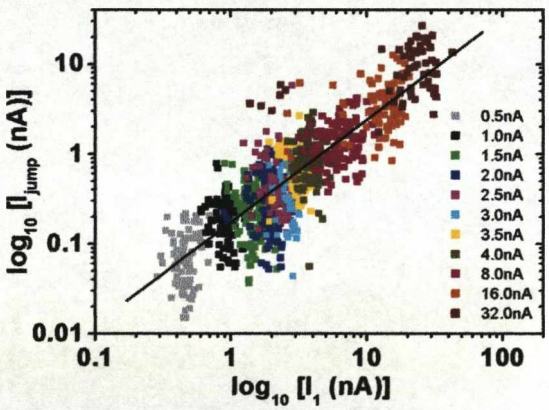

Figure App. 2. I(t) jumps as a function of the setpoint current. U_{bias} = 0.2 V.

The jumps have an approximately logarithmic relation to the setpoint current. When the same measurements were performed under argon atmosphere (after purging the closed cell for 12 h) current jumps were still observable, however, at a reduced frequency. Finally measurements were carried out on a SAM modified gold surface (using pentanethiol to form a reasonable coverage) under Ar atmosphere. Very few current jumps could be seen under these conditions. This lead us to believe that the unexplained current jumps could either be caused by organic contamination on the surface (which could come from the ambient environment, but not allowed

to contaminate a passivated surface) or by diffusion of gold atoms on the surface. Essentially any species which jumps into or out of the tunnelling gap could cause a jump in the current by facilitating tunnelling.

Telegraphic current switching has also been reported by other groups on 'clean' surfaces. In one of the cases the switching was attributed to water, acting as a scatterer, jumping in and out of the electric field between tip and surface. In the second case current switching was seen on plasma cleaned Si (110). Indeed telegraphic current switching has been seen over single molecules embedded in an insulating matrix. This, however, was attributed to fluctuations at the metal-molecule interface.

At this stage we cannot give any indication about the probability of observing the unexplained current jumps over true molecular jumps. Certainly it would seem, however, that in the presence of dithiol compounds it is possible to observe single molecules spontaneously bridging the tip-surface gap, which was evidenced in chapters four and seven. In both the chapters the I(t) data was supported by I(s) measurements.

Further work shall be needed in order to determine the ultimate cause of the jumps. However, we would recommend based on these results that I(t) measurements on molecular wires should be carried out under inert conditions with as clean a surface as possible.

Chemical control of double barrier tunnelling in α,ω-dithiaalkane molecular wires†

Edmund Leary, Simon J. Higgins,* Harm van Zalinge, Wolfgang Haiss and Richard J. Nichols

Received (in Cambridge, UK) 26th June 2007, Accepted 7th August 2007
First published as an Advance Article on the web 13th August 2007
DOI: 10.1039/b709576g

Single molecule conductance measurements on 1,4-bis-(6-thiahexyl)-benzene derivatives reveal (i) that benzene rings serve as an effective indentation in the tunnelling barrier, and (ii) that more electron-rich benzene rings give higher conductances, consistent with hole conduction (*i.e. via* the benzene HOMO).

The advent of reliable techniques for measuring the electrical properties of single molecules bridging two metallic contacts has led to an explosion of interest in this field.[1,2] There is still a lack of understanding of basic structure–property relationships in molecular electronics. Attempts to address this are often complicated by the fact that more than one potentially significant parameter (*e.g.* molecular length, conformation, contact geometry, steric and electronic effect of substituents) is varied simultaneously.[3–5] A common approach in molecular electronics has been to search for organic molecular devices capable of basic electrical functions. Molecules designed to act as molecular wires,[6,7] switches[8–10] and diodes[11] have recently been examined theoretically and/or experimentally, and devices have been produced which show rectification and negative differential resistance (NDR) behaviour. This points to the possibility of generating organic devices that mimic inorganic semiconductor junctions, although technological deployment seems some way off.

An architecture that is expected to be important in future generations of devices is the double tunnelling barrier junction.[12] These have been introduced recently into field effect transistors,[13] diodes[14] and bipolar transistors.[15] In these inorganic devices, metalorganic vapour phase epitaxy is used to assemble a 'well' or barrier indentation, sandwiched between the two tunnelling barriers.

We recently determined the single molecule conductance of the molecule 6V6 (Fig. 1).[16,17] When contacted to gold electrodes *via* the thiol groups, this can be regarded as the single molecule equivalent of a double tunnelling barrier because the frontier orbital energies for the alkyl groups lie far from the gold Fermi energy, while the frontier orbitals for the π-system of the viologen are much closer to the Fermi energy. This is apparent upon comparing the single molecule conductance of 6V6 (0.5 nS)[16,18] with that of dodecane-1,12-dithiol (*i.e.* two back-to-back barriers with no well; 0.028 nS).[19] Even though 6V6 is *longer* than dodecane-1,12-dithiol, it is more conductive due to the influence of the viologen acting as a barrier indentation.

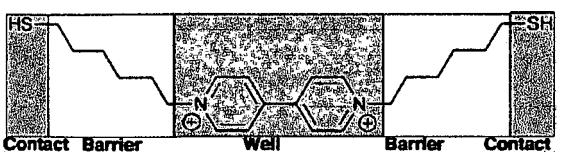

Fig. 1 The molecule 6V6 as a double tunnelling barrier junction.

The viologen group in 6V6 is electroactive. When measured under potential control in aqueous electrolyte, the conductance increased approximately six-fold as the potential was swept negative to access the viologen cation radical redox state, giving a value approximately the same as that for a single C_6 alkane barrier (in hexane-1,6-dithiol; 2.5 nS[16,17]), indicating that the viologen radical cation acts as a particularly deep well.

In this paper, we address the following questions. Firstly, do smaller, non-redox-active moieties also act as "wells"? Secondly, if so, can they be chemically tuned by altering the electronic structure of the well? Thirdly, is there a relationship between the frontier orbital energies of the well and the conductance of the whole junction? Accordingly, we have made a range of molecules **1–4** in which the contacts and barriers are constant ($HS(CH_2)_6$–) and the wells are varied. These are listed in Table 1 together with the HOMO and LUMO energies determined using the SPARTAN04 implementation of DFT (B3LYP/6-31G**).

Table 1 Well structures used, and their frontier orbital energies (in eV). R = $HS(CH_2)_6$– in all cases

Molecule	Well structure	HOMO	LUMO
1	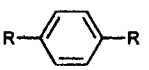	−6.25	+0.06
2		−6.62	−0.59
3	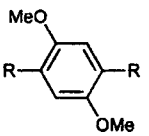	−5.23	+0.09
4	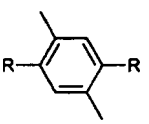	−5.97	+0.12

Department of Chemistry, University of Liverpool, Crown Street, Liverpool, UK L69 7ZD. E-mail: shiggins@liv.ac.uk; Fax: +44 (0) 151 794 3588; Tel: +44 (0) 151 794 3512

† Electronic supplementary information (ESI) available: Syntheses and characterisation of **1–4**; experimental details. See DOI: 10.1039/b709576g

Molecules **1–4** (Table 1) were synthesised (as dithioacetates) and fully characterised by microanalytical and spectroscopic methods.‡ We then employed the scanning tunnelling microscopy (STM) based *I(t)* technique of Haiss[20] to determine the single molecule conductances of **1–4**. A flame-annealed gold-coated glass slide is dipped into a dilute (10^{-4}–10^{-5} M) solution of the appropriate dithioacetate for one minute to allow the formation of a low coverage monolayer (our recent experience is that it is not necessary to employ $CH_3C(O)Cl$–MeOH deprotection[21] prior to monolayer formation). A gold STM tip is then brought to a fixed distance above the gold surface under perfluorodecane, controlled using the set point current. The feedback loop is switched off and the current is monitored as a function of time. As molecules spontaneously form and break bridges between tip and surface, jumps in the tunnelling current are observed (for example, Figure S4 in Supplementary Information) due to conductance through the molecule(s). These jumps are analysed statistically. Fig. 2 shows a typical histogram for such an experiment. For molecules **1–4**, we repeated this experiment at different tip–substrate bias potentials, and the mean single molecule current was then plotted against the bias potential. The slope gives the molecular conductance (Table 2).

The results were checked using a complementary method, the *I(s)* technique. Here, the tip is withdrawn while maintaining a constant x–y position, and a current–distance (*I(s)* where s = relative tip–sample distance) curve is collected. We typically observe current–distance behaviour characteristic of the formation of molecular wires (Figure S1, Supplementary Information) with a plateau in the current (*I(w)*) due to conductance through the fully-extended molecule in its lowest-energy conformation. As the tip is withdrawn further, the molecule then detaches at a distance characteristic of its length. Again, the experiment is repeated many times, and the results are analysed statistically as for the *I(t)* measurements. The results (Table 2) are valuable in two ways. Firstly, results for the two techniques are in good agreement, giving us added confidence in the *I(t)* measurements. Secondly, they provide confirmation that we are dealing with molecular

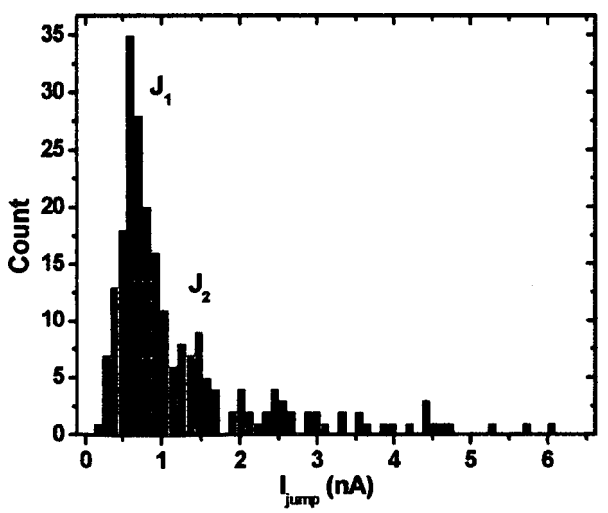

Fig. 2 Histogram of the current jumps observed in one of the *I(t)* measurements on molecule **4**. The tip–substrate potential in this example was +600 mV. The large peak, J_1, corresponds to jumps involving a single molecule, and the smaller peak J_2 to jumps involving two molecules.

Table 2 Conductances (standard deviations in parentheses) of **1–4** measured using *I(t)* and *I(s)* methods, and mean detachment distances (standard deviations in parentheses) measured using *I(s)* method

Molecule	*I(t)* (nS)	*I(s)* (nS)	$s_{1/2}$ (nm)
1	0.67 (0.07)	0.74 (0.24)	1.83 (0.19)
2	0.48 (0.05)	0.40 (0.09)	2.35 (0.28)
3	0.92 (0.14)	0.90 (0.19)	1.33 (0.14)
4	0.77 (0.11)	0.69 (0.27)	1.38 (0.15)

events, because the mean break-off distances are reasonably consistent with the lengths of the molecules (2 nm S–S distances for the fully-extended, transoid conformers of **1–4** as determined by molecular mechanics). The degree of uncertainty in the detachment distance measurement (see the histogram in Figure S2) is larger than in the determination of conductance because of the range of contact geometries, and the difficulty of maintaining a constant starting-point in the measurements.

The results in Table 2 are interesting in several respects. Firstly, it is clear that the conductances are considerably greater than would be expected for an alkanedithiol of the same length as **1–4**. This indicates that the aromatic units do indeed act as a "well" in the tunnelling barrier for **1–4**. Secondly, it is clear that the conductance varies with substituent; electron-donating groups lead to higher conductances. In Fig. 3, we plot the conductances against the HOMO energy for the aromatic unit, obtained from the Spartan04 implementation of DFT (B3LYP, 6-31G**; equilibrium geometry calculated for the transoid, extended form of **1–4** minimised using molecular mechanics).

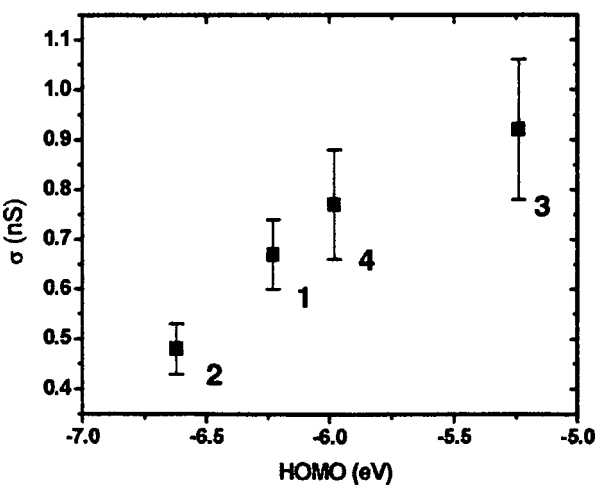

Fig. 3 Plot of conductances determined by *I(t)* method (with standard deviations) against HOMO energy for molecules **1–4**.

For molecules such as alkanedithiols in which superexchange is the conductance mechanism, conductance G decreases exponentially with the length of the molecule ($G = A\exp(-\beta_N N)$, equation 1) where A is characteristic of the metal–molecule coupling and is therefore contact-dependent, β_N is a decay constant characteristic of the repeat unit (–CH_2–), and N is the number of repeat units. Superexchange is also expected to be the operable mechanism for molecules **1–4**, especially given that the central chemical group (the

"well") is off-resonance.[18] However, simple barrier tunnelling (equation 1, where the decay constant β or κ is proportional to the square root of barrier height) cannot adequately describe tunnelling across **1–4** since the "well" leads to a double tunnelling barrier with the barrier height only reduced at the well rather than across the entire molecule. Fig. 3 is plotted in linear form since *a priori* the relationship between conductance and the HOMO position is not known and in any case is not likely to follow the simple single barrier tunnelling model implicit in equation 1. The observation that a clearly apparent but rather weak (linear) relationship exists between conductance and HOMO position is noteworthy, and demonstrates that these molecular double tunnelling barriers are not represented adequately by equation 1, for which a reduction in barrier height across the whole molecular wire would lead to a non-linear relationship between conductance and frontier orbital position. Indeed, for a selection of conjugated molecular wires in which a single frontier orbital extends between the two sulfur terminal groups, we observe that ln(conductance) scales with the square root of the frontier orbital position, consistent with the barrier tunnelling model of equation 1.[22]

A detailed theoretical description of the mechanism of conduction is outside the scope of this paper. A very recent study of the single molecule conductances of a series of very short conjugated molecules (substituted 1,4-diaminobenzenes) using an STM-based break junction technique found that electron donating substituents resulted in higher molecular conductances, and there was a (very approximate) correlation between the conductance and the Hammett σ_p parameter, consistent with hole transport (*i.e.* one could regard the molecule as being in a 'positive transition state' as it conducts).[5] Also, recent thermoelectric effect measurements on conjugated dithiols trapped between gold electrodes in the presence of a temperature gradient gave positive values for the junction Seebeck coefficients, indicating hole conduction.[23] In our molecules, the presence of the alkyl tunnelling barriers means that the aryl substituents are far removed from the gold contacts during measurement, so that possible complications from steric effects, and consequent differences in contact geometry, are much less likely. It is interesting that although the conduction mechanism may well be different for short, conjugated molecules, the effect of substitution is the same.

We thank EPSRC (grant no. EP/C00678X/1) for funding.

Notes and references

‡ Sonogashira cross-coupling of the appropriate 1,4-dibromo-arene with 6-chloro-hex-1-yne, H_2/Pd reduction of the resulting di-alkyne, and subsequent KSAc–NaI(cat.)–acetone treatment of the 1,4-bis(6-chloro-hexyl)arene afforded the corresponding thioacetic acid *S*-{6-[4-(6-acetylsulfanyl-hexyl)-aryl]-hexyl} esters, **1–4**; full details are in the Supplementary Information.

1 S. M. Lindsay and M. A. Ratner, *Adv. Mater.*, 2007, **19**, 23.
2 N. J. Tao, *Nat. Nanotechnol.*, 2006, **1**, 173.
3 L. Venkataraman, J. E. Klare, C. Nuckolls, M. S. Hybertsen and M. L. Steigerwald, *Nature*, 2006, **442**, 904.
4 J. R. Quinn, F. W. Foss, L. Venkataraman, M. S. Hybertsen and R. Breslow, *J. Am. Chem. Soc.*, 2007, **129**, 6714.
5 L. Venkataraman, Y. S. Park, A. C. Whalley, C. Nuckolls, M. S. Hybertsen and M. L. Steigerwald, *Nano Lett.*, 2007, **7**, 502.
6 A. V. Danilov, S. E. Kubatkin, S. G. Kafanov, K. Flensberg and T. Bjornholm, *Nano Lett.*, 2006, **6**, 2184.
7 G. J. Ashwell, B. Urasinska, C. S. Wang, M. R. Bryce, I. Grace and C. J. Lambert, *Chem. Commun.*, 2006, 4706.
8 A. M. Moore, A. A. Dameron, B. A. Mantooth, R. K. Smith, D. J. Fuchs, J. W. Ciszek, F. Maya, Y. X. Yao, J. M. Tour and P. S. Weiss, *J. Am. Chem. Soc.*, 2006, **128**, 1959.
9 A. S. Blum, J. G. Kushmerick, D. P. Long, C. H. Patterson, J. C. Yang, J. C. Henderson, Y. X. Yao, J. M. Tour, R. Shashidhar and B. R. Ratna, *Nat. Mater.*, 2005, **4**, 167.
10 L. H. Yu, Z. K. Keane, J. W. Ciszek, L. Cheng, M. P. Stewart, J. M. Tour and D. Natelson, *Phys. Rev. Lett.*, 2004, **93**, 266802.
11 M. Elbing, R. Ochs, M. Koentopp, M. Fischer, C. von Hanisch, F. Weigend, F. Evers, H. B. Weber and M. Mayor, *Proc. Natl. Acad. Sci. U. S. A.*, 2005, **102**, 8815.
12 L. L. Chang, L. Esaki and R. Tsu, *Appl. Phys. Lett.*, 1974, **24**, 593.
13 D. P. Wang, B. R. Perkins, A. J. Yin, A. Zaslavsky, J. M. Xu, R. Beresford and G. L. Snider, *Appl. Phys. Lett.*, 2005, **87**, 152102.
14 T. Kanazawa, R. Fujii, T. Wada, Y. Suzuki, M. Watanabe and M. Asada, *Appl. Phys. Lett.*, 2007, **90**, 092101.
15 W. C. Liu, W. S. Lour and Y. H. Wang, *IEEE Trans. Electron Devices*, 1992, **39**, 2214.
16 W. Haiss, H. van Zalinge, S. J. Higgins, D. Bethell, H. Höbenreich, D. J. Schiffrin and R. J. Nichols, *J. Am. Chem. Soc.*, 2003, **125**, 15294.
17 W. Haiss, H. van Zalinge, H. Höbenreich, D. Bethell, D. J. Schiffrin, S. J. Higgins and R. J. Nichols, *Langmuir*, 2004, **20**, 7694.
18 W. Haiss, T. Albrecht, H. van Zalinge, S. J. Higgins, D. Bethell, H. Höbenreich, D. J. Schiffrin, R. J. Nichols, A. M. Kuznetsov, J. Zhang, Q. Chi and J. Ulstrup, *J. Phys. Chem. B*, 2007, **111**, 6703.
19 W. Haiss, unpublished observations, 2007.
20 W. Haiss, R. J. Nichols, H. van Zalinge, S. J. Higgins, D. Bethell and D. J. Schiffrin, *Phys. Chem. Chem. Phys.*, 2004, **6**, 4330.
21 W. Haiss, R. J. Nichols, S. J. Higgins, D. Bethell, H. Höbenreich and D. J. Schiffrin, *Faraday Discuss.*, 2004, **125**, 179.
22 W. Haiss, C. S. Wang, I. Grace, C. Lambert, M. R. Bryce, S. J. Higgins and R. J. Nichols, manuscript in preparation, 2007.
23 P. Reddy, S. Y. Jang, R. A. Segalman and A. Majumdar, *Science*, 2007, **315**, 1568.

J|A|C|S
COMMUNICATIONS

Published on Web 08/23/2008

Structure–Property Relationships in Redox-Gated Single Molecule Junctions – A Comparison of Pyrrolo-Tetrathiafulvalene and Viologen Redox Groups

Edmund Leary,[†] Simon J. Higgins,*[,†] Harm van Zalinge,[†] Wolfgang Haiss,[†] Richard J. Nichols,[†] Sune Nygaard,[‡] Jan Oskar Jeppesen,*[,‡] and Jens Ulstrup[§]

Department of Chemistry, University of Liverpool, Liverpool L69 7ZD, U.K., Department of Physics and Chemistry, University of Southern Denmark, Campusvej 55, DK-5230 Odense M, Denmark, Department of Chemistry and NanoDTU, Technical University of Denmark, DK2800 Kgs. Lyngby, Denmark

Received March 6, 2008; E-mail: shiggins@liv.ac.uk; joj@ifk.sdu.dk

There is a growing realization of the important role that electrochemistry plays in molecular and organic electronics and of the potential for creating new electronic devices which use electrochemistry to control an electrical response. Electrochemical processes have been implicated in controlling the electrical behavior of a number of molecular devices such as rotaxane based switches and negative differential resistance (NDR)[1] devices, although it is not always straightforward to ascertain the mechanism. It has recently been demonstrated that the electrical properties of single molecules incorporating redox groups (e.g., viologens,[2,3] oligophenyleneethynylenes,[4] perylene tetracarboxylic diimides (PTCDI),[5] and oligo-anilines[6]) can be characterized as they are electrochemically switched between redox states, opening the possibility to examine directly the link between redox state and conductance of individual molecules.[2] Such experiments typically use a scanning tunneling microscope (STM), with individual redox active molecules tethered via Au–S bonds between a gold substrate and tip, under potential control.

There is a clear analogy in these experiments to a molecular transistor, with the tip and surface acting as source and drain, I_{SD} being the current flow between these two electrodes, while the counter electrode acts as a "gate". It has been shown in several instances that electrochemically gated conductance increases occur concomitantly with redox changes.[2−6] The following questions now arise: can other device characteristics be controlled by the structural, chemical or electronic properties of the redox group, and can structure–property relationships be derived? Here, we show that the nature of the I_{SD} vs electrochemical gating potential (E_{Gate}) profile can be controlled by the nature of the redox group: the pyrrolo-tetrathiafulvalene (PTTF) molecular bridge 6PTTF6 (Figure 1) exhibits a sharp *off–on–off* transition as E_{Gate} is swept through the redox transition, while the viologen 6V6 exhibits a much broader *off–on* switching profile. We discuss possible reasons for these observations.

The two molecular bridges shown in Figure 1 (left) only differ in the central redox moiety. In this configuration, the redox groups are electronically "decoupled" from the enclosing metal contacts by the $-(CH_2)_6SH$ arms, giving double tunneling barriers. It has been previously shown[2] that the conductance of 6V6 increases as the potential is swept negative, but no peak is observed in the conductance–overpotential relation around the $V^{2+}/V^{\bullet+}$ equilibrium potential. Instead, a broad rise occurs across the redox wave, which does not level off within the attainable negative potential limit. This unusual behavior has been attributed to configurational fluctuations

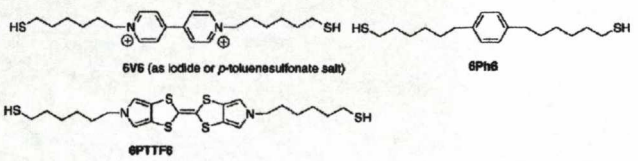

Figure 1. Structures of redox-active double tunneling barriers 6V6 and 6PTTF6 (left) and redox-inactive control 6Ph6[7] (right).

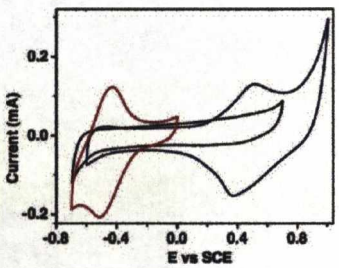

Figure 2. Cyclic voltammograms of 6PTTF6 (blue), 6V6 monolayer (red), and 6Ph6 (black) monolayers on Au(111) single crystal electrodes, recorded in 10 mM Na_2HPO_4/NaH_2PO_4, pH 6.8 at 1 V s^{-1}. The irreversible oxidation at >+0.8 V seen for 6PTTF6 is due to oxidative desorption of Au–S.

of the flexible polymethylene chains.[2b] This process leads to a "soft gating" of superexchange-based electron transport across 6V6, as the molecular bridge attains configurations in which tunneling is more facile by preorganization of the nuclear coordinates and environment.

We next examined structurally related molecules, to test whether "soft gating" is a general phenomenon. Tetrathiafulvalene (TTF) derivatives have already served as π-electron donors in molecular and supramolecular systems designed for molecular electronics.[8] We chose the PTTF redox moiety (Figure 1) since (i) possible complications arising from cis and trans mixtures for "symmetrically" disubstituted TTFs[9] are obviated[10] and (ii) PTTFs are particularly electron-rich and show two fully reversible, one-electron oxidations, the first of which lies well within the potential range where Au–S bonds are stable in aqueous electrolyte. Compound 6PTTF6 was synthesized and fully characterized[11] (see Supporting Information (SI)).

Figure 2 shows cyclic voltammograms of monolayers of 6PTTF6, 6V6, and 6Ph6 on Au(111) in aqueous buffer, and Figure 3 shows single molecule conductance data for each molecule as a function of the overpotential (redox active molecules) or electrode potential (6Ph6). For 6PTTF6, the data show a conductance rise from ~0.5 nS in its neutral state to a maximum of 2.5 nS, which falls again to the "off" conductance value of ~0.5 nS at positive overpotentials. The width of the conductance peak is ~0.2 V, in the range

[†] University of Liverpool.
[‡] University of Southern Denmark.
[§] Technical University of Denmark.

10.1021/ja8014605 CCC: $40.75

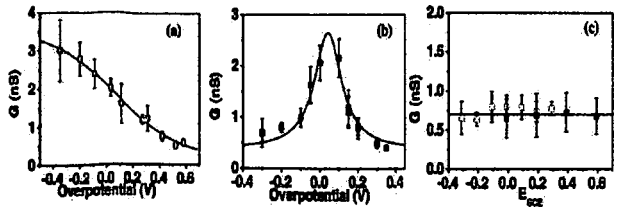

Figure 3. Single molecule conductance of (a) 6V6 (red), (b) 6PTTF6 (blue), and (c) 6Ph6 (black), versus the overpotential (η) for the redox molecules and the electrode potential for 6Ph6. Data for filled symbols obtained using I(s) method; for open symbols using I(t) method (see SI).

expected[12] for the tip-to-sample bias voltage of 0.2 V employed in these experiments. The conductance of the redox-inactive 6Ph6[7] is similar to that of the "off" states of 6V6 and 6PTTF6 but does not change as a function of potential; the frontier π-orbitals of the benzene ring are too far from the Fermi energy of Au to be brought into resonance by gate potentials accessible in these experiments. The "classical" behavior of the gold|6PTTF6|gold single molecule junction, with a symmetrical peak close to the first oxidation potential for PTTF, can be rationalized in terms of both two-step (hopping) mechanisms and superexchange (tunneling) modes. In the hopping mechanism the oxidized ($PTTF^{\bullet+}$) and reduced ($PTTF^{0}$) forms would contribute comparably at the equilibrium redox potential to the tunneling current across the molecular junction.[13] A maximum would then result in the conductance vs overpotential relationship, as is experimentally observed. A maximum is also expected in the tunneling or superexchange mechanisms when the two redox states of PTTF are comparably populated at the reversible potential.[13a] The question is why does the PTTF moiety behave classically, while the viologen moiety does not?

The conductance of both 6V6 and 6PTTF6 in the "off" state and the factor by which the conductance changes on reduction (6V6) or oxidation (6PTTF6) are similar. The difference clearly must lie in the properties of the central redox moiety, because the flexible alkyl spacers are present in all three molecules. Both the neutral PTTF moiety[14] and structurally characterized $TTF^{\bullet+}$ derivatives[16] are planar in the solid state. DFT calculations[15] show that the PTTF core of an isolated molecule (as found in metal−molecule−metal junctions) is also planar for both states. Viologen dications can be planar or twisted about the inter-ring C−C bond, depending upon the anion, suggesting that inter-ring twisting is a low-energy process.[17] Strong $\pi-\pi$ interactions in the solid state mean that the sole crystal structure of a $V^{\bullet+}$ salt[18] can tell us little about the likely configuration of an isolated molecule, but greater coplanarization upon reduction and increased inter-ring C−C double bond character is predicted.[15,19] There are therefore significant configurational differences between V^{2+} and $V^{\bullet+}$ that are not apparent in the PTTF system.[20] We suggest that these are the likely cause of the differences in the two systems and that the tunneling factor depends upon the instantaneous nuclear configuration of the twisting mode for the viologen, giving the different form of the current/overpotential relation.

In summary, we have shown that well-defined redox switching can be obtained in gold|6PTTF6|gold single molecule junctions. We have achieved *off−on−off* switching (in accord with theoretical expectations and the simplest view of the two-step process[13b]) in these junctions, controlled by the redox electrochemistry of the PTTF group. Differences between the conductance−overpotential behavior of 6V6 and 6PTTF6 are rationalized in terms of conformational dynamics of the respective systems.

Acknowledgment. We thank the EPSRC (Grant EP/C00678X/1) for funding and for provision of the Chemical Database Service. The Danish groups thank the DSRC (2117-05-0115) and the DRCTPS (274-07-0272) for funding.

Supporting Information Available: Details of the synthesis and characterization of 6PTTF6, molecular conductance determinations, and SPARTAN calculations. This material is available free of charge via the Internet at http://pubs.acs.org.

References

(1) (a) Flood, A. H.; Stoddart, J. F.; Steuerman, D. W.; Heath, J. R. *Science* **2004**, *306*, 2055. (b) Chen, J.; Reed, M. A.; Rowlett, A. M.; Tour, J. M. *Science* **1999**, *286*, 1550.
(2) (a) Haiss, W.; van Zalinge, H.; Higgins, S. J.; Bethell, D.; Höbenreich, H.; Schiffrin, D. J.; Nichols, R. J. *J. Am. Chem. Soc.* **2003**, *125*, 15294. (b) Haiss, W.; Albrecht, T.; van Zalinge, H.; Higgins, S. J.; Bethell, D.; Höbenreich, H.; Schiffrin, D. J.; Nichols, R. J.; Kuznetsov, A. M.; Zhang, J.; Chi, Q.; Ulstrup, J. *J. Phys. Chem. B* **2007**, *111*, 6703. (c) Haiss, W.; Van Zalinge, H.; Höbenreich, H.; Bethell, D.; Schiffrin, D. J.; Higgins, S. J.; Nichols, R. J. *Langmuir* **2004**, *20*, 7694.
(3) Li, Z. H.; Han, B.; Meszaros, G.; Pobelov, I.; Wandlowski, T.; Blaszczyk, A.; Mayor, M. *Faraday Discuss.* **2006**, *131*, 121.
(4) Xiao, X. Y.; Nagahara, L. A.; Rawlett, A. M.; Tao, N. J. *J. Am. Chem. Soc.* **2005**, *127*, 9235.
(5) Li, X. L.; Xu, B. Q.; Xiao, X. Y.; Yang, X. M.; Zang, L.; Tao, N. J. *Faraday Discuss.* **2006**, *131*, 111.
(6) (a) Chen, F.; He, J.; Nuckolls, C.; Roberts, T.; Klare, J. E.; Lindsay, S. *Nano Lett.* **2005**, *5*, 503. (b) He, J.; Chen, F.; Lindsay, S.; Nuckolls, C. *Appl. Phys. Lett.* **2007**, *90*, 072112. (c) Chen, F.; Nuckolls, C.; Lindsay, S. *Chem. Phys.* **2006**, *324*, 236.
(7) Leary, E.; Higgins, S. J.; van Zalinge, H.; Haiss, W.; Nichols, R. J. *Chem. Commun.* **2007**, 3939–3941.
(8) Dichtel, W. R.; Heath, J. R.; Stoddart, J. F. *Philos. Trans. R. Soc. London, Ser. A* **2007**, *365*, 1607.
(9) Giacalone, F.; Herranz, M. A.; Gruter, L.; Gonzalez, M. T.; Calame, M.; Schonenberger, C.; Arroyo, C. R.; Rubio-Bollinger, G.; Velez, M.; Agrait, N.; Martin, N. *Chem. Commun.* **2007**, 4854.
(10) Jeppesen, J. O.; Becher, J. *Eur. J. Org. Chem.* **2003**, 3245.
(11) (a) Jeppesen, J. O.; Takimiya, K.; Jensen, F.; Becher, J. *Org. Lett.* **1999**, *1*, 1291. (b) Jeppesen, J. O.; Takimiya, K.; Jensen, F.; Brimert, T.; Nielsen, K.; Thorup, N.; Becher, J. *J. Org. Chem.* **2000**, *65*, 5794.
(12) Kuznetsov, A. M.; Medvedev, I. G.; Ulstrup, J. *J. Chem. Phys.* **2007**, *127*, 104708.
(13) (a) Kuznetsov, A. M.; Ulstrup, J. *Electron Transfer in Chemistry and Biology: An Introduction to the Theory*; John Wiley: Chichester, U.K., 1999. (b) Zhang, J.; Chi, Q.; Kuznetsov, A. M.; Hansen, A. G.; Wackerbarth, H.; Christensen, H. E. M.; Andersen, J. E. T.; Ulstrup, J. *J. Phys. Chem. B* **2002**, *106*, 1131.
(14) Doi, I.; Miyazaki, K.; Takimiya, K.; Kunugi, Y. *Chem. Mater.* **2007**, *19*, 5230.
(15) Spartan'04, DFT implementation, B3LYP at the 6-31G* level.
(16) Honda, K.; Takasaki, S.; Yamada, J.-I.; Nakatsuji, S. I.; Anzai, H. *Acta Crystallogr., Sect. C* **1998**, *C54*, 261.
(17) Fletcher, D. A.; McMeeking, R. F.; Parkin, D. *J. Chem. Inf. Comput. Sci.* **1996**, *36*, 746.
(18) Bockman, T. M.; Kochi, J. K. *J. Org. Chem.* **1990**, *55*, 4127.
(19) Hester, R. E.; Suzuki, S. *J. Phys. Chem.* **1982**, *86*, 4626.
(20) The small difference in electron self-exchange rate constants (k_{ex}) between viologens (e.g., $MV^{2+/\bullet+}$; k_{ex} 8.1 × 10^{8} [21]) and TTFs (e.g., $Me_4TTF^{\bullet/\bullet+}$; k_{ex} 3.3 × 10^{9} $M^{-1}s^{-1}$ [22]) cannot account for the different forms of the current−overpotential relations for 6V6 and 6PTTF6. Note that self-assembled monolayers incorporating $[M(terpy)_2]^{2+/3+}$ (M = Co, Os) units both show current−overpotential relations in scanning tunneling spectroscopy experiments similar in form to 6PTTF6, yet they have very different interfacial electron transfer rates, > 10^{6} s^{-1} (M = Os) and ca. 10^{3} s^{-1} (M = Co).[23]
(21) Grampp, G.; Mladenova, B. Y.; Kattnig, D. R.; Landgraf, S. *Appl. Magn. Reson.* **2006**, *30*, 145–164.
(22) Rosokha, S. V.; Kochi, J. K. *J. Am. Chem. Soc.* **2007**, *129*, 828–838.
(23) Albrecht, T.; Moth-Poulsen, K.; Christensen, J. B.; Guckian, A.; Bjørnholm, T.; Vos, J. G.; Ulstrup, J. *Faraday Discuss.* **2006**, *131*, 265–279.

JA8014605